Medium Scale Morphodynamics of the Central Dithmarschen Bight

Dissertation
zur Erlangung des Doktorgrades
der Mathematisch-Naturwissenschaftlichen Fakultät
der Christian-Albrechts-Universität zu Kiel

vorgelegt von

Jort Wilkens

Kiel
2004

Referent:	Prof. Dr. Roberto Mayerle
Koreferent:	Prof. Dr.-Ing. Werner Zielke
Tag der mündlichen Prüfung:	5. Mai 2004
Zum Druck genehmigt	Kiel, den 24. März 2005

Contents

List of Figures

List of Tables

Acknowledgements

First of all, I would like to thank my supervisor Prof. Dr. Roberto Mayerle. He invited me in 1999 to come to Kiel and join his research group for a period of six months, forming the basis for the much longer stay. I thank him for his support and valuable discussions.

Secondly, I would like to thank Prof. Dr.-Ing. Werner Zielke. As project leader of the Promorph project he shared his knowledge and experience with our project group. Many thanks also for his readiness to be part of the jury of this dissertation.

Also, I would like to thank all of the colleagues who were or are part of the Coastal Research Laboratory group for their friendship and making the work enjoyable. I thank my friends Fernando Toro and Christian Winter, with whom I had many good times, not only during working hours.

Furthermore, I thank my colleagues at the Research and Technology Centre Westcoast. They made our measurement campaigns on the Wadden Sea an enjoyable experience, despite the sometimes rough and other times tedious conditions. Many thanks to Nils Asp for his friendship and interesting discussions, as well as to Klaus Ricklefs for sharing his knowledge and his useful comments on my work.

I would like to thank our partners in the Promorph project and the collaborating authorities and institutes for sharing their knowledge, discussions and making available the necessary data for the underlying work.

Special thanks go to my dear parents Akke and Dirk Wilkens and to my sister Rixt, for their love, support and for standing by me during these years. And finally, Brigitte, thank you for your love and the good times we had and will have.

Jort Wilkens
Kiel, March 24^{th}, 2005

Abstract

Medium scale morphodynamics. Along many coastlines in the world tidal flat areas can be found. Their morphology is generally changing at varying temporal and spatial scales due to natural influences, e.g. tides and waves, and anthropological activities, such as the construction of coastal structures and dredging. The processes which are responsible for these morphological changes are the hydrodynamics and the sediment transport. Depending on the bathymetry, these processes can be highly complex. The morphological changes on the medium scale are here defined as changes on the scale of tidal channels, tidal flats and sand banks. Their dynamics occur on the medium term periods of up to about ten years.

Analysis of the relevant morphodynamic processes. The understanding of the hydrodynamics and sediment dynamics can be improved through a variety of measurements as well as by representing the processes in a mathematical model. Both methods have been applied to analyse the relevant processes for the medium scale morphological evolution over the last twenty years of the tidal channel system of the central Dithmarschen Bight, a tidal flat area on the German coast in the southeastern North Sea. Extensive field data of the hydrodynamics and sediment dynamics have been analysed and a complex numerical model was set up.

Analysis of observed morphological evolution and relevant processes. The tidal channel system in the central Dithmarschen Bight consists of two channels that connect to the open North Sea and merge in the middle of the area to form a single channel that penetrates further into the tidal flat area. Enclosed by and adjacent to these channels several tidal flats and shoals are found. The large mean tidal range of 3.2 m and incoming waves of up to 3.5 m, in combination with mean sediment grain sizes in the order of 100 to 250 μm, allow for significant medium scale morphological changes. These include a general narrowing and deepening of the channels, channel migration and a shoreward migration of the enclosed tidal flat.

Modelling of the medium scale morphodynamics. Partly in previous works, extensive calibration and validation studies have been carried out for the individual process models for flow, waves and sediment transport. The resulting models have

been coupled to a model for morphological updating to form a morphodynamic model.

An approach has been followed in which a limited number of representative conditions in terms of tides, swell, wind and storm conditions were defined. The obtained representative tidal cycle has a tidal range close to the mean tidal range in the area, slightly (7 to 20 %) lower than the ranges proposed in literature. The influence of storm conditions on the morphodynamic model results was found to be very limited and these have thus been considered as part of the representative swell and wind climates. These climates were considered as first estimates and have been adjusted in the calibration.

The morphodynamic model has been calibrated and validated, considering the medium scale morphological evolution over periods of approximately ten years. The evaluation of the model results was based on the changes in the location of depth contours, volumetric analysis of several sub-domains and comparison of the medium scale sedimentation and erosion patterns. The most significant improvements in the calibration were achieved by adjustment of the representative swell and wind climates and by the application of a variable definition of the Bijker's constant in the applied sediment transport formula. It led to a model that reproduced the majority of the observed medium scale morphodynamics rather well. The validation showed that the medium scale behaviour of the investigated area can be properly represented by the morphodynamic model.

Analysis of modelled morphodynamic processes. The validated morphodynamic model has been applied to analyse the significance of the main driving forces, i.e. tide, swell, locally generated waves and wind, for the medium scale morphodynamics, on the basis of comparisons of the modelled morphological changes over a period of two years. It could be concluded that the tidal and swell conditions have the most significant effects on the western and middle parts of the study area, which could thus be classified to be mixed energy coastal areas. The eastern, sheltered part could be identified as highly tide-dominated.

The main driving force behind the observed expansion of the central tidal flat Tertiussand to the Northeast and South, as well as the erosion of its western part, was concluded to be swell. The medium scale morphological evolution of the investigated area mainly depends on the balance of the tide, responsible for initiating and maintaining the channels, and the swell, causing an equalising of the tidal flats and channels.

Prediction of ten years of morphological evolution. The extensive calibration and validation of the medium scale morphodynamic model, as well as of the underlying individual process models, gives good confidence in the prediction of the morphological evolution over periods of about ten years. The model predicts the breakthrough of the tidal flat Tertiussand, causing some significant morphological changes.

Zusammenfassung

Mesoskalige Morphodynamik. Viele Küstengebiete der Erde bestehen aus Wattgebieten. Deren Morphologie ändert sich im Allgemeinen in variierenden zeitlichen und räumlichen Skalen auf Grund von natürlichen Einflüssen wie z.B. Tiden und Seegang, und anthropologischen Eingriffen wie z.B. den Bau von Küstenbauwerken und Baggermaßnahmen. Die Prozesse, die für diese morphologischen Änderungen verantwortlich sind, sind die Hydrodynamik und der Sedimenttransport. In Abhängigkeit der Bathymetrie können diese Prozesse hochkomplex sein. Die mesoskaligen morphologischen Änderungen sind hier definiert als Änderungen in der Größenordnung von Tiderinnen, Wattflächen und Sandbänken. Deren Dynamik erfolgt in mittelfristigen Perioden von bis zu etwa zehn Jahren.

Analyse der maßgeblichen morphodynamischen Prozesse. Das Verständnis der Hydrodynamik und der Sedimentdynamik kann durch eine Vielzahl von Messungen sowie durch die Abbildung der Prozesse in einem mathematischen Modell verbessert werden. Beide Methoden wurden verwendet, um die maßgeblichen Prozesse der mesoskaligen morphologischen Entwicklung der letzten zwanzig Jahre im Gebiet der zentralen Dithmarscher Bucht zu analysieren, ein Wattengebiet an der deutschen Küste in der südöstlichen Nordsee. Umfangreiche Naturmessungen der Hydrodynamik und der Sedimentdynamik wurden analysiert und ein komplexes numerisches Modell wurde erstellt.

Analyse der beobachteten morphodynamischen Entwicklung und maßgebliche Prozesse. Das Gebiet in der zentralen Dithmarscher Bucht besteht aus zwei Rinnen, die mit der Nordsee verbunden sind und sich in der Mitte der Bucht zu einer dritten Rinne vereinigen, die weit in das Wattengebiet hineinreicht. Eingeschlossen und angrenzend an diese Rinnen befinden sich mehrere Wattflächen und Untiefen. Der große mittlere Tidehub von 3.2 m und Wellen von bis zu 3.5 m in Verbindung mit mittleren Korngrößen von 100 bis 250 μm lassen signifikante mittelfristige Änderungen zu. Diese beinhalten eine generelle Verengung und Vertiefung der Rinnen, Rinnenmigration und eine landwärtsgerichtete Verlagerung des eingeschlossenen Wattengebietes.

Modellierung der mesoskaligen Morphodynamik. Teilweise in vorangegangenen Arbeiten, wurden umfangreiche Kalibrierungs- und Validierungsstudien für die einzel-

nen Prozessmodelle für Strömung, Wellen und Sedimenttransport durchgeführt. Die entstandenen Modelle wurden zu einem morphologischen Update-Modell gekoppelt um zusammen ein morphodynamisches Modell zu bilden.

Ein Ansatz wurde verwendet in dem eine begrenzte Anzahl von repräsentativen Bedingungen im Hinblick auf Tiden, Dünung, Wind und Sturmbedingungen definiert wurde. Der daraus entstandene Tidezyklus hat einen Tidehub, der in der Nähe des mittleren Tidehubs liegt. Dieser ist niedriger (7 bis 20 %) als die in der Literatur vorgeschagene Tidehübe. Der Einfluss von Sturmbedingungen auf die Ergebnisse des morphodynamischen Modells stellte sich als sehr begrenzt heraus und wurde deshalb als Teil der repräsentativen Dünungs- und Windklimas berücksichtigt, die als erste Abschätzung angesehen und während der Kalibrierung angepasst wurden.

Das morphodynamische Modell wurde unter Berücksichtigung der mesoskaligen Entwicklung in einem Zeitraum von etwa zehn Jahren kalibriert und validiert. Die Auswertung der Modellergebnisse basiert auf den Änderungen von Tiefenlinien, volumetrischen Analysen von verschiedenen Teilgebieten und Vergleich von mesoskaligen Sedimentations- und Erosionsmustern. Die signifikantesten Verbesserungen in der Kalibrierung wurden durch die Anpassung der repräsentativen Dünungs- und Windklimas und durch die Anwendung einer variablen Definition der Bijker Konstanten in der verwendeten Sedimenttransport-Gleichung erzielt. Dies führte zu einem Modell, das die Mehrheit der beobachteten mesoskaligen morphodynamischen Änderungen gut nachbilden kann. Die Validierung zeigte, dass das mesoskalige Verhalten des Untersuchungsgebietes vom morphodynamischen Modell passend nachgebildet werden kann.

Analyse der modellierten morphodynamischen Prozesse. Das validierte morphodynamische Modell wurde angewandt, um die Bedeutung der wichtigsten Antriebskräfte, d.h. Tide, Dünung, örtliche Windsee und Wind für die mesoskalige Morphodynamik zu analysieren, auf der Basis von Vergleichen zwischen modellierten morphologischen Änderungen im westlichen und mittleren Teil des Untersuchungsgebietes. Deshalb kann dieser Bereich als *mixed energy* klassifiziert werden. Der östliche, geschützte Teil des Gebietes wurde hingegen als stark tide-dominiert identifiziert.

Die wichtigste Kraft für die beobachtete Ausbreitung des Wattgebietes Tertiussand in Richtung Nordost und Süd, sowie die Erosion dessen westlichen Teils ist Dünung. Die mesoskalige morphologische Entwicklung des Gebietes ist hauptsächlich abhängig vom Gleichgewicht der Tide, die die Ursache für die Schaffung und Erhaltung der Rinnen ist, und der Dünung, die einen Ausgleich zwischen Wattflächen und Rinnen verursacht.

Zehnjährige Vorhersage der morphologischen Entwicklung. Die umfangreiche Kalibrierung und Validierung des morphodynamischen Modells, sowie der zugrundeliegenden Prozess-Modelle gibt Vertrauen in die Vorhersage der morphologischen Entwicklung über einen Zeitraum von zehn Jahren. Das Modell sagt einen Durchbruch von Tertiussand vorher, der signifikante morphologische Änderungen verursacht.

Chapter 1

Introduction

1.1 General

Along many coastlines in the world tidal flats can be found. In the North Sea, tidal flat areas are present along the Dutch, German and Danish coasts, together building the Wadden Sea. The bathymetries of many of these areas are changing at varying temporal and spatial scales, under the natural influence of the tides, waves, wind and storm conditions, as well as the anthropological influences, such as dredging, suppletion and the construction of coastal structures. In return, these morphological changes have an effect on the tidal flow and waves. The interactions between the hydrodynamics and the morphology are defined as morphodynamics. They take place in the form of transport of sediment and the subsequent re-orientation of the hydrodynamics.

Morphodynamic processes occur at various spatial scales, ranging from small scale ripples over medium scale sand banks and tidal flats to large scale dynamics of coastal areas. De Vriend [1997] presented an overview of processes at different temporal and spatial scale as shown in Figure 1.1. It shows the relationship between the spatial and temporal scales. The spatial scale is defined by dimensions of the process or underlying feature; the temporal scale by the period over which significant changes are expected.

This thesis focusses on the medium scale morphodynamics, concerning the behaviour of morphological features on the scale of large tidal channels, tidal flats and sand banks. Their dynamics occur on the medium term, here defined as periods of up to circa ten years.

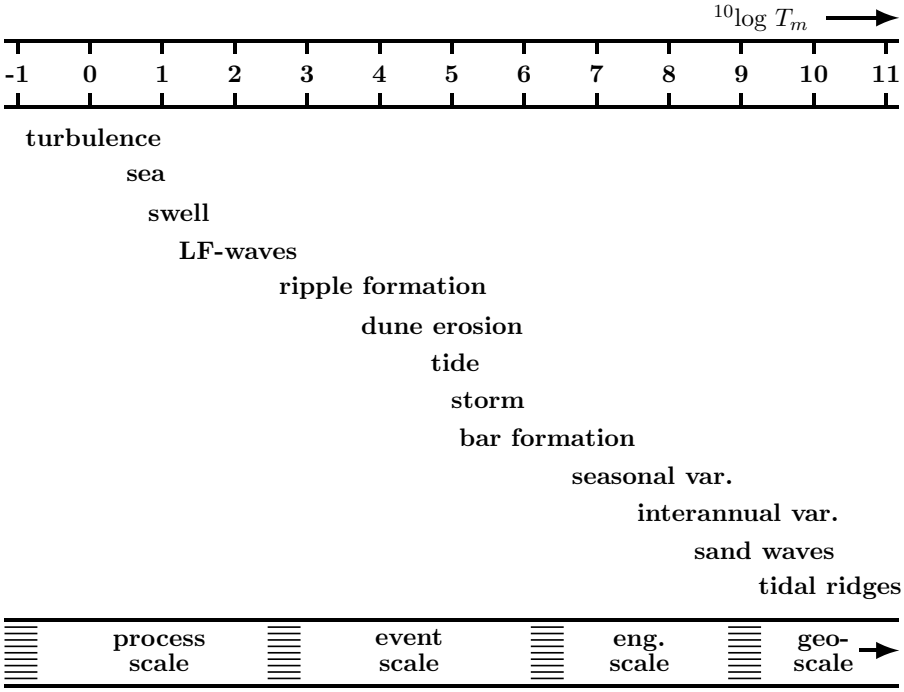

Figure 1.1: Scale range in coastal morphology (morphological time scale T_m in seconds). After [De Vriend, 1997].

The understanding of the medium scale morphodynamic behaviour of coastal areas can be improved through the analysis of:

- measurements of the hydrodynamics, sediment dynamics and morphology, and related characteristics of the considered area; and
- results of a mathematical model representation of the area and its dynamics.

The necessary **measurements** include – the spatial and temporal variation of – the characteristics of the hydrodynamic processes, such as water levels, current velocities and wave heights, periods and directions at various locations in the investigation area. These are completed by observations of the local wind conditions inducing wind-induced currents and generating waves. Secondly, the main characteristics of the available sediment and the sea bed have to be known, e.g. the grain size distribution, cohesiveness and presence of non-erodible features. Furthermore, observations concerning the quantity and direction of the sediment transport, both as bed and as suspended load transport are important. And finally, bathymetric measurements on the considered temporal and spatial scale to analyse the morphological evolution of the study area are needed.

An extensive collection of measurements and observations concerning the above-mentioned processes and characteristics has been analysed in this study.

Several **mathematical modelling** approaches are available for simulation of coastal morphodynamics. An overview is presented by Hanson *et al.* [2003]. Line models can be applied for estimation of the horizontal progress or retreat of an iso-depth line, e.g. the coastline (*shoreline models*), or the vertical changes of a cross-shore coastal profile (*profile evolution models*). Although they can incorporate multiple lines, the two-dimensional horizontal behaviour of the underlying processes is not represented in this type of models. Instead of line models, multi-dimensional, process-based models can be used at various levels of aggregation, ranging from parameterised *conceptual models* to *complex numerical models*. This approach is appropriate when phenomena in the horizontally two-dimensional, or even three-dimensional space are to be represented. Conceptual models can be applied to analyse the main hydrodynamic and morphodynamic mechanisms of an area, considering the exchange of water and sediment between a limited number of sub-domains. These models do not provide information about the transformation of morphological features. For this purpose, complex numerical models can be used. In complex models the significant hydrodynamic and morphodynamic processes are resolved at a much higher spatial resolution, enabling a detailed representation of the hydrodynamics, sediment dynamics and morphology.

In the underlying work, the complex numerical modelling approach has been applied to represent and investigate the medium scale morphological evolution and significant hydrodynamic and morphodynamic processes. On the basis of previous works, a medium scale morphodynamic model has been created, consisting of calibrated and validated individual process models for flow, waves and sediment transport.

1.2 Main research topic

In this study both of the afore-mentioned approaches, i.e. measurements and mathematical modelling, have been combined to increase the understanding of the medium scale morphodynamics for the tidal channel system in the central Dithmarschen Bight.

This tidal flat area is part of the German Wadden Sea between the estuaries of the rivers Elbe and Eider. The central Dithmarschen Bight contains large tidal flats and shoals, and a number of channels of varying size. The relatively large tidal range, with a mean value of approximately 3.2 m, and the unsheltered outer tidal flats, in combination with largely available – mainly non-cohesive – sediments with relatively small median grain sizes (100 to 250 μm) make the area highly dynamic.

Where in previous model studies of the medium scale morphodynamics of the central Dithmarschen Bight [Hirschhäuser & Zanke, 2002; Hoyme, 2002] the focus has been on the sheltered Meldorf Bight in the eastern part, here it is concentrated on the more exposed tidal channel system, where significant wave action can be found.

The *main goals* of this study have been to analyse the morphological evolution over the last 20 years on a medium scale and to identify the relevant processes of the tidal channel system of the central Dithmarschen Bight on the basis of observations of the relevant physical processes and properties and the results of a process-based, numerical model.

To achieve these goals, the following objectives have been defined:

- analysis of the morphological evolution over the last 20 years and characterisation of the dominant processes in terms of hydrodynamics, sediment dynamics and geological build-up, on the basis of field measurements;
- combination of validated process models for tidal flow, waves and sediment transport into a morphodynamic model;
- definition of an optimal approach for medium scale morphodynamic modelling as well as representative boundary conditions to drive the model;
- calibration and validation of the optimised morphodynamic model on the basis of simulations over a period of 10 years; and
- application of the model to determine the dominant processes for the observed morphological changes and to predict future morphological evolution.

1.3 Outline of the thesis

In **Chapter 2** the investigated area of the central Dithmarschen Bight is described. The geological build-up and the main characteristics of the hydrodynamics, sedimentology, sediment transport and morphological changes are discussed on the basis of previous investigations and recently carried out measurements.

Chapter 3 describes the process models for simulation of tidal currents, swell and locally generated waves and suspended and bed load sediment transport. The applied modelling approaches and the results of the calibration and validation of each of these (coupled) models is presented.

In **Chapter 4** the applied approach for medium scale morphodynamic modelling is discussed, followed by the description of the coupling of the process models and the model for morphological evolution to build the medium scale morphodynamic model. The extraction of representative conditions in terms of tides, waves and winds is presented.

Chapter 5 presents the calibration and validation of the medium scale morphodynamic model on the basis of periods of 10 years.

Chapter 6 discusses the application of the morphodynamic model to define the dominating processes for selected morphological changes in the study area, in the light of the observed characteristics. It is followed by the presentation of the results of a prediction of the medium scale morphological evolution over a period of 10 years.

In **Chapter 7** the main conclusions of the study are presented, followed by some suggestions for future research.

Chapter 2

The Dithmarschen Bight

2.1 Introduction

The underlying dissertation focuses on the morphodynamic processes of the tidal channel system in the central part of the Dithmarschen Bight, located in the southeastern part of the German Bight between the Elbe estuary in the South and Eider estuary in the North (see Figure 2.1).

The domain of interest within the Dithmarschen Bight consists of the Piep tidal channel system, formed by the channels Norderpiep, Suederpiep and Piep, and the neighbouring tidal flats. The western boundary of the domain lies in depths of 10 – 15 m. In the East the Meldorf Bight can be found, surrounded by the dike-protected coastline.

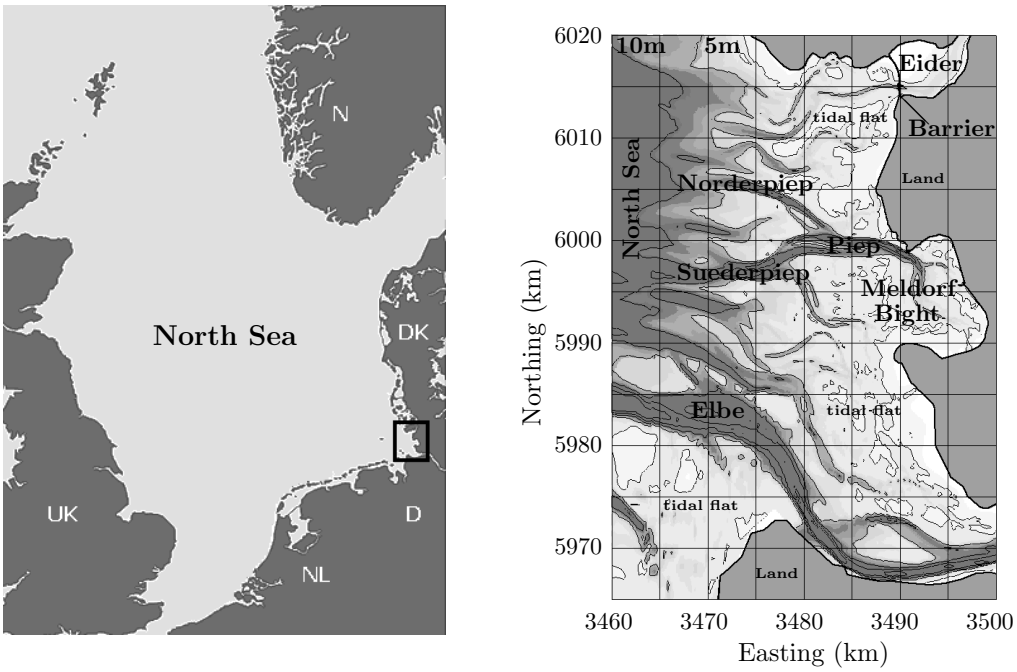

(a) North Sea. (b) Dithmarschen Bight.

Figure 2.1: Location of the Dithmarschen Bight in the southeastern part of the North Sea.

In this Chapter the characteristics of the area of investigation are discussed. In Section 2.2 the geomorphological background and classification are presented. This is followed by a description of the hydrodynamics in Section 2.3. Subsequently, the spatial and temporal variation of the salinity and temperature of the water is described (Section 2.4) and the meteorological conditions are discussed (Section 2.5). The sedimentological aspects are presented in Section 2.6. Finally, in Section 2.7 an analysis of the morphological changes over the last 20 years is presented.

2.2 Geomorphology and classification

2.2.1 Geomorphology

A brief description of the general geomorphology of the study area is presented here. For a detailed description is referred to Asp [2003]. After the last Ice Age the sea level rose relatively quickly from a level some 100 m lower than at present. During this Holocene Transgression the North Sea started to progress in southern direction. The rise continued up to about 5000 B.C. at approximately 1.2 m per 100 years. During this period the sedimentation of the Wadden Sea area was initiated [Behre, 1994].

After 5000 B.C. the Holocene Transgression continued at a lower pace and was subject to fluctuations leading to temporary steady states of the coastline and even some regression. The currently existing morphology of the Dithmarschen Bight started to develop around 1600 B.C., from whereon the sedimentation of the bight could no longer be followed by the sea level rise of the Holocene transgression [Wieland, 1984; Ehlers, 1988]. The coastline was located some 10 km more eastward than at present.

The gradual sedimentation initiated the building of the extensive tidal flat areas. Westward of the former coastline, sedimentation continued, resulting in marshes which in time became main-land [Dittmer, 1960], also due to a sequence of dike constructions. The last dike constructions took place in 1972 (see Figure 2.2), reclaiming 11.5 km^2 in the southeastern part of the Meldorf Bight, and in 1978, reducing the area of the Meldorf Bight by another 22.5 km^2. These land reclamations reduced the area of the Meldorf Bight by 40 %.

Rohde [1977] studied the more recent sea level rise along the German North Sea coast. He estimated the sea level rise at 0.3 m per 100 years between 1600 and 1920 A.D. and a reduced 0.2 m per 100 years up to present. Wieland *et al.* [1984] also found an average rise of circa 2 mm/year for the mean high water level at Buesum over a 30-year period up to 1979. The current trend of global warming can cause an increase in the speed at which the sea level rise takes place in the future. Depending on this speed and the availability of sediment, the tidal flats of the Wadden Sea may increase or decrease on the long-term. Although important for the general long-term evolution of the Wadden Sea, the effects of the sea level rise will not be addressed in this thesis since it is focussed on the medium-term morphodynamics.

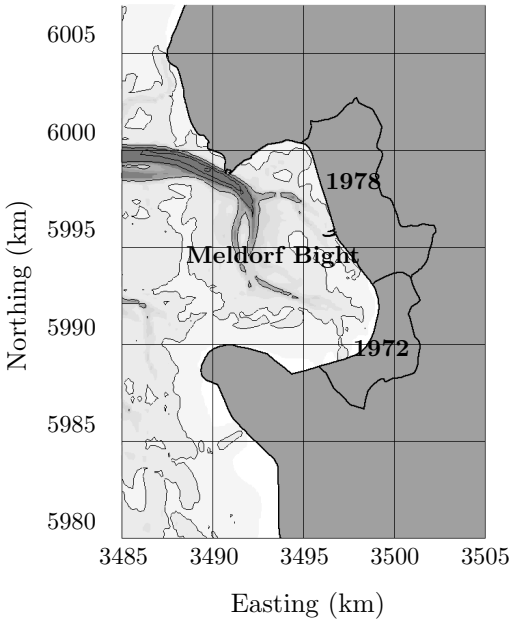

Figure 2.2: Dike constructions in the Meldorf Bight in 1972 and 1978.

2.2.2 Morphological classification

The current state of the tidal flats, with absence of barrier islands, depends strongly on the tidal range [Ehlers, 1988]. For the Dithmarschen Bight the mean tidal range is about 3.2 m. Davies [1964] classifies an area as microtidal for a tidal range between 0 and 2 m, mesotidal for a tidal range between 2 and 4 m and macrotidal for tidal ranges over 4 m. Hence, the Dithmarschen Bight is classified as mesotidal (see also Section 2.3).

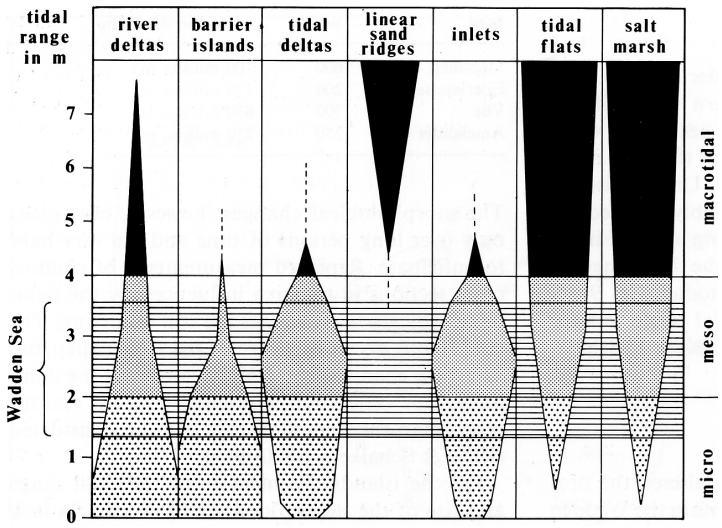

Figure 2.3: Morphological variations depending on the tidal range according to Hayes [1975].

Hayes [1975, 1979] presented a model whereby the morphology of coastal plain shorelines of tide-dominated coasts can be explained as a result of the governing tidal range. The aforementioned categories for the tidal range formed the basis for this model, as shown in Figure 2.3. It shows a preference for areas with a mesotidal range for tidal inlets and tidal deltas. Furthermore, an inverse correlation between tidal range and the occurrence of barrier islands can be seen. With increasing tidal range a tendency towards tidal flats and marshes can be found.

Ehlers [1988] concluded that this classification does not hold for the region of tidal flats in the southeastern German Bight, including the Dithmarschen Bight. In this area tidal flats and sand ridges are dominant, although the tide is classified as mesotidal by Davies [1964] and Hayes [1975]. Therefore, Ehlers [1988] modified the tidal classification of the model, as shown in Figure 2.4. From this adapted model, it follows that the dominant morphological features for the lower macrotidal range are tidal flats, salt marshes and linear tidal ridges, where barrier islands, inlets and tidal deltas may be present on a smaller scale.

The hence indicated presence of these features can be verified from Figure 2.1. Tidal flats are widely spread over the area. Salt marshes can be found at a smaller scale on the lee side of the shoal Trischen [Ehlers, 1988] and in the transition zone between the tidal flats and the main land where no dike construction took place. Barrier islands cannot be found, although the shoal Trischen tends towards supratidal dimensions. Logically, inlets as such are therefore absent. However, the entrance of the channel Suederpiep, enclosed between the flat Tertiussand and the shoal D-Steert, does show similarities with typical Wadden Sea inlets.

A more extensive description of the individual morphological features and their behaviour follows in Section 2.7.

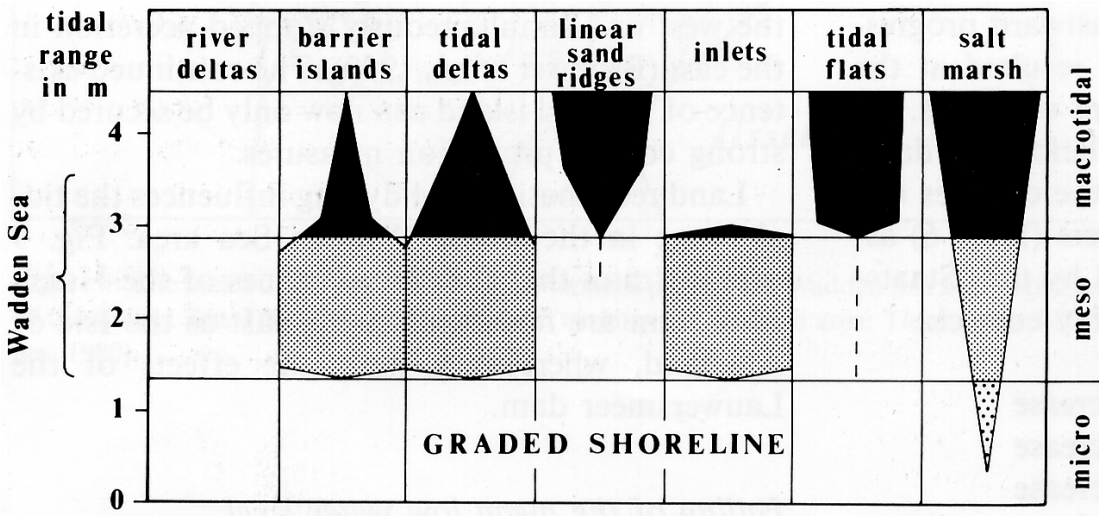

Figure 2.4: Adapted model for dependency of the morphological variations on the tidal range. From [Ehlers, 1988].

2.3 Hydrodynamics

2.3.1 Tidal conditions

The tidal conditions in the Dithmarschen Bight depend on the rotation of the semi-diurnal tidal wave around the amphidromic point in the southeastern North Sea (see Figure 2.5). The tidal wave progresses counter-clockwise along the German Wadden Sea coast, where the tidal range increases from West to East.

Reineck [1978] presented an overview of the main direction and magnitude of the tidal currents, as shown in Figure 2.6, based on the spatial variation of the tidal ranges and the morphology in shallower areas. It gives a general impression of the dominant water movement in the German Bight. It shows that the main current directions due to the tidal wave are either East to West or vice versa in the Dithmarschen Bight. The flow characteristics shown in this figure are rather generalised and do not show the more detailed local variations due to bathymetry-determined flow convergences and divergences.

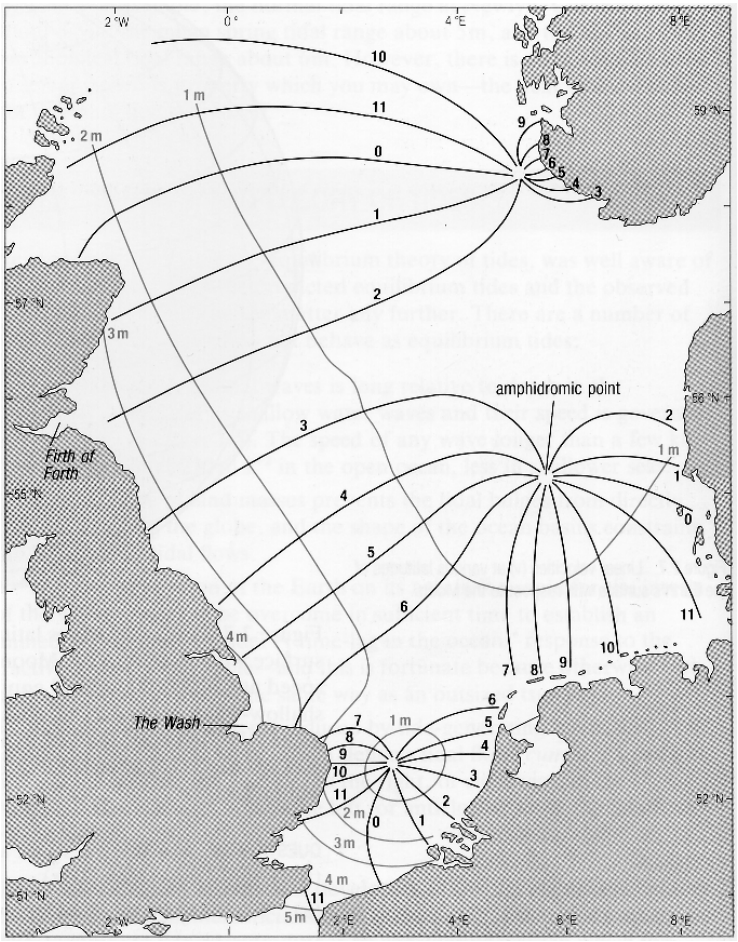

Figure 2.5: Amphidromic systems in the North Sea, with co-tidal and co-range lines in metres [Brown *et al.*, 1989].

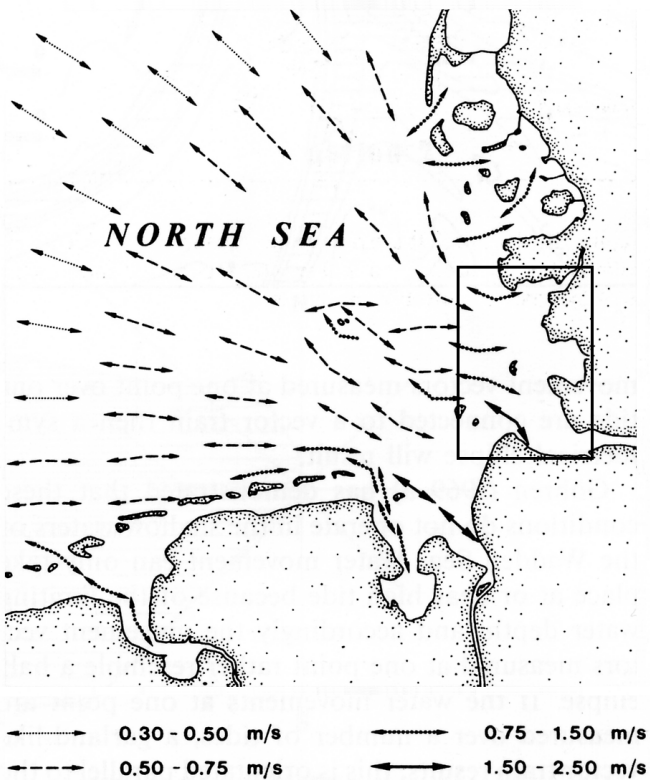

Figure 2.6: Direction and magnitude of the tidal currents in the German Bight. The rectangle indicates the Dithmarschen Bight. Adapted from Ehlers [1988], after Reineck [1978].

The tidal conditions can be differentiated into vertical and horizontal conditions. The *vertical tide* concerns the amplitude, period and shape of the tidal wave, whereas the *horizontal tide* indicates the induced tidal currents.

Vertical tide

The tidal signal is dominated by the semi-diurnal M2 constituent, with a period of approximately 12 hours and 25 minutes. The average tidal range in the central Dithmarschen Bight measures about 3.1 m in the southern and 3.4 m in the northern part. Near Buesum the average high water level reaches circa 1.6 m above mean sea level (MSL) – or *Normal Null (NN)* as it is generally referred to in Germany – and the average low water level about 1.6 m below MSL. The difference between neap and spring tidal range is approximately 0.9 m. The most severe onshore storms can result in a water level set-up of more than 4 m.

Besides by its period and amplitude, the shape of the tidal curve is furthermore defined by its asymmetry. The tidal wave is essentially a shallow-water wave and is thus influenced by the sea bed. This influence becomes stronger with decreasing water depth. The Dithmarschen Bight is a typical *type 1* tidal basin, defined by Dronkers [1986] as a basin where the tidal basins have deep channels – depth much larger than

the tidal amplitude – and/or high tidal flat areas – above MSL. The major channels in the central Dithmarschen Bight are circa 10 to 15m deep and about 50 % of the area dries during low tide. With increasing water level, this type 1-basin has a smaller relative increase of the flow cross-section than the relative increase of storage surface. Based on Dronkers [1986], this leads to a longer slack water period before flood than before ebb, resulting in a shortened flood phase and a lengthened ebb phase. From an analysis of water level measurements in the Norderpiep and Suederpiep, an average flood phase duration of 6 hours and an ebb phase duration of 6 hours and 20 minutes has been found. Thus, the water level measurements confirm the described behaviour.

Horizontal tide

The asymmetry of the tidal curve leads to higher flood velocities and more moderate ebb velocities in the channels, although this also depends on the available cross-section through which the water flows into or out of the domain. The local flow paths are strongly influenced by the presence of the channels and shoals. The mean maximum velocities are about 1.2 to 1.5 m/s in the channels and 0.3 to 0.7 m/s on the tidal flats [Reimers, 1999]. The hydrodynamics may vary significantly due to wind- and wave-effects, especially those related to severe storm events. Extreme velocities may reach up to 2 m/s in tidal channels and up to 1 m/s on the tidal flats.

From 1999 until 2002 a large number of vessel-based ADCP-measurements (Acoustic Doppler Current Profiler) have been carried out within the central Dithmarschen Bight[1]. The measurements were taken along various transects, as shown in Figure 2.7. During a full tidal cycle of approximately 12.5 hours, the vessel sailed constantly from North to South and vice versa along a single transect. Depending on the length of the transect and the vessel speed, this resulted in typically 30 minute intervals between measurements at the same location along a transect.

The transects T1, T2 and T3 formed the basis for the majority of the carried out measurements. Every three months a campaign has been carried out, where different phases of the spring tidal cycle were covered. The results of these measurements resulted in an extensive set of data which yields a high quality insight in the current velocities in the main tidal channels.

Based on the limitations of the vessel and measurement devices, these campaigns have only been carried out during relatively calm weather conditions. Rough conditions, with high waves and stronger currents, would result in failing devices or unacceptably large measurement inaccuracies.

[1]These measurements were carried out within the PROMORPH research project, carried out by the Research and Technology Centre Westcoast, Buesum, Germany. See Zielke *et al.* [2000]

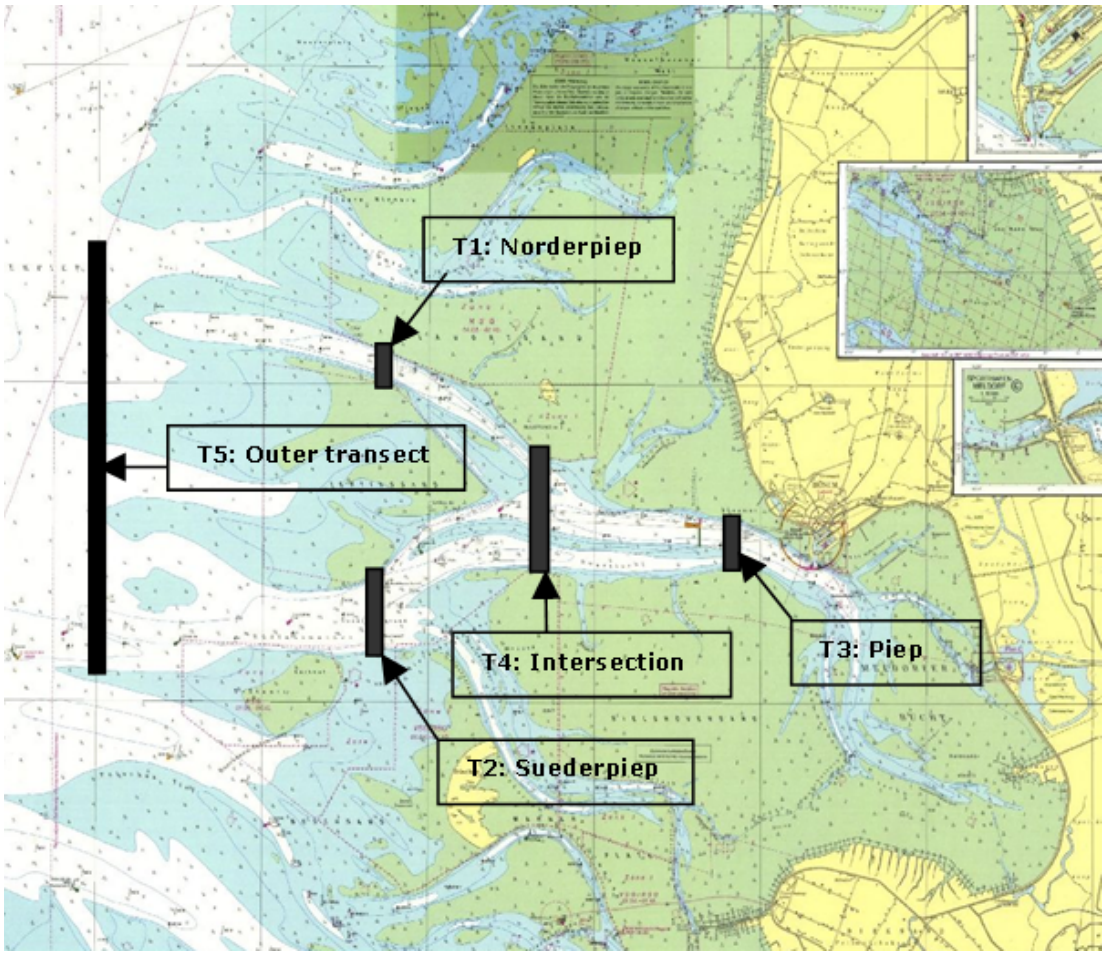

Figure 2.7: Locations of the transects along which vessel-based ADCP-measurements have been made.

2.3.2 Wave conditions

The wave conditions in the area depend on the *swell waves* approaching from the open North Sea as well as on the locally generated *wind waves*. The *distribution of the wave conditions* over the study area depends strongly on the local bathymetry. The local variation of the average wave characteristics is discussed below, followed by descriptions of the observed swell and wind wave conditions.

Distribution of the wave conditions

At the western edge of the domain the water depths range between 10 and 16 m. Swell waves therefore enter the area practically undisturbed by the bathymetry. Within 5 to 10 km from the western edge, water depths reduce to values between 0 and 4 m on the tidal flats, depending on the stage in the tidal cycle. Thus, most incoming swell waves will break in this part of the domain. Only in the tidal channels the waves can penetrate further into the domain, however they may be hindered by the out-flowing

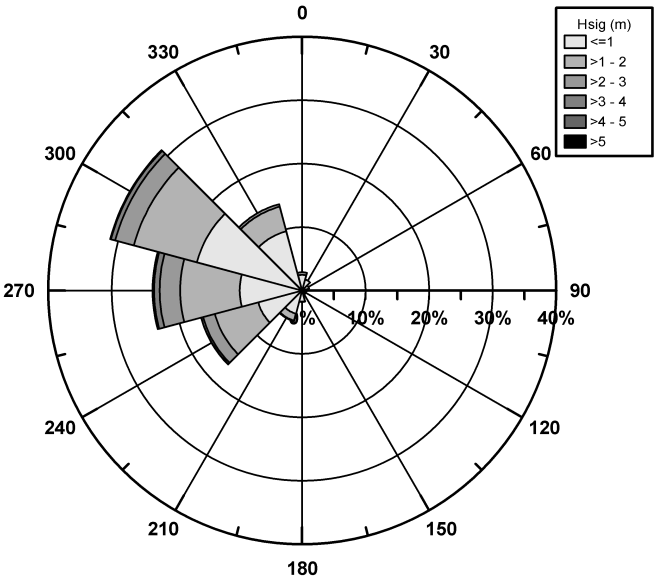

Figure 2.8: Wave rose - probability of occurrence per combination of direction (nautical convention) and significant wave height interval. Based on measurement data at Sylt from 1986 to 1993 from Froehle & Kohlhase [1995].

ebb currents. Generally, only little swell energy remains eastward of the edge of the tidal delta. During storm surges this dissipation area shifts landward but is still located on the same tidal flats. Hence the eastern part of the domain is dominated by locally generated wind waves. This can be seen from wave measurements which show shorter wave periods, typical for wind generated waves.

Swell

The swell depend on the wave energy generated on the remote wind conditions on the North Sea. The amount of energy and characteristics of these waves are related to the fetch length and duration of the wind condition. Furthermore, swell from different source areas may be superimposed. This depends on the time of occurrence of the generating wind events and the travelling time of the waves from the source area to the Dithmarschen Bight.

Due to its location, the Dithmarschen Bight is only subject to swell waves from the sector West-Southwest to North-Northwest. The largest fetch lengths can be found within the sector Northwest to North-Northwest.

Long-term measurements

The only available long-term wave statistics are from the nearby Island of Sylt, some 70 km north of the study area. These statistics are based on data recorded from 1986 to 1993 by a wave buoy about 5 km off the coastline at the centre of the island [BMFT, 1994; Froehle & Kohlhase, 1995].

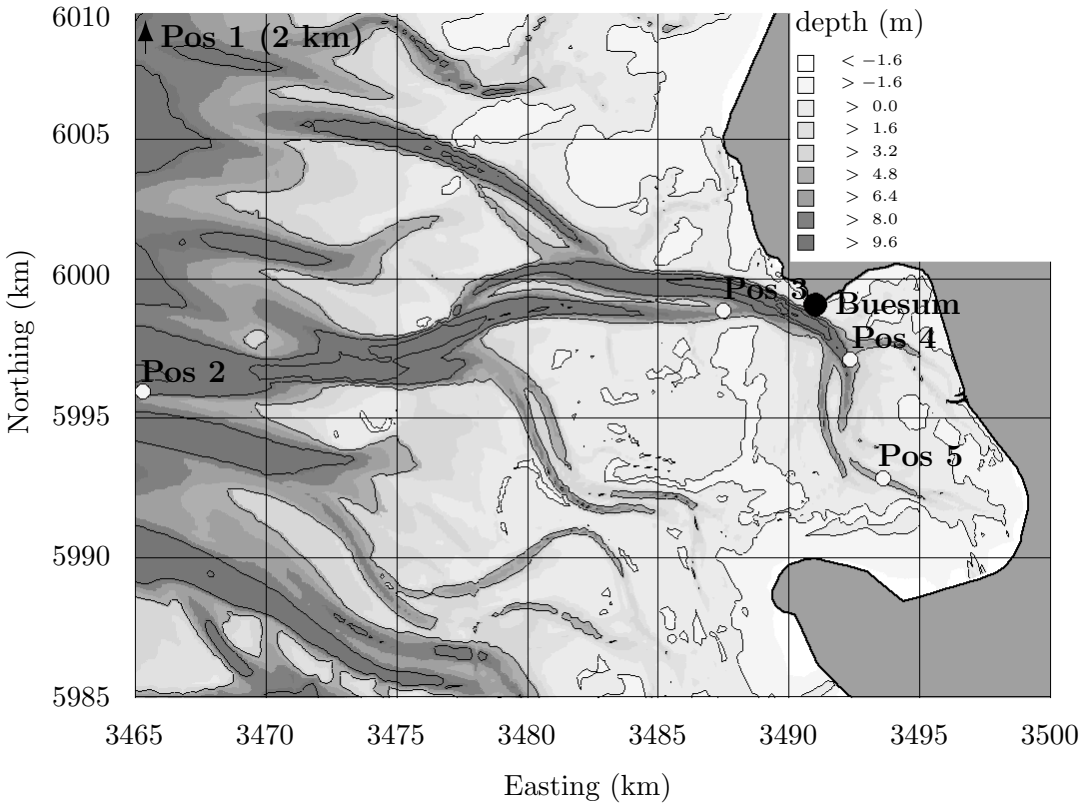

Figure 2.9: Location of the wave buoys from the measurements by [Niemeyer *et al.*, 1995].

The average water depth at the buoy location is about 13 m. The conditions are relatively similar to those at the western edge of the study area since depth-induced wave breaking is negligible at this location. The probability of occurrence per wave height and direction is shown in the wave rose of Figure 2.8.

As can be seen, swell waves up to 2 metres have their highest probabilities at 300°N (West-Northwest). For waves higher than 2 m, the dominating direction shifts towards the West. Some 60 % of the occurring waves came from the sector between 270 and 330°N. The highest waves in this data set have heights of 5.5 m and the average wave height is 1.07 m.

Local short-term measurements

Shorter term measurements[2] have been made during September 1996 with two wave buoys near the western edge of the domain and three in the Meldorf Bight [Niemeyer *et al.*, 1995]. One of the outer buoys was located in the northern part of the Dithmarschen Bight, the approximate locations of the other four are shown in Figure 2.9.

The western buoy, denoted as *Pos 2*, was situated at a water depth of about 14 m. The buoys *Pos 3, Pos 4 and Pos 5* were located near the banks of the main channel and in one of its branches at approximate water depths of respectively 6, 5 and 3 m.

[2]These measurements have been carried out by the Coastal Research Station of the Lower Saxon State Board for Ecology at Norderney (CRS) and the Office of Rural Development in Husum (ALR).

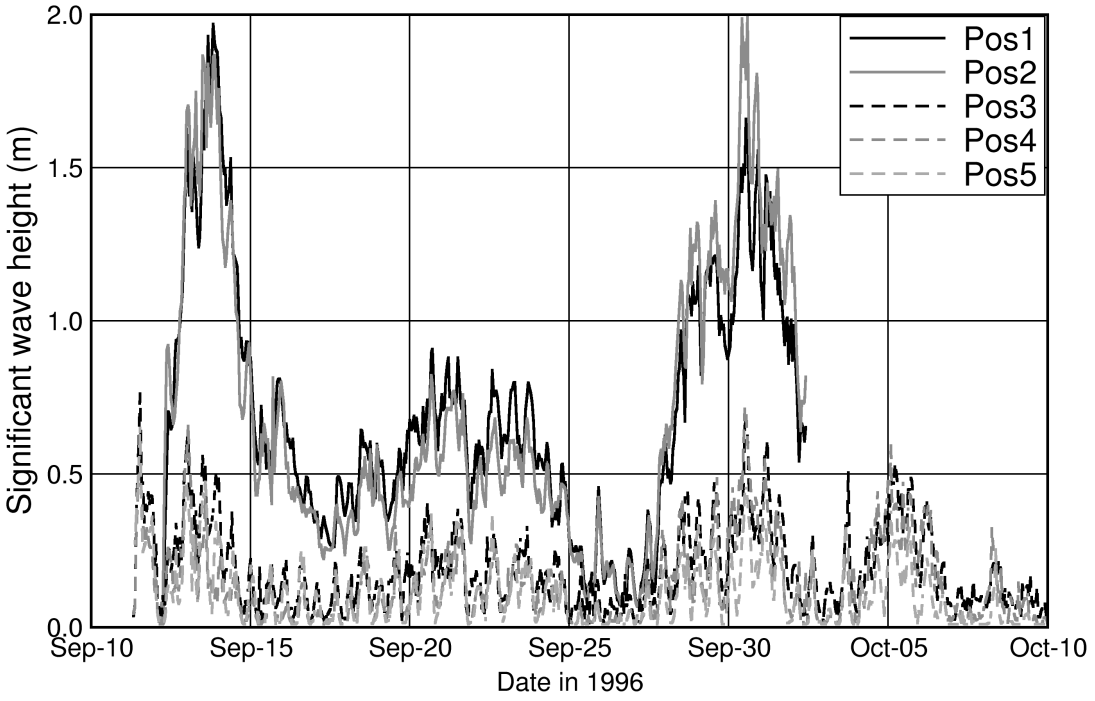

Figure 2.10: Time series of the significant wave heights at the five wave buoys.

An analysis of the recordings yields the time series of the significant wave heights shown in Figure 2.10. The highest significant wave heights occurred at the two western buoys, measuring about 2 m. These peaks coincide with the peaks of the three eastern buoys. However, at these locations the significant wave heights have a maximum value of circa 0.8 m at Pos 3. This is related to the previously discussed wave breaking in the middle of the domain. Wind speeds varied between 0 and 15 m/s, where the highest wind speeds coincided with the largest waves. In the middle of the period the wind speed was about 10 m/s from the East. Therefore, an increase in wave height can be seen at the western positions whereas the wave heights at the eastern points continue to be very small due to the limited fetch.

Wind waves

Due to the sheltering effect of the tidal flats, the wave energy in the eastern part of the domain is dominated by locally generated wind waves. The height of these waves depends on the local wind conditions, fetch length and water depth. The latter are subject to large relative changes due to the tidal range. Where waves can be generated over the entire domain during high water, during low water this can only happen in the channels and submerged flats. Hence, the wind direction and local bathymetry are the main constraining factors for local wave generation. This is confirmed by the measurements shown in Figure 2.10.

Observations in the eastern part of the domain show wave heights that are generally between 0.1 and 0.3 m, with some peaks up to 0.5 m during storm events. In the channels wave heights up to 1 m can be reached.

2.4 Salinity and water temperature

Large vertical variations of the salinity and temperature of the water may cause stratification. The typical values for the Wadden Sea and results from measurements in the central Dithmarschen Bight are discussed below.

2.4.1 Salinity

The salinity in the Wadden Sea is somewhat less than the typical salinity of the North Sea, measuring circa 35 ‰. Salinity variations over the year can be found due to the season-induced variations in the river discharges. The highest values can be measured around October when the fresh water input of the rivers is minimal. In spring the lowest salinity values are found. Conductivity measurements[3] at several locations in the study area showed values between 20 and 21.5 ‰ in spring and between 27 and 29.5 ‰ in autumn. The vertical variations were insignificant. Based on the high mixing due to the tides Ehlers [1988] concluded that significant salinity-induced stratification is not found in the Wadden Sea, when not directly adjacent to a river mouth.

2.4.2 Temperature

Due to the relatively small water depths, the temperature of the water fluctuates more strongly in the tidal flat areas than on the open North Sea. The water temperature varies between values close to 0°C up to 18°C, depending on the season. The tides and wave action cause a strong mixing over the water column. Therefore, the variations of temperature over the depth is rather small, preventing significant stratification.

2.5 Meteorology

The hydrodynamics in the Dithmarschen Bight depend also strongly on the wind conditions on the North Sea as well as in the area itself. The meteorological conditions on the North Sea may cause storm surges of up to 5 m, as recorded in 1967 in Buesum during a severe storm (see Figure 2.9 for its location). Furthermore, distant storms may cause strong swell wave action. Local extreme wind conditions do not cause such clearly visible effects but they do induce relatively strong wind-induced currents and locally generated waves in the shallow areas, which play an important role in the morphodynamics of the flats and channels.

[3]This measurement campaign was part of the PROMORPH research project, carried out by the Research and Technology Centre Westcoast, Buesum, Germany. See Zielke *et al.* [2000]

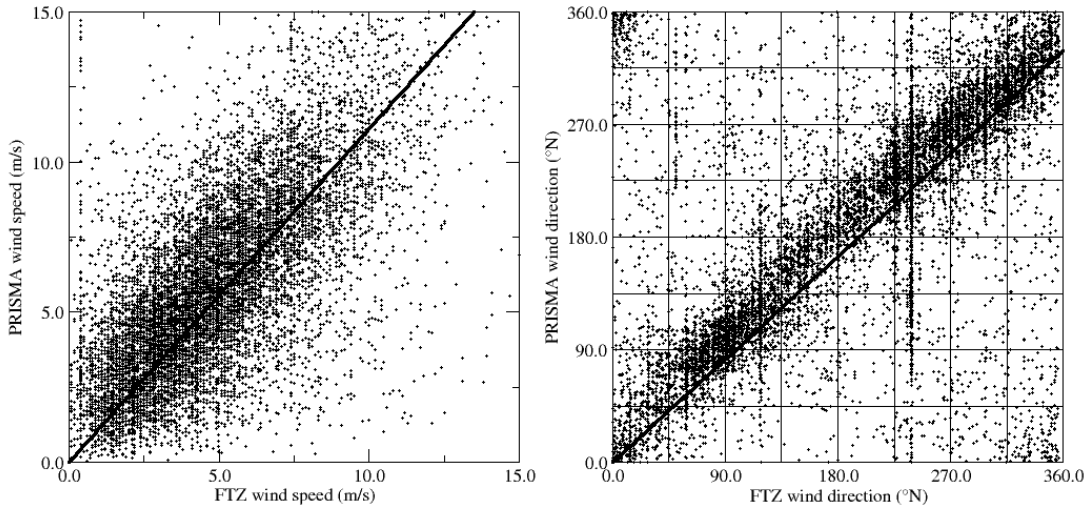

Figure 2.11: Comparison of wind speed (m/s) and direction (°N) from the measurement station at Buesum (Research and Technology Centre Westcoast) and the PRISMA wind model. Based on measurements between March, 1991 and December, 1998.

Luthardt [1987] describes the PRISMA[4] synoptic wind model which generates wind and pressure fields that cover the entire North Sea. The model assimilates wind measurement data from numerous wind measurement stations along the North Sea coastline as well as observations from other sources, such as oil platforms. The generated wind speed data are stored as mean velocities over 10 minutes at 3-hourly intervals.

An advantage of the data generated by the PRISMA model over direct wind measurement data is the full coverage of the investigation area. This is required for a proper representation in the hydrodynamic model, as described in Chapter 3. Furthermore, a continuous data set is available for a period of 12 years, from 1989 to 2000. Therefore, the PRISMA data served as the basis for the evaluation of the wind climate and for providing meteorological information for the hydrodynamic modelling within this study. The wind model results have been compared to wind measurements at the measurement station in Buesum for a period of eight years, as shown in Figure 2.11.

The PRISMA model grid has approximately a 42 km grid spacing. This caused the selected output location from the PRISMA model to be located some 20 km westward (offshore) from Buesum. As a result, the wind velocities from the PRISMA model are slightly (up to 10 %) higher than those measured at the Research and Technology Centre Westcoast in Buesum (FTZ), as indicated by the linear trend line. Another reason for the higher velocities from the PRISMA model is that for wind from the sector West to North the measured wind speeds are up to 6 m/s lower do to the upwind buildings and vegetation (pers. comm. Mr. Vanselow, FTZ). The plot of the wind direction shows a good correlation of both data sets.

[4]The PRISMA model has been developed at the Max Planck Institute of Meteorology of the University of Hamburg.

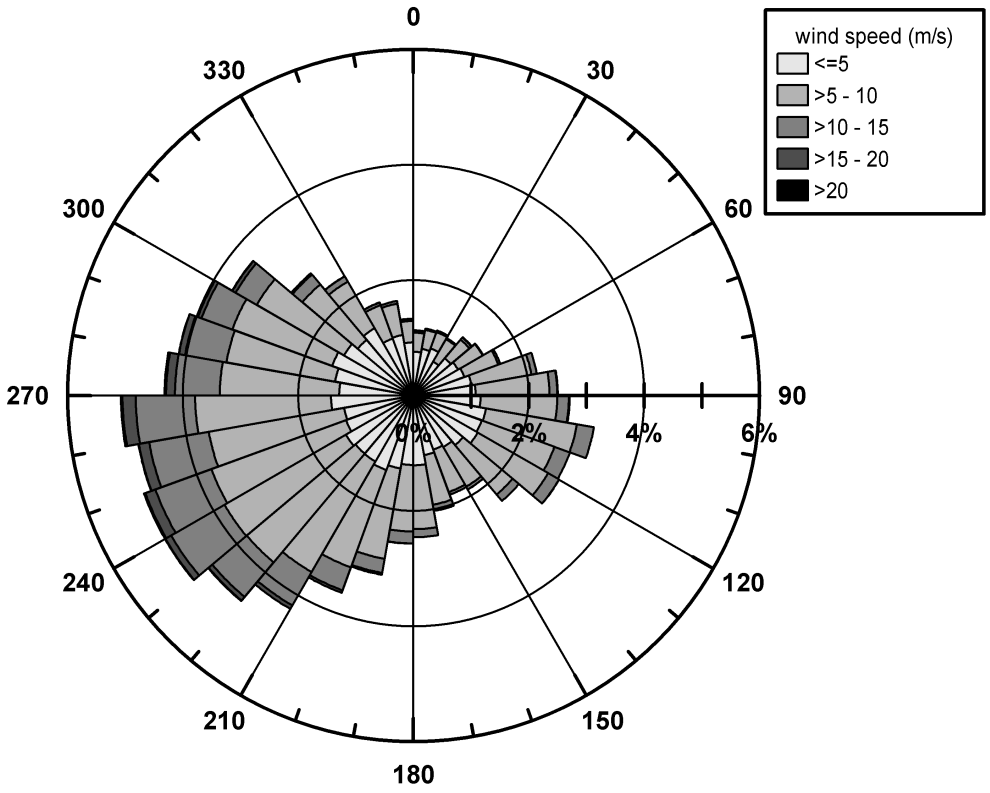

Figure 2.12: Wind rose for the Dithmarschen Bight - probability of occurrence per combination of wind direction (nautical convention) and wind speed interval. Based on data from 1989 to 2000, from the PRISMA data assimilation model by [Luthardt, 1987]

Based on the synoptic data, the wind climate in the Dithmarschen Bight has been analysed for the period from 1989 to 2000. The results are summarised in the wind rose of Figure 2.12, showing the probability of occurrence for combinations of wind speed and direction.

The wind rose shows a clear dominance of winds from the sector Southwest-West. This dominance holds for all of the wind velocity intervals. Circa 40 % of the time the wind direction was between 200 and 280°N.

The different dominant direction compared to the wave rose in Figure 2.8 is mainly related to the varying fetch lengths for the various directions. The differing measurement locations for the underlying data are considered to have a limited influence.

2.6 Sedimentology and bed characteristics

The domain of interest has been subject of a number of surveys and investigations over the last 50 years with respect to its sedimentological and geological characteristics. These concern on the one hand the build-up of the *bed sediments* and on the other hand the *suspended sediments*. These studies and their findings are presented hereafter.

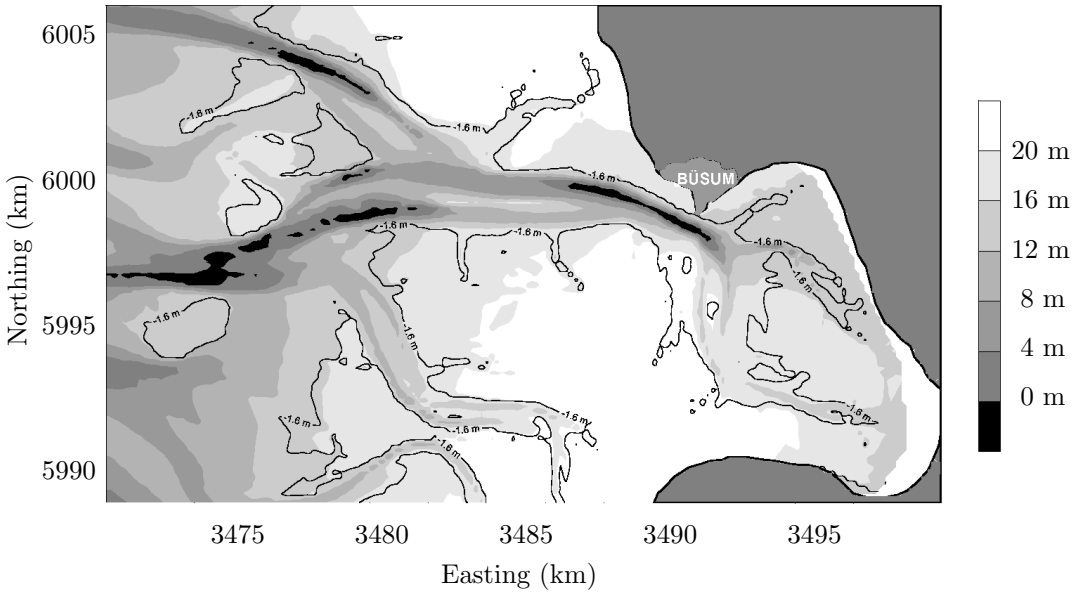

Figure 2.13: Thickness of the non-cohesive sediment layer above the *Dithmarscher Klei* clay layer [Asp, 2003].

Bed sediments

The build-up of the sea bed can be differentiated into the *vertical sediment stratification of the bed* and the *horizontal surface sediment distribution.*

Dittmer [1938] studied the vertical geological structure of the sea bottom in the Dithmarschen Bight. Based on core analysis, he showed the sea bottom build-up from bottom to top starting with the presence of the pleistocene sands up to a level of 25 to 30 m below mean sea level, covered by a layer consisting of cohesive silty clay deposits. The clay layer is known as the *Dithmarscher Klei* and can reach a thickness of more than 10 m. The clay layer again is covered by non-cohesive sandy sediments up to the bottom surface. This sandy layer can be as thick as 20 m at locations on the tidal flats and is absent in some of the deepest sections of the tidal channels. At these locations, shown in Figure 2.13, the consolidated cohesive sediments hinder further erosion and therefore form a restriction in the morphological development of these channels in the vertical [Asp, 2003]. Apart from this clay layer, the pleistocene surface forms a restriction for further erosion due to its coarse sediments [Zeiler *et al.*, 2000; Asp, 2003]. Due to its deep location, however, this does not has a direct influence on the morphology in the Dithmarschen Bight. At some locations, the sandy layer is interrupted by smaller layers of consolidated mud and clay, e.g. at a depth of circa 10 m at the flat Blauortsand and at about 8 m depth at the mouth of the channel Bielshoevener Loch [Asp, 2003]. Thus, the geological structure forms the basis for the composition and spatial distribution of the outcropping sediments.

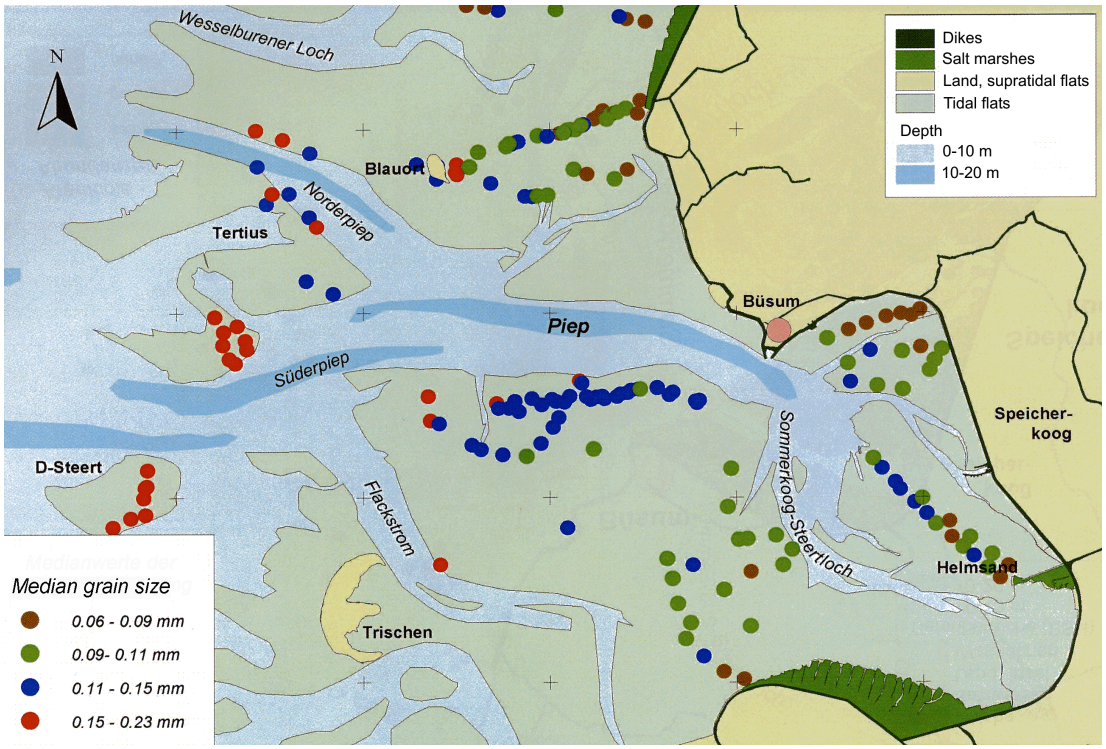

Figure 2.14: Location and results of the bed sediment measurements during 1999 and 2000. Adapted after Reimers [2003].

The horizontal sediment distribution in the Meldorf Bight has been the topic of several recent studies. Figge [1981] created a map of the sediment distribution for the German Bight, showing that more than 50 % of the sand fraction has a diameter between 63 and 250 μm and up to 40 % between 250 and 500 μm in the central Dithmarschen Bight. The sand fraction varies between 20 and 90 % and the silt and clay fraction may reach up to 50 %. The large scale of the study area prevented the representation of local variations in the Dithmarschen Bight.

Besides the large-scale study by Figge [1981], several surveys concerning small-scale areas within the central Dithmarschen Bight have been carried out, see for example Gast [1980]; Gast *et al.* [1984]; Runte [1994]; Kesper [1992]; Reimers [1999]. The most recent studies were carried out by Reimers [2003] for the tidal flats and by Vela Diez [2001] for the tidal channels.

Reimers carried out an extensive measurement campaign[5] concerning the sediments on the tidal flats in the central Dithmarschen Bight. The locations of the measurements and the estimated median grain sizes (d_{50}) are shown in Figure 2.14.

Reimers found median grain sizes of 150 to 230 μm (fine sand) on the southwestern part of Tertiussand and the shoal D-Steert. On the northeastern part of Tertiussand, the western part of Blauortsand and on the northern part of Bielshoevensand grain

[5]These measurements were carried out within the SEDIMORV project by the GKSS Research Centre in Geesthacht, Germany

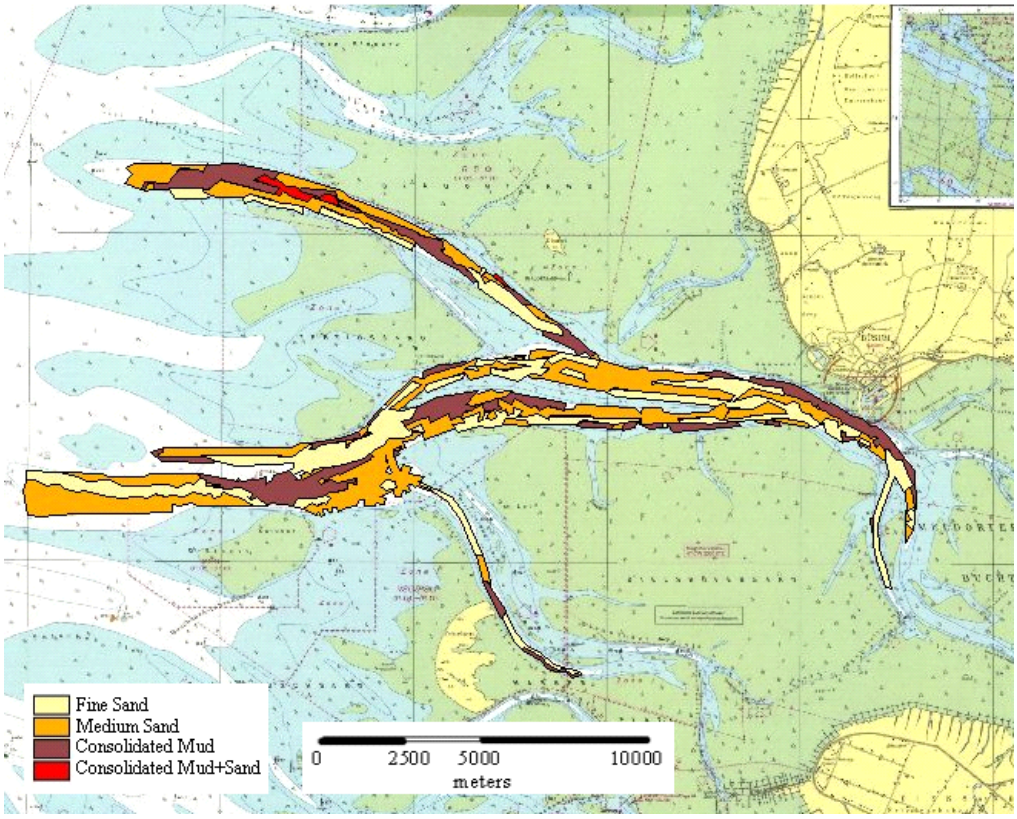

Figure 2.15: Distribution of sediment types, after Vela Diez [2001].

sizes between 110 and 150 μm were found. The eastern part of Blauortsand and the tidal flats in the Meldorf Bight contained mainly very fine sand with median grain sizes between 90 and 110 μm. Hence, a gradual decrease of the grain sizes from West to East has been found on the tidal flats. This agrees with the general principles of sediment re-distribution in sandy coastal areas where the grain sizes decrease from the more exposed to the more sheltered locations. Next to the variation in the median grain sizes, a gradual increase of the silt fraction (grain size smaller than 63 μm) from 10 % in the western and middle part of the domain to over 50 % in the eastern part has been found.

Vela Diez [2001] analysed the bed sediments in the tidal channels Norderpiep, Suederpiep and Piep on the basis of side-scan sonar measurements and grab samples during 1999 and 2000. The analysis of the side-scan sonar results was calibrated with the results of the grab samples, resulting in a comprehensive map of the grain size distribution of the bed sediments, as shown in Figure 2.15. It shows that the channel beds consist mainly of medium to fine sand, with stretches of consolidated mud. The median grain sizes of the bed sediment samples vary from 80 to 230 μm, where two third are below 100 μm. A strong correlation between the magnitude of the sand fraction and the median grain size was found, i.e. for median grain sizes over 100 μm the sand fraction was above 95 %.

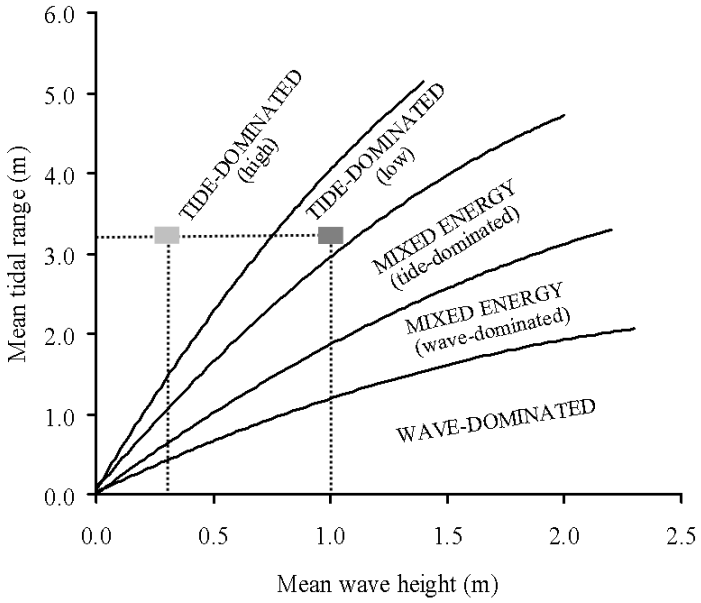

Figure 2.16: Classification of tidal areas, differentiated on the mean tidal range and mean wave height. The western (dark grey) and eastern part (light grey) of the Dithmarschen Bight are indicated by the two rectangles. Adapted after Hayes [1979].

Suspended sediments

Measurements of suspended particle matter have been carried out along several cross-sections of the channels Norderpiep, Suederpiep and Piep, as presented in Poerbandono & Mayerle [2003] and Poerbandono [2003]. From the analysis of these samples the particle size of the suspended sediment was found to be between 6 and 86 μm. About 60 % of the samples had a median value between 10 and 25 μm. No clear pattern could be determined with respect to the spatial and temporal variation of the sediment sizes.

The maximum depth-averaged suspended sediment concentrations along the cross-sections in Figure 2.7 measured 0.27 kg/m^3 at T1, 0.52 kg/m^3 at T2 and 0.39 kg/m^3 at T3 [Poerbandono, 2003]. Generally a fairly uniform vertical concentration profile was found, which Poerbandono [2003] concluded to be related to the small grain sizes and the related small settling velocities.

2.7 Morphology and morphodynamics

As mentioned in Section 2.3, the tidal range in the central Dithmarschen Bight measures approximately 3.2 m and the mean wave height approximately 1.0 m, based on the long-term wave data set from the nearby island of Sylt. Applying the classification of Hayes [1979] as shown in Figure 2.16, the western part of the Dithmarschen Bight may be characterised as mildly tide-dominated, and the sheltered, eastern part as highly tide-dominated.

Based on yearly bathymetric measurements during the period from 1977 through 2000[6], the various morphological features have been identified and their recent morphodynamics have been calculated and analysed. The measurements from the BSH are generally limited to the main channels and the tidal flat Tertiussand. The ALR measurements provide data for the entire Dithmarschen Bight but are limited to one single data set, which includes data from 1986 to 1993.

A description of the morphology, location of the individual features and recent morphodynamics for the whole study area follows in the next Paragraph. The comparison of the measured bathymetries leads to a general overview of the dynamics of the domain. Subsequently, the individual features and their changes are discussed on the basis of a number of cross-sectional bathymetric profiles and volume analyses.

It should be noted that the coverage of the bathymetric data varies strongly per year. Furthermore, data is usually sparse on the tidal flats, since these domains cannot be measured by ship-based echo-soundings and hence measurement campaigns are more costly here. Van Rijn *et al.* [2002a] note the fact that bathymetric measurements may contain errors due to a number of factors, e.g. effects of waves on survey accuracy, ship characteristics and the accuracy of the positioning in the horizontal plane. Also, the water level at the time of the measurement has to be estimated to determine the depth with respect to the reference level, e.g. MSL. Westlake [1996] reported errors up to 0.25 m for water depths below 6 m and up to 0.1 m for larger depths, at the Dutch North Sea coast. For the Dithmarschen Bight, considering the relatively difficult measuring conditions, e.g. strong and varying currents, as well as the complex bathymetry, these inaccuracies may be higher. The quality of the estimation of the instantaneous water level depends on the distance from one or more water level gauges and the local variation of the water level. These local variations are larger in areas with a complex bathymetry and large tidal range, such as the study area. The institutes that carried out the bathymetric surveys, the Federal Maritime and Hydrographic Agency of Germany (BSH) and the Office of Rural Areas (ALR), indicates an overall inaccuracy of 0.1 to 0.2 m [pers. comm. Mr. Klueger (BSH) and Mr. Christiansen (ALR)] for more recent measurements. Older measurements, based on less accurate devices and methods, may have larger discrepancies.

For comparison of bathymetric data, an interpolation needs to be carried out. This has been carried on the basis of the applied model grid (see Chapter 4), with a typical grid spacing of 100 to 180 m in area of analysis. This spacing agrees with the spacing of the bathymetric measurements, which varies between 50 and 200 m with typical values of 150 m. The interpolation error was found to be approximately 0.3 m, depending on the local spacing of the grid as well as of the measured data.

[6]The bathymetric measurements have been carried out by the Federal Maritime and Hydrographic Agency of Germany in Hamburg (BSH) and the Office for Rural Areas in Husum (ALR).

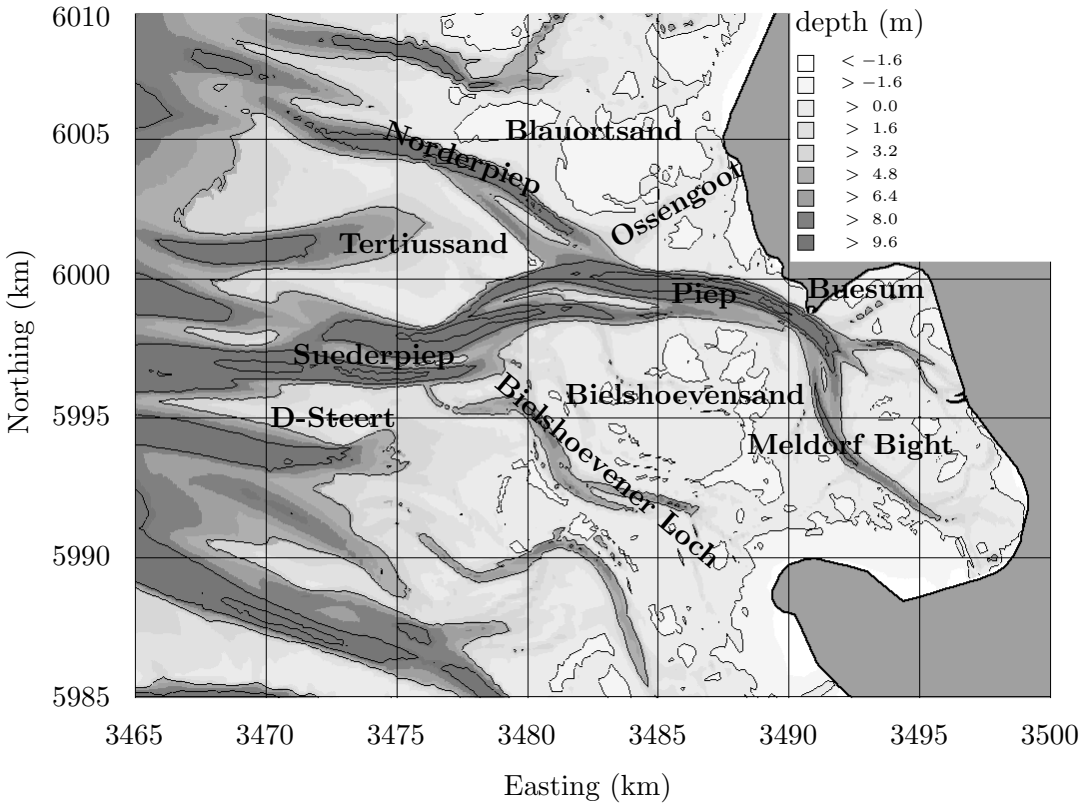

Figure 2.17: Location of the morphological features in the central Dithmarschen Bight (bathymetry from 1977).

When considering bathymetric differences over a longer period of time, the relative influence of the inaccuracies on the correctness of the interpretation will be reduced. In this study a period of 20 years is considered, which is sufficiently long for a sound interpretation.

2.7.1 The central Dithmarschen Bight

The area contains several primary and secondary channels, divided by a number of shoals and tidal flats. These are shown in Figure 2.17.

The channel system consists of the main channel *Piep*. The Piep bifurcates in western direction into the *Norderpiep* and *Suederpiep* channels, which connect the system to the North Sea. Towards the East, the Piep bends in southern direction near *Buesum*, after which it spreads over the *Meldorf Bight* through several smaller channels. From the Suederpiep the smaller channel *Bielshoevener Loch* branches in southeastern direction. Between the Norderpiep and Suederpiep, the tidal flat *Tertiussand* can be found. The flat *Blauortsand*, located north of the Norderpiep and Piep, forms the northern limit of the study area. The shallow channel *Ossengoot*, is located just northeast of the Piep bifurcation. In the middle of the domain is the flat *Bielshoevensand*, which marks the southern limit of the investigated area, together with the shoal *D-Steert*.

Recent morphological changes

The yearly bathymetric data have been interpolated onto the model grid to enable intercomparison and the calculation of the sedimentation and erosion patterns.

The interpolated bathymetric measurements are shown in Figure 2.18 for the years 1977 and 1999. The currently existing coastline has been included, since bathymetric data for the diked areas (see Figure 2.2) are scarce for 1977 and naturally not available for 1999. The 1999-bathymetry has been preferred over the bathymetric data for 2000 because of the better area coverage. For these years, the bathymetric data coverage was relatively high and the channels as well as the flat Tertiussand were covered to a large extent. Where no data were available, those of preceding and following years have been used. An overview of the sedimentation and erosion between 1977 and 1999 is shown in Figure 2.19(a).

From Figures 2.18 and 2.19(a) can be clearly seen that the morphology is rather dynamic. The migrations and evolution of the morphological features is schematically shown in Figure 2.19(b). For instance the western edge of the flat Tertiussand is retreating and (part of) the eroded material is transported onto its eastern part. It shows furthermore an expansion in southern direction, forcing the Suederpiep southward. Since the shoal D-Steert prevents a southward migration, the Suederpiep became narrower and deeper. Other significant changes are the sedimentation of Bielshoevensand, the migration of the submerged bar near the Piep bifurcation and the clockwise rotation of the North-South oriented part of the Piep in the Meldorf Bight. These and other morphological changes are discussed in more detail in the following Paragraphs.

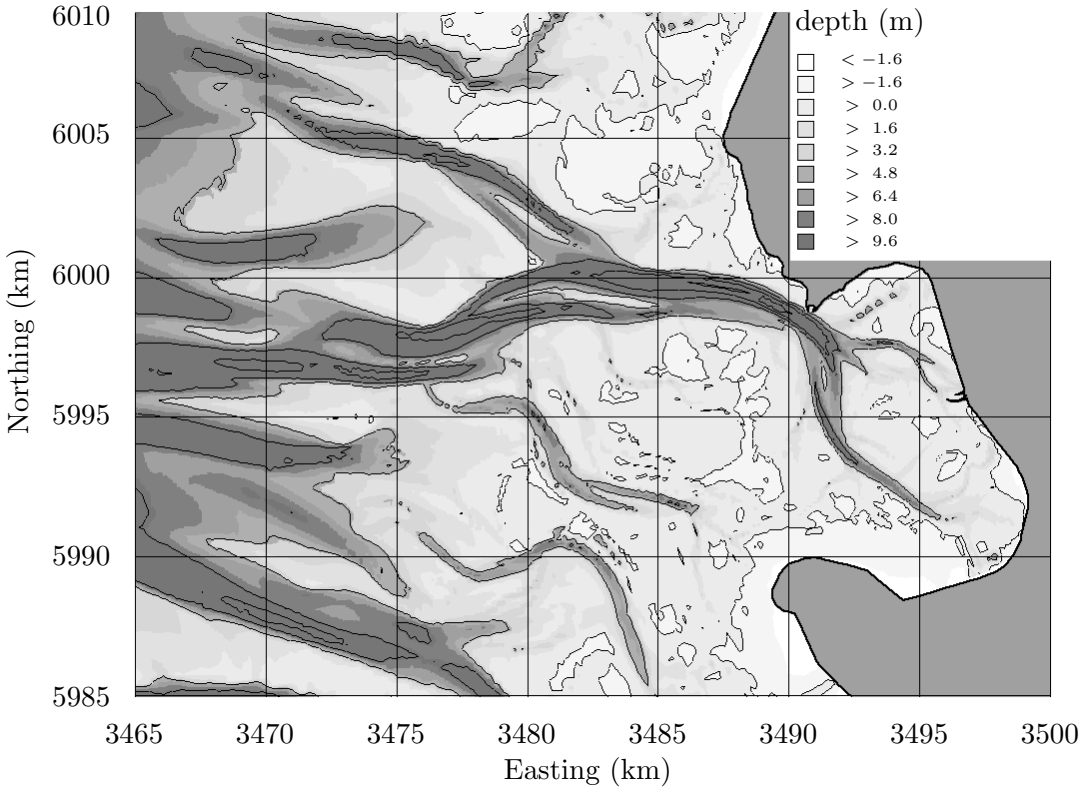

(a) 1977

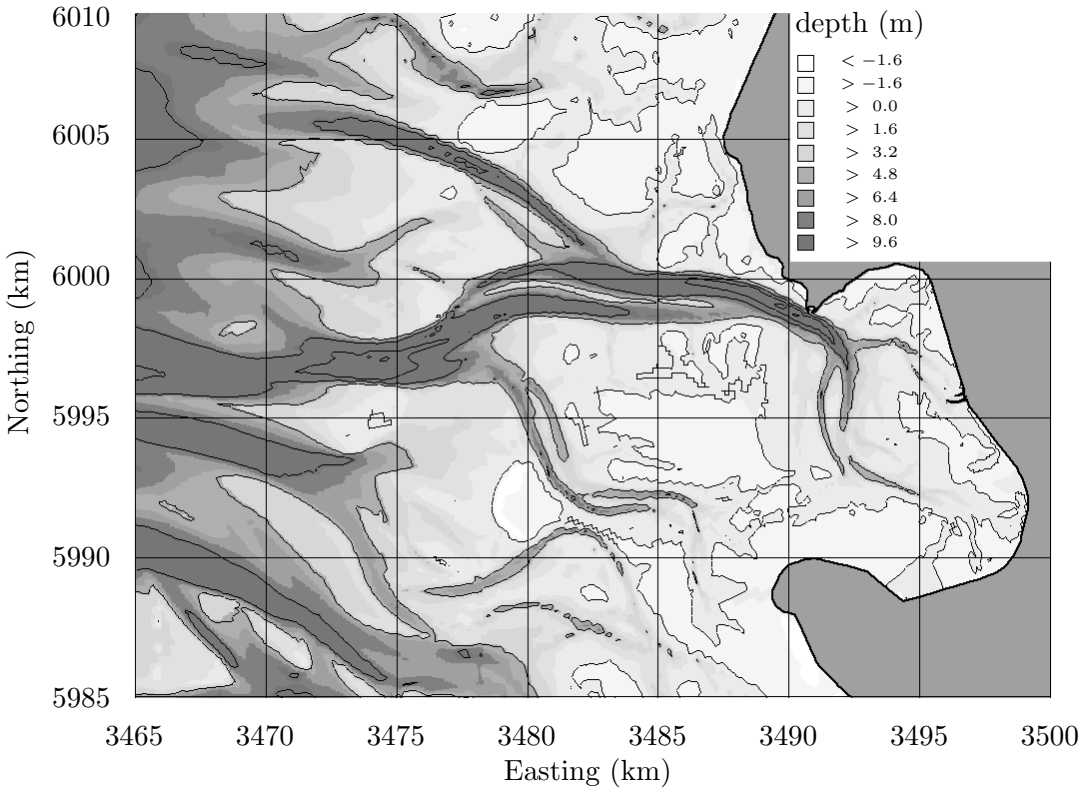

(b) 1999

Figure 2.18: Measured bathymetry in the central Dithmarschen Bight.

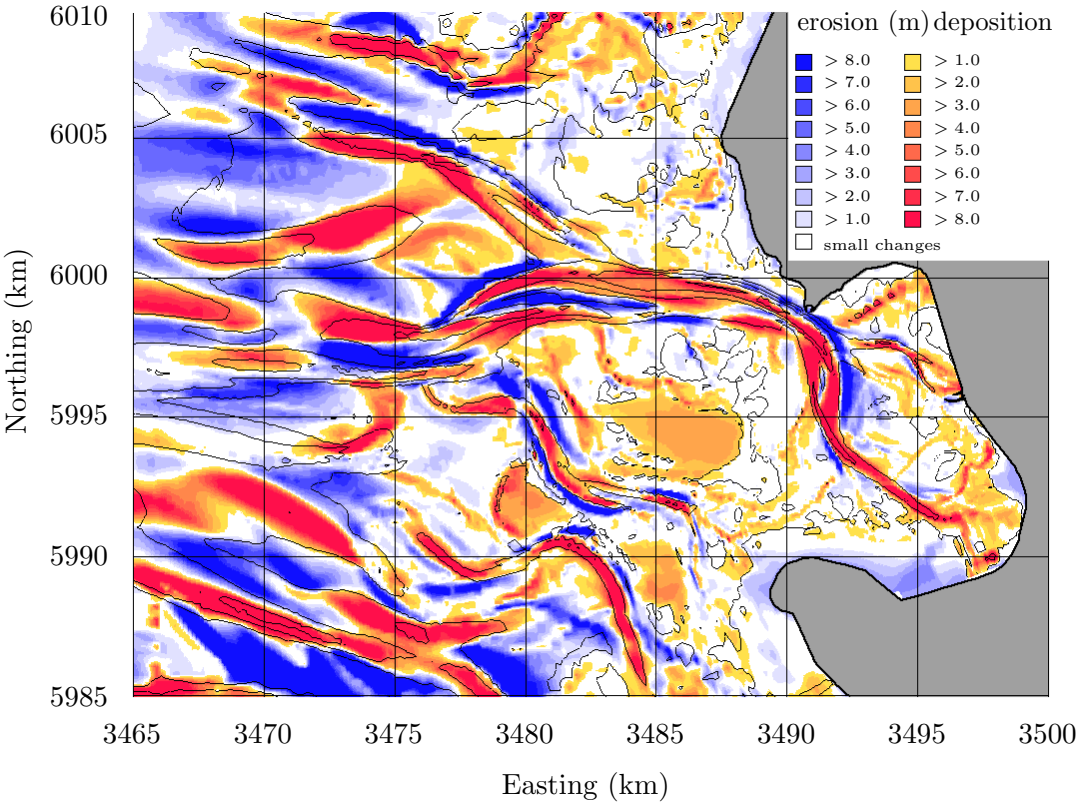

(a) Sedimentation and erosion between 1977 and 1999 (isolines from 1977).

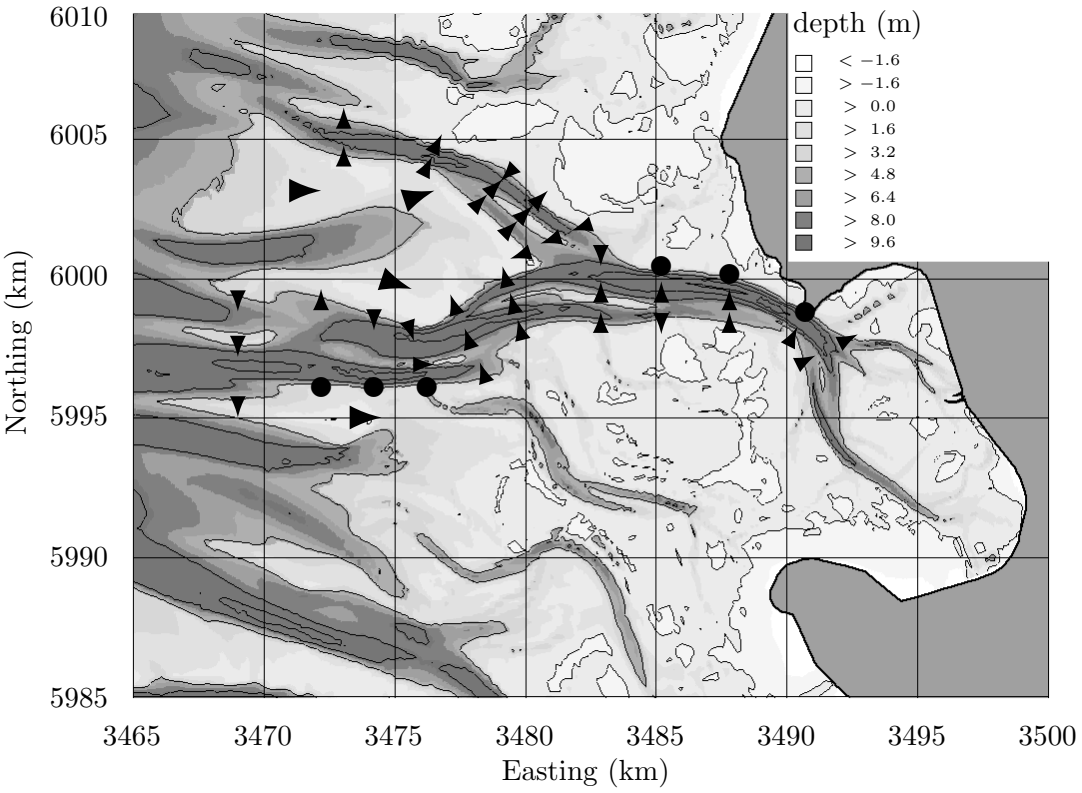

(b) Migration (indicated by the arrowheads) and stability (circles) (isolines from 1977).

Figure 2.19: Morphodynamics in the central Dithmarschen Bight.

2.7.2 Individual morphological features and their behaviour

In the following, the current state of each of these units is described, followed by their morphodynamic behaviour over the last 20 years. The characterisation is based on the analysis of a number of cross-sectional profiles, as shown in Figure 2.20, as well as on the comparison of the bathymetries of 1977 and 1999, shown in Figure 2.18. The profiles are limited to the years 1977, 1983, 1990, 1996 and 1999, to ensure easily readable plots. These data sets have 3 to 7-year intervals and a relatively high coverage of the channels. Where data for 1999 were not providing a good coverage they were completed with the measurements from 2000.

Furthermore, for several sub-domains a volume analysis has been carried out. Due to the coverage of the measurements, this could not be done for the entire domain and has therefore been limited to the main channels and the tidal flat Tertiussand. The locations of the analysed sub-domains are shown in Figure 2.21. The volume changes have been indexed to the volumes of the starting bathymetry for 1977 as follows:

$$V_{rel,i} = \frac{V_i}{V_{1977}} * 100\ \% \tag{2.1}$$

with:

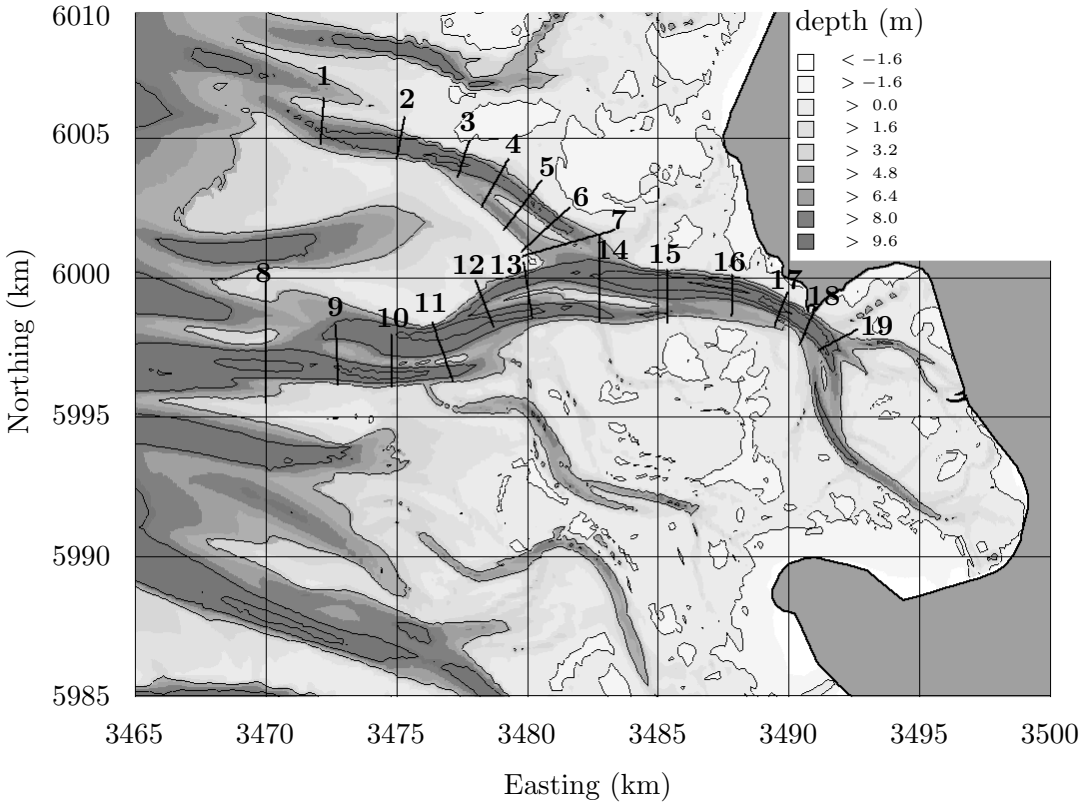

Figure 2.20: Location of the channel cross-sections for the channel profile analysis. The cross-sections have been defined approximately equidistantly along the main channels (bathymetry from 1977).

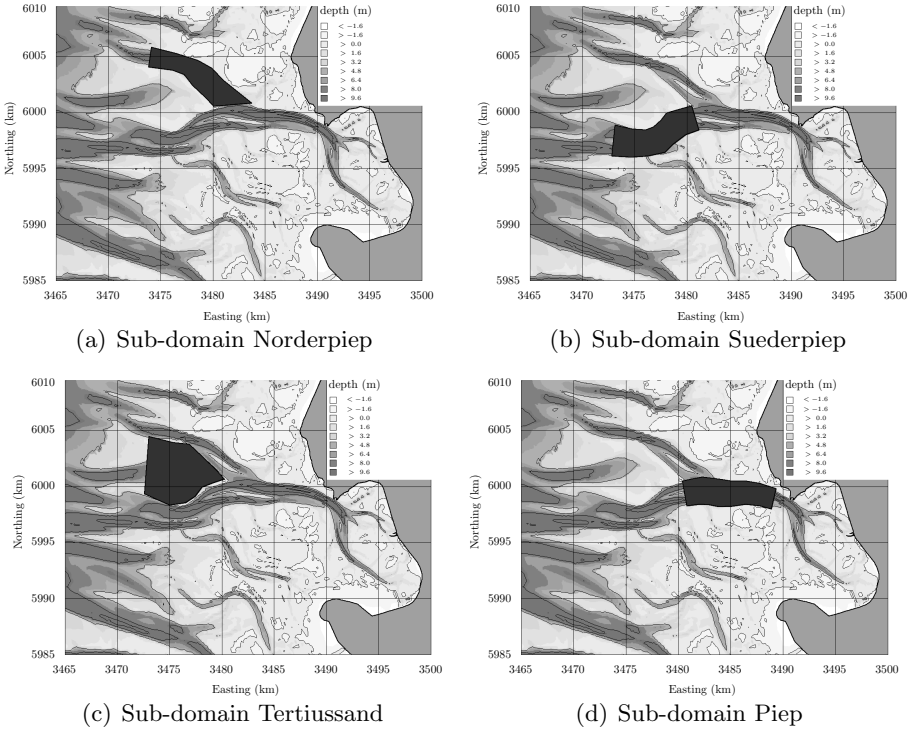

(a) Sub-domain Norderpiep (b) Sub-domain Suederpiep

(c) Sub-domain Tertiussand (d) Sub-domain Piep

Figure 2.21: Location of the considered sub-domains in the volume analysis.

$V_{rel,i}$	relative wet volume below MSL of a sub-domain in year i
V_{1977}	wet volume below MSL of a sub-domain in 1977
V_i	wet volume below MSL of a sub-domain in year i

The tidal channel Piep

The main channel in the domain is the channel Piep. This channel accounts for the major part of the tidal flow between the Meldorf Bight and the open sea. The Piep can be divided into three sections. The most western section starts at the junction of the channels Norderpiep and Suederpiep. This channel section contains two subchannels with depths of 12 to 14 m, divided by a submerged bar with a depth of approximately 2 m. The second channel section, near Buesum, consists of a single channel with depths up to 22 m which bend sharply towards the South. The third section starts just southeast of Buesum and continues further towards the South. In this section the Piep consists of two sub-channels with gradually decreasing depths. In the latter two sections smaller gullies branch towards the shallower parts of the Meldorf Bight.

Morphodynamics of the Piep

The submerged bar has extended in eastward direction which caused a more distinctive separation of the two sub-channels just westward of Buesum. The southeastern part of the Piep has reduced in size and length.

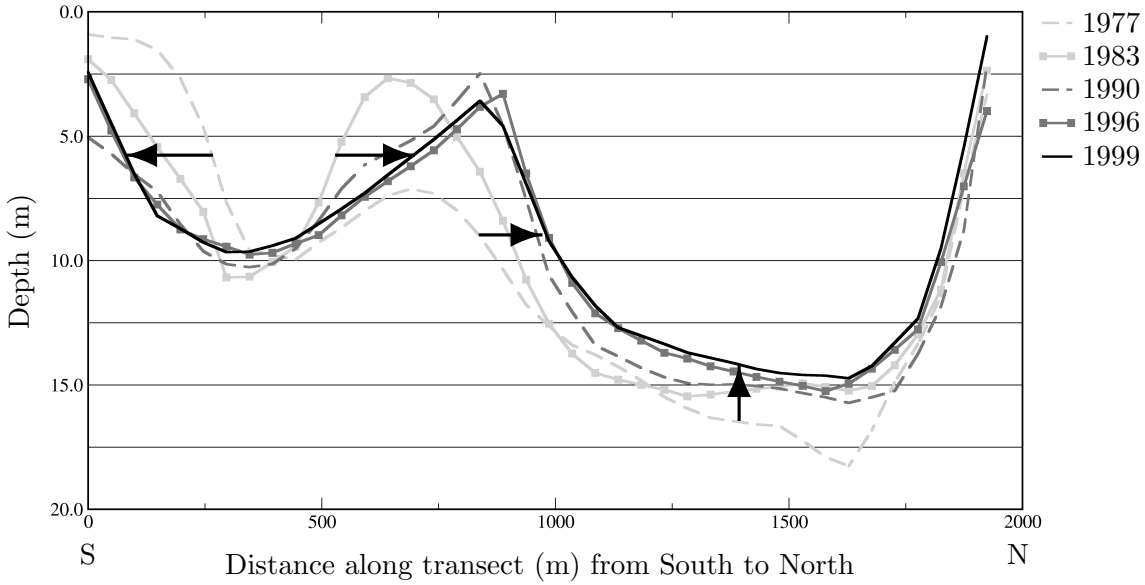

Figure 2.22: Measured channel profile at cross-section 15 in the Piep.

In the West-East oriented part of the Piep the southern sub-channel has slowly increased at the cost of the northern sub-channel. The submerged bar has gained in height and is gradually moving northward to allow the afore-mentioned changes in channel cross-sections. This can be clearly seen in Figure 2.22 which shows the channel profiles for several years at cross-section 15 (see Figure 2.20). Note that due to the vertical exaggeration the changes appear to be rather extreme. The southern channel bank has moved in southern direction whereas the northern bank is relatively stable. The maximum channel depth was rather stable, after an initial decrease until 1983.

In the bend near Buesum the inner bank gradually migrated in northeastern direction. This is shown in Figure 2.23. The outer bank is quite stable, mainly due to the presence of the harbour entrance. The Piep maintained its cross-sectional area through deepening by approximately 1 m.

The North-South oriented part of the Piep in the Meldorf Bight has changed from one main channel to a two-channel system. The maximum depth reduced from approximately 12 to 7 m. The reduction may well be related to the dike constructions that reduced the drainage area of the channel.

Figure 2.24 shows the relative changes of wet volume of the Piep sub-domain as indicated in Figure 2.21. A gradual reduction of the volume can be seen. The variations on the scale of years may well be based on the accuracy of the underlying data and thus does not necessarily represent a back and forth behaviour.

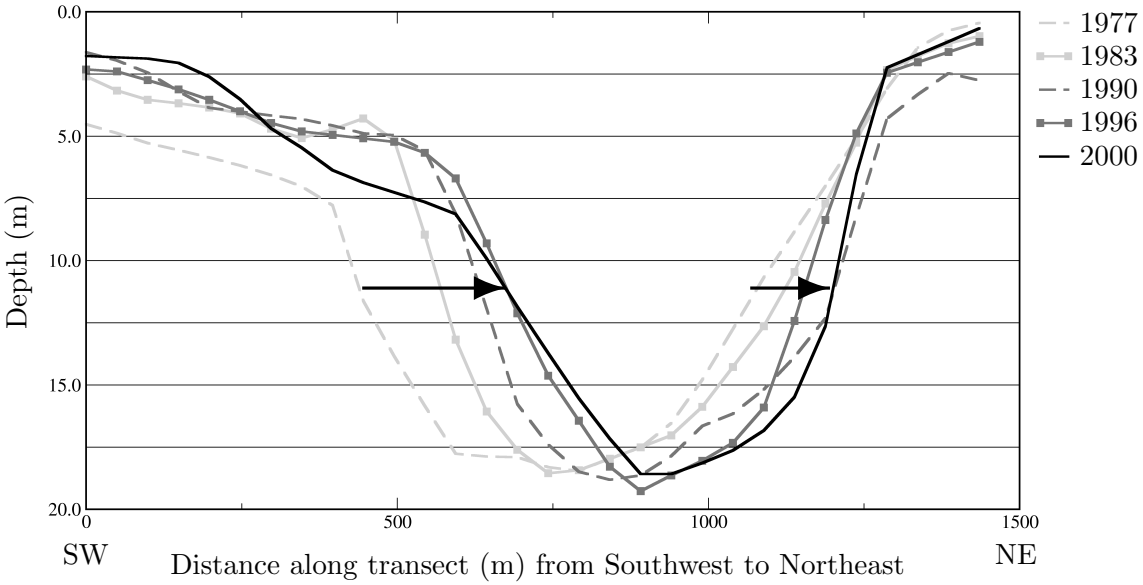

Figure 2.23: Measured channel profile at cross-section 18 in the Piep.

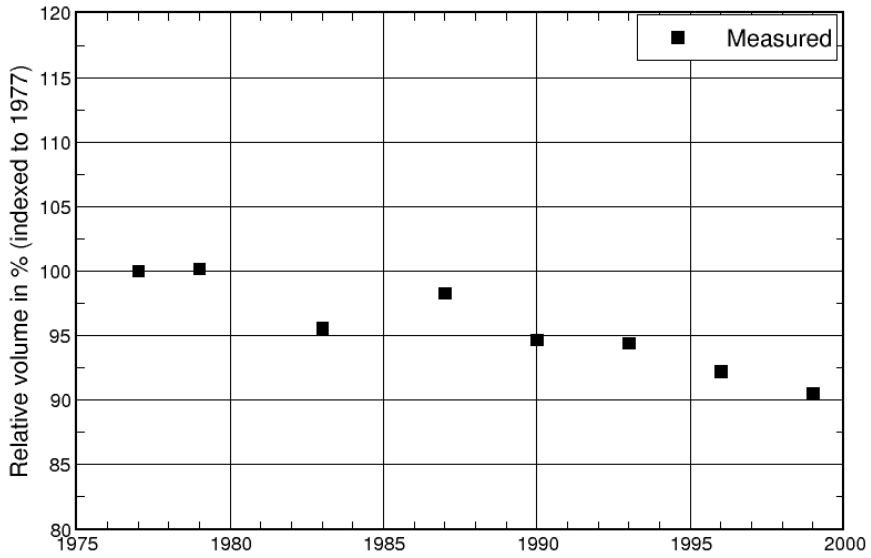

Figure 2.24: Changes in the wet volume below mean sea level of sub-domain Piep.

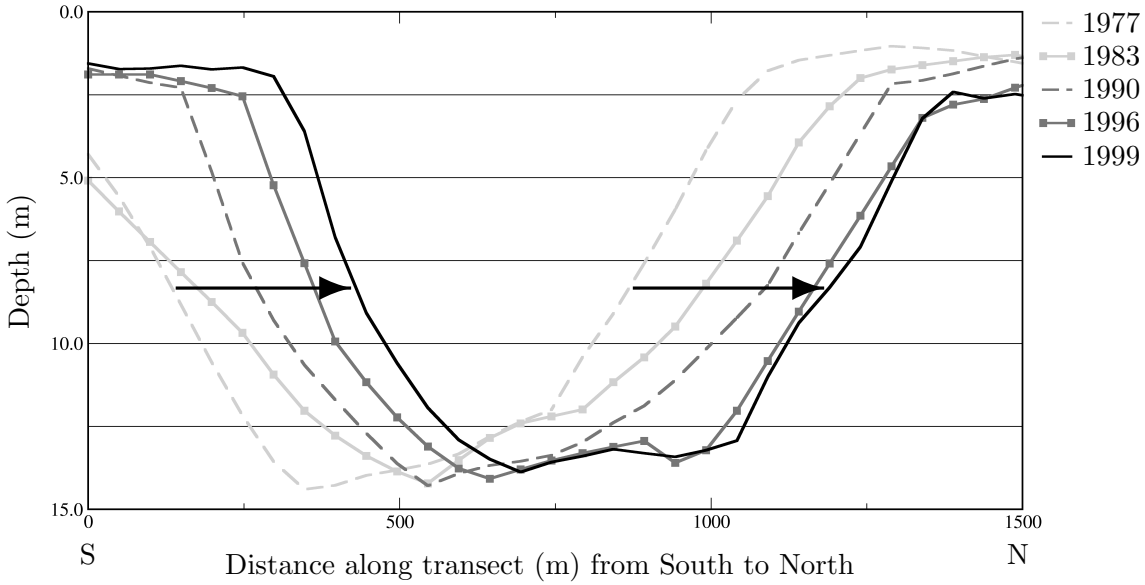

Figure 2.25: Measured channel profile at cross-section 2 in the Norderpiep.

The tidal channel Norderpiep

The channel Norderpiep enters the domain from the Northwest. The western part is a single channel with depths ranging between 10 m at cross-section 1 and 17 m at cross-section 3. The Norderpiep bifurcates towards the Southeast. The southwestern sub-channel is 5 to 7 m and the northeastern sub-channel 12 to 16 m deep.

Morphodynamics of the Norderpiep

The orientation of the mouth of the Norderpiep has changed from West-Northwest to West. This reorientation and the eastward movement of Tertiussand caused the northern part of the channel to migrate gradually towards the Northeast. The middle part of the channel is rather stable on the northeastern side, mainly because of the presence of the consolidated mud at this location (see Section 2.6). In the southeastern section of the channel, the reduction of the western sub-channel is the most distinct difference between 1977 and 1999. The submerged bar attached to Tertiussand at its northern tip and the western sub-channel diminished both in depth and in width.

From the development of the profile at cross-section 2 in Figure 2.25 can be seen that the Norderpiep has migrated northward by 300 to 400 m at this location. The maximum depth of the channel is almost constant. A steepening of the southern bank can be seen. The northward extension of the flat Tertiussand is responsible for this.

Figure 2.26 shows the evolution of the channel at cross-section 4. It can be seen that the submerged bar has increased in height. The northeastern sub-channel is rather sta-

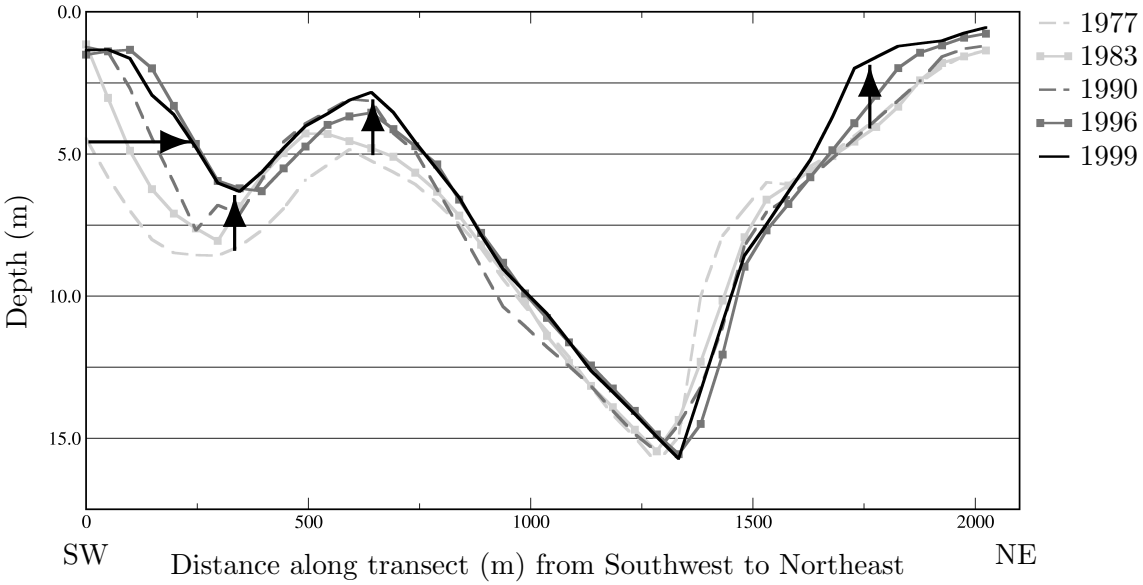

Figure 2.26: Measured channel profile at cross-section 4 in the Norderpiep.

ble with a depth of about 16 m, except for a slight steepening of the northeastern bank bordering the flat Blauortsand. The cross-section of the southwestern sub-channel has reduced significantly. This is caused on the one hand by the progressing flat Tertiussand and on the other hand by the sedimentation of the channel itself. The maximum depth of this sub-channel reduced from circa 8 to 6.5 m.

The changes in volume, presented in Figure 2.27, show a reduction of circa 10 % of the volume over the considered period.

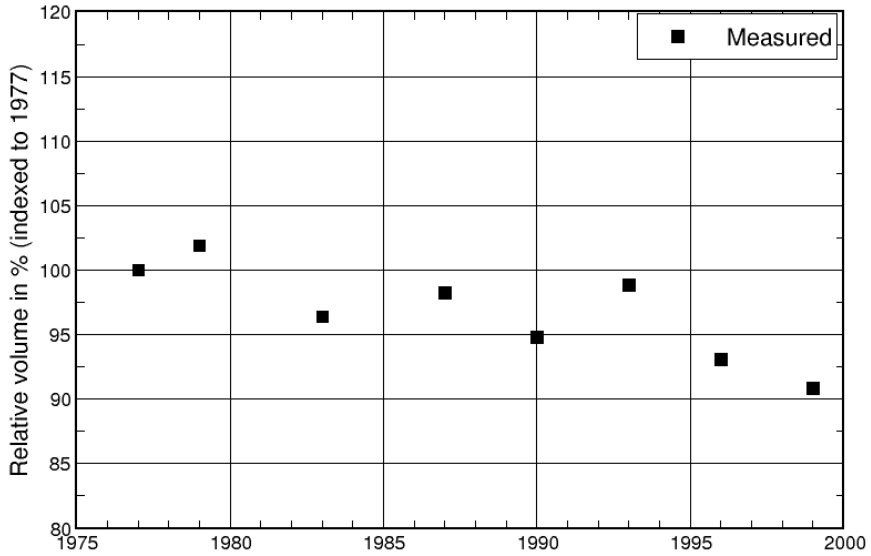

Figure 2.27: Changes in the wet volume below mean sea level of sub-domain Norderpiep.

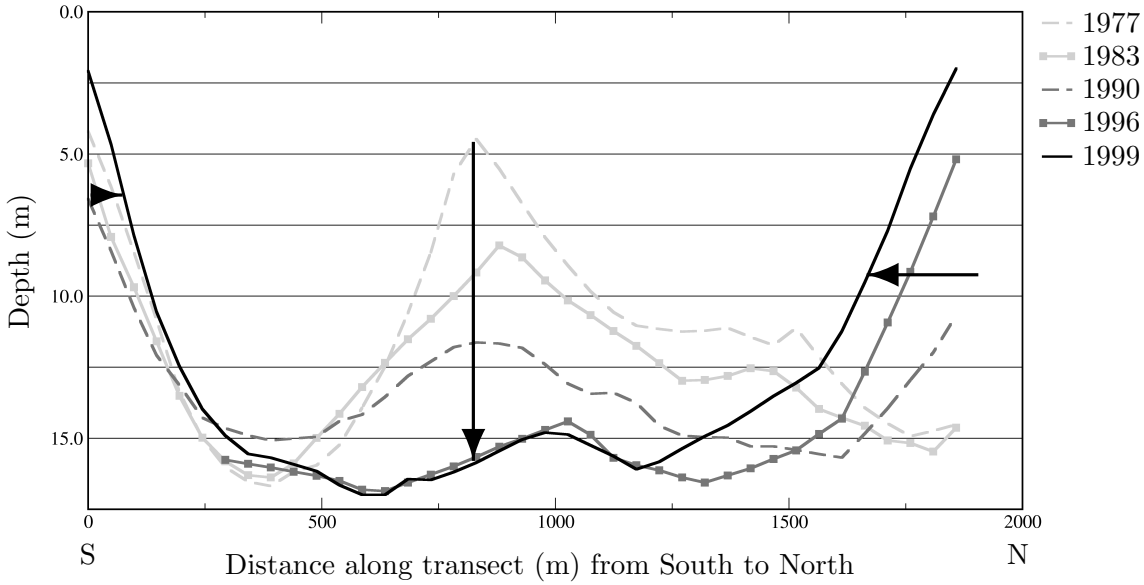

Figure 2.28: Measured channel profile at cross-section 10 in the Suederpiep.

The tidal channel Suederpiep

The Suederpiep, entering the domain from the West, is the largest channel in the study area. It can be split-up into two parts, divided by the mouth of the channel Bielshoevener Loch. The western channel section consists of one main channel with a depth of approximately 17 m. Towards the East this channel bends slightly towards the East-Northeast. A smaller branch into the mouth of the Bielshoevener Loch can be seen. Eastward of the Bielshoevener Loch, the Suederpiep is split-up into two sub-channels, divided by a submerged bar. Initially the southern sub-channel is dominant whereas the dimensions of the northern channel increase and those of the southern channel decrease when progressing eastward. At this location the Suederpiep returns to its eastward orientation.

Morphodynamics of the Suederpiep

The western section of the Suederpiep consisted of two sub-channels in 1977 which gradually merged into one main channel towards 1999. The channel mouth has shifted southward, together with the southwestern tip of the flat Tertiussand. North of the shoal D-Steert the channel is deepened from 15 to 17 m. Due to the confinement of the channel by the southward expanding Tertiussand and the northern edge of D-Steert, the channel had to become deeper to maintain its cross-section. In the curve where the Suederpiep changes its orientation to the East-Northeast, the channel is getting shallower by up to 3 m. The second curve, in which the channel returns towards the East, migrates in northwestern direction where it erodes the edge of Tertiussand. The stretches of strong erosion and sedimentation (see Figure 2.19(a)) indicate this process.

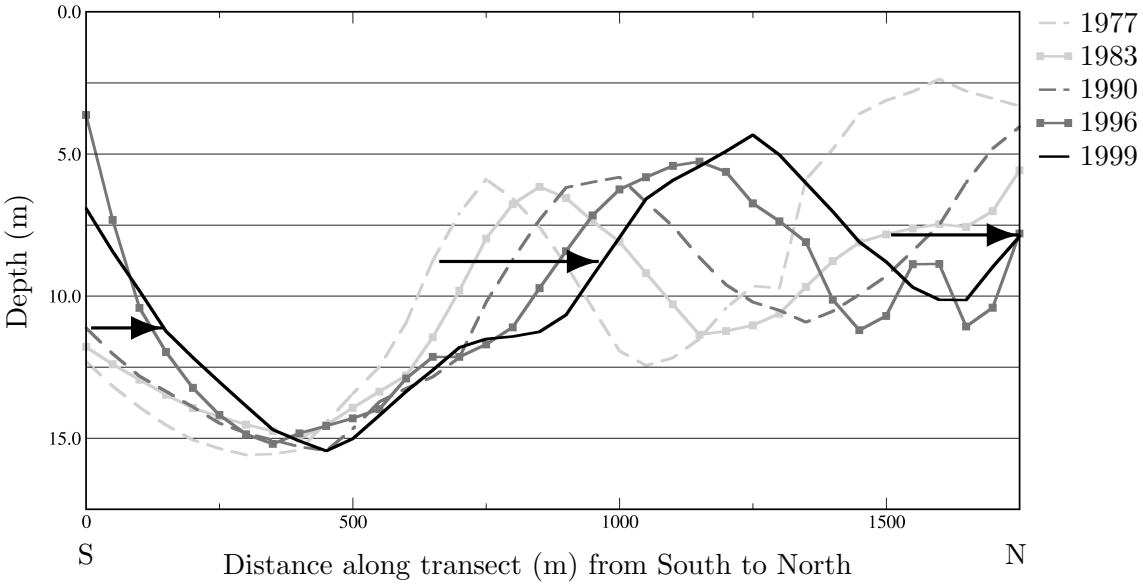

Figure 2.29: Measured channel profile at cross-section 12 in the Suederpiep.

The channel profiles at cross-section 10, as shown in Figure 2.28, show the gradual disappearance of the submerged bar, causing increases in depth of up to 10 m. The southern bank at the edge of D-Steert showed to be relatively stable whereas the northern bank migrated by up to 500 m southward in the 20-year period. The maximum depth stayed constant at a level of approximately 17 m. Asp *et al.* [2001] showed the presence of the *Dithmarschen Klei* – clay layer at this location, which explains the heavy erosion of the bar in combination with the stable depths of the sub-channels.

Figure 2.29 shows the evolution of the channel at cross-section 12. The channel migration can be clearly seen. The channel banks and the submerged bar moved up to 350 m in northwestern direction. The shape of the channel profile is rather stable except for the northern sub-channel, showing a decrease in depth by over 2 m. The strange hump in this sub-channel in the 1996-profile is almost certainly the result of an erroneous measurement.

The volume changes of the analysed sub-domain Suederpiep show a relative stability (Figure 2.30). The slight increase in volume in the first ten years is balanced by a reduction in the following period.

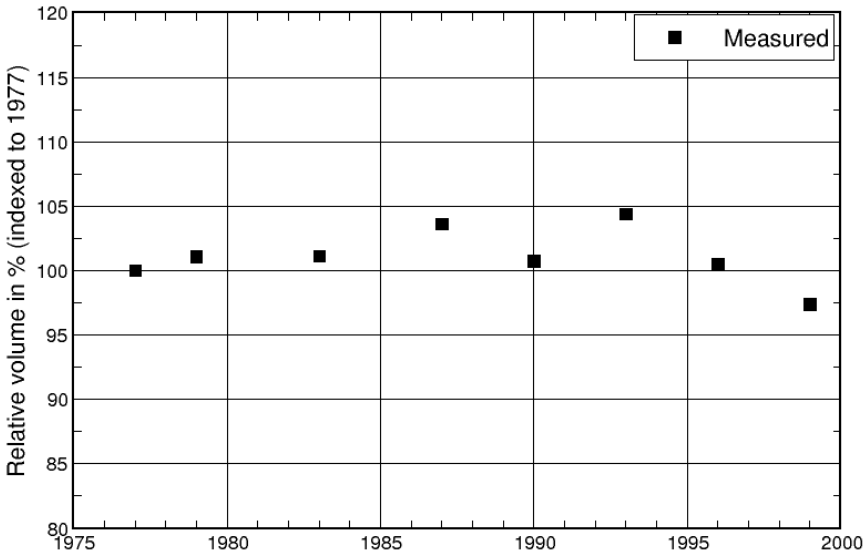

Figure 2.30: Changes in the wet volume below mean sea level of sub-domain Suederpiep.

The tidal flat Tertiussand

The tidal flat Tertiussand is situated between the channels Norderpiep and Suederpiep. From North to South it measures about 7 km and from West to East maximally 10 km. Its highest (but relatively small) parts are just above mean sea level but the entire flat is flooded during high water. In the middle of Tertiussand, on its western side, a secondary channel can be found with a maximum depth of 8 m. The slopes are relatively gentle on the North Sea side and much steeper where the flat meets the channels.

Morphodynamics of Tertiussand

The secondary channel in the middle of Tertiussand was oriented mainly towards the Northeast. Over the years, the significance of the northeastern end of the channel has reduced. An extension towards the Southeast has developed, that connected with the northern sub-channel of the Suederpiep. The western side of the secondary channel moved northward. Both effects caused a clockwise rotation of the channel by circa 20°.

The northern and eastern parts of Tertiussand are moving eastward, which is probably related to the erosion of the northwestern side, providing sediments. This migration causes sedimentation at its northeastern and eastern edges, pushing the Norderpiep in the same direction. The deposition of sediments at the Norderpiep's western bank induces the merging of the its submerged bar with Tertiussand.

The southern part of the tidal flat shows strong sedimentation at its southern edge, pushing the Suederpiep southward and causing a stronger curvature of the northern sub-channel of the Suederpiep. The combined effect of the dynamics of the southern and eastern parts of Tertiussand, together with the erosion in the middle channel, may result in the connection of both channels.

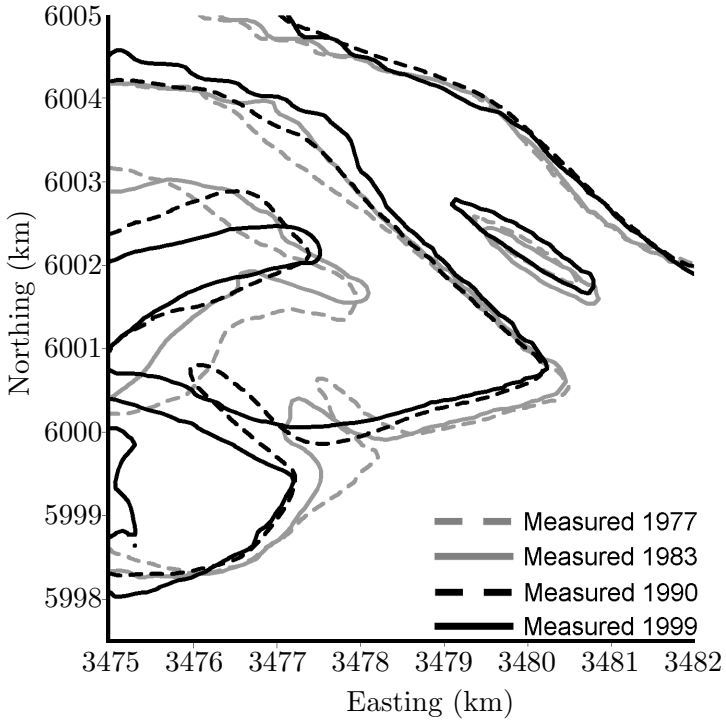

Figure 2.31: Changes of the 3 m depth contours near Tertiussand.

The 3 m depth contours near Tertiussand are shown in Figure 2.31 for the years 1977, 1983, 1990 and 1999. Gradual progression of the tidal flat towards the Northeast can be seen. In the Southeast, the flat is retreating, giving more space to the channel Suederpiep. In the Southwest an expansion of Tertiussand can be recognised. Furthermore a small channel is slowly increasing in size, branching of from the Suederpiep. The deeper central area is changing shape and reducing in size over the considered period.

As shown in Figure 2.32 the wet volume is gradually decreasing, indicating an increase in sediment volume below mean sea level. This is either the result of an actual import of sediment or the levelling of higher areas.

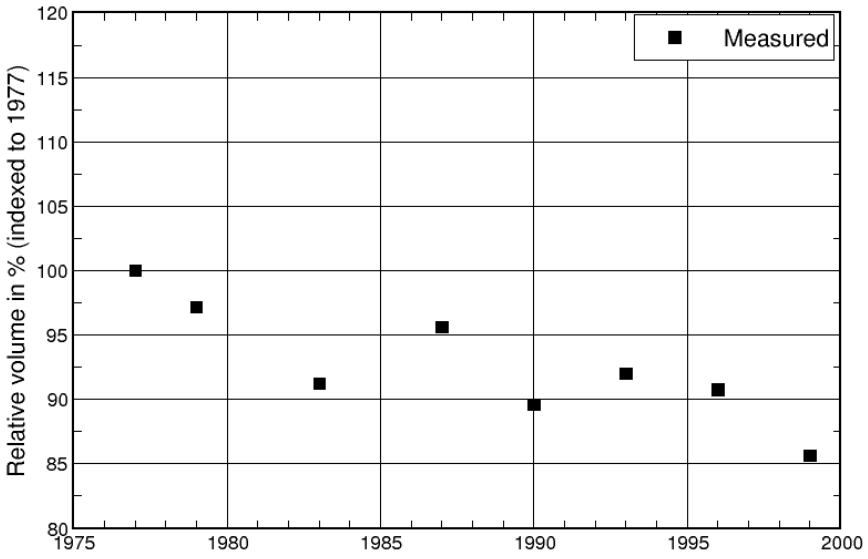

Figure 2.32: Relative changes in the wet volume below mean sea level of sub-domain Tertiussand, indexed to 1977.

The tidal channel Bielshoevener Loch

At the mouth of the Bielshoevener Loch the channel is West-East oriented and consists of a single channel. After the bend towards the South-Southeast, it splits into two sub-channels of equal width that meander further towards the Southeast. The western sub-channel is slightly deeper (circa 9 m) than the eastern sub-channel which has depths around 7 m.

Morphodynamics of the Bielshoevener Loch

The original mouth of the channel Bielshoevener Loch as it existed in 1977 has disappeared totally over the years. A new connection to the Suederpiep developed gradually into the new entrance. Furthermore, the middle section with North-South orientation rotated clockwise by some 15° and switched from one main channel to two sub-channels.

The tidal flat Blauortsand

Blauortsand is the tidal flat at the northern edge of the domain of investigation. It stretches from the western edge of the Norderpiep up to the main land in the East over circa 20 km. Except for the a small area, named Blauort, the flat is intertidal with a large area above mean sea level. The southwestern edge of Blauortsand forms the channel bank of the Norderpiep. In the southern part, the secondary channel Ossengoot can be found, with depths below 5 m.

Morphodynamics of Blauortsand

Relatively little morphological activity can be seen on the flat Blauortsand, except for the stretch of erosion along the Norderpiep.

The shoal D-Steert

The shoal D-Steert is located just South of the Suederpiep in the western part of the domain. It is rather exposed to the open sea. The bathymetry may be up to 1 m above mean sea level. D-Steert measures some 4 km^2.

Morphodynamics of D-Steert

The shoal D-Steert is relatively stable in North-South direction, with only a slight extension towards the North of less than 50 m in 20 years. The eastward migration, however, is clearly visible. A large stretch of erosion can be seen at its western side, combined with strong sedimentation to its East. The eastern front of the shoal migrated circa 1.5 km over the analysed 22 years, giving an average of 70 m/year.

The tidal flat Bielshoevensand

In the centre of the tidal flat Bielshoevensand can be found. It is bordered in the North and East by the Piep and in the West and Southwest by the Bielshoevener Loch. In the Southeast the flat is connected to the main land. The depth varies generally around mean sea level by circa 1 m although some small channels have larger depths.

Morphodynamics of Bielshoevensand

The morphologically most active part is the northwestern tip, which splits the Suederpiep and the Bielshoevener Loch. Over the years, strong sedimentation can be seen at this location. However, this is the combined result of heavy deposition up to 1990 and erosion afterwards. From 1990 onward the influence of the changed Suederpiep can be seen. The Suederpiep concentrated into one main channel and directed the incoming flood currents increasingly towards the tip, leading to erosion. Therefore, erosion of the tip combined with deposition at the southern channel bank of the Suederpiep can be found after 1990, causing a deepening and widening of the northwestern edge of Bielshoevensand. It pushes the Suederpiep northward, enforcing the migration of the sub-channels and submerged bar of this channel.

The rest of the tidal flat shows generally minor sedimentation. However, the extent of data coverage is limited and thus precise comparisons cannot be made. Most protruding is the sedimentation of the smaller drainage channels that flow over the tidal flat into the Piep. The largest of these channels, flowing into the Piep near the bifurcation, has diminished gradually over the considered period.

The Meldorf Bight

The Meldorf Bight contains the landward part of the drainage area of the Piep. Several small streams that transport water to this channel can be found. The western part of the Bight consists of parts of the previously mentioned Bielshoevensand. The depths in the eastern part are between -1 and 1 m with respect to mean sea level. Close to the coastline the bathymetry may be higher.

Morphodynamics of the Meldorf Bight

The eastward tidal flats in the Meldorf Bight, east of the Piep channel, show sedimentation throughout the area. A relation with the dike constructions seems logical, since this decreased the drainage areas of the several contributory channels. The western side of the Meldorf Bight is part of the flat Bielshoevensand.

Chapter 3

The Dithmarschen Bight model – process models

3.1 Introduction

In this Chapter, the set-up and calibration of the model components for the central Dithmarschen Bight are discussed. In Section 3.2 the definition of the model domain is presented. This is followed by the description of the model components for flow, waves and sediment transport in Sections 3.3 through 3.5. In Section 3.6 the results are discussed.

The model has been set-up within the modelling system Delft3D-MOR which contains modules for simulating tidal flow, waves, sediment transport and morphological updating. A description of the modelling system and its main characteristics is given in Appendix 3.A.

3.2 Model domain

The model domain, being the area for which the physical processes will be simulated, forms the basis for the morphodynamic model. For the Dithmarschen Bight model it is identical for all of the applied modules. In Paragraph 3.2.1, the general aspects to be considered when defining the model domain are discussed. In an iterative procedure, in which these aspects have been accounted for, the model domain of the Dithmarschen Bight model has been defined. The resulting domain is introduced in Paragraph 3.2.2.

3.2.1 General aspects

The definition of the model domain is the first step in the set-up of a morphodynamic model. It should be based on an optimal balance between the models reproductive capability and the needed calculation time. To this end, the location of the model boundaries, the boundary conditions to be imposed, the area of interest, the period to be simulated and the needed computing time have to be considered.

Natural and artificial boundaries

The domain is limited by boundaries, which may either be open or closed. Furthermore, a division can be made between horizontal and vertical boundaries.

At open boundaries interaction between the model domain and the "world outside" is possible. At vertical open boundaries that limit the horizontal extensions of the model domain, examples of these interactions are tidal flow, river discharge, swell wave energy or sediment exchange. These boundaries are artificial in the sense that there is no such division in real nature. At the horizontal open boundaries, consisting of the free water surface and the bottom, meteorological circumstances (wind and air pressure) and sediment exchange may influence the conditions within the model.

Closed boundaries are the limits of the domain where no interaction is present, generally representing the coastline. These are natural boundaries, that may nevertheless be based on man-made dikes and structures. They form a physical limitation to the movement of the modelled property.

Boundary conditions

At all boundaries, the model requires information about the state just outside of the model domain. At closed boundaries the fluxes across them are set to zero, preventing interaction with the outside world. At the open boundaries the fluxes may be locally and temporally varying, generally causing the boundary conditions at these locations to be more complex. The higher the complexity of the interactions, the more difficult it is to define proper boundary conditions. Therefore, the choice of their location is very important and should be based on both the availability of information and the preferably unambiguity of the local physical state. The latter is usually satisfied when the gradients of the bathymetry and the related current velocity and sediment transport gradients are relatively small.

Another important aspect is the fact that, in case of a current velocity boundary condition, only the velocity components normal to the open boundary are imposed within Delft3D. Therefore it is important to locate the open boundaries in such a way that they cut the main current paths at an angle close to 90 degrees.

In general the boundary conditions will not be perfect, introducing deviations of the modelled state with respect to the real state.

Area of interest

The area of interest, being the area that will be taken into consideration when evaluating and interpreting the model results, has to be defined. Furthermore, the surrounding areas that have significant influence on the hydro- and morphodynamic state of the area of interest have to be identified. Generally, these surrounding areas should be included in the model and should be large enough to prevent significant influence on the area of interest by the previously mentioned deviations of the boundary conditions.

Simulation period

When the simulation period is longer, the influence of the boundary conditions may progress further into the model domain. Thus, the surrounding area has to be large enough to prevent progression into the area of interest during the simulation period. Due to the complexity of the interacting physical processes its size can usually only be determined through comparison of the model results of simulations with varying extent of the surrounding areas.

Computation time

The computation time of the model depends on the number of grid cells, the number of time steps, the time needed by the model to solve the included equations for one point and one time step, and the size of the simulation period. The number of grid cells is determined by the extent of the model domain and the grid resolution. The latter has to based on balancing the feasibility of the calculation time on the one hand, and the representation of the hydro- and morphodynamic physical state on the other hand.

For an instationary model, the maximally allowable time step is limited by the size of the grid cell (see Paragraph 3.2.3) and the progression celerity of the modelled quantity, e.g. the current velocity. For explicit models this limit ensures numerical stability, whereas for implicit models the limitation concerns the accuracy of the model results. Within the Delft3D-MOR system, the flow module is semi-implicit whereas the sediment transport and morphodynamic modules are explicit. The wave module is stationary.

3.2.2 Model domain of the Dithmarschen Bight model

Based on the afore-mentioned considerations, the model domain of the Dithmarschen Bight has been defined. The area of interest contains the Piep tidal channel system with its contributory channels and adjacent tidal flats. This is shown in Figure 3.1. It includes the channels Norderpiep, Suederpiep and Piep, together with the adjacent tidal flats Tertiussand, Blauortsand and Bielshoevensand.

To ensure a proper representation of the hydro- and morphodynamics in this area, the model domain has been extended in northern, western and southern direction. This is shown in Figure 3.2. The eastern side coincides with the coastline and is therefore a closed boundary.

Under normal circumstances the fluxes across the northern and southern boundary are rather small. However, under storm conditions with a strong water level set-up and redirected current patterns, this is not necessarily the case. These effects can not be expected to be properly imposed through the open boundary conditions, since there is no clearly dominant flow direction. As described in Paragraph 3.2.1, only the velocity component normal to the open boundary can be prescribed. Therefore it is necessary

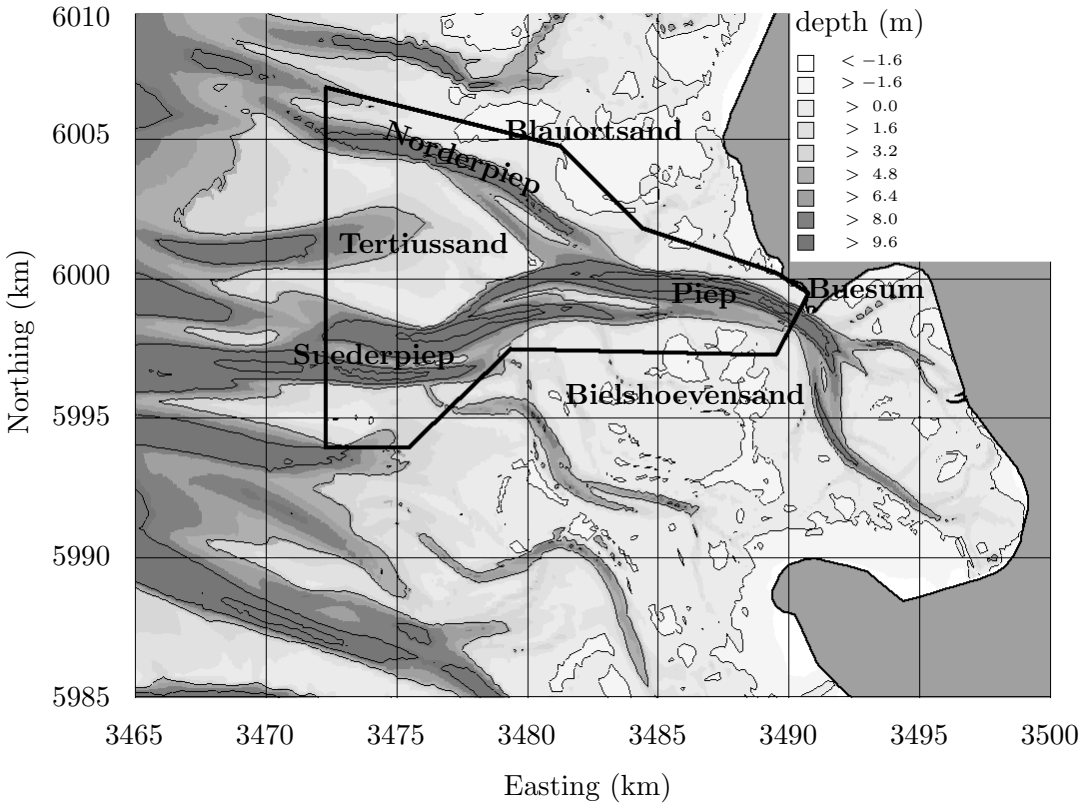

Figure 3.1: The defined area of interest (bathymetry from 1977).

to extend the model domain in northern and southern direction. This extension also eliminates the problematic imposition of wave boundary conditions at these sides.

The western side forms the link between the model domain and the open North Sea, making it the most important open boundary. Here, the imposed conditions for the exchange of water, wave energy and sediment are the driving forces in the morphodynamic model, together with the imposed meteorological conditions. To simplify the determination of these conditions, the western boundary has been located in relatively deep water. Here, the incoming current velocities and waves are still relatively undisturbed by the bathymetry and therefore have a more uniform character.

In the Northeast, the tidally influenced part of the Eider river, together with the barrier at its mouth, has been schematically included in the model domain. This approach prevents the need for complex boundary conditions at the barrier.

Part of the Elbe river, in the Southeast, is also included. The Elbe enters the model domain in the Southeast and flows out into the North Sea in the Southwest. Due to the extensive tidal flats just northward there is almost no direct exchange of water between the area of interest and the Elbe river. Its inclusion is motivated by the elimination of the southern open boundary, which has been replaced by a closed boundary that mainly follows the coastline.

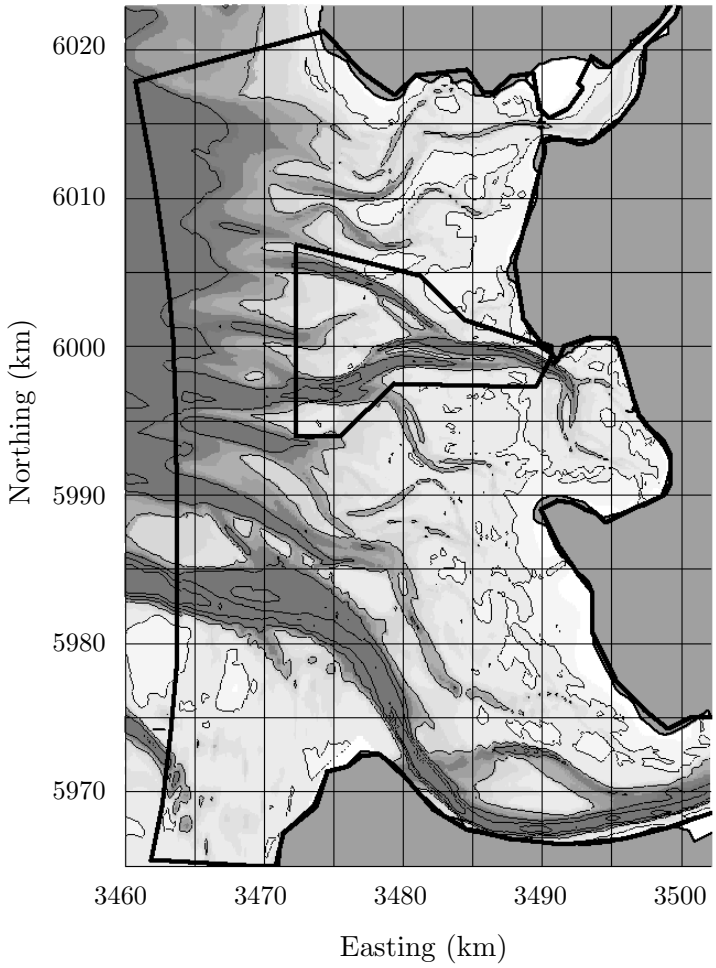

Figure 3.2: The model domain of the Dithmarschen Bight model, with the area of interest (bathymetry from 1977).

The defined dimensions of the model domain ensure that the open boundaries are minimally 10 km away from the area of interest. The model results confirm that this is sufficient for morphodynamic simulations with a simulation period of up to 10 years.

3.2.3 Grid definition and model bathymetry

After the model domain has been defined the grid layout and resolution, i.e. the number of grid cells per unit of area, is defined. The combination of the layout and grid resolution should be such, that the to-be-modelled processes and the underlying bathymetry are represented optimally and the grid requirements are met, without making the model simulations prohibitively expensive in terms of the computational costs, i.e. computation time and computer requirements.

Grid requirements

The numerical solving methods within Delft3D are based on finite-difference grids. It allows the grid to be curvilinear, although there are some requirements with respect to the shape of the grid. To ensure an optimal numerical accuracy, the angles between the horizontal and vertical grid lines should be close to 90 degrees and the grid cell size should not vary too much from one cell to the adjacent cells. The rectangular character of the model grid is defined by the so-called orthogonality, which is the cosine of the angle between the crossing grid lines in both horizontal directions. For angles close to 90 degrees, the orthogonality is therefore close to 0. In the Delft3D manual values lower than 0.02 (angle between 88.85 and 91.15 degrees) in the area of interest to 0.04 (87.7 – 92.3 degrees) in remote areas are suggested. The grid smoothness is defined by the relative cell size with respect to the adjacent grid cells, in both horizontal directions. The relative change in grid cell size in both horizontal directions should be below 30 – 40 %. Furthermore, it is preferred that the grid lines follow the main velocity patterns [WL | Delft Hydraulics, 2003a,c].

Model grid

On the basis of the defined model domain and considering the previously described grid requirements, the model grid has been generated. Since the focus of the study is on the medium scale morphodynamics, the maximally allowed grid spacing in the area of interest has been set to follow the spacing of the bathymetric measurements, being 100 to 200 m. The curvilinear grid has been defined in such a way that it follows the main channels to a high extent.

The resulting grid is shown in Figure 3.3 for the entire model domain and in Figure 3.4 for the area of interest. In the area of interest the model grid follows the tidal channels, with a focus on the dominant Suederpiep and Piep channels. The highest resolution can be found here, with a spacing between 80 and 180 m. In remote areas the resolution is lower, to limit the number of computational cells. With this resolution the medium scale morphology can be represented properly.

The open boundary on the western side of the model is located perpendicularly to the main East-West oriented tidal currents. The depth measures between 10 and 20 m at this boundary. In the middle of the boundary, one of the wave buoys was located (see Paragraph 2.3.2), enabling the direct imposition of the measured conditions at these buoy onto the boundary for the wave model evaluation.

Since the northern and southern open boundaries are located in shallow water, relatively small current velocities occur and very little wave energy enters. These conditions and the remote location of these open boundaries ensure that these boundaries have no influence on the model results for the area of interest.

In the North the Eider estuary is included and in the South the grid orientation follows the Elbe river.

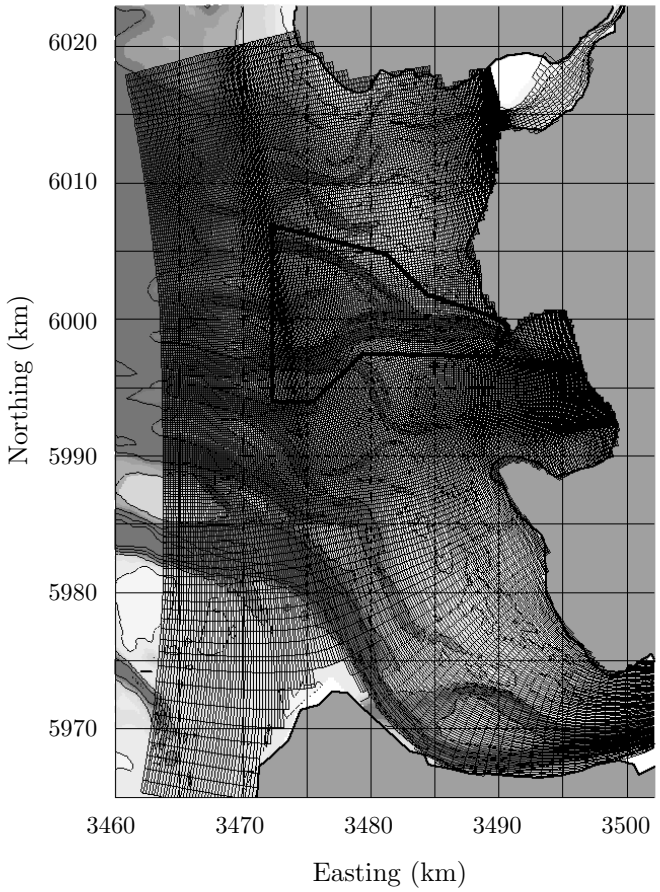

Figure 3.3: The curvilinear model grid.

The grid has a total of circa 43,000 cells. The smallest cells are found in the central channels, where tidal currents up to 2 m/s may be expected. Considering the advised maximum Courant number of 10 ([WL | Delft Hydraulics, 2003a], see Appendix 3.A for the definition of the Courant number in this case), the resulting time step is set at 60 s. This results in an acceptable calculation time of circa 30 minutes per simulated lunar day (flow only) on a PC with 3.0 GHz processor and 1 Gb RAM.

Model bathymetry

The bathymetric data, as described in Chapter 2, have been interpolated onto the model grid to form the model bathymetry. Several model bathymetries have been created, to generate the proper starting conditions for the various modelling periods. Since the data coverage is generally limited to the main channels and parts of the tidal flats, data from previous and following years have been added to gain a larger coverage. For the remaining uncovered areas, generally located on the tidal flats or shoals, data have been taken from other years and have sometimes been adapted to follow the observed, but not measured, trends. Although this is a rather subjective

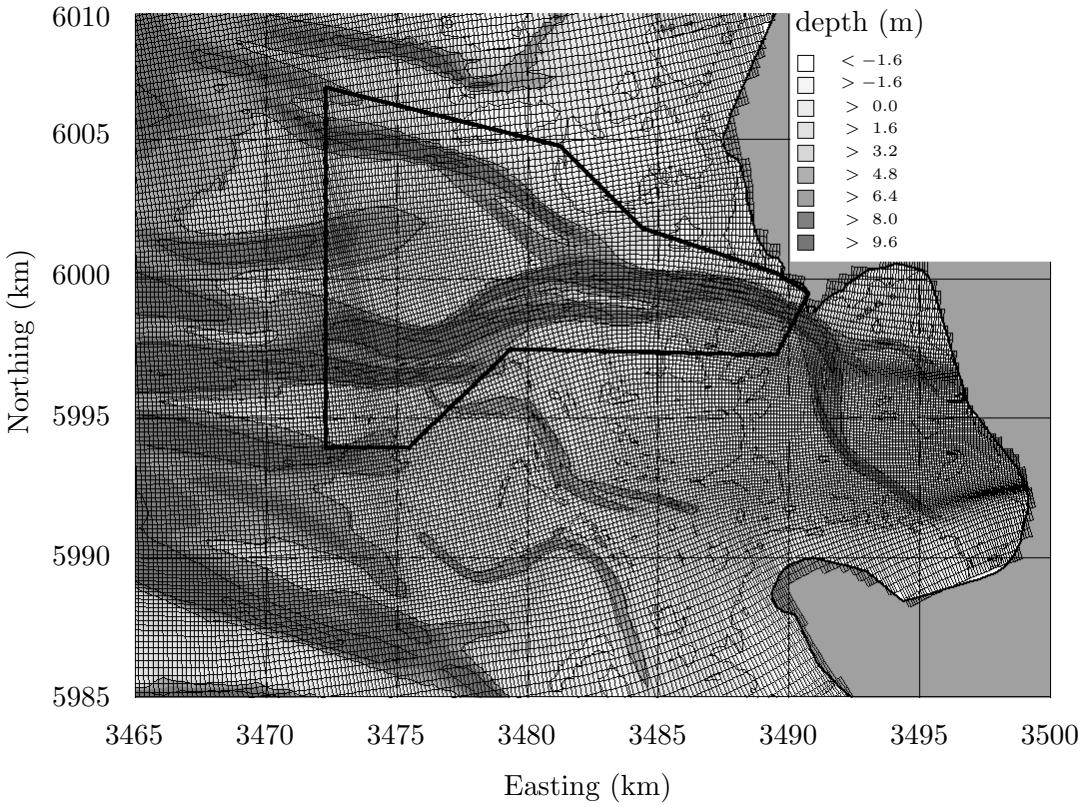

Figure 3.4: The grid in the area of interest with a higher resolution (bathymetry from 1977).

approach and may introduce inaccuracies in the starting bathymetries, this method yielded the best possible bathymetric conditions for the model simulations.

The channel profiles that have been presented in Chapter 2 have been based on the model grid. The channel profiles were properly represented and confirm that the applied resolution is sufficient for a good representation of the medium scale morphology.

3.3 Tidal flow model

A brief description of the basic concepts of the Delft3D flow module is given in Paragraph 3.A.2 of Appendix 3.A. The following Paragraph describes the flow model set-up, followed by the model validation in Paragraph 3.3.2.

3.3.1 Flow model set-up

Several decisions have to be made when setting up a numerical model for flow simulation, e.g. the choice of a depth-integrated or three-dimensional approach and the definition of the boundary conditions that incorporate the forcing of the hydrodynamics in the model. To obtain a reliable model set-up an iterative procedure, of setting-up the model and making sensitivity analyses to evaluate the effects of these decisions, has to be carried out. The main characteristics of the flow model are discussed in the following.

Depth-integrated versus three-dimensional approach

The necessity for three-dimensional modelling depends on the importance of the three-dimensional effects that cannot be sufficiently represented in a parameterised way by the depth-integrated model. The significance can be evaluated on the basis of the carried out field measurements an general knowledge of the governing physical processes.

The Elbe river, in the southern part of the domain, is not directly connected due to the separating tidal flats. It therefore spills its fresh or brackish water into deeper parts of the German Bight, where it mixes with the saline water of the North Sea. Although the salinity is subject to seasonal effects (see Section 2.4), these effects are expected to be rather uniform for the Dithmarschen Bight [Ehlers, 1988]. The same mixing occurs with respect to the temperature of the water. The smaller Eider river in the North does not play a significant role either, both due to its limited discharge and the in-between tidal flats. These considerations, together with the limited water depths, strong tidal action and wave action, lead to the conclusion that stratification due to salinity or temperature differences can be considered to have an insignificant role in the hydrodynamics of the area of interest.

Various calibration and validation studies for flow modelling in the study area showed that a 2Dh-approach resulted in good results [Mayerle & Palacio, 2002; Palacio *et al.*, 2001; Palacio, 2002]. In Palacio *et al.* [2001] a comparison between the results of a 2Dh-model and three dimensional model with 10 layers has been made, leading to the conclusion that only minor differences in terms of water levels at several locations and flow discharges at several channel cross-sections were found.

On a small scale, three-dimensional behaviour may occur however, e.g due to spiral flow in the channel bend near Buesum and on the western part of the model domain due to wave action. The focus on medium scale behaviour in this thesis excludes these small-scale processes.

The significance of the influence of the three-dimensional behaviour on the medium scale morphodynamics has been weighted against the extra computational costs. An extension of the flow model from a 2Dh- to a 3D-model would require a reduction of the model domain to maintain manageable calculation times, especially for longer simulations (up to 10 years). Based on the results of morphodynamic modelling with a smaller model domain it has been concluded that a domain reduction is not acceptable (see Wilkens *et al.* [2001]). Therefore, the two-dimensional depth-integrated approach has been applied.

Boundary conditions

At each of the open boundaries, conditions have to be defined to represent the interaction between the hydrodynamics in the model domain and those outside. These boundaries have been split into a number of segments, to ensure a proper representation of the varying conditions along them. For each segment conditions are imposed at the beginning and end; between them these conditions are linearly interpolated.

Sensitivity tests showed that the best results were obtained when imposing current velocity conditions at the western open boundary and water level conditions at the northern and southern boundaries. Water levels are imposed at the open boundary in the Elbe river in the southeast of the domain. The relatively small Eider river is represented by a discharge source.

Since neither water level nor velocity measurement data with sufficient resolution in time and space are available for the open boundaries, the conditions are determined by nesting the Dithmarschen Bight model into larger models. This nesting sequence (see Figure 3.5) starts with a model for the entire North Sea, the Continental Shelf Model, presented by Verboom *et al.* [1992]. At the open boundaries of the Continental Shelf Model astronomical components for the water levels are imposed. The results of the Continental Shelf Model are imposed onto the open boundaries of the German Bight Model. This is an adapted version of the model developed by Hartsuiker [1997].

The sequence of these two models has been validated by Winter [2003] for the German North Sea coast. The resulting water levels and current velocities of the German Bight Model are subsequently interpolated onto the open boundaries of the Dithmarschen Bight Model. Depending on the simulated period, wind fields may be imposed onto the large scale models, to include wind-induced currents and storm surges.

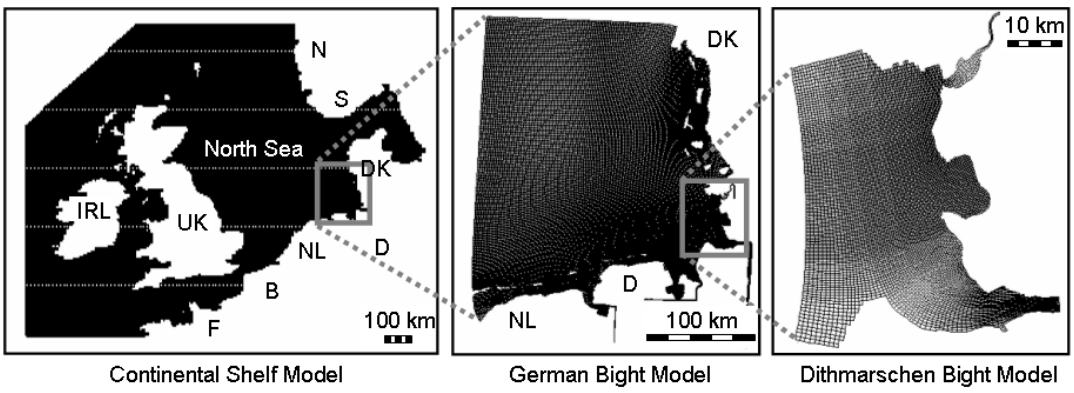

Figure 3.5: The applied nesting sequence for the generation of the boundary conditions.

Wind

Synoptic wind data are available from the PRISMA interpolation model, presented by Luthardt [1987]. These data are described in Section 2.5. Depending on the goal of the simulation, either these data have been imposed in the flow model or a constant wind speed and direction have been specified.

3.3.2 Flow model validation

The settings of the flow model have been based on the results of an extensive calibration and validation study of a flow model by Palacio [2002], see also Palacio *et al.* [2001]; Mayerle & Palacio [2002]. The best results in this study were obtained when imposing measured water levels at the open boundaries. Since no water level measurements are available at the open boundaries of the Dithmarschen Bight model, this approach is not used. Instead, the model is nested in larger scale models - an approach that also yielded acceptable results in the mentioned calibration and validation studies.

Meldorf Bight flow model by Palacio [2002]

Palacio's flow model (*Meldorf Bight flow model*) covers not only the Meldorf Bight, but approximately the area of interest shown in Figure 3.1. The open boundaries on the northern, western and southern side of the model more or less coincide with the boundaries of this area of interest. The study focussed on the flow conditions at several channel cross-sections of the channels Piep, Norderpiep and Suederpiep.

The model results have been compared to the measured water levels at several gauges as well as to the current velocities and deducted channel discharges of the ADCP-measurements described in Section 2.3.1. The comparison has been based on integrated parameters, such as the cross-sectional discharge, the depth-integrated and the width-integrated velocities. Since the current measurements are only available for relatively calm periods, such conditions were considered exclusively. The hydrodynamic modelling did not include the modelling of waves and therefore the local wave effects were not accounted for. This was considered acceptable since only calm periods were simulated.

In conjunction with the calibration and validation, Palacio [2002] considered several approaches for the definition of the open boundary conditions, e.g. applying a nesting sequence similar to the one shown in Figure 3.5 or imposing synoptic water level data on the basis of nearby gauges. Furthermore, the influence of inaccuracies of the bathymetry on the tidal flats has been investigated.

Validation

The validation of the model showed its capability to reproduce the hydrodynamics of the tidal channels on the basis of five water level gauges and three channel cross-sections, for

both spring and neap tides. Palacio [2002] reported a Root Mean Square Error (RMSE) around 0.15 m/s in the Piep and Norderpiep and circa 0.25 m/s in the Suederpiep for the depth-integrated current velocities. The RMS-error of the water levels was between 0.02 and 0.04 m for high tide and between 0.05 and 0.12 m during low tide, based on the maximum and minimum water levels of a two-month period. The cross-sectional discharges are reproduced with discrepancies below of 10 to 15 % of the maximum discharge, with the highest accuracy during spring tide for the three considered cross-sections. Exemplarily, the comparison of the depth-integrated measured and modelled velocities at the indicated cross-section in the Suederpiep are shown in Figure 3.6.

Discussion

The afore-mentioned values are satisfactory, considering the complex bathymetry and current velocity patterns in the model domain. When evaluating these results, a few aspects should be taken into consideration.

Firstly, the high accuracy of the water level predictions can be partly explained by the fact that the imposed boundary conditions have been based on extrapolated water level measurements. The expected high correlation between the measured values at different locations will not be easily lowered by the model. However, since the predictions at more remote gauges (with respect to the open boundaries) are quite good, it is assumed that the physical settings of the model are optimal for the study area.

Secondly, the definition of a channel cross-section is not unambiguous. Parts of the channel close to the banks will not be measured (too shallow or too risky). In the comparison these parts are therefore not taken into account, although they may represent an important part of a channel's discharge.

Finally, it should be noted that the measurements of the hydrodynamics in tidal flat areas are not always as straight-forward as they seem. Strong local currents and waves, together with the limited size of the vessel may cause inaccuracies, in addition to the device-related uncertainties. For example, Van Rijn *et al.* [2002a] mention an accuracy of circa 0.05 m/s for a typical vessel-mounted ADCP under calm conditions.

Taking the above into account, it can be concluded that the main hydrodynamics are captured rather well by Palacio's model. The optimal settings as determined within this study have been used in setting up the flow model for the Dithmarschen Bight. The open boundary conditions, however, are based on model nesting instead of imposing measured water levels. There are no water level gauges in the direct vicinity of the more remote open boundaries of the Dithmarschen Bight model. Thus, the approach of extrapolating the water level measurements onto the open boundary would presumably lead to large inaccuracies. Furthermore, the nesting method allows the simulation of hypothetical events as well as making forecasts.

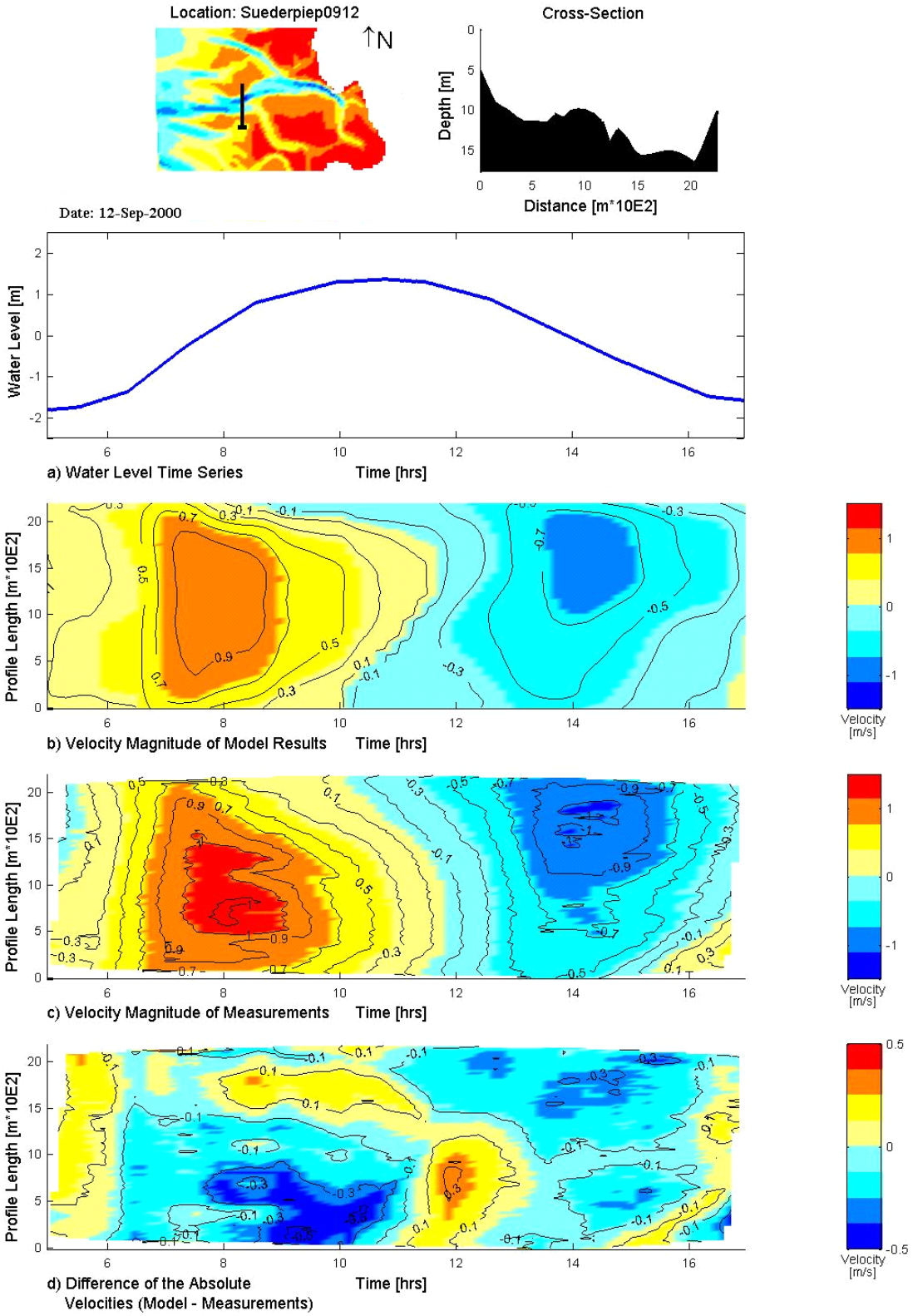

Figure 3.6: Comparison of measured and modelled depth-integrated velocities at the indicated cross-section in the channel Suederpiep. Adapted after Palacio [2002].

3.4 Wave model

The background of the implemented wave models within Delft3D are discussed in Paragraph 3.A.3 of Appendix 3.A. The general set-up of the wave model is presented in Paragraph 3.4.1. This is followed by the description of the model validation in Paragraph 3.4.2.

3.4.1 Wave model set-up

In the modelled tidal flat area local current velocities can be relatively high – up to 2 m/s. Furthermore, the total water depth can be influenced significantly by the phase of the tidal cycle and wind- or wave-induced water level changes. These dynamics can have a strong influence on the wave characteristics. Therefore, the wave model has been coupled to the flow model.

HISWA versus SWAN

Within Delft3D, the underlying model for calculating the wave characteristics can be either the HISWA or the SWAN wave model (see Holthuijsen *et al.* [1989] for HISWA; Booij *et al.* [1999] and Ris *et al.* [1999] for SWAN). Both have been applied to the central Dithmarschen Bight, as presented in Wilkens & Mayerle [2002]. This calibration and validation study led to the conclusion that the SWAN model produced better results than the HISWA model. Furthermore, the application of SWAN has several advantages over the use of HISWA. Therefore, SWAN has been applied for the morphodynamic modelling. The advantages of SWAN over HISWA are discussed in Paragraph 3.A.3 of Appendix 3.A.

Model grid

The previously defined model grid has been used to set-up the wave model. Since the SWAN model is rather expensive in terms of computation time, a comparison has been made between the wave results of a simulation with this grid and a simulation based on a coarsened version. It has been concluded that the coarsened version yields approximately the same results. Therefore, the coarsened version has been applied for the wave simulations.

Boundary conditions

The model domain contains three open boundaries through which wave energy may enter, i.e. in the North, West and South. The northern and especially the southern boundary are relatively unimportant, since the conditions at these locations do not significantly influence the wave characteristics in the area of interest. At the western boundary the wave conditions are very important. These represent the incoming swell energy from the North Sea.

At each of the open boundaries, swell wave conditions have been specified. For the model calibration and validation, these conditions are based on the wave measurements at the buoys near the western open boundary. When simulating other periods, for which no measured wave conditions are available, the imposed conditions are based on model results from larger scale models. This nesting procedure is similar to the one applied for the flow model nesting, see Paragraph 3.3.1.

Wind

As for the flow model, either synoptic data from the PRISMA interpolation model have been imposed in the wave model or a constant wind speed and direction have been specified.

3.4.2 Wave model validation

The evaluation of the coupled flow-wave model has been carried out on the basis of the wave measurement campaign of September 1996, as presented in Wilkens & Mayerle [2002]. This campaign, described in Paragraph 2.3.2, yielded information about the wave characteristics at five locations within the Dithmarschen Bight. Thus, not only the characteristics at these locations are known, but also knowledge about the transformation of the waves and penetration of wave energy into the area of interest is gathered. The four locations near the area of interest are shown in Figure 3.7. Forming the only known data set of this kind for the Dithmarschen Bight, the following procedure has been applied for the model evaluation.

From the covered measurement period, five one-day periods with varying conditions have been selected for the calibration. After the optimal set-up and both physical and numerical parameters have been determined, the entire period has been modelled for the model validation. In Figure 3.8, the measured and computed significant wave heights at Pos3 are shown for the validation period. The results at Pos4 an Pos5 show a similar accuracy.

Discussion

As can be seen, the model is able to capture not only the variations of the wave height during the tidal cycle, but also the increasing wave heights during storm events. In some cases there are significant differences between the model results and the measurements. However, these occur mainly during calm conditions where the wave heights are lower than 0.2 to 0.3 m. Considering the complex morphology and highly varying currents, this is within accuracy that can reasonably be expected from the wave model.

Generally, representative wave conditions are imposed in simulations with the morphodynamic model. Therefore, it is more important that approximately the right amount of wave energy is predicted than that the exact time series are reproduced. The model results show that this is the case for the created flow-wave model.

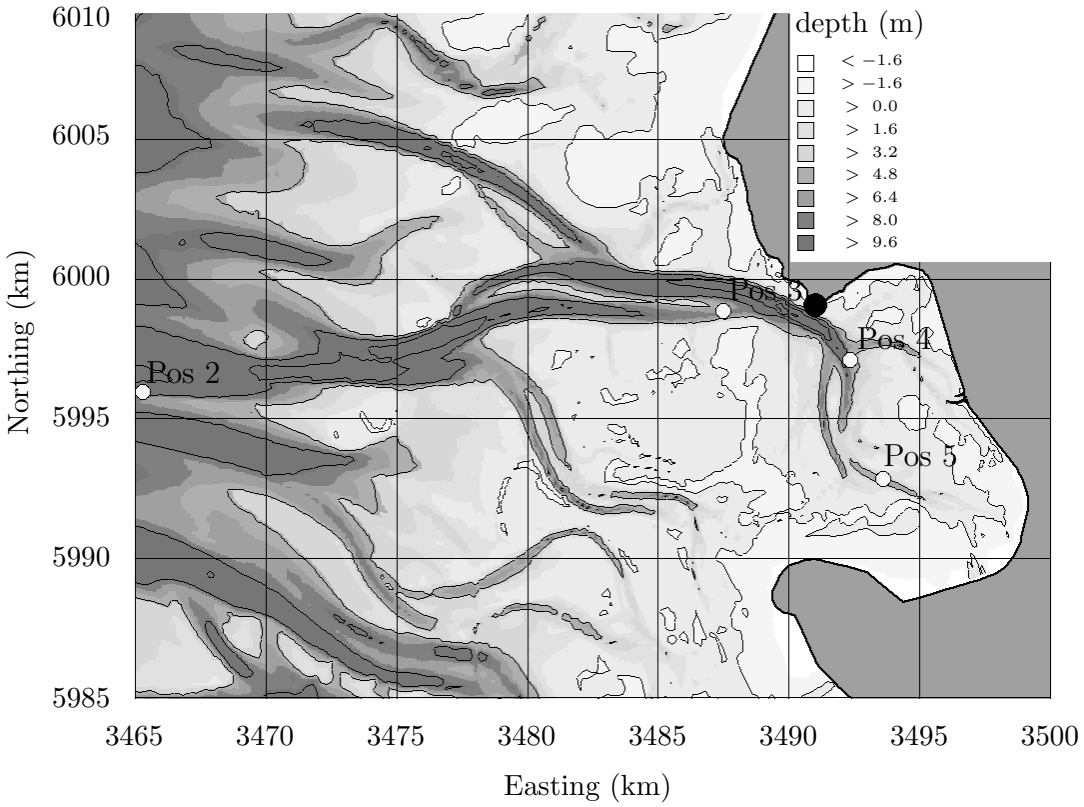

Figure 3.7: Location of the wave buoys.

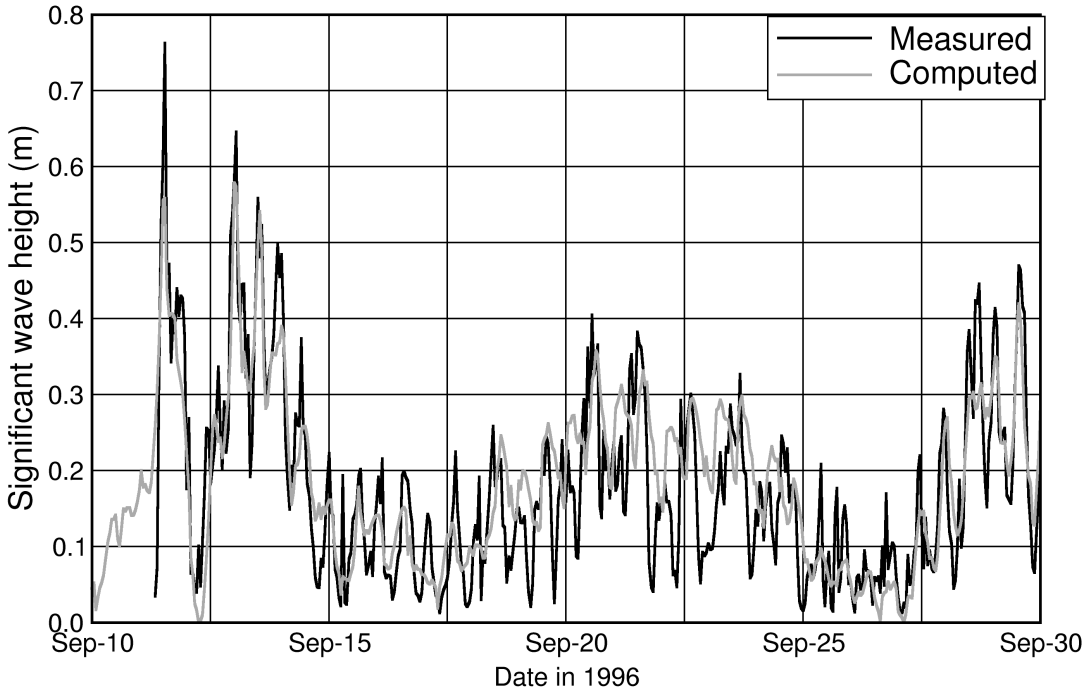

Figure 3.8: Measured and computed significant wave heights at Pos3.

3.5 Sediment transport model

The sediment transport model determines the bed and suspended load transports with a 2Dh-approach on the basis of the time-varying state of the hydrodynamics, as computed by the flow and wave models. The underlying model concepts are described in Paragraph 3.A.4 of Appendix 3.A. The set-up of the sediment transport model, which has been coupled to the flow and wave models for providing the hydrodynamic conditions, is presented in Paragraph 3.5.1. This is followed by the calibration and validation of the model in Paragraph 3.5.2.

3.5.1 Sediment transport model set-up

The sediment transport model is coupled to the hydrodynamic models that provide the hydrodynamic conditions. The main characteristics of the set-up of the sediment transport model are discussed in the following Paragraphs.

Selection of the sediment transport formula

One of the most important decisions to be taken when setting-up a sediment transport model is the selection of the sediment transport formula. Within the Delft3D-MOR sediment transport module various formulae are available. Their applicability depends on the processes taken into account by the formulae and their numerical stability to ensure proper sediment transport and morphodynamic simulations.

From an initial model study it has been seen that the amount of suspended load sediment transport is the main transport mode in the central Dithmarschen Bight [Wilkens *et al.*, 2001]. Furthermore, it showed that the wave action plays an important role in the sediment dynamics, especially in the western part of the area. One of the - in Delft3D included - sediment transport formulae, that takes account for suspended load sediment transport as well as wave influences, is the Bijker formula [Bijker, 1971]. Based on the high stability of the sediment transport and morphodynamic computations with this formula and the results of the calibration and validation (see Paragraph 3.5.2), this formula has been applied exclusively for the sediment transport calculations in this study.

Model grid

The underlying model grid for the sediment transport model is identical to the flow model grid. It therefore retrieves the necessary information about the water levels and current velocities without any interpolation steps from the flow model. Since the wave model is based on a coarsened version, the wave information is interpolated, to yield data for each computational cell of the transport model grid. A sensitivity analysis showed that this approach does not have a significant influence on the morphodynamic model results.

Boundary conditions

Similar to the flow and wave models, boundary conditions need to be specified to represent the sediment fluxes across the open boundaries. The lack of accurate data caused the need for theoretically defined conditions.

For the bed load transport the boundary condition can be defined by prescribing the time-dependent bed load or total load transport or by defining the time-dependent bed level changes. No accurate data about these quantities are available from measurements at the needed time scale. Therefore the bed level at the boundary has been defined as constant in time. This approach introduces an effect on the morphological development of the model domain. However, since the open boundaries have been located far away from the area of interest, this is acceptable.

Since the suspended load transport is accounted for separately, a boundary condition has to be specified for the suspended sediment flux as well. In the here-described model these conditions have been defined as follows. During inflow conditions, the local equilibrium concentration is imposed and for outflow conditions the computed local concentration of the upstream grid cell is specified.

The initial model study of the morphodynamics showed that a distance of circa 5 km between the open boundaries and the area of interest is sufficient for modelling periods of up to 5 years. For the underlying model, this distance measures at least 12 km. The open boundaries are therefore considered to be sufficiently remote for modelling periods up to 10 years.

3.5.2 Sediment transport model validation

The modelling of the bed and suspended load sediment transport in the study area has been the topic of several studies, e.g. Winter & Mayerle [2003]; Poerbandono [2003]. The results of these studies served as a basis for the settings of the sediment transport model for the Dithmarschen Bight, and are presented below.

Meldorf Bight sediment transport model by Winter & Mayerle [2003]

Winter & Mayerle [2003] present the set-up and calibration of a sediment transport model, coupled to a depth-averaged hydrodynamic model accounting for tidal flow and local wave action. The model has been set-up within the Delft3D modelling system. The HISWA wave model has been applied. The bed load and suspended load sediment transports were accounted for separately, where both the formulae of Bijker [1971] and Van Rijn [1984] were evaluated. The presence of the layer of consolidated cohesive sediments (see Section 2.6) was not accounted for.

The calibration took place on the basis of measurements of current velocities and suspended sediment concentrations along three channel cross-sections, as shown in Figure 3.9. For each of the cross-sections, measurements have been made over a full tidal

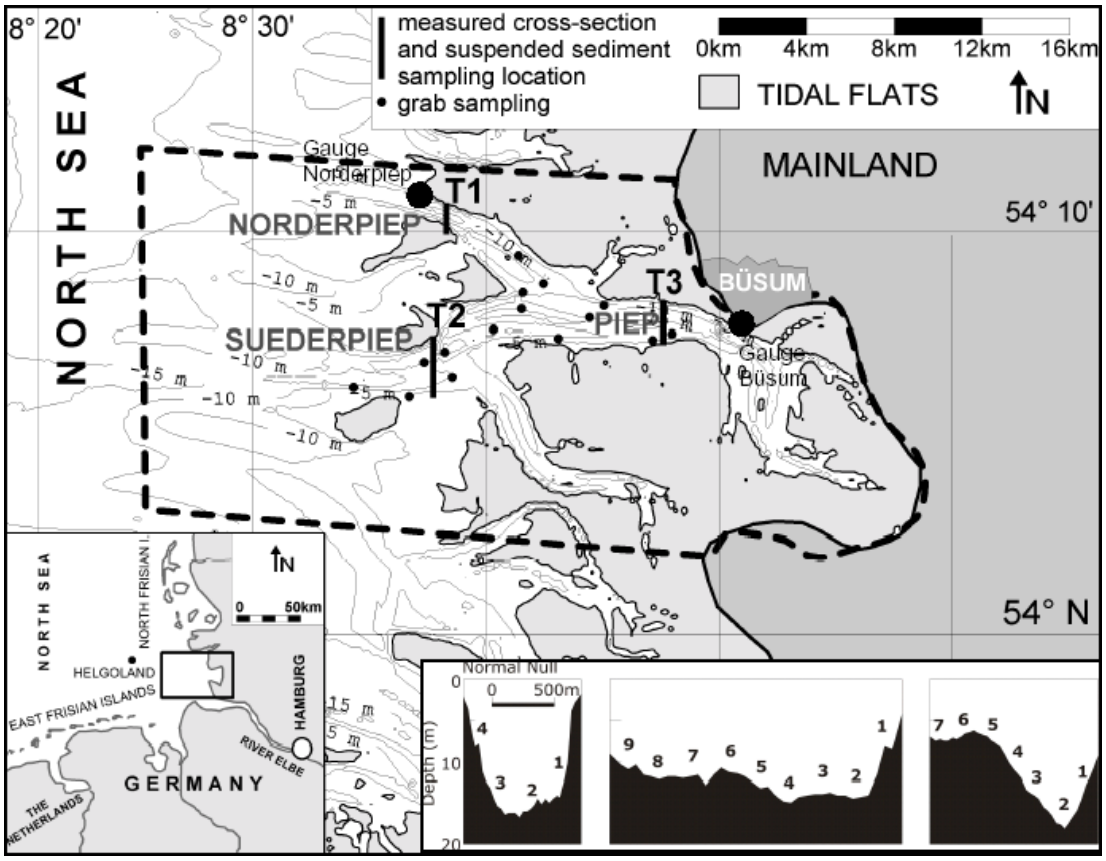

Figure 3.9: Model domain (dashed line) and location of the channel cross-sections, along which the current velocity and suspended sediment measurements were carried out [Winter & Mayerle, 2003]. In the bottom-right the depth profiles along the cross-sections are depicted, together with the locations of the sediment concentration measurements.

cycle during calm weather conditions, resulting in a complete overview of the variations of the tidal flow and sediment transport characteristics.

The applied tidal flow model has been based on the previously described validation by Palacio [2002] and Mayerle & Palacio [2002]. Winter & Mayerle [2003] report that the water levels are reproduced with a discrepancy between 3 and 10 % of the maximum tidal range of 3.6 to 3.9 m. Differences between the modelled and measured flow velocities at the three cross-sections are less than 0.3 m/s.

From simulations of the wave-induced currents the authors concluded that the influence of locally-generated wind waves on the currents is moderate on the tidal flats and negligible in the tidal channels for the modelled (calm) period.

Based on the statistical evaluation parameter RMAE (Relative Mean Absolute Error), as proposed by Van Rijn *et al.* [2002b], the model has been calibrated to obtain optimal values for selected input parameters, e.g. the median grain size and the settling velocity. Although these parameters were imposed uniformly, it has been concluded that the observed characteristics of the sediment transport could be reproduced reasonably

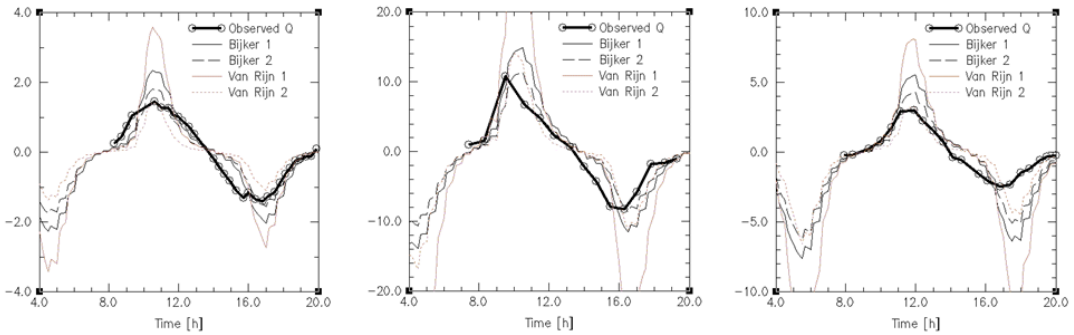

Figure 3.10: Observed and computed suspended sediment load (10^3 kg/s) for varying settings in the sediment transport calculation at cross-sections T1, T2 and T3 [Winter & Mayerle, 2003].

well, apart from too high concentrations during the flood phase at cross-section T2 (see Figure 3.9 for its location). Exemplarily, the observed and computed suspended sediment loads during a tidal cycle are shown for the three examined cross-sections in Figure 3.10. Both optimised sediment transport formulations show their capability to follow the observations. The optimised Bijker formulation – Bijker 2 in Figure 3.10) – showed the best results.

Sediment transport modelling by Poerbandono [2003]

The calibration by Winter & Mayerle has been extended by Poerbandono, who added two data sets which each cover approximately a tidal cycle. The same three channel cross-sections have been considered, as shown in Figure 3.9. After the extended calibration, the model has been validated with two further data sets. The current and suspended matter measurements could only be carried out during calm weather conditions, due to the vessel size and requirements for the applied devices. Thus, the calibration is limited to these conditions. Wave effects on the currents and on the sediment transport have been ignored, which were assumed to be acceptable for the considered calm periods. The presence of the layer of consolidated cohesive sediments (Section 2.6) was not considered.

The validation showed that the sediment transport calculations on the basis of the Bijker [1971] formula performed slightly better than the Van Rijn [1984] formula. Exemplarily, the computed total loads are shown for several data sets for the three cross-sections in Figure 3.11.

Poerbandono & Mayerle conclude that for cross-section T1 the results agree quite well with the observations, although a time lag of approximately 1 hour can be observed. At cross-sections T2 and T3, the sediment loads tend to be somewhat underestimated and time lags reach up to 90 minutes. Circa 50 % of the data lie within a factor two of the observed values for the Bijker formula.

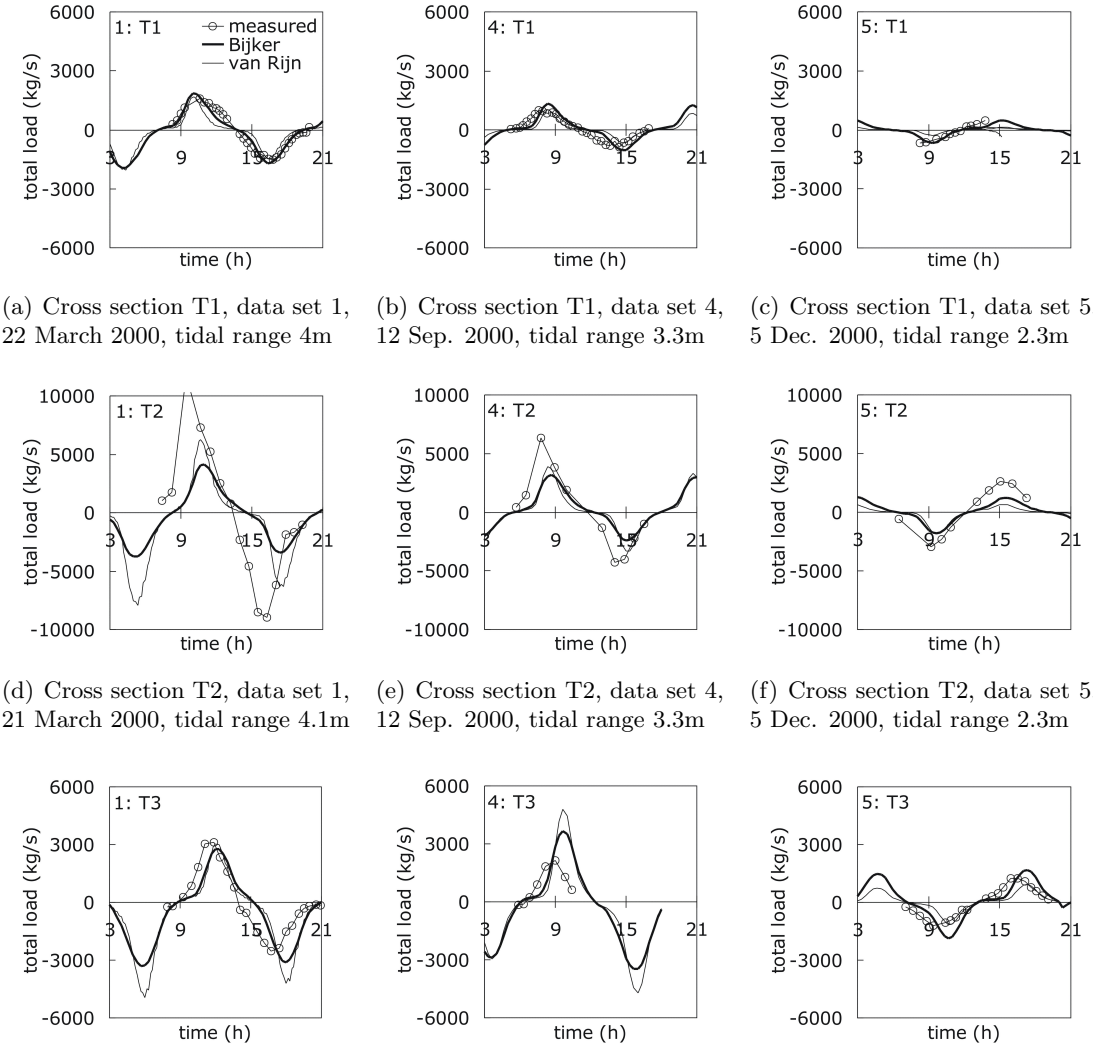

(a) Cross section T1, data set 1, 22 March 2000, tidal range 4m

(b) Cross section T1, data set 4, 12 Sep. 2000, tidal range 3.3m

(c) Cross section T1, data set 5, 5 Dec. 2000, tidal range 2.3m

(d) Cross section T2, data set 1, 21 March 2000, tidal range 4.1m

(e) Cross section T2, data set 4, 12 Sep. 2000, tidal range 3.3m

(f) Cross section T2, data set 5, 5 Dec. 2000, tidal range 2.3m

(g) Cross section T3, data set 1, 23 March 2000, tidal range 4.2m

(h) Cross section T3, data set 4, 13 Sep. 2000, tidal range 3.5m

(i) Cross section T3, data set 5, 6 Dec. 2000, tidal range 2.5m

Figure 3.11: Observed and computed suspended sediment load (kg/s) for several data sets at cross-sections T1, T2 and T3 [Poerbandono & Mayerle, 2003].

Discussion

The calibration and validation of the sediment transport model took place on the basis of a vast amount of observations. Since the measurements have been carried out from research vessels, they are limited to the tidal channels that ensure a sufficient draught. Therefore, no evaluation of the model results could be made for the shallower areas, i.e. near the channel banks and on the tidal flats. Furthermore, the measurements are limited to calm weather conditions, since strong wave action and high local currents did not allow measurements during rough conditions.

Nevertheless, an extensive data set has been collected, yielding an extensive insight in the sediment dynamics of the main tidal channels. The applied sediment transport model could be significantly improved on their basis.

Winter & Mayerle [2003] concluded that for the considered calm periods the effects of the relatively low locally generated waves on the computed suspended sediment concentrations are insignificant. The effect of swell wave energy has not been investigated in this study.

From Wilkens & Mayerle [2002] it is known that swell waves generally break on the outer tidal flats. A sensitivity analysis showed that limited swell (0.5 m wave height at the western open boundary) induces circa 5 % larger sediment concentrations during flood conditions at the edge of the tidal flat Tertiussand and no significant changes in the concentrations along the rest of the cross-section. This confirms the correctness of the assumption by Winter & Mayerle [2003] that waves are of negligible importance during calm conditions.

As can be seen from the results of the subsequent study by Poerbandono & Mayerle [2003], as shown in Figure 3.11, the percentage of data within a factor two of the observed values would increase when the phase lag is absent. Since the tidally averaged sediment loads are used for morphodynamic modelling, the results of the sediment transport validation are of acceptable quality for this purpose.

The presence of the consolidated cohesive sediments has been ignored in both studies. The size of the areas where this layer may influence the sediment transports is relatively small with respect to the medium scale at which the simulations were made. When considering a smaller scale the effects of these areas on the sediment transports may become of increasing importance. Since the underlying study focuses on the medium scale the influence of this layer has not been further investigated.

Although both studies have been based on uniform settings of the considered parameters, i.e. a uniform d_{50} of 100 μm and d_{90} of 150 μm and k_s of 0.2 m, the model showed the ability to represent the observed conditions at the evaluated cross-sections rather well. A non-uniform approach is expected to further improve the results. However, this should be based on realistic assumptions with respect to the horizontal variations and would require a huge and prohibitively expensive increase of the needed measurement activities when carried out for the entire area. On the basis of the available data which already give a very good insight in the local conditions throughout the area, it can be concluded that optimal settings for the coupled sediment transport model have been determined in a proper manner. These settings have been adopted for the sediment transport model for the entire Dithmarschen Bight.

3.6 Discussion

As described in the previous Sections, each of the process models has been calibrated and validated and it is therefore assumed that they represent the dominating physical processes in a correct manner. The validation of the flow and sediment transport mod-

els is limited to calm wind and wave conditions, due to the lack of data for more severe situations. The considered validation period for the wave model includes two storm events as well as the in-between calm periods.

The individual process models have been coupled to create a morphodynamic model for the central Dithmarschen Bight, as discussed in Chapter 4. Considering on the extensive evaluation of the individual models this yields a very good basis for the morphodynamic modelling.

3.A Delft3D-MOR modelling system

3.A.1 Introduction

The morphological components of the Delft3D modelling system[1] are described in this Appendix. For more detailed information is referred to Roelvink & Van Banning [1994] and Roelvink *et al.* [1994] as well as to the Delft3D user manuals (see WL | Delft Hydraulics, 2003a,b,c).

The morphological components of the modelling system, combined referred to as Delft2D-MOR, include modules for simulating currents, waves, bed load and suspended load sediment transports, and morphological development. Exchange of the results of each of these individual models ensures the representation of the various interactions between the simulated physical processes, e.g. wave-induced currents.

Each of the modules and their basic concepts are described in the following Paragraphs.

3.A.2 Flow

The flow module can be applied to simulate the non-steady flow conditions in coastal areas. It takes both tidal and meteorological forcing into account and, coupled to the wave module, also includes wave-induced changes in the flow conditions. Stratification due to salinity and temperature variations can be accounted for. Drying and flooding of tidal flats can be represented as well.

The model can be applied with both a two- and a three-dimensional approach. Within this study the two-dimensional, depth-averaged approach has been applied and is therefore considered exclusively hereafter.

Basic equations

The 2Dh flow model solves the instationary shallow-water equations. The assumptions of incompressible fluid and hydrostatic pressure are made.

These equations are solved by a finite difference method on a rectilinear or curvilinear grid. The grid is a so-called *staggered grid*, where the water levels are solved for the middle of the grid cells and the velocity components on the cells sides, whereas the depth is specified at the cell vertices. This allows an easy implementation of boundary conditions and needs less discrete variables than a non-staggered grid. The geographic space is defined in (ξ, η) co-ordinates along the grid.

The applied numerical scheme is an *alternating direction implicit* (ADI) scheme. The main advantage of the resulting semi-implicit scheme is that a relatively large time step can be applied which is limited by the grid spacing and the Courant number, as

[1] Delft3D has been developed by Delft Hydraulics in the Netherlands.

follows:

$$Cr = 2\Delta t\sqrt{gH}\sqrt{\frac{1}{\Delta x^2} + \frac{1}{\Delta y^2}} < 10 \tag{3.1}$$

with:

Cr	Courant-Friedrich-Levy number
Δt	time step
g	gravitational acceleration
h	water depth
Δx	grid cell size in x-direction
Δy	grid cell size in y-direction

Boundary conditions

Along the open boundaries, i.e. the boundaries where water can freely enter or leave the model domain, boundary conditions have to be prescribed. For inflow, two conditions need to be defined, for outflow only one. Within the flow model, the one, permanently needed boundary conditions is to be specified, whereas the second inflow condition is internally defined. The permanent condition may be defined as water level, velocity, discharge or partially reflective boundary conditions (Riemann invariants).

The internal condition is defined by prescribing a zero-velocity component *along* the boundary. This implicates that diagonally (with respect to the open boundary) inflowing water is represented by the perpendicularly component only. When defining the open boundaries approximately perpendicular to the main inflowing currents and keeping them well away from the area of interest, this approach functions satisfactory.

Along the closed boundaries, representing the natural *land-water* boundaries, two boundary conditions are imposed. Obviously, the normal velocity is set to zero, to prevent any flow across this boundary. This is done internally by the flow model. The second boundary condition concerns the shear stress along the boundary. This is either set to zero, as usually the case for mild-slope coastlines, or as a partial slip boundary, to represent the retarding effect of for example a vertical quay or flume wall.

Drying and flooding

The computational domain, limited by the afore-mentioned boundaries, may be reduced due to the presence of dry cells. Dry cells are grid cells in which the bottom level is higher than the instantaneous water level. During each time step, the model determines if a cell is either in- or excluded in/from the hydrodynamic computation.

Turbulence closure

Since the applied model grid is generally too coarse and the time step too large to resolve turbulent processes, these should be represented by a parametrisation. Since the flow

model does not contain such a parametrisation, the turbulence has to be represented by the values of the horizontal viscosity and eddy diffusivity coefficients ν_{2Dh} and D_h. They depend on the grid size and can be specified as space-varying.

Spiral flow

Although spiral flow in the bend of a river or tidal channel cannot be resolved by a 2Dh model, it can be included indirectly. This is done by extending the depth-averaged momentum equations and the continuity equation. An advection-diffusion equation is added to take account for the generation and adaptation of the spiral flow intensity.

Wave-current interaction

The wave-induced effects on the currents are included in the momentum equations through additional terms. There are two approaches available for the calculation of these quantities. The first is based on the use of the radiation stresses, the second on the wave energy dissipation, as proposed by Dingemans *et al.* [1987].

3.A.3 Waves

The Delft3D system offers the application of two wave models. The first wave model is the second-generation HISWA wave model[2] (see Holthuijsen *et al.* [1989]), the second the third-generation SWAN model[6] (see Ris *et al.* [1999]; Booij *et al.* [1999]. Within this study the SWAN model has been applied for both physical and numerical reasons.

With respect to the physical representation there are two advantages of SWAN over HISWA. Firstly, SWAN incorporates the state-of-the-art formulations, whereas HISWA is based on highly parameterised formulations. Secondly, SWAN is fully spectral in frequency and direction where HISWA is parameterised in the frequency domain.

There are three numerical reasons to use the SWAN instead of the HISWA model. The first is that the SWAN model is not limited to a directional sector, where HISWA is. Secondly, the HISWA model grid(s) should be oriented in the mean wave direction - for SWAN there is no such restriction. And thirdly, SWAN simulations can be made on the basis of a curvilinear grid, whereas HISWA is limited to rectilinear grids. Thus, SWAN simulation can be made on the basis of the flow model grid (which is curvilinear in this study) and therefore prevents inaccuracy-incurring interpolations.

In the following only the - in Delft3D incorporated - SWAN model will be described. The SWAN model can be applied to simulate the evolution of random, short-crested, wind-generated waves in coastal areas. The model is fully spectral, implying that random wave fields propagating from different directions can be simulated, e.g. locally generated waves from one direction and incoming (through the open boundaries) from another direction. The evolution is calculated by taking local current conditions into

[2]The HISWA and SWAN wave models have been developed at the Technical University of Delft, the Netherlands

consideration. The model accounts for refraction, wave generation by a local wind, and dissipation due to bottom friction, depth-induced wave breaking, whitecapping and non-linear wave-wave interactions, as well as wave blocking due to opposing currents.

Basic equations

The wave model is based on the two-dimensional wave action density spectrum $N(\sigma,\theta)$, where σ denotes the relative frequency and θ the wave direction. The action density is equal to the energy density divided by the relative frequency:

$$N(\sigma,\theta) = \frac{E(\sigma,\theta)}{\sigma} \tag{3.2}$$

with:

$N(\sigma,\theta)$	spectral wave action density
σ	relative wave frequency
θ	wave direction
$E(\sigma,\theta)$	spectral wave energy density

On Cartesian co-ordinates, the spectral action balance equation is written as:

$$\frac{\delta N}{\delta t} + \frac{\delta c_x N}{\delta x} + \frac{\delta c_y N}{\delta y} + \frac{\delta c_\sigma N}{\delta \sigma} + \frac{\delta c_\theta N}{\delta \theta} = \frac{S}{\sigma} \tag{3.3}$$

with:

$c_x, c_y, c_\sigma, c_\theta$	propagation velocities in x-, y-, σ- and θ-space
S	source term

The equation balances the rate of change of action density in time, the propagation in x- and y- space, and the shifting to different relative frequency and direction to the source term on the right-hand side. The generation and dissipation of wave energy are represented by this source term. The definition of the source term based on the generation and dissipation is given by:

$$S = S_{in}(\sigma,\theta) + S_{ds,b}(\sigma,\theta) + S_{ds,br}(\sigma,\theta) + S_{ds,w}(\sigma,\theta) \tag{3.4}$$

with:

$S_{in}(\sigma,\theta)$	source term for wind generation
$S_{ds,b}(\sigma,\theta)$	source term for dissipation through bottom friction
$S_{ds,br}(\sigma,\theta)$	source term for dissipation through wave breaking
$S_{ds,w}(\sigma,\theta)$	source term for dissipation through white-capping

For the definition of these source terms and for non-linear wave-wave interactions is referred to Ris *et al.* [1999]; WL | Delft Hydraulics [2003b].

Numerical solving method

The integration of the action balance equation has been implemented in SWAN with finite difference schemes in all five dimensions (time, geographic space and spectral space). In Delft3D, SWAN is applied in a stationary mode so that time has been omitted from the equations. The geographic space can be either in (x,y) or in (ξ, η) coordinates, dependent on the character of the model grid (i.e. rectilinear or curvilinear).

In geographic space the discretisation is based on the underlying grid; in spectral space a user-defined, constant directional resolution and constant relative frequency resolution are used.

Boundary conditions

Wave boundary conditions may be specified at up to four sides of the model grid. The conditions of these incoming waves (swell) may be specified by representative wave parameters (i.e. significant wave height H_s, peak period T_p, mean direction and energy width distribution), together with a predefined wave spectrum shape, e.g. the JONSWAP spectrum. An other possibility is to provide an exact wave spectrum, which for example has been obtained from wave measurements.

Current-wave interaction

The results from the previously described flow model may be included in the wave simulations, to take account for the effects of changing water level and current conditions on the waves. This is especially important in shallow-water areas, where the relative change of the total water depth as well as the current velocities can be rather high. In coupled simulations, the model bathymetry can be read from the flow model, so ensure equal depths in both models.

3.A.4 Sediment transport

The Delft3D sediment transport model uses the results of the flow and, optionally, the wave model to compute the two-dimensional, depth-averaged bed load and suspended load sediment transports. The model can be applied in (1) total mode, in which an algebraic total load sediment transport relation is applied, in (2) suspended mode, in which the suspended load transport is modelled with an advection-diffusion equation in addition to the algebraic relation for the total load transport, or in (3) silt mode which includes the advection-diffusion equation only.

The sediment transport model uses the time-dependent results from the flow and wave models, together with the bathymetry of the flow model. After calculating the sediment transport for a user-defined simulation period and time step it also determines the time-averaged transport for a given sub-period of the simulation period, to be used for the calculation of the new bathymetry (see Paragraph 3.A.5).

Retardation (lagging) of the sediment concentration is important in tidal flat areas with relatively high gradients in the current velocities and small grain sizes, having low settling velocities. Therefore the adaptation lengths scale of the suspended sediment transport can be considerably larger than the spatial scale of the velocity gradients. This leads to differences between the equilibrium concentration and the local concentration, which can only be correctly represented by inclusion of the advection-diffusion equation.

The suspended mode model is able to calculate the local sediment concentrations, by taking the conditions of the surrounding area into account whereas the total model only considers the local conditions. Considering the above, the suspended mode has been applied in the underlying study.

Basic equations

Within this study the equation of Bijker [1971] has been applied. Within Delft3D it can be applied for calculation of total load and suspended load transports. Furthermore, the effect of waves on the sediment transport is represented in this formulation, which is especially important for the exposed tidal flats. Within this model, the calculated total sediment transport rate can be corrected for bed slope effects and the effects of the presence of a non-erodible layer.

Following Bijker [1971], the bed load sediment transport S_b is defined as:

$$S_b = bd_{50}\frac{U}{C}\sqrt{g}exp\left\{-0.27\frac{\Delta d_{50}\rho_w g}{\mu\tau_{cw}}\right\} \tag{3.5}$$

with:

b	Bijker calibration constant (range: 1-5)
d_{50}	median grain size
U	horizontal flow velocity magnitude
C	Chézy bottom roughness coefficient
g	gravitational acceleration
Δ	relative density $(\rho_s - \rho_w)/\rho_w$
ρ_w	density of the water
ρ_s	density of the sediment
μ	ripple factor $\left(\frac{C}{18log_{10}(12h/d_{90})}\right)^{1.5}$
h	water depth
d_{90}	90^{th} percentile of the sediment grain size distribution
τ_{cw}	combined current- and wave-induced bed shear stress

The suspended load sediment transport calculation by Bijker [1971] follows from:

$$S_s = 1.83 S_b \left\{ I_1 ln(\frac{33h}{r_c}) + I_2 \right\} \tag{3.6}$$

with:

S_s	Suspended load sediment transport
I_1, I_2	Einstein integrals, functions of the relative bottom roughness r_c/h
r_c	bed roughness height for currents

The median sediment grain size can be defined spatially varying over the model domain. However, a time-varying approach is not included in the sediment transport model. Therefore, the model does not record where sediments with a certain grain size are transported to. Furthermore, a grain size distribution (sieve curve) can not be specified. Double-peaked sediment grain size distributions can therefore not be represented accurately.

When applied in suspended mode, the calculated suspended sediment transport is used to calculate the equilibrium concentration. This concentration is then entered as the bed boundary condition into the depth-averaged advection-diffusion equation, which is subsequently solved for the suspended sediment concentration.

The effects of the bed gradients on the total sediment transport are included by multiplication of the determined transport with an adaption factor.

A non-erodible sea bed or layer underneath an erodible sea bed can be represented by the model. The presence of such a layer will reduce the amount of sediment transport in the model. The depth of the layer has to be specified after which the model computes the relative thickness of the surfacing erodible layer. Based on the relative thickness, a fixed layer reduction factor for the computed sediment transport is determined.

Due to the applied formulations, for a certain erodible layer thickness on top of a non-erodible layer, an increase in total water depth will decrease the effect of the non-erodible layer on the sediment transport rate. When the erodible layer thickness is less than the total water depth multiplied by a user-defined factor, the sediment transport will be reduced.

Boundary conditions

At the open boundaries, i.e. the boundaries through which sediment transport is possible, boundary conditions have to be defined. The sediment transport model offers three possibilities for imposing boundary conditions in suspended mode. In the first two cases the bed load transport rate or total load transport rate have to be specified, together with a condition to determine the suspended load transport rate. For the third option the bed level has to be specified in combination with a condition for specifying the suspended load transport rate.

In this study the third option has been applied by setting the bed level constant. This implies that no changes will occur in the morphology directly at the open boundaries. When these open boundaries are far away from the domain of interest, this is considered acceptable. Furthermore, the definition of the suspended load sediment transport rate in case of inflow has been based on the equilibrium concentration, as calculated by the algebraic equation. In the case of outflow, the upstream concentration is used.

3.A.5 Morphological evolution

The development of the bathymetry is determined by solving the continuity equation for the bed level. The components for the bed load and suspended load sediment transports are averaged sediment transports over a user-defined sub-period of the sediment transport simulation period. The so-determined bed level change rate can be multiplied by a certain period to get an estimation of the morphological changes over this period.

Due to the applied explicit discretisation scheme FTCS (Forward in Time, Centred in Space), this period is limited by the Courant-Friedrich-Levy criterion (CFL-criterion) and the total sediment transport rates. The Courant number for the bed Cr_{bed} should stay below 1 for stability reasons and is determined by:

$$Cr_{bed} = c_{bed}\frac{\Delta t_{bed,max}}{\Delta s} \leq 1 \tag{3.7}$$

with:

Cr_{bed}	Courant number for the bed
c_{bed}	bed celerity
$\Delta t_{bed,max}$	maximal time step for bed evolution calculation
Δs	local grid cell size, depending on the sediment transport direction

The value of Δs is determined by the local sediment transport direction and the local dimensions of the grid cell. Several formulations for calculating the local bed celerity are available. Based on the calculated time-averaged total sediment transports and the determined optimal time step, the changes in the bathymetry can be calculated. This results in the determination of a new bathymetry, which subsequently can be passed on to the other modules for continuation of the simulation.

3.A.6 Time management of the modules

To combine the individual process modules into a user-defined sequence for simulation of the morphodynamic processes, the main module of Delft2D-MOR can be used. This module allows the user to set-up a *model tree* in which the to be included modules are defined, together with a set of rules for the module simulation periods and number of repetitions.

The exchange of model results takes place over a set of general result files in which all mutually used parameters and data are stored.

Continuity update

An especially useful option is the possibility of a so-called *continuity update*. Instead of using the velocity fields calculated by the hydrodynamic modules directly, the discharge fields together with the actual total water depth are used. From these quantities the local velocities are calculated as:

$$\begin{aligned} u &= q_\xi/(d+\zeta) \\ v &= q_\eta/(d+\zeta) \end{aligned} \tag{3.8}$$

with:

u	depth-averaged flow velocity in ξ-direction
v	depth-averaged flow velocity in η-direction
q_ξ	discharge in ξ-direction per unit of width
q_η	discharge in η-direction per unit of width
d	water depth with respect to MSL (pos. downward)
ζ	water level with respect to MSL (pos. upward)

After the calculation of the sediment transport rates and the update bathymetry, the same discharge values are entered in the equations above, together with the updated depths. This way an adapted velocity field is determined for each time step without making a new hydrodynamic computation. The latter is by far the most expensive part of a morphodynamic simulation in terms of computing time and therefore the continuity update significantly reduces the calculation time of a morphodynamic simulation.

The continuity update can only be applied as long as the assumption holds that the determined bathymetric changes do not cause large changes in the horizontal velocity patterns in the model domain. The user can determine the criterion for allowing a continuity update or making a new hydrodynamic computation. This can be either a fixed number of continuity updates or a maximum allowable change of, for example, the bed level.

In general, the application of the continuity update significantly enhances the speed of morphodynamic simulations without a large loss of accuracy.

Chapter 4

The Dithmarschen Bight morphodynamic model

4.1 Introduction

To increase the understanding of the physical processes underlying the morphological development of the central Dithmarschen Bight, a morphodynamic model has been created. It has been based on the widely-used approach of complex numerical modelling, where individual models for the driving forces, i.e. tides and wave action, are coupled to a sediment transport model.

In the previous Chapter, the individual process models have been presented. The described calibration and validation of these models showed their capability of reproducing the observed characteristics of the physical processes in a good manner. The optimal settings of these evaluations have been adopted for the set-up of the coupled morphodynamic model. In this way an optimal basis for modelling the medium scale morphological evolution of the domain is achieved.

In Section 4.2, an overview of the basic model concepts of morphodynamic modelling is presented. A differentiation is made between Initial Sedimentation and Erosion (ISE) models, Medium Term Morphodynamic (MTM) models and Long Term Morphodynamic (LTM) models. The first two include the use of individual process models, whereas in the latter they are not. In ISE-models the morphological changes over a limited period of time are computed without back coupling of these changes to the hydrodynamic and sediment transport models. When the morphological changes are fed back to these models, thus including two-way interaction, the model is called a MTM-model. Due to the included interaction much larger periods in time can be simulated realistically. In this study the ISE-approach has been adopted for the sensitivity analyses, whereas the MTM-approach has been applied for the hindcasting and forecasting of the morphological evolution of the study area.

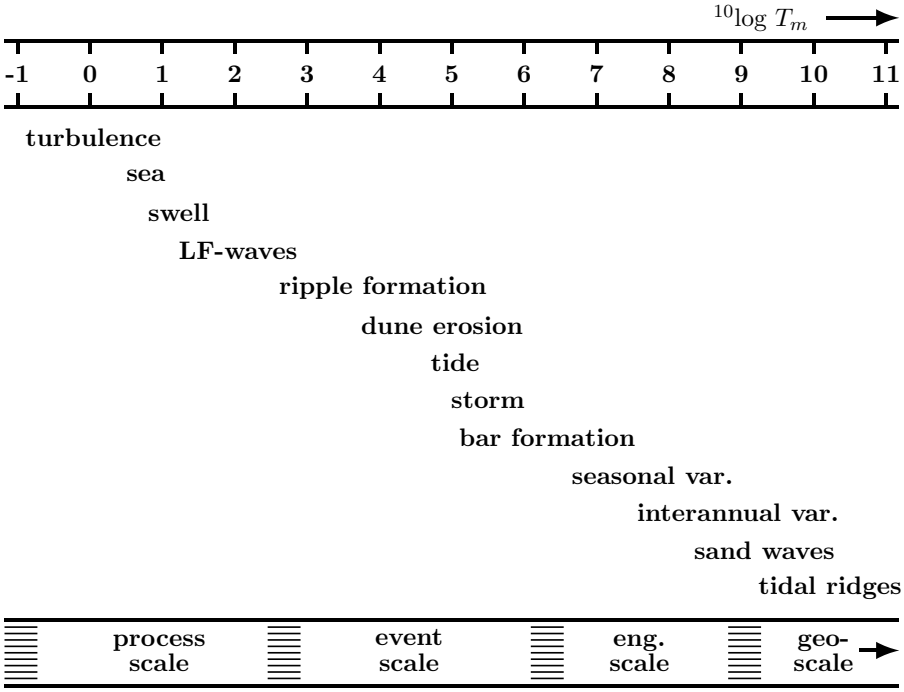

Figure 4.1: Scale range in coastal morphology (morphological time scale T_m in seconds). After [De Vriend, 1997].

In this study short term is defined as several days and medium term as a period of up to 10 years. The scale of the considered morphodynamic changes is related to the considered time span [De Vriend, 1997], as shown in Figure 4.1. On the short term the small scale effects of tides and storms are considered. On the medium term the morphological changes are considered in terms of the evolution of channels, tidal ridges, shoals and tidal flats.

The coupling of the individual models into the morphodynamic model is discussed in Section 4.3. The process models are driven by specified open boundaries and coupled to a model for calculation of the morphological changes over the considered period of ten years. The specification of the boundary conditions for tidal flow, wind, swell and sediment transports is the topic of Section 4.4.

To assess the sensitivity of the morphodynamic model to the defined conditions, a hindcast study of a real storm has been carried out. This is described in Appendix 4.A. Furthermore, a comparison has been made between the application of representative tidal conditions and a full neap-spring tidal cycle. This study is presented in Appendix 4.B.

4.2 Model concepts for coastal area modelling

As stated by De Vriend *et al.* [1993a], the combined individual process models constitute a new system. This system forms a new model and, subsequently, the phases

of sensitivity analysis and model evaluation should be carried out anew. The combined individual process models can be applied in three ways, schematically shown in Figure 4.2:

- ISE-model – Initial Sedimentation / Erosion model;
- MTM-model – Medium-Term Morphodynamic model;
- LTM-model – Long-Term Morphological model.

The sequence in the left column shows the initial bathymetry and constituent process models, together building an ISE-model. When the bathymetry is updated by the time stepping mechanism on the basis of the sediment balance and subsequently re-entered in the process models, an MTM-model is formed. Instead of time-stepping, the processes can be temporally integrated to build an LTM-model. Based on De Vriend *et al.* [1993a], these models can be described as follows.

ISE-models

Within an ISE-model, the sediment balance for each grid cell is determined from the computed sediment transports, that are based on the calculated wave and current velocity characteristics. No updating of the bathymetry occurs. This type of model can therefore only yield information at a time scale that is much smaller than the morphological time scale [De Vriend *et al.*, 1993b], typically one or two tidal cycles. However, it does provide information on the reaction of the morphology to the specified settings and imposed conditions.

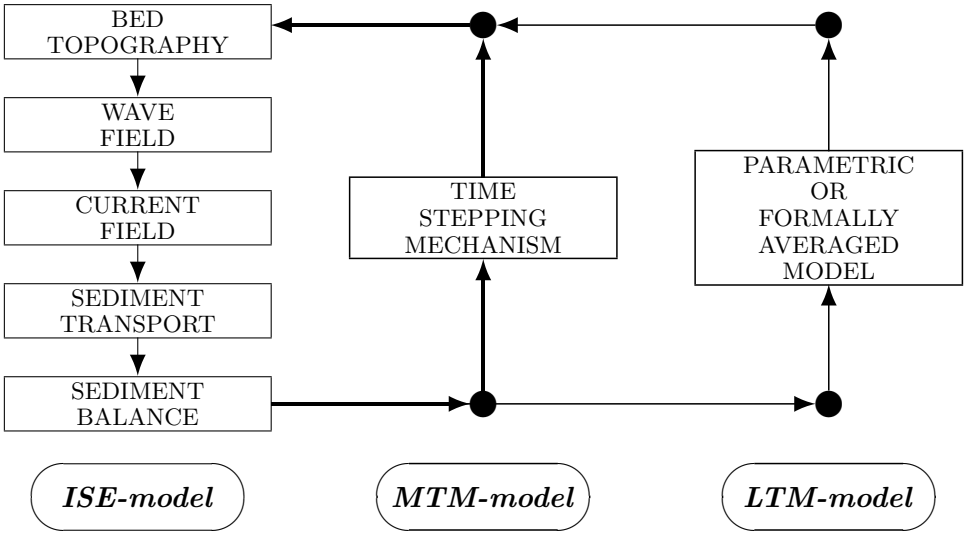

Figure 4.2: Compound morphological model concepts, adapted after De Vriend *et al.* [1993b].

MTM-models

When the dynamics of the morphology over a longer time scale are to be considered, the short-term approach of the ISE-model no longer holds. The non-linear interactions between the bathymetric changes on the one hand and the hydro- and sediment dynamics on the other have to be taken into account by updating the bathymetry. The time stepping mechanism in these MTM-models is the algorithm that controls this updating.

LTM-models

On an even larger scale, the LTM-models can be applied. In this type of model the underlying equations describe the morphodynamics in an integrated manner instead of on the basis of the process-resolving method of the first two model types.

4.2.1 Applied concepts for the Dithmarschen Bight model

Initially, the created model has been applied in ISE-mode to analyse the sensitivity of the model results to a variety of settings and conditions. Examples of the varied settings are the number of flow-wave iterations, the number of wave calculations per tidal cycle and time interval at which tidal flow information is passed to the sediment transport model. With respect to the conditions, a large number of varying swell, wind and tidal conditions have been considered. This resulted in a good overall understanding of the performance of the model. Furthermore, it gave insight in the sensitivity of the model results to the settings taken from calibration and validation of the individual process models summarised in Chapter 3.

Subsequently, the model has been applied as a MTM-model for the calibration. The MTM-approach as opposed to the ISE-approach is considered here to include the back-coupling of the morphological changes to the hydrodynamics and sediment transports. This allows for longer simulation periods, i.e. in the order of the time scale of medium scale morphodynamics. As described in Section 2.7, bathymetric data are available on a yearly basis with a varying coverage of the area of interest. Furthermore, inaccuracies in the measured data, morphological fluctuations within a single year – which are not investigated in this study – and inaccuracies due to interpolation onto the model grid necessitate to consider periods of several years when comparing the observed and modelled medium scale morphological changes. The MTM-approach requires the imposition of realistic representations of the occurred tidal, wind and wave climates, as well as intermediate morphological updating. To that purpose, the model has been applied in MTM-mode for the model calibration and validation, as presented in Chapter 5, considering a modelling period of about 10 years.

In Chapter 6 the application of the calibrated and validated MTM-model is described. An analysis has been made of the dominant processes for the morphological behaviour, followed by a prediction of the morphological evolution.

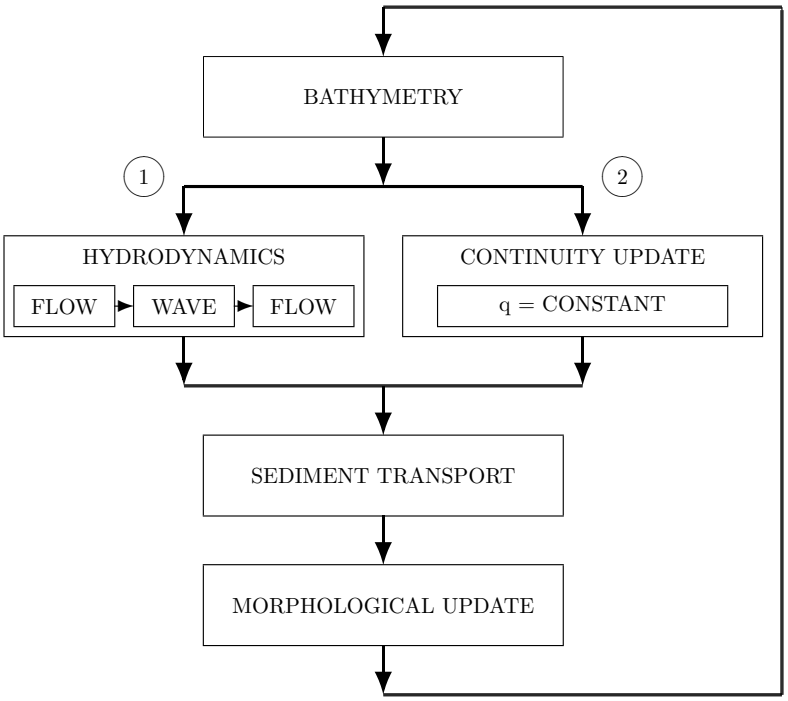

Figure 4.3: Morphological modelling scheme for the Dithmarschen Bight model.

4.3 Set-up of the morphodynamic model

The morphodynamic model is the result of the coupling of the individual process models to each other and to the morphological updating model. Within the Delft3D system, these are linked within a simulation by a main model that imposes the time management (see also Paragraph 3.A.6). The time management prescribes the order of calculation by the constituent models as well as the time stepping mechanism for updating the bathymetry. The here applied modelling scheme is shown in Figure 4.3.

For application of the ISE-model concept, the initial bathymetry is entered into the hydrodynamic process models in *path 1*, followed by the sediment transport computation. On the basis of the tide-averaged sediment transport fields the initial sedimentation and erosion patterns are determined for a short-term period.

In MTM-mode, either *path 1* or *path 2* is taken to determine the hydrodynamics, followed by the computation of the sediment transports and a morphological update. Every 5^{th} loop *path 1* is taken. In either case, the morphological time step, i.e. the period between the initial and updated bathymetry, is not fixed. Instead, the CFL-criterion is applied on the basis of the tide-averaged sediment velocity for each grid cell. This results in a morphological step, being the smallest allowable time step for all grid cells. The updated bathymetry is subsequently applied for the next loop. The loop is repeated until the end of the defined simulation period has been reached.

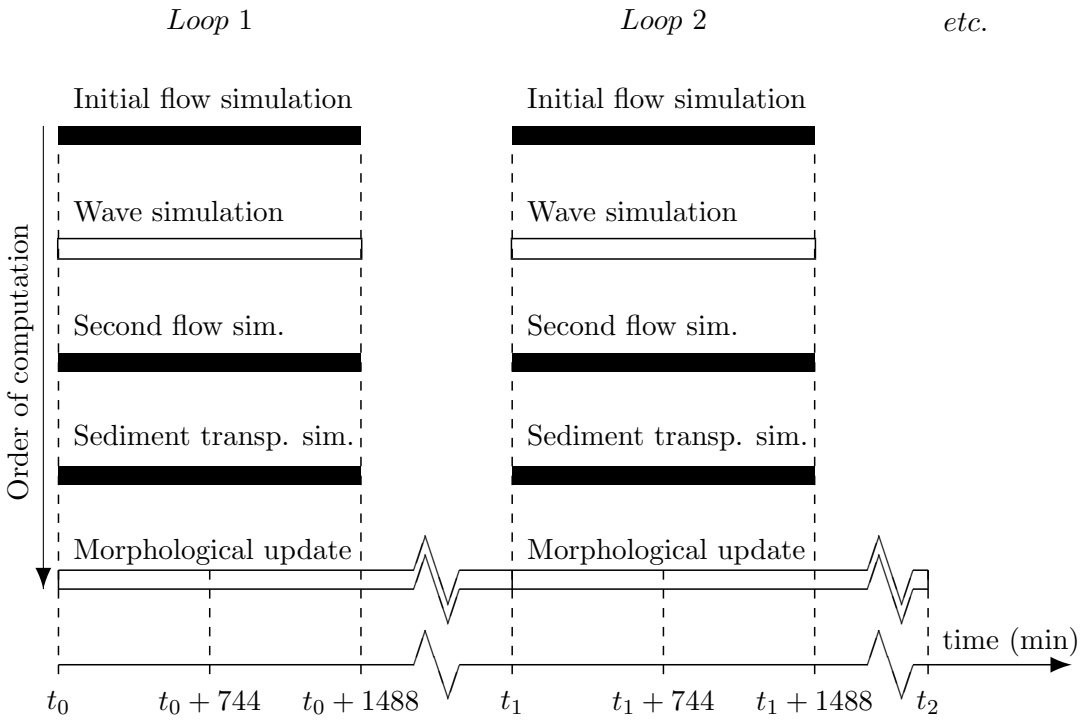

Figure 4.4: Simulated time series within the simulation set-up.

4.3.1 General simulation set-up

In terms of the simulated time series, the simulation can be schematised as shown in Figure 4.4.

Basic process model simulation

The initial bathymetry at t_0 is entered into the process models for flow, waves and sediment transport. The first loop follows *path 1* of Figure 4.3. First an initial flow simulation over two tidal cycles (of 12 hours and 24 minutes) is carried out. This provides the tide-varying conditions for the subsequent wave simulation for the same period. Subsequently, a wave calculation is made every 2 hours, being the optimised interval on the basis of a sensitivity analysis. The wave characteristics are interpolated linearly between the 2-hourly wave calculations to yield data for each flow time step.

A second flow simulation is then carried out in which the wave effects are taken into account. This results in current velocity fields including both tidal and wave-induced currents. The results of the second flow simulation and those of the wave simulation provide the conditions for the sediment transport model. After calculating the sediment transports for both suspended and bed load transport, the time-averaged transports over the second tidal cycle are calculated, viz. from $t_0 + 744$ to $t_0 + 1488$ minutes. The model results of the first tidal cycle are ignored to exclude initialisation effects.

Sedimentation and erosion calculation in ISE-mode

In ISE-mode, the time-averaged transports are multiplied by 24 hours. Then, the initial sedimentation and erosion patterns for a one-day period are calculated on the basis of the continuity equation for the bed level (see also Paragraph 3.A.6 in Appendix 3.A).

Sedimentation and erosion calculation in MTM-mode

In MTM-mode, the time-averaged transports are used to determine a theoretical *bed celerity*, followed by the computation of the maximally allowable morphological time step Δt_{bed} on the basis of the CFL-criterion (see Formula 3.7). This is explained more extensively in Paragraph 3.A.5. The time-averaged transports are multiplied by the morphological time step to obtain the resulting sediment movements. Subsequently the sedimentation and erosion are calculated. These are added to the bathymetry at the start of the loop (t=t_0). As long as the end of the simulation period has not yet been reached, a new loop is started on the basis of the updated bathymetry for t_1, where $t_1 = t_0 + \Delta t_{bed}$.

Subsequent loops in MTM-mode

Subsequent loops follow either *path 1* or *path 2* of Figure 4.3. Since the execution of the hydrodynamic process model simulations require a relatively large computational effort, inducing long calculation times, a shortcut is available in the Delft3D modelling system. This so-called *continuity update* estimates the flow conditions for the updated bathymetry (see also Paragraph 3.A.6). The assumption is made that no significant changes of the horizontal current patterns will take place on the basis of the morphological changes after one loop. Thus, the adapted current velocities can be determined by combining the flow discharges and slightly changed total water depth for each grid cell and time step. A decrease in water depth will increase the velocity and vice versa. The adapted current velocities and the original wave characteristics are subsequently entered into the sediment transport model.

4.3.2 Simulation of scenarios with varying conditions

When the morphodynamic model is applied to simulate in MTM-mode, the imposed conditions with respect to the tide, waves and wind can be varied. In this way a representative *climate* can be imposed. The definition of representative conditions is discussed in Section 4.4. To this end, the total simulation period, e.g. one year, is split up into a number of shorter periods. For each period different conditions are imposed and the length of the period depends on the probability of occurrence of the combination of the imposed conditions. This is shown schematically in Figure 4.5. In every sub-simulation the modelling scheme of Figure 4.4 is carried out anew.

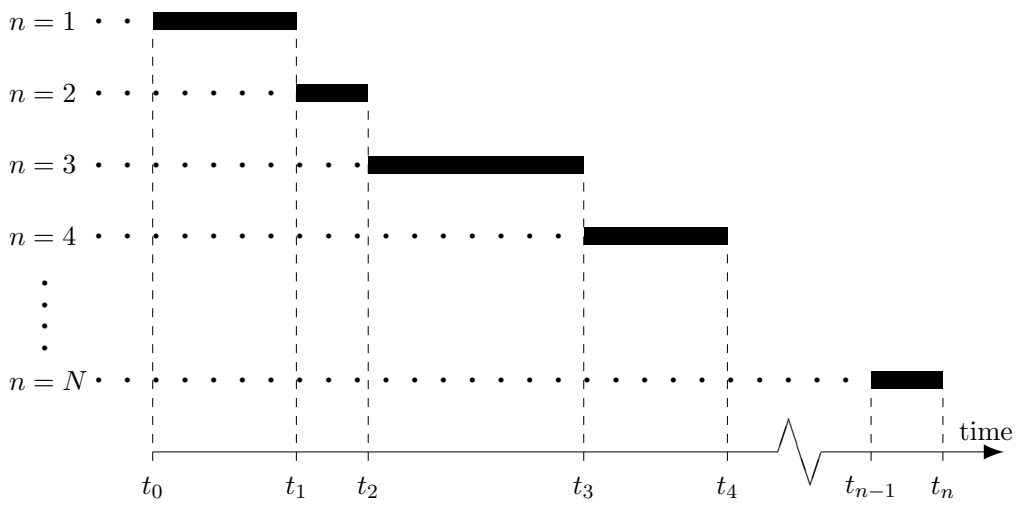

Figure 4.5: Scheme for splitting-up the simulation into N sub-simulations with varying conditions and simulation periods. For each sub-simulation n the scheme of Figure 4.4 is carried out.

4.4 Definition of the open boundary conditions

Depending on the applied model concept, either a single combination of boundary conditions for the process models or a series of sequential combinations have been imposed. For the ISE-concept, applied in the sensitivity analysis, a single combination of boundary conditions has been imposed. For the calibration of the morphodynamic model, based on the MTM-concept, a series of combinations have been imposed. A first estimation of these conditions was made through the application of input filtering techniques, as explained below. In the calibration (Section 5.3) an optimisation of this initial estimation has been carried out.

In Paragraph 4.4.1 the topic of input filtering is discussed, together with its necessity for medium-term morphodynamic modelling. This is followed by the description of the applied methods for determining representative boundary conditions in Paragraphs 4.4.2 through 4.4.8.

4.4.1 Input filtering

When applying complex morphodynamic models for coastal areas, the combination of the required high grid resolution with the relatively long modelling period leads to prohibitively expensive calculations in terms of computational efforts [Steijn, 1992; De Vriend *et al.*, 1993a; Latteux, 1995]. De Vriend *et al.* [1993a] mention three approaches for overcoming the problem of too expensive simulations, viz.:

- Input reduction – reduction of the chronologically sequence of conditions during the modelling period to a limited number of *representative* conditions;
- Model reduction – reformulation of the model, based on integration of smaller-scale effects (e.g. flow and waves) into the effects on a morphological scale;
- Behaviour-oriented modelling – representation of the morphodynamics without considering the underlying processes.

The method of input reduction has been applied exclusively within this study, as explained in the following Paragraph. The essence of input filtering is to reduce the number of input conditions for complex coastal morphological models to an economically and scientifically acceptable minimum [Steijn, 1992].

4.4.2 Applied input reduction methods

In this study the individual hydrodynamic and sediment transport processes are to be represented within the process models of the morphodynamic model. Therefore, only the first approach, input reduction, has been considered.

The input reduction approach has been carried out for the driving forces of the hydrodynamic models, i.e. the tide, swell, wind and storm conditions. Since locally generated wind waves may play a significant role in the eastern part of the study area (see Paragraph 2.3.2), the representative conditions for tide and waves have been further extended with several wind conditions.

The first step in determining the representative boundary conditions has been to define the representative tidal conditions, as explained in Paragraph 4.4.3. Secondly, a representative wave climate has been determined. The applied method for doing this is described in Paragraph 4.4.4. And finally, in Paragraph 4.4.5 the applied method for determining the representative conditions for the wind climate is presented. The combination of the afore-mentioned conditions into a set of conditions for the morphodynamic model is described in Paragraph 4.4.6. Storm conditions are discussed in Paragraph 4.4.7. The combination of swell and wind conditions together with the open boundary conditions for the sediment transport and morphology models (Paragraph 4.4.8) forms the representation of the interactions between the model domain and its surroundings.

4.4.3 Flow boundary conditions

The method for selection of representative tidal conditions has been based on the approaches presented by Latteux [1995] and Steijn [1992]. As will be described hereafter, the use of a single representative tidal cycle yields good results. Nevertheless, a comparison of the morphodynamic model results of a simulation on the basis of a full

spring-neap tidal cycle and a simulation based on the defined representative tidal conditions has been made. As shown in Appendix 4.B, the results are rather similar. To find the tidal cycle that yields an optimal result for the whole area the following procedure has been applied:

- Definition of representative locations – selection of a number of locations throughout the study area that are assumed to be representative for the whole study area;
- Calculation of the average sediment transport over a neap-spring tidal cycle – application of the numerical model to calculate the sediment transport time series in each of the locations and determining their average values;
- Calculation of the average sediment transport over each single tidal cycle during the entire neap-spring tidal cycle – calculation of the average sediment transport values per tidal cycle on the basis of the time series of the simulation of the previous step;
- Selection of the optimal tidal cycle – comparison of the averaged sediment transports of each tidal cycle to the neap-spring tidal cycle averages and selection of the tidal cycle for which most locations show similarity.

A number of locations has been selected throughout the study area, which consists of the main tidal channels and surrounding tidal flats. The locations have thus been positioned in and along these channels as well as on the tidal flat Tertiussand. A total of 17 locations in the tidal channels and 14 on the tidal flats has been defined, as shown in Figure 4.6.

Subsequently, a sediment transport simulation has been made over a complete neap-spring tidal cycle on the basis of a flow simulation over the same period. The tidal flow boundary conditions have been generated with the previously described model nesting sequence and constituted the only driving force. This resulted in time series of the sediment transport for the selected locations.

From these time series the average values $\overline{S_x(i,tot)}$ and $\overline{S_y(i,tot)}$ over the entire period have been determined for all locations i, separated in x- and y-components. Similarly, the average values $\overline{S_x(i,j)}$ and $\overline{S_y(i,j)}$ per tidal cycle j for location i were calculated.

The representativity factor λ_x and λ_y for both directions are defined as:

$$\begin{aligned} \lambda_x(i,j) &= \overline{S_x(i,j)}/\overline{S_x(i,tot)} \\ \lambda_y(i,j) &= \overline{S_y(i,j)}/\overline{S_y(i,tot)} \end{aligned} \tag{4.1}$$

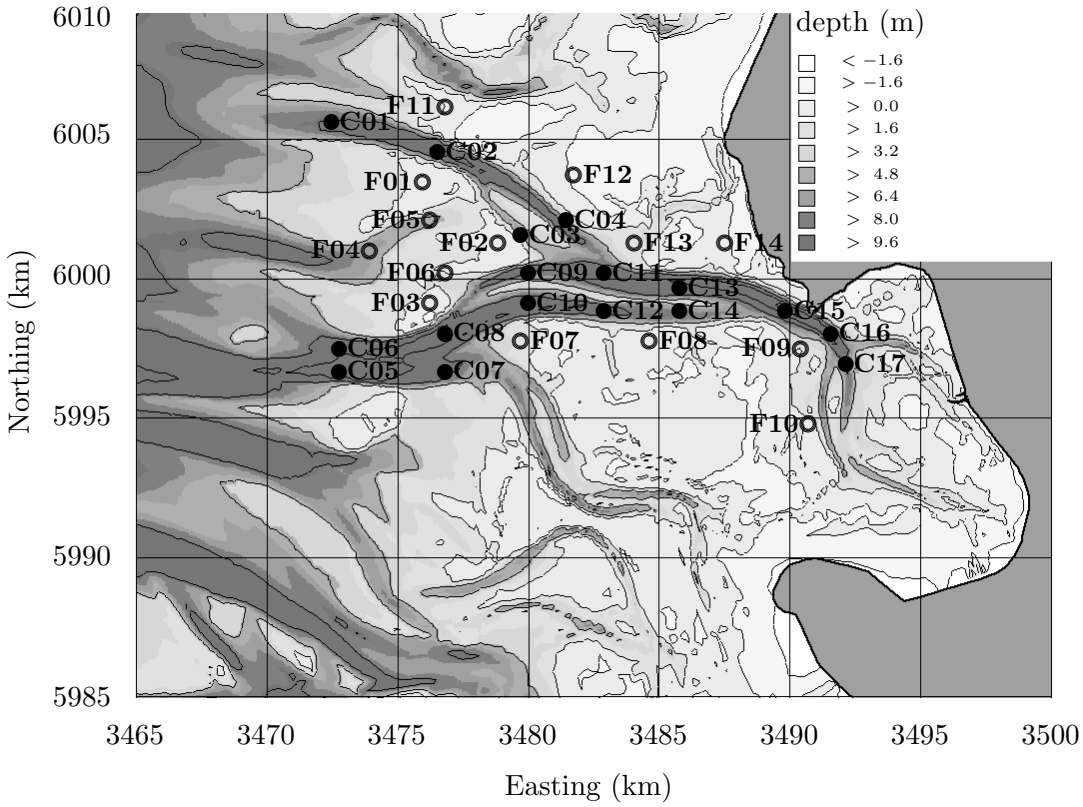

Figure 4.6: Location of the defined locations in the channels (dots) and on the tidal flats (circles).

with:

$\lambda_x(i,j)$ and $\lambda_y(i,j)$	representativity factor of tide j at point i in x- and y-direction
$\overline{S_x(i,j)}$ and $\overline{S_y(i,j)}$	average sediment transport during tide j at point i in x- and y-direction
$\overline{S_x(i,tot)}$ and $\overline{S_y(i,tot)}$	average sediment transport during whole Neap-Spring period in x- and y-direction

A value of 1 therefore indicates an optimal representation of the average sediment transport rate over the neap-spring cycle by the considered tide. Values larger than 1 result from transport rates that are higher than the average. When the tide-averaged transport rate is lower than the average rate over the whole period, the value of λ_x or λ_y is between 0 and 1 when the direction is correct, and between -1 and 0 when the direction is opposite. Values lower than -1 result when the transport rate is higher than the average rate over the whole period and in the wrong direction. Inherent to the definition of λ_x or λ_y, very small average transport rates over the entire period may result in extreme values of λ_x or λ_y, even for small tide-averaged transport rates.

The resulting values for λ_x and λ_y are shown in Figures 4.8(a) and 4.8(b) for the selected locations in the tidal channels, and in Figures 4.8(c) and 4.8(d) for those on the tidal flats. The focus is on the maximum and minimum values, whose deviations

from the value 1 should be as small as possible. These are indicated by the black lines, whereas the connected λ_x or λ_y-values for the individual locations are shown in grey.

The tide which on the one hand generated λ_x or λ_y-values close to 1 for the majority of examined locations and on the other hand did not show large deflections of λ_x or λ_y for any of the locations has been selected as the representative tidal cycle. The maximum deflection measured about 30 %, corresponding to a λ_x or λ_y between 0.7 and 1.3. The selected tide is indicated in Figure 4.8 by the vertical line.

In Figure 4.7 the water level near Buesum is shown exemplarily, together with the selected representative tidal cycle. The tidal range of this tide is circa 3.1 m, being close to the mean tidal range in the area. Therefore a mean tidal cycle has been used as representative tidal cycle for the morphodynamic simulations in this study.

Compared to the results of Latteux [1995] and Steijn [1992], the representative tidal range is slightly lower. Latteux found the representative tide to have a tidal range between 7 and 20 % higher than the mean tidal range and in the study by Steijn a 10 % higher range was found for the southern North Sea. These differences may well be related to differences in the studied areas, such as the dominant forces and sediment characteristics.

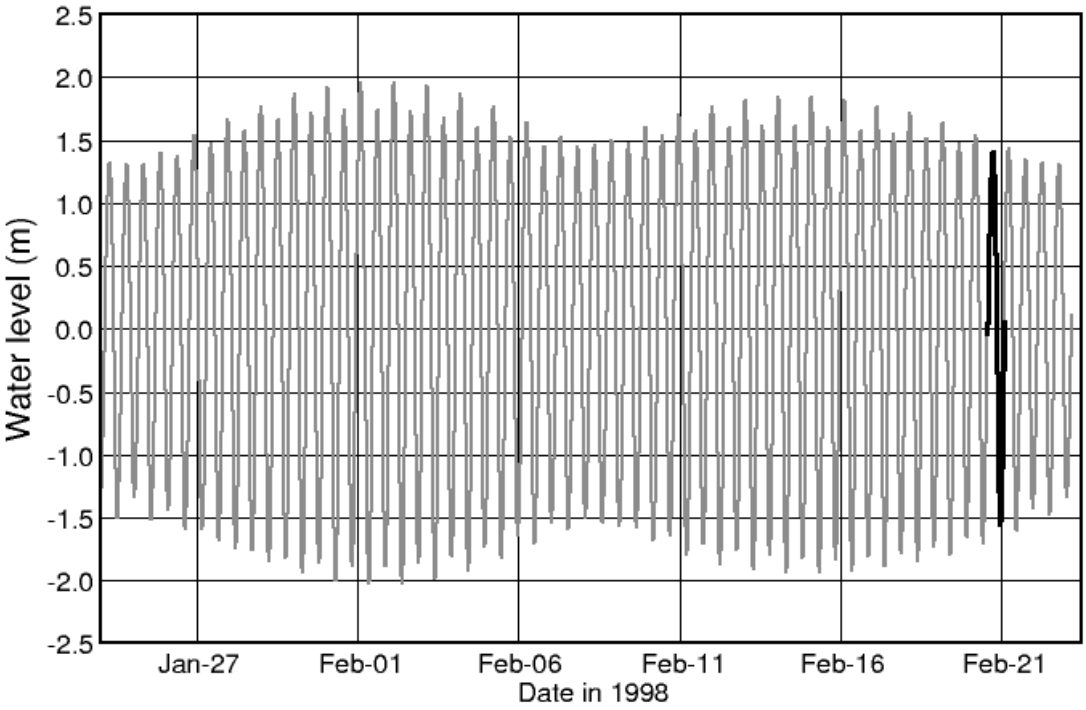

Figure 4.7: Computed water level at Buesum for the examined Spring-Neap period. The selected representative tidal cycle is indicated in black.

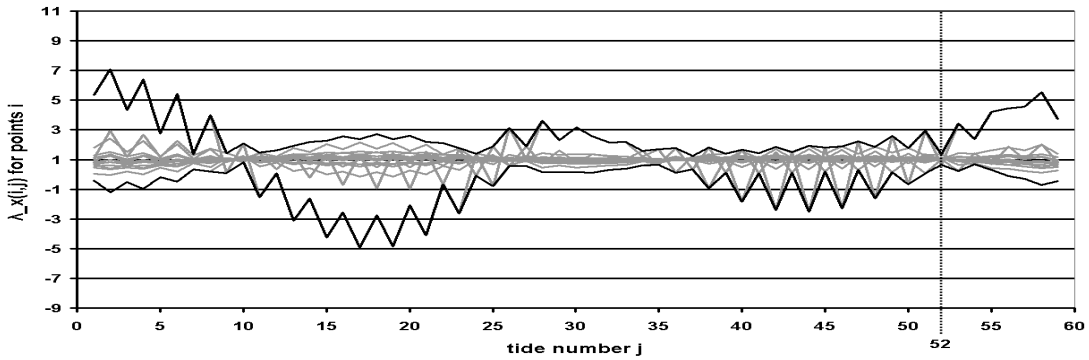

(a) x-component of the tidal channel locations.

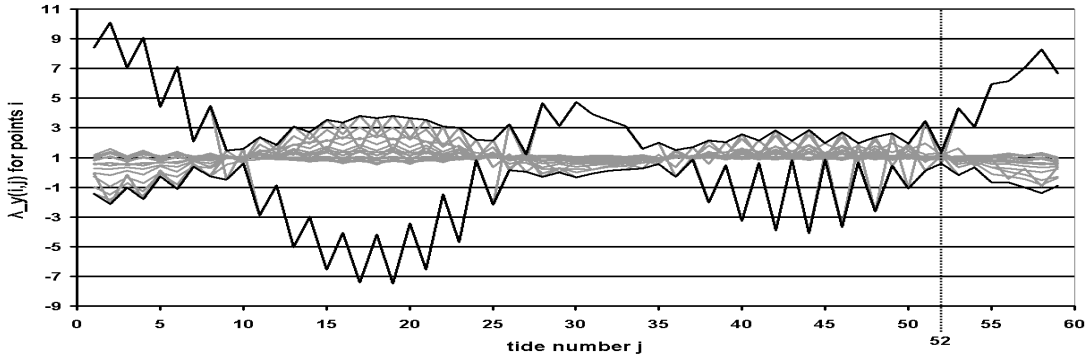

(b) y-components of the tidal channel locations.

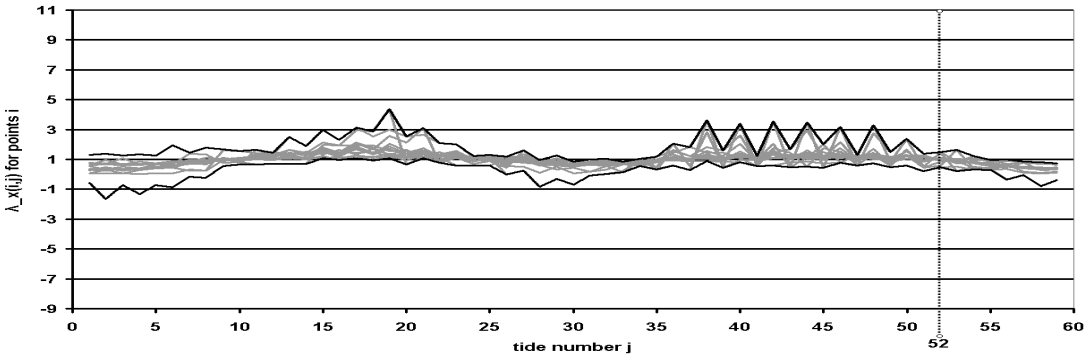

(c) x-component of the tidal flat locations.

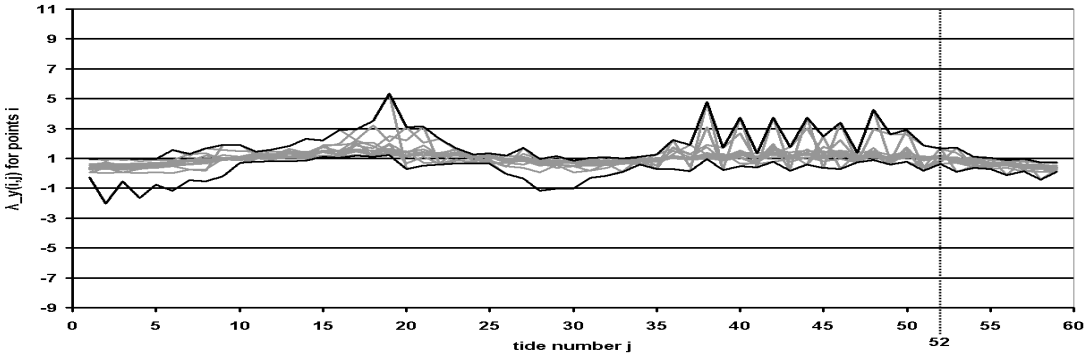

(d) y-component of the tidal flat locations.

Figure 4.8: λ-values (grey) for x- and y-components in the tidal channels (a and b) and on the tidal flats (c and d). The black lines indicate the maximum and minimum values.

4.4.4 Swell wave boundary conditions

Where the above-described tidal conditions are deterministic, the swell wave conditions are stochastic. They depend on the non-predictable – for periods longer than a few days – meteorological conditions. Therefore the schematisation of the expected wave climate can only be based on observations from the past. The observations should cover a sufficiently long period – generally in the order of several years – to be representative.

Since long-term wave measurements are not available for the study area itself, wave statistics from observations near the Island of Sylt have been used. These are presented in Paragraph 2.3.2 and constitute the nearest long-term wave data collection. This location is located approximately 70 km north of the area of study. It is more exposed to incoming swell from the North Sea than the western edge of the here-investigated tidal flats and channels.

The swell statistics consist of a table with the probability of occurrence per wave direction interval and wave height interval, as shown in Table 4.1. The wave directions are differentiated in 30-degree intervals, whereas the wave heights are split-up into intervals of 0.25 m. For each class with non-zero probability, the average wave period and water level set-up is available as well. As can be seen, the highest observed waves had a significant wave height between 5.25 and 5.50 m.

To transform these data into a limited number of representative conditions for the hydrodynamic model, an approach similar to the one presented by Steijn [1992] has been followed. As Steijn [1992] stated, the essence of this approach is to determine the effect of all conditions on the sediment transport and subsequently determine a small number of conditions that yield approximately the same effect. The effects on the sediment transport can be determined either by:

- making a coupled hydrodynamics-sediment transport simulation for each of the conditions in Table 4.1, and weighted addition of the resulting sediment transports on the basis of the probabilities;
- using an approach in which the effects on the sediment transport are estimated through simplified relationships between wave conditions and sediment transports.

Since simulation of all of the conditions of Table 4.1 is computationally too expensive, the second approach has been applied. Steijn [1992] differentiated between two (indirect) effects of waves on sediment transport, i.e. the *wave-induced currents* and the *stirring effect*. The former is the basis for the advective long-shore and cross-shore sediment transport, whereas the latter only enhances sediment transport in combination with currents due to other processes, e.g. tidal currents, river outflow or wind-induced currents. As discussed in Section 2.7, the study area can be classified as medium

Table 4.1: Probability of occurrence (%) per wave direction and significant wave height. Based on BMFT [1994].

Dir. (°N) H_s **(m)**	**0**	**30**	**60**	**90**	**120**	**150**	**180**	**210**	**240**	**270**	**300**	**330**	**total**
0.125	0.10	0.06	0.04	0.02	0.03	0.02	0.02	0.13	0.28	0.71	0.95	0.33	**2.71**
0.375	1.19	1.25	0.74	0.43	0.41	0.41	0.73	1.41	1.72	2.79	5.63	3.09	**19.81**
0.525	0.76	0.36	0.28	0.22	0.15	0.23	0.78	1.31	2.53	3.19	5.82	4.00	**19.63**
0.875	0.42	0.10	0.06	0.02	0.01	0.02	0.23	0.93	2.62	3.14	4.75	2.24	**14.54**
1.125	0.25	0.01	0.01	0.01	0.00	0.01	0.05	0.57	2.73	3.32	3.84	1.54	**12.33**
1.375	0.13	0.00	0.00	0.00	–	–	0.00	0.24	1.86	2.46	2.89	1.27	**8.86**
1.525	0.02	–	–	–	–	–	0.00	0.20	1.48	2.07	2.01	0.75	**6.55**
1.875	0.01	–	–	–	–	–	–	0.11	1.00	1.52	1.52	0.44	**4.59**
2.125	0.00	–	–	–	–	–	–	0.08	0.77	1.23	1.19	0.21	**3.47**
2.375	–	–	–	–	–	–	–	0.02	0.55	0.82	0.89	0.12	**2.41**
2.525	–	–	–	–	–	–	–	0.01	0.35	0.69	0.60	0.04	**1.69**
2.875	–	–	–	–	–	–	–	0.00	0.24	0.48	0.37	0.03	**1.12**
3.125	–	–	–	–	–	–	–	–	0.13	0.32	0.24	0.00	**0.69**
3.375	–	–	–	–	–	–	–	–	0.07	0.25	0.17	0.00	**0.49**
3.525	–	–	–	–	–	–	–	–	0.07	0.18	0.17	–	**0.42**
3.875	–	–	–	–	–	–	–	–	0.04	0.13	0.10	–	**0.28**
4.125	–	–	–	–	–	–	–	–	0.02	0.08	0.08	–	**0.18**
4.375	–	–	–	–	–	–	–	–	0.01	0.08	0.05	–	**0.15**
4.525	–	–	–	–	–	–	–	–	0.00	0.03	0.01	–	**0.05**
4.875	–	–	–	–	–	–	–	–	–	0.03	–	–	**0.03**
5.125	–	–	–	–	–	–	–	–	–	0.01	0.00	–	**0.01**
5.375	–	–	–	–	–	–	–	–	–	0.00	–	–	**0.00**
total	**2.89**	**1.79**	**1.15**	**0.71**	**0.60**	**0.69**	**1.81**	**5.0**	**16.46**	**23.55**	**31.29**	**14.06**	**100.00**

to highly tide-dominated, from West to East. The presence of relatively strong tidal currents increases the significance of the stirring effect with respect to effect of wave-induced currents.

Steijn [1992] showed that the current-inducing wave energy flux P is proportional to $H_s^{2.5}$, and the stirring parameter τ_w is proportional to H_s. On the basis of these relationships and the known probabilities, the contributions $P(H_i, \theta_i)$ and $\tau_w(H_i, \theta_i)$ to the total effects P_{tot} and $\tau_{w,tot}$ can be determined for all conditions through:

$$P(H_i, \theta_i) \propto p(H_i, \theta_i) * H_i^{2.5} \tag{4.2}$$

and:

$$\tau_w(H_i, \theta_i) \propto p(H_i, \theta_i) * H_i \tag{4.3}$$

with:

i	identifier of a combination of wave height direction
H_i	average wave height of condition i
θ_i	average wave direction of condition i
$p(H_i, \theta_i)$	probability of occurrence for the combination of H_i and θ_i
$P(H_i, \theta_i)$	energy flux contribution for H_i and θ_i
$\tau_w(H_i, \theta_i)$	stirring effect contribution for H_i and θ_i

The totals, for all directions and wave heights, then follow from:

$$P_{tot} \propto \sum_i P(H_i, \theta_i) \tag{4.4}$$

and

$$\tau_{w,tot} \propto \sum_i \tau_w(H_i, \theta_i) \tag{4.5}$$

with:

P_{tot}	total energy flux, summed over all conditions i
$\tau_{w,tot}$	total stirring effect, summed over all conditions i

Subsequently, the relative contributions to the totals can be determined per wave height and direction by:

$$P_{rel}(H_i, \theta_i) = \frac{P(H_i, \theta_i)}{P_{tot}} * 100\% \tag{4.6}$$

and

$$\tau_{w,rel}(H_i, \theta_i) = \frac{\tau_w(H_i, \theta_i)}{\tau_{w,tot}} * 100\% \tag{4.7}$$

with:

$P_{rel}(H_i, \theta_i)$	relative contribution to the total energy flux
$\tau_{w,rel}(H_i, \theta_i)$	relative contribution to the total stirring effect

This has been carried out for conditions within the sector from 225 – 345°N, corresponding to the sector from which swell enters the model domain (as opposed to the wider spectrum of directions at the location of the wave measurements). Furthermore, the number of wave height intervals has been reduced by adding the contributions of the lumped wave height intervals. The relative contributions, with respect to the total of all classes, are shown for the wave energy flux in Table 4.2 and for the stirring effect in Table 4.3.

It can be seen that the selected directional sector is responsible for over 90 % of the generated energy flux and stirring effect generated by all conditions, showing that the neglect of direction outside of this sector is acceptable. For the wave energy flux the wave heights between 2.0 and 3.5 m are dominant, whereas for the stirring effect the dominance shifts to the interval 0.5 to 2.0 m. For both effects the sector from 285 to 315 °N is dominant up to wave heights of 2.0 m. For higher waves the sector from 255 to 285 °N is yielding the largest contributions, although this is less pregnant.

Based on the dominating directions, the selected directions for the to-be-imposed representative conditions at the western model boundary have been defined as 270 °N for high waves and 300 °N for low waves. These conditions are consistent with the

Table 4.2: Relative contribution (%) to wave energy flux per direction θ and wave height H_s.

θ (°N) H_s (m)	225-255	255-285	285-315	315-345	total
0.0-0.5	0.1	0.1	0.2	0.1	**0.5**
0.5-2.0	8.7	11.7	13.2	5.3	**38.8**
2.0-3.5	10.1	20.8	18.2	1.5	**50.6**
3.5-5.5	0.5	4.2	2.4	0.0	**7.0**
total	**19.3**	**36.8**	**34.0**	**6.9**	**96.9**

Table 4.3: Relative contribution (%) to the stirring effect per direction θ and wave height H_s.

θ (°N) H_s (m)	225-255	255-285	285-315	315-345	total
0.0-0.5	0.6	1.1	2.1	1.1	**4.9**
0.5-2.0	12.9	16.9	20.7	9.3	**59.8**
2.0-3.5	5.2	10.0	9.0	0.9	**25.2**
3.5-5.5	0.1	1.0	0.6	0.0	**1.7**
total	**18.8**	**29.0**	**32.4**	**11.3**	**91.6**

Table 4.4: Overview of the imposed wave conditions.

Condition	**Description**	H_s **(m)**	θ **(°N)**
Low	representing calm conditions (0.0$\leq H_s \leq$0.5 m)	0.20	300
Medium	intermediate wave action (0.5$< H_s \leq$2.0 m)	1.00	300
High	rough conditions (2.0$< H_s \leq$3.5 m)	2.00	270

presented wave rose in Paragraph 2.3.2 and are summarised in Table 4.4. The wave height for each condition is defined somewhat lower than the average wave heights per interval (of Tables 4.2 and 4.3) to reflect the more sheltered location of the study area. The highest interval has been ignored. These wave heights are considered as storm conditions, which will be represented individually as discussed in Paragraph 4.4.7.

Comparison to the wave rose shows that swell from the direction West-Southwest is ignored, which can be explained by the fact that swell from this direction is much less significant at the edge of the model domain than at the location whereat the measurements were taken.

The number of conditions has been kept relatively small since they have been combined with a number of local wind conditions, as described in Paragraph 4.4.5, and the number of input conditions should be reduced to an economically acceptable minimum [Steijn, 1992]. A sensitivity analysis showed that a larger number of conditions does not significantly improve the model results.

Based on the relative contributions a representative probability has subsequently been defined for each of the selected combinations of wave height and direction. Both the wave energy flux and stirring effects have been considered. The resultant effects of the representative conditions are therefore similar to those generated by the full spectrum of wave heights and directions. This approach resulted in the representative probabilities listed in Table 4.5.

These representative swell conditions have been combined with several representative local wind conditions, as described in the following Paragraph.

Table 4.5: Representative swell conditions.

Condition	H_s **(m)**	θ **(°N)**	**Probability (%)**
Low	0.20	300	16
Medium	1.00	300	73
High	2.00	270	11

4.4.5 Wind conditions

As locally generated waves are more important for the sheltered part of the study area, local wind conditions have been represented in the morphodynamic model as well.

The synoptic wind data, presented in Section 2.5, served as a basis for the statistical analysis of the wind conditions in the area of investigation. These data cover a period of 12 years, from 1989 to 2000. The probabilities of combinations of wind speed U_w and wind direction θ_w are shown in Table 4.7. The directional intervals with the highest probability per wind speed interval are indicated by the underlined values. These combinations of wind direction and speed have been selected for representation of the local wind climate. The related probabilities have been based on the total probability per wind speed interval. For each interval (of wind speed and of wind direction) the average value has been taken, leading to the representative local wind conditions in Table 4.6. The order of simulation is not necessarily the order shown.

4.4.6 Combination of swell and wind conditions

The combination of the defined swell and wind climate has been based on a straightforward pairing of each of the swell conditions to each of the wave conditions, where the probability of each pair has been obtained through multiplication of the individual probabilities. Due to the low probability of the wind condition with a 22.5 m/s wind speed, this condition is only represented in combination with the medium swell wave class. The resulting combined climate is listed in Table 4.8.

In the morphodynamic simulations, the probability of occurrence has been multiplied by a period of one year to obtain the model period for each condition per year of simulation. This resulted in the imposed start time t_{n-1} and stop time t_n for the n loops in Figure 4.5. A sensitivity analysis with respect to the order of conditions has been carried out. Several morphodynamic simulations over a period of ten years were made, in which the order of conditions was varied. It could be concluded that the differences between the resulting bathymetries of these simulations were very limited in comparison to the computed morphological changes. Relatively, the differences were below 5 % of the computed morphological changes.

Table 4.6: Representative local wind conditions.

U_w **(m/s)**	θ_w **(°N)**	**Probability (%)**
2.50	180	27.7
7.50	240	49.8
12.50	255	19.3
17.50	270	3.0
22.50	300	0.3

Table 4.7: Probability of occurrence (%) per wind direction and wind speed. Based on the PRISMA-model by Luthardt [1987].

θ_w (°N) / U_w (m/s)	**0**	**30**	**60**	**90**	**120**	**150**	**180**	**210**	**240**	**270**	**300**	**330**	**total**
0.0 - 5.0	2.29	1.71	2.19	2.16	3.25	2.26	2.95	2.50	2.57	2.43	1.78	1.58	**27.67**
5.0 - 10.0	1.37	1.44	1.23	4.01	3.36	3.56	3.42	6.61	7.67	6.88	6.47	3.73	**49.76**
10.0 - 15.0	0.03	0.07	0.00	1.03	1.34	0.41	0.38	2.95	4.55	4.55	2.95	1.03	**19.28**
15.0 - 20.0	0.00	0.00	0.00	0.00	0.03	0.00	0.07	0.51	0.82	1.06	0.45	0.00	**2.95**
20.0 - 25.0	0.00	0.00	0.00	0.00	0.00	0.00	0.00	0.03	0.00	0.10	0.21	0.00	**0.33**
Total	**3.70**	**3.22**	**3.42**	**7.19**	**7.98**	**6.23**	**6.82**	**12.60**	**15.62**	**15.03**	**11.85**	**6.34**	**100.00**

Table 4.8: Combined climate for swell and wind.

H_s **(m)**	θ **(°N)**	U_w **(m/s)**	θ_w **(°N)**	**Probability (%)**
0.20	300	2.50	180	4.43
0.20	300	7.50	240	7.97
0.20	300	12.50	255	3.09
0.20	300	17.50	270	0.48
1.00	300	2.50	180	20.22
1.00	300	7.50	240	36.35
1.00	300	12.50	255	14.09
1.00	300	17.50	270	2.19
1.00	300	22.50	300	0.22
2.00	270	2.50	180	3.05
2.00	270	7.50	240	5.48
2.00	270	12.50	255	2.12
2.00	270	17.50	270	0.33

4.4.7 Storm conditions

Since storm conditions are generally including a significant change in water level, current velocities and wave action, these may have to be represented separately from the above-described swell and wind conditions. The statistical probability of occurrence of storms is rather insignificant in the afore-presented tables. However, due to the extreme circumstances during storms, they can have a significant effect on coastal morphology and therefore should not be ignored.

To properly evaluate the effects of a storm, an actually occurred storm has been modelled with the morphodynamic model. The selected storm, named "Anatol" by the meteorologists, formed one of the strongest storms of the last decade [DWD, 2000]. It was a typical low pressure area that moved from West to East over the central North Sea, causing strong onshore winds when passing by north of the study area. A detailed description of this model study is given in Appendix 4.A.

From the study it has been concluded that the inclusion of one or two storms in a one-year morphodynamic simulation has a very limited effect on the resulting morphodynamics in the here-applied model set-up. Therefore, instead of representing storms separately in the morphodynamic simulations they have been considered as part of the previously described representative wave and wind climates.

4.4.8 Sediment transport and morphological boundary conditions

Next to the open boundary conditions for the hydrodynamic models, conditions have to be imposed onto the open boundaries of the models for sediment transport and mor-

phological updating. Within the Delft3D modelling system three options are available:

- Prescription of the bed load transport rate;
- Prescription of the total load transport rate;
- Specification of the bed level.

Each of these has to be defined together with a condition to determine the suspended load transport rate.

Due to the absence of measured sediment transport rates near the open boundaries, the prescription of realistic time-dependent bed load or total load transport rates has been omitted. Instead, the third option, involving the specification of the bed level has been applied and set to remain at the initial value. The remote location of the open boundaries and the small morphological changes along them assure that this approach does not influence the model results in the area of interest.

The definition of the boundary condition for the suspended load transport is divided into inflow and outflow. Depending on the inflow or outflow state at the open boundary, the appropriate condition will be imposed. For inflow, the equilibrium concentration, computed through the algebraic sediment transport relation is imposed. In case of outflow, the concentration at the up-stream cell is imposed, effectively setting the concentration gradient to zero.

The effect of the definition of the sediment transport conditions at the open boundaries has been evaluated by Rizzo [2003] for the central Dithmarschen Bight. On the basis of a sensitivity analysis for various open boundary definitions and hydrodynamic conditions (e.g. neap tide, spring tide, wave action), he concluded that differences in computed concentrations can only be found within approximately 5 km of the open boundary. In the medium term morphodynamic simulations the definition of these open boundary conditions may have an influence on the net inflow or outflow of sediment. In this study it has been assumed that this influence is limited and does not significantly affect the area of interest, as it is located about 10 km from the nearest open boundary.

4.5 Discussion

On the basis of the general concepts for medium-term modelling the morphodynamic model for the Dithmarschen Bight has been set-up. Consisting of the calibrated and validated process models for tides, waves and sediment transports, it forms a sound basis for the hindcasting and forecasting of the morphological evolution in the study area. The defined scheme for splitting the morphodynamic simulation into a number of sub-simulations allows for a variety of driving conditions to be imposed.

Several input filtering techniques have been applied to define representative conditions for the driving forces in the model, considering the available (synoptic) measurement data.

A single representative tidal cycle has been defined, based on the widely accepted approaches by Latteux [1995] and Steijn [1992]. The selected tidal cycle has a tidal range close to the mean tidal range, whereas the aforementioned authors present tidal ranges slightly higher than the mean value as representative (between 7 and 20 %). A direct comparison between the model results on the basis of the representative tidal cycle and those based on a full neap-spring cycle showed that the defined tidal conditions do not significantly influence the computed morphological changes. Thus the selected tidal cycle can be used to represent the neap-spring cycle.

The available long-term wind and swell data have been subjected to a statistical analysis, resulting in a limited number of representative conditions. From a model study, in which the model predictions for a storm period have been evaluated, it was found that the inclusion of storm conditions affects the model results rather limitedly when considering medium-term to long-term simulation periods. The defined wind and swell conditions form an initial estimate for the model calibration, which is the subject of the following Chapter.

4.A Model study: Anatol storm

4.A.1 Introduction

The storm "Anatol" has been modelled with the morphodynamic model to evaluate the effects on the morphodynamics in the central Dithmarschen Bight. The ISE-approach has been applied, thus no back-coupling of the bathymetric changes to the hydrodynamic and sediment transport models is considered. In Paragraph 4.A.2 the characteristics of the storm are presented. For proper modelling of the storm, the wind conditions over the entire North Sea have been taken into account. To this purpose, the entire model nesting sequence (see also Paragraph 3.3.1) has been applied, as described in Paragraph 4.A.3, together with the model set-up. The results of the hydrodynamic models of the Dithmarschen Bight Model have subsequently been evaluated on the basis of the available water level and wave measurements (Paragraph 4.A.4). This was followed by the coupling of the hydrodynamic models to the sediment transport model and the model for morphological updating to build the morphodynamic model. The morphodynamic model has been applied to compute the morphodynamic changes due to the considered storm, as presented in Paragraph 4.A.5. The conclusions of this study are given in Paragraph 4.A.6.

4.A.2 Characteristics of Anatol

The selected storm, named "Anatol" by the meteorologists, formed one of the strongest storms of the last decade [DWD, 2000]. Anatol was a typical storm for the study area, with a low pressure area moving from West to East over the central North Sea and causing strong onshore winds when passing by north of the study area. The path of the centre of the storm is shown in Figure 4.9.

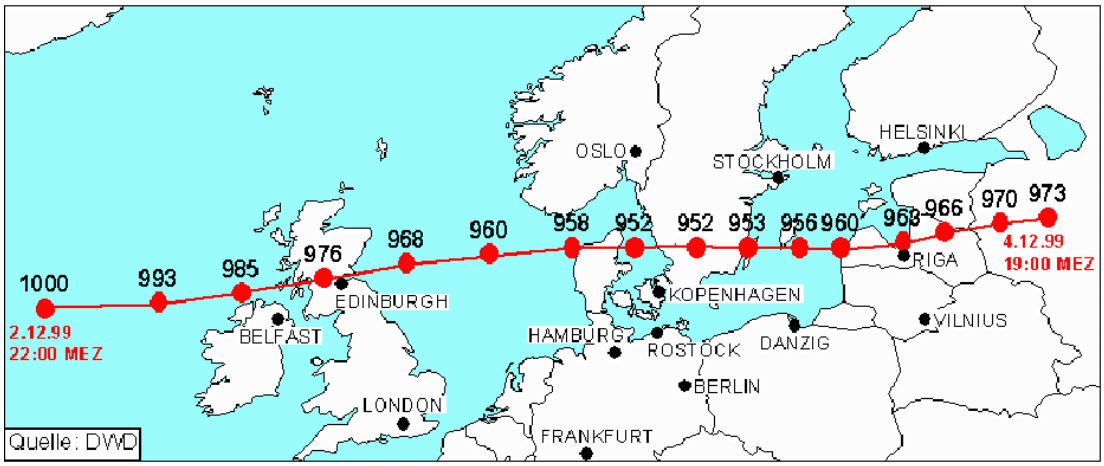

Figure 4.9: Path of the low pressure field of Anatol in 3-hourly intervals (times in UTC+1). The values indicate the air pressure in hPa [DWD, 2000].

A good impression of the storm characteristics can be found when looking at the wind velocity distribution over the area. This is shown in Figure 4.10. It can be seen that the wind velocities in the southeastern North Sea start to increase after December $3^r d$, 09.00 UTC, and the wind direction gradually shifts from West-Southwest to West. On December $4^t h$, 03.00 UTC, the low pressure area has passed and the wind reduces to moderate conditions.

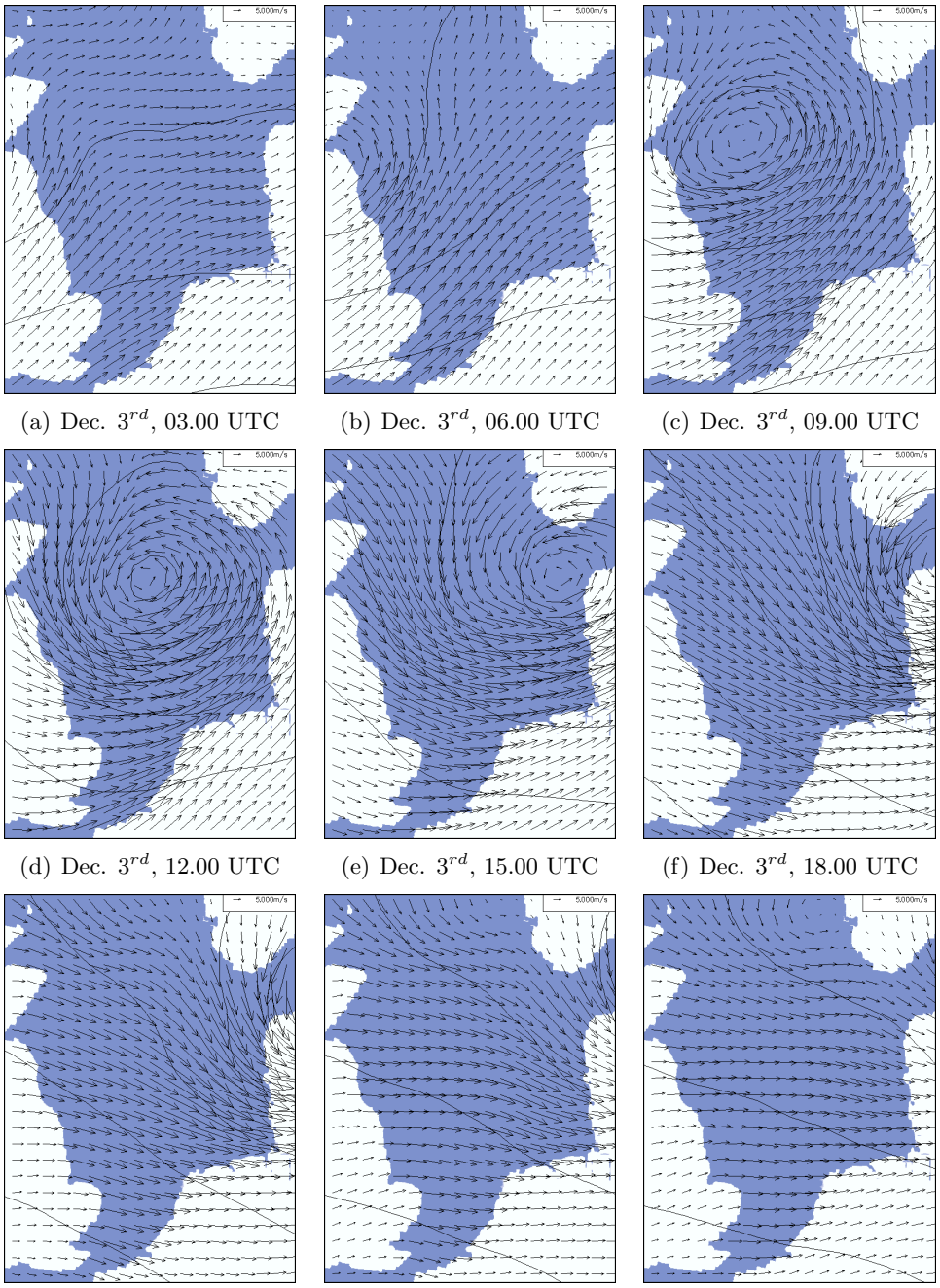

(a) Dec. 3^{rd}, 03.00 UTC (b) Dec. 3^{rd}, 06.00 UTC (c) Dec. 3^{rd}, 09.00 UTC

(d) Dec. 3^{rd}, 12.00 UTC (e) Dec. 3^{rd}, 15.00 UTC (f) Dec. 3^{rd}, 18.00 UTC

(g) Dec. 3^{rd}, 21.00 UTC (h) Dec. 4^{th}, 00.00 UTC (i) Dec. 4^{th}, 03.00 UTC

Figure 4.10: Wind velocity distribution during storm Anatol over the North Sea, including isobars. Based on synoptic data from the PRISMA model [Luthardt, 1987].

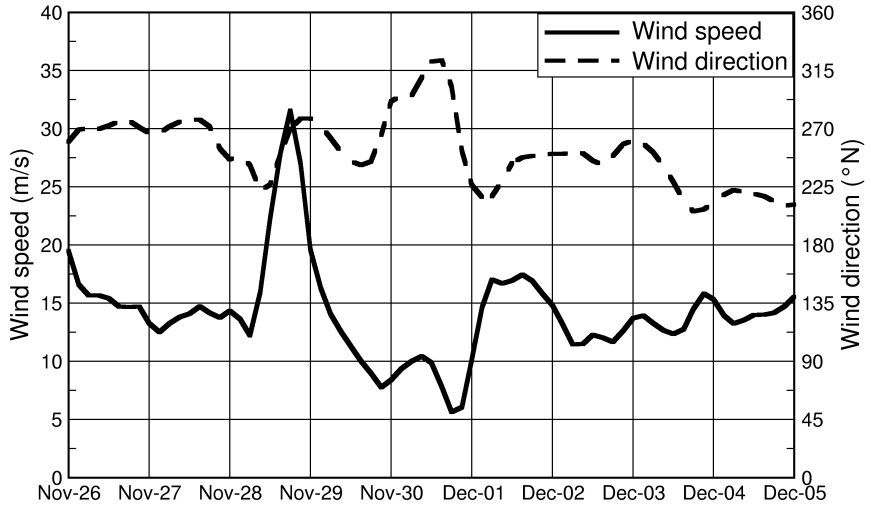

Figure 4.11: Wind speed and direction in the study area. Based on synoptic data from the PRISMA model [Luthardt, 1987].

In Figure 4.11 the time series of the wind velocity and direction in the study area are shown. As can be seen, the wind velocity increased rapidly from a moderate 15 m/s to a maximal value of over 30 m/s – corresponding to a force of 11 on the Beaufort scale – at 18.00 UTC on December 3^{rd}, in combination with a shift in direction from Southwest to West. After the low pressure area passed, the wind velocity reduced again to 10 – 15 m/s and the direction turned back to West-Southwest.

4.A.3 Model nesting and coupling

The storm surge generated by the storm Anatol is the result of the influence of the wind and pressure field on the water movements in the entire North Sea. Therefore, the whole model nesting sequence of Figure 4.12 has been applied for the hydrodynamic hindcast. This nesting sequence is described in more detail in Paragraph 3.3.1.

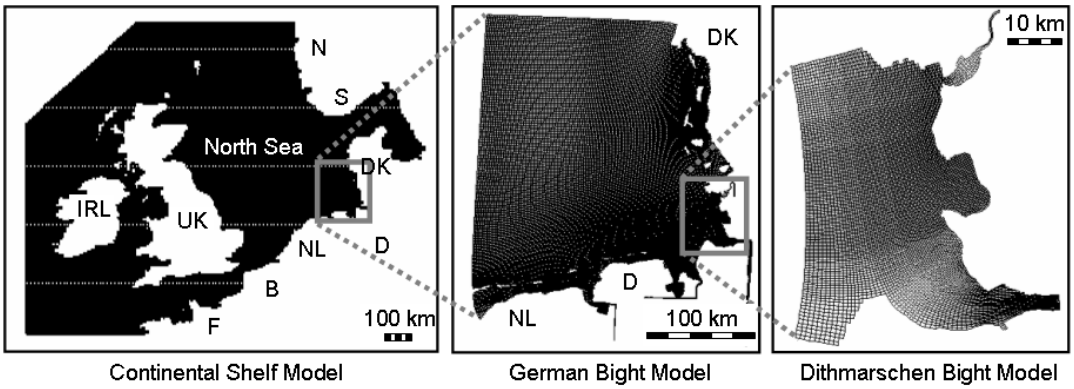

Figure 4.12: Nesting sequence from the large scale Continental Shelf Model, over the German Bight Model, to the Dithmarschen Bight Model.

The Continental Shelf Model has been applied to model the currents and water levels due to the astronomical tide and the imposed wind and pressure fields from the PRISMA assimilation model, developed by Luthardt [1987]. The results have subsequently been interpolated onto the open flow boundaries of the German Bight Model, thus introducing the large scale effects of the storm in this model. Similarly, the results of the German Bight Model have been transferred to the open flow boundaries of the Dithmarschen Bight Model. The meteorological data are updated in steps of one hour. Since the PRISMA data are only available every three hours, a linear interpolation in time has been carried out to generate hourly data.

Although the applied wave model (SWAN) can only be run in stationary mode within coupled simulations in Delft3D, it has been applied to generate swell boundary conditions for the Dithmarschen Bight model. The high variability of the wind conditions during the modelled period in conjunction with the relatively large dimensions of the German Bight Model make the use of a stationary wave model questionable. However, since no proper wave measurement data near the open boundaries of the Dithmarschen Bight Model were available for the considered period, it has been decided to follow this approach as a best option. As will be shown in the following Section, the stationary approach produces acceptable results. The wave boundary conditions have been nested to the Dithmarschen Bight model in steps of one hour. The applied model sequence is shown in Figure 4.13.

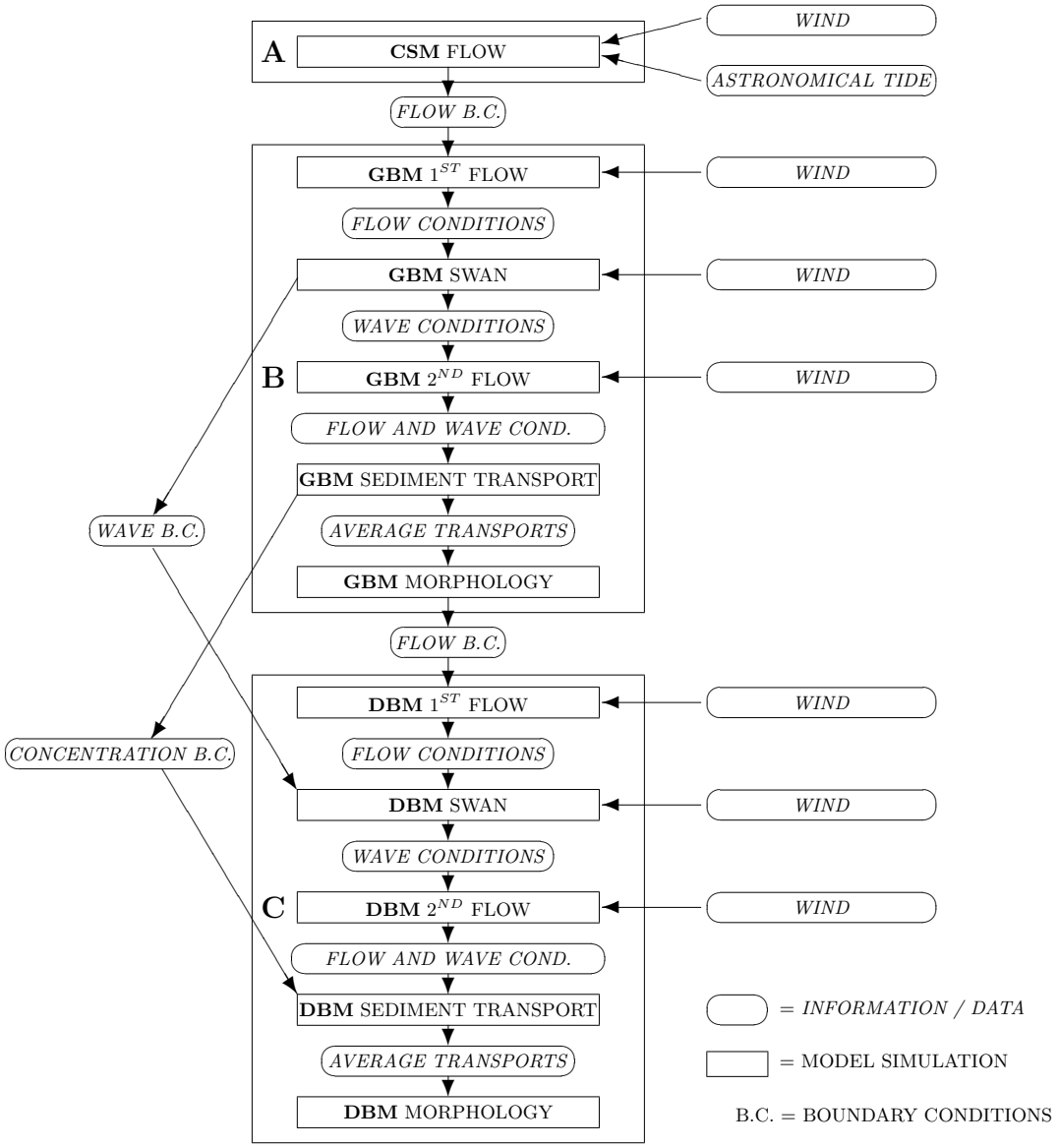

Figure 4.13: Schematic overview of the applied model approach, (A) the Continental Shelf Model (CSM), (B) the German Bight Model (GBM), and (C) the Dithmarschen Bight Model (DBM).

4.A.4 Hydrodynamics

The results of the hydrodynamic models have been evaluated on the basis of measured water levels and wave heights. The locations of the wave buoys and water level gauges are shown in Figure 4.14. For two wave measurement stations in the southeastern German Bight data are available during the storm Anatol. One is located near the island of Helgoland, the other at the edge of the Elbe estuary. Data from the water level gauges at Helgoland, at the locations in the channels Norderpiep and Suederpiep and near Buesum are available as well.

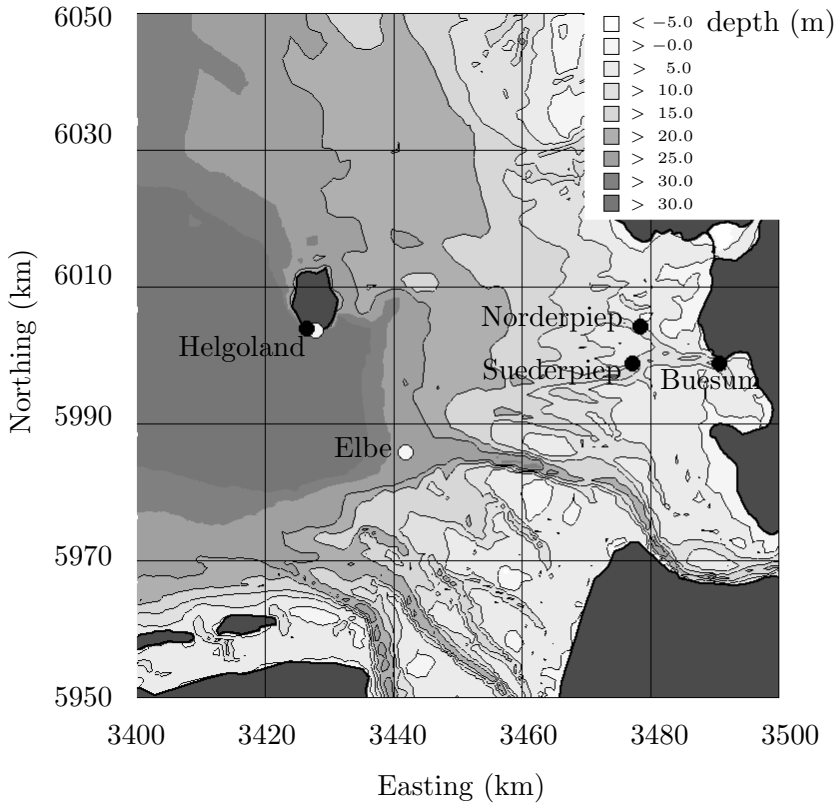

Figure 4.14: Location of the wave buoys (white) and water level gauges (black) in the south-eastern German Bight, for which data are available during the storm Anatol.

Water levels

Initially, the computed water levels from the German Bight Model have been compared to the observed water levels. The computed water levels include wave effects on the flow as they stem from the second flow simulation (see Figure 4.13). As can be seen from Figure 4.15, the computed water level at the Helgoland gauge fits quite well with the measurements. For the other three gauges the trends of the storm surge are reproduced very well, although some discrepancies can be found. These are expected here, since the horizontal resolution of the German Bight Model does not resolve the complexity of the bathymetry of the inner Dithmarschen Bight.

After execution of the afore-mentioned nesting procedure, the coupled flow-wave model for the Dithmarschen Bight was run for the same period. The results of the second flow simulation, i.e. including wave effects on the flow (see Figure 4.13), are shown in Figure 4.16, together with the observed water levels in the Norderpiep, Suederpiep and near Buesum. The island of Helgoland is outside of the Dithmarschen Bight Model domain and has thus been omitted. As can be seen, the results of the Dithmarschen Bight Model are better than those of the German Bight Model. During the storm the water level at low water is underpredicted, however.

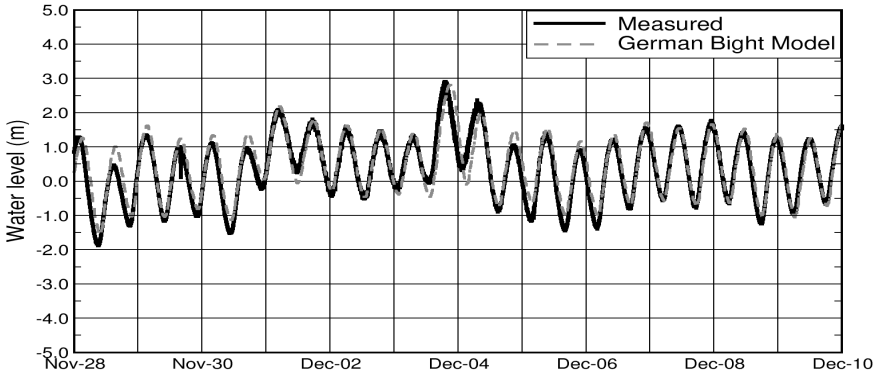

(a) Helgoland

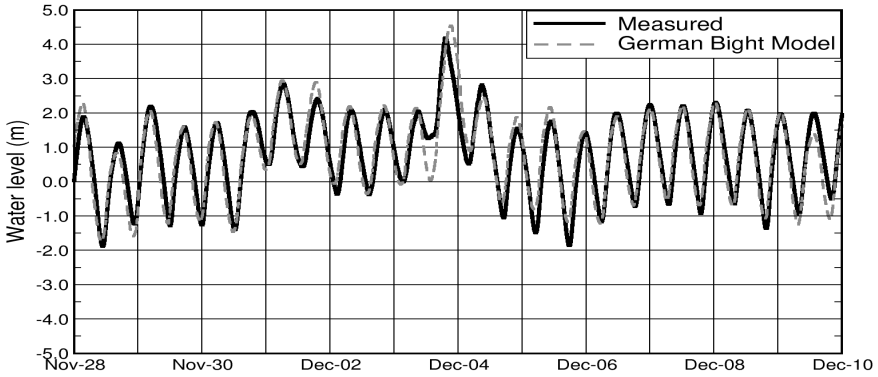

(b) Norderpiep

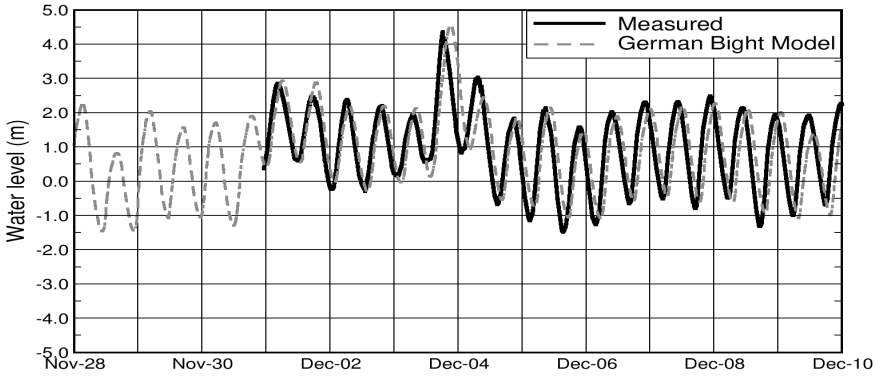

(c) Suederpiep

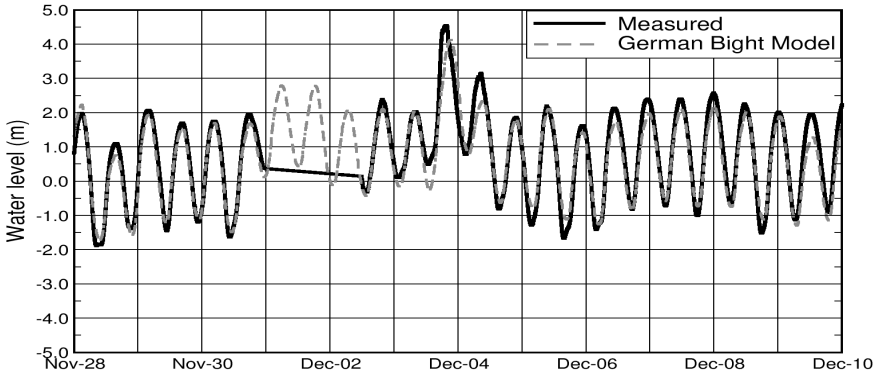

(d) Buesum

Figure 4.15: Observed and computed water levels, using the German Bight Model.

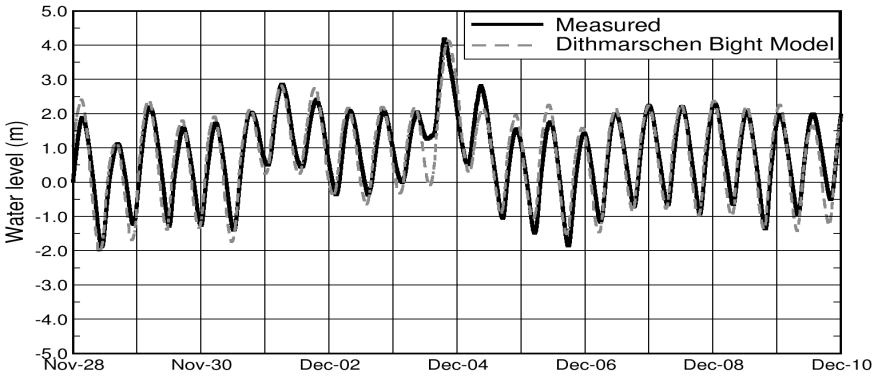

(a) Norderpiep

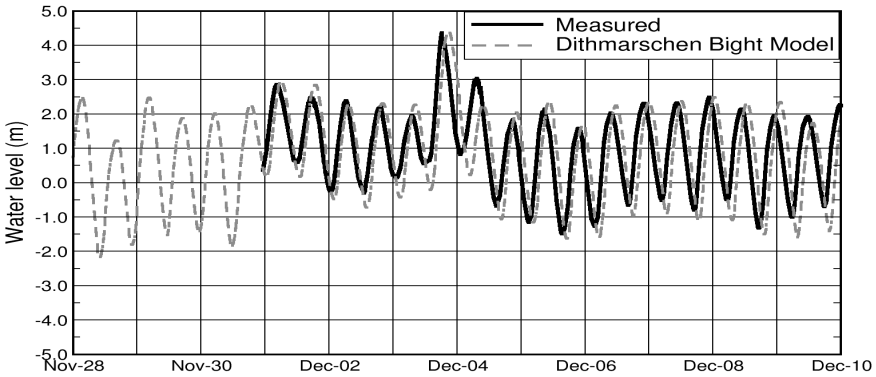

(b) Suederpiep

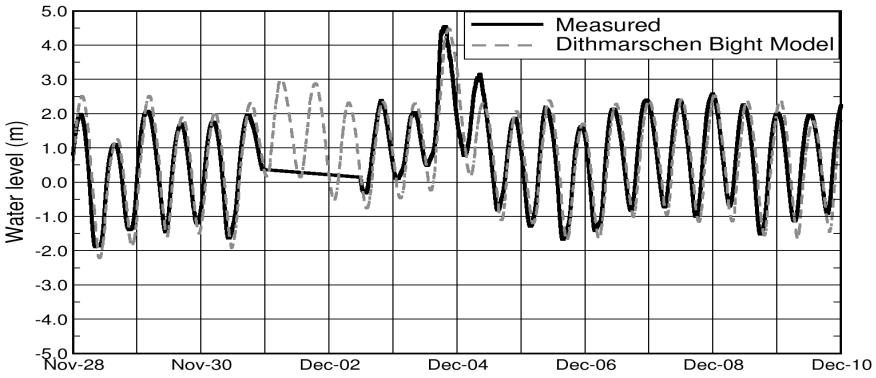

(c) Buesum

Figure 4.16: Observed and computed water levels, using the Dithmarschen Bight Model.

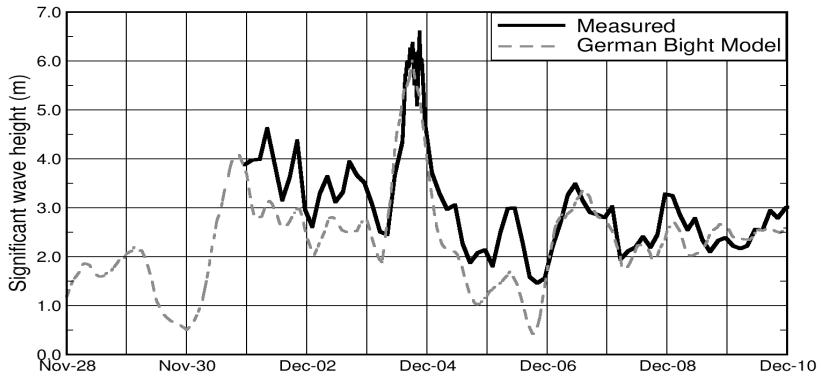

(a) Helgoland

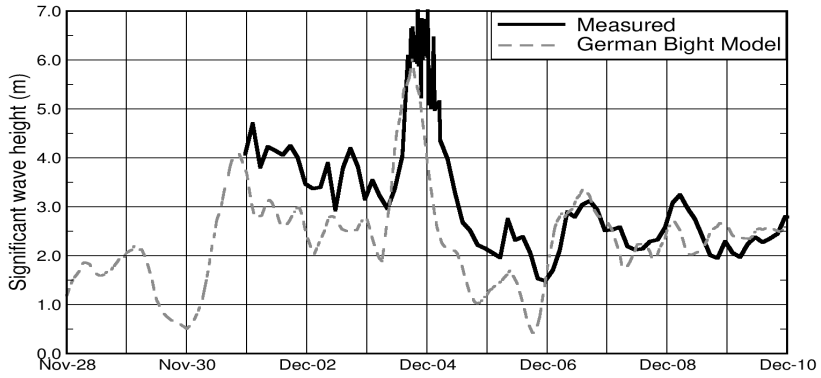

(b) Elbe buoy

Figure 4.17: Observed and computed significant wave heights, using the the German Bight model.

Wave heights

The location of the wave buoys for which data are available during the simulated period, are located outside the domain of the Dithmarschen Bight Model. Therefore, only the results of the German Bight wave model could be evaluated on the basis of these data. The computed significant wave heights are shown in Figure 4.17, together with the observations. The peak in the evening of December 3^{rd} is reproduced well by the model. Before and after this peak the wave heights are underestimated. They do reflect the trends in the time series of the wave heights during the storm period rather well.

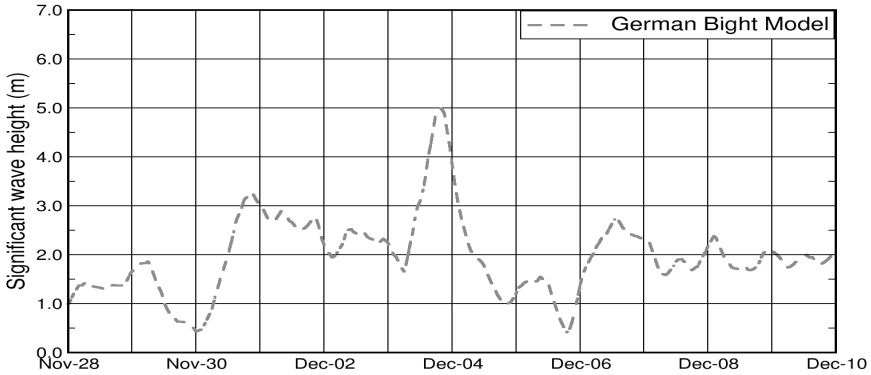

Figure 4.18: German Bight wave model results at the open boundary of the Dithmarschen Bight Model.

4.A.5 Morphodynamics

Based on the coupled flow-wave model the suspended and bed load sediment transports have been modelled, followed by morphological updating. Where applicable, the model settings were obtained from the calibrated and validated morphodynamic model.

The total simulation consisted of a sequence of sub-simulations of one hour, in which the sequence of Figure 4.13 was executed. In each sub-simulation the hydrodynamics, sediment dynamics and bathymetry resulting from the previous sub-simulation were used as initial conditions. This ensured a smooth continuation over the entire model period.

The time series plots in Figure 4.16 indicate the imposed water levels. Figure 4.18 shows the significant wave heights computed with the German Bight model at a location near the centre of the western boundary of the Dithmarschen Bight model. The time series show the imposed wave conditions at the open boundary of the latter model.

The morphodynamic simulation has been carried out for the period from November 25^{th}, 0.00 UTC, until December 6^{th}, 0.00 UTC. The evaluation of the effects of the storm on the morphodynamics has been based on the computed morphological changes from November 30^{th} until December 6^{th}, to exclude initialisation effects. This period approximately covers the period where the storm surge can be clearly recognised in the water level records.

Model results

The sedimentation and erosion patterns that resulted from the simulation are shown in Figure 4.19. When the storm conditions are imposed, much larger changes can be seen in the model results. However, the maximum changes are still within the range of 40 mm. On the western tidal flats erosion can be seen, caused by the incoming swell waves. The here eroded sediment is deposited in the surrounding channels, viz. the

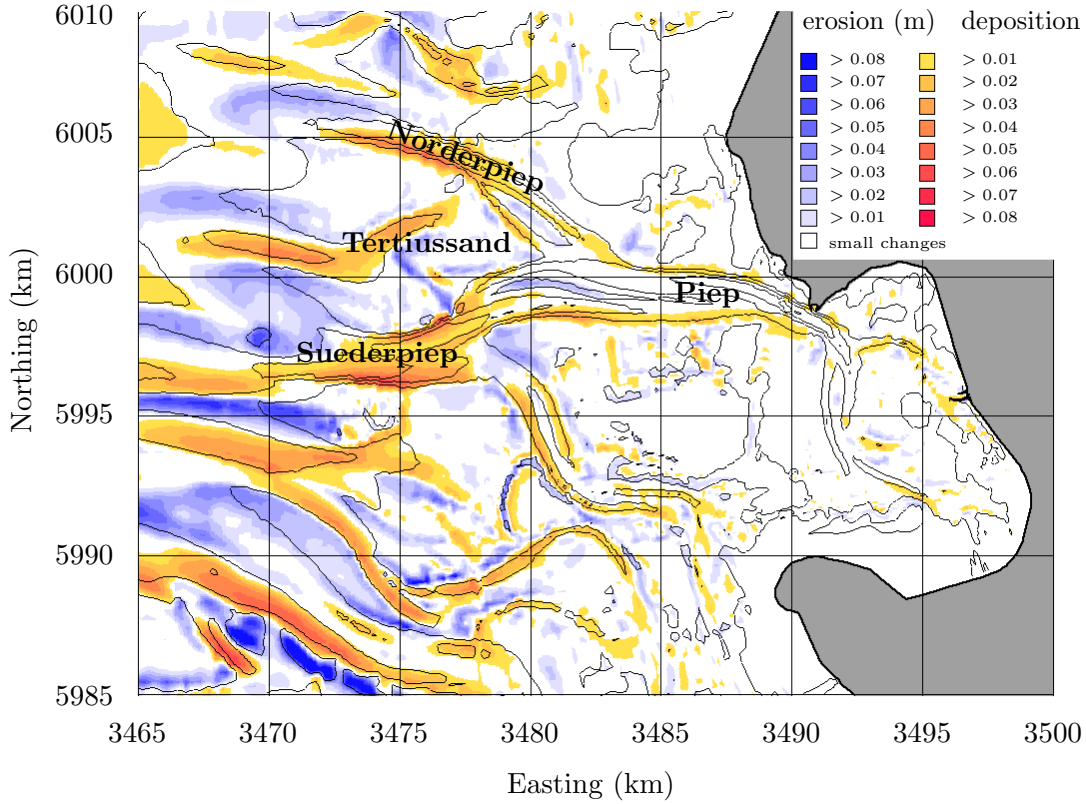

Figure 4.19: Sedimentation and erosion (in m) during the storm period of six days.

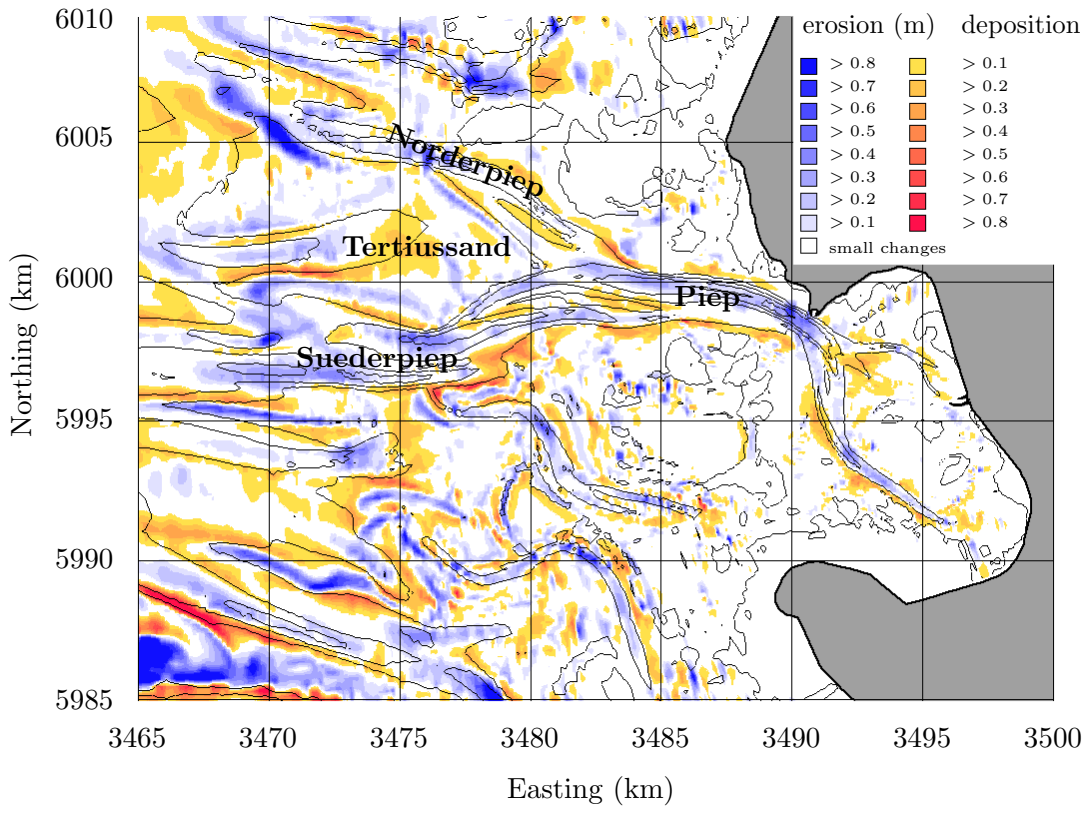

Figure 4.20: Sedimentation and erosion over a one-year period with representative conditions.

small channel in the middle of Tertiussand and the channels Norderpiep and Suederpiep on its Northeast and South. Along the channel Piep sediment is deposited along its banks.

For comparison, the modelled morphological changes over a one-year period with varying conditions is shown in Figure 4.20, starting from the same bathymetry as the afore-mentioned simulations. The computed maximum changes over a year are in the range of 0.6 m. The computed storm-induced changes are therefore relatively small.

4.A.6 Conclusions

With the presented approach, the hydrodynamics during the storm Anatol could be reproduced quite well with the applied sequence of nested models. The main differences that are found in the hindcasts of the water levels concern the results during low tide, when both the German Bight Model and the Dithmarschen Bight Model underestimate the water level. With the wave model for the German Bight the wave heights at the two measurement locations could be simulated in a good manner. In the model results the peak wave heights were very close to the observed values. Around the peak they were under-predicted but showed the correct trends. In general the storm surge was reproduced reasonably well, resulting in proper input for the sediment transport and morphodynamic models.

The morphodynamic model results showed that the maximum morphological changes during the storm were at most about 0.05 m for small areas during the evaluated 6-day period. In comparison to the morphological changes of a one-year simulation, in which representative conditions for tide, waves and wind were imposed, these changes are relatively small. The model results of the one-year simulation showed morphological changes of up to 0.6 m over much larger parts of the study area. The influence of storm conditions on the morphological behaviour of the domain over medium-term periods is therefore limited within the applied model.

From the above is concluded that the inclusion of storm conditions in medium scale morphodynamic simulations does not significantly influence the morphodynamic results within the current model set-up.

4.B Model study: representative tide

4.B.1 Introduction

The morphodynamic simulations with the Dithmarschen Bight model are based on a limited number of imposed boundary conditions. In this Appendix a model study to evaluate of the significance of the representation of the varying tidal cycles during a full spring-neap tidal cycle by a representative tide is presented. The influence of this simplification has been analysed through comparison of model results from one-year morphodynamic simulations.

In the following Paragraph the variation of the tidal range is briefly presented, followed by the explanation of the set-up of the morphodynamic simulation in Paragraph 4.B.3. The evaluation of the influence of the imposed tidal cycle(s) has been carried out for two cases. In the first case only tide has been imposed, whereas in the second case the representative swell and wind climates have been added. The results are presented in Paragraphs 4.B.4 and 4.B.5.

4.B.2 Tidal variation

The variation of the tidal range in the Dithmarschen Bight is rather strong with a neap tidal range of approximately 2.9 m and a spring tidal range of circa 3.8 m. This is depicted in the modelled water levels near Buesum for a full spring-neap tidal cycle in Figure 4.21. The variations in tidal range may influence the tide-averaged sediment transport rates, which are used in the morphodynamic model to compute the morphological changes. These changes may be quantitative as well as qualitative, i.e. a change of direction at a certain location. The computed morphological changes on the basis of the defined representative tide may therefore be different from those computed on the basis of the full spring-neap tidal cycle.

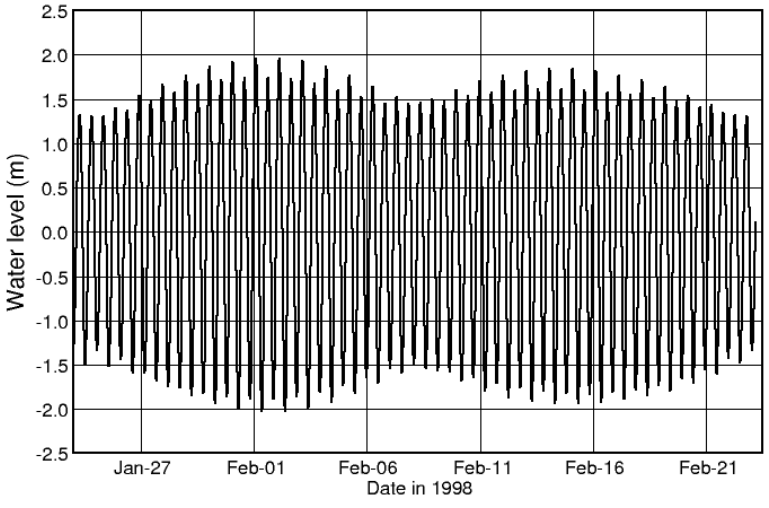

Figure 4.21: Computed water level (purely tide-induced) at Buesum.

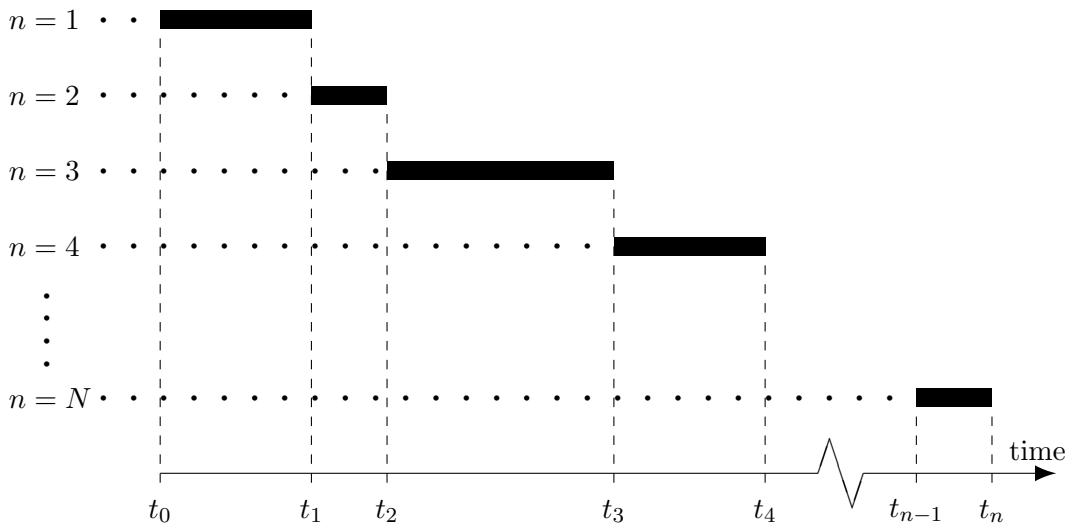

Figure 4.22: Scheme for splitting-up the simulation into N sub-simulations with varying conditions and simulation periods.

4.B.3 Morphodynamic simulation set-up

In the case of imposing one representative tidal cycle during the whole model period, the modelling scheme of Figure 4.22 has been executed (see also Paragraph 4.B.3). For each n a new loop is started in which the morphodynamic model is restarted with the most recently computed bathymetry. Based on the imposed representative wind and wave climate, as described in Paragraph 4.4.6 a total of 13 loops are made per year of simulation, one for each representative condition. In these loops, the representative tide (see Paragraph 4.4.3) has been imposed exclusively.

To simulate the entire spring-neap tidal cycle, this scheme has been adapted. Instead of repetition of the representative tide, the entire tidal cycle has been imposed. To this purpose, each condition n has been split-up into 30 sub-loops. For each day a loop as in Figure 4.22 has been carried out in which the next 24 hours of hydrodynamics have been imposed, followed by a sediment transport computation and a morphodynamic update for $\frac{1}{30}$ of the original loop simulation period $(t_n - t_{n-1})$. Thus, after simulation of one loop thirty sub-loops have been carried out with a final bathymetry based on the entire spring-neap tidal cycle as a result. This bathymetry has subsequently been entered in the next loop. The settings for the constituent models have been based on the results of their calibration and validation (Chapter 3).

For the here-presented morphodynamic simulations over a period of one year, it takes almost ten days for the tide-only case and four weeks when including wave simulations, on a 3 GHz processor with 1 Gb RAM. For comparison, the representative tide-approach needs circa one day per simulated year on the same computer.

4.B.4 Tidal conditions only

The computed sedimentation and erosion of the simulation with the normal model set-up and representative tide are shown in Figure 4.23(a) and the results of the simulation with the full spring-neap cycle in Figure 4.23(b). Since no wind or waves have been imposed in these simulations, the computed changes are purely based on the tide.

It can be seen that the sedimentation and erosion patterns are highly similar. In the western part of the domain some local quantitative differences can be found that do not exceed 0.2 m. In the remaining part of the domain, almost no differences can be found. Also, in the results of both simulations the morphological changes have the same sign, i.e. either sedimentation or erosion. Thus it can be concluded that the application of a representative tide instead of simulating the entire spring-neap cycle can very well be selected for the here-considered case without wind and waves.

4.B.5 Including representative wind and swell climates

Since waves have an significant influence on the morphological evolution of the domain, the previous test has been repeated for a case in which the representative wind and swell conditions have been imposed. The morphological changes over the considered period of one year, as computed by the model in the original set-up are shown in Figure 4.24(a). Figure 4.24(b) shows the model results of the adapted set-up, with the spring-neap tidal cycle imposed.

Similar to the case without wind and waves, the results of both simulations are highly similar. When imposing the full spring-neap cycle, the changes are slightly larger. However, the character of the changes (sedimentation or erosion) is generally identical. Hence, also for the simulations with swell and wind included, the representation of the tide can be applied without significantly influencing the model results.

4.B.6 Conclusions

From the results of the two test cases, it can be concluded that there is no significant change in the computed morphological changes when representing the tidal conditions by a representative tidal cycle, as opposed to simulating the entire spring-neap cycle. It confirms that the adopted approach to impose the representative tidal conditions in the morphodynamic simulations of the applied morphodynamic model is scientifically sound. In terms of the computational requirements it results in a significant reduction in the time needed for the simulations.

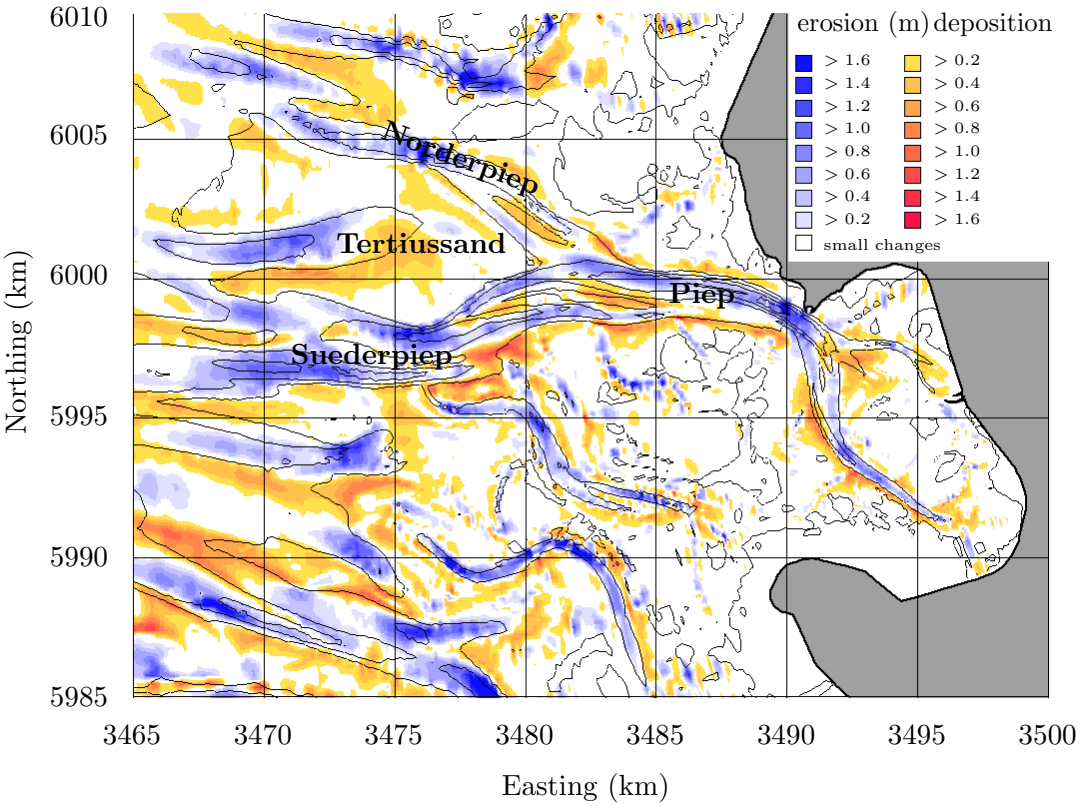

(a) Normal model set-up and representative tide.

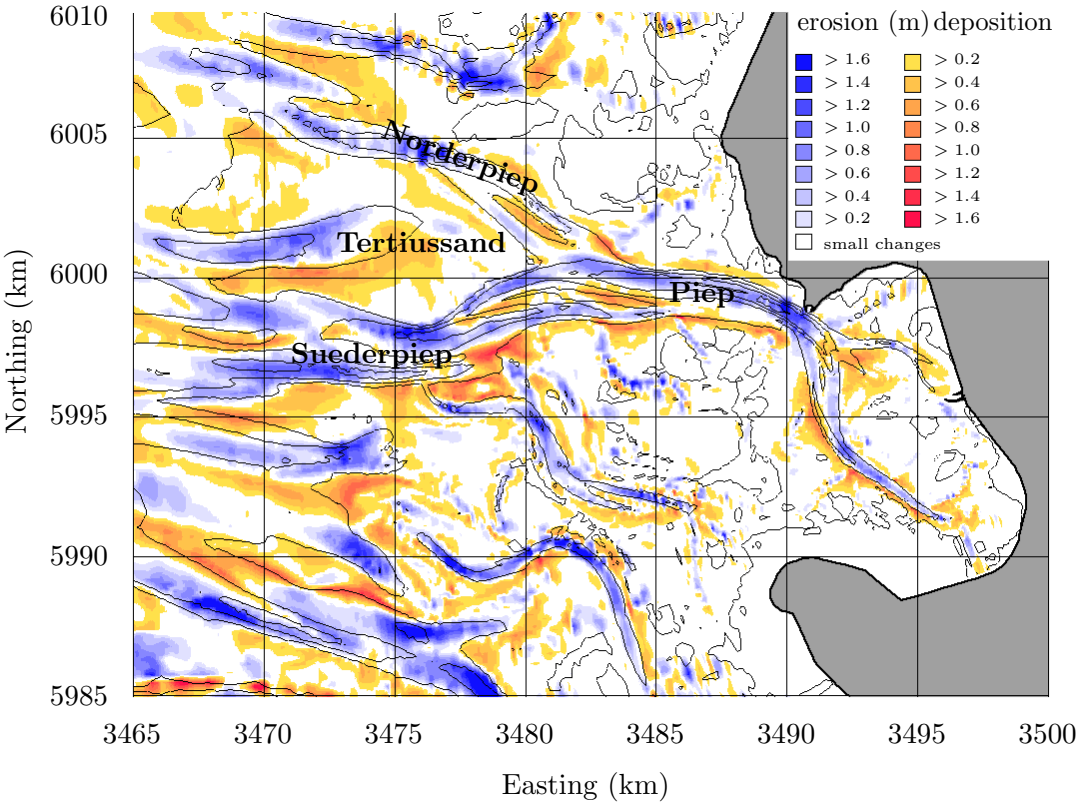

(b) Adapted model set-up and spring-neap cycle.

Figure 4.23: Computed sedimentation and erosion over a period of one year, no wind and waves.

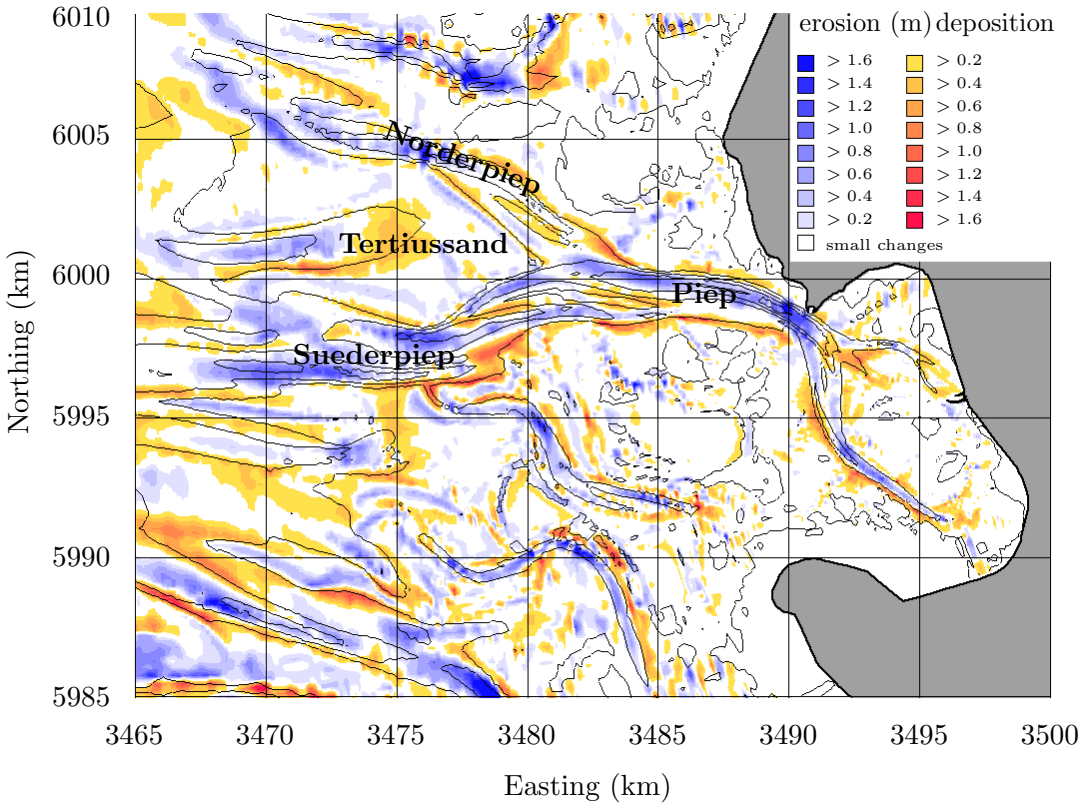

(a) Normal model set-up and representative tide.

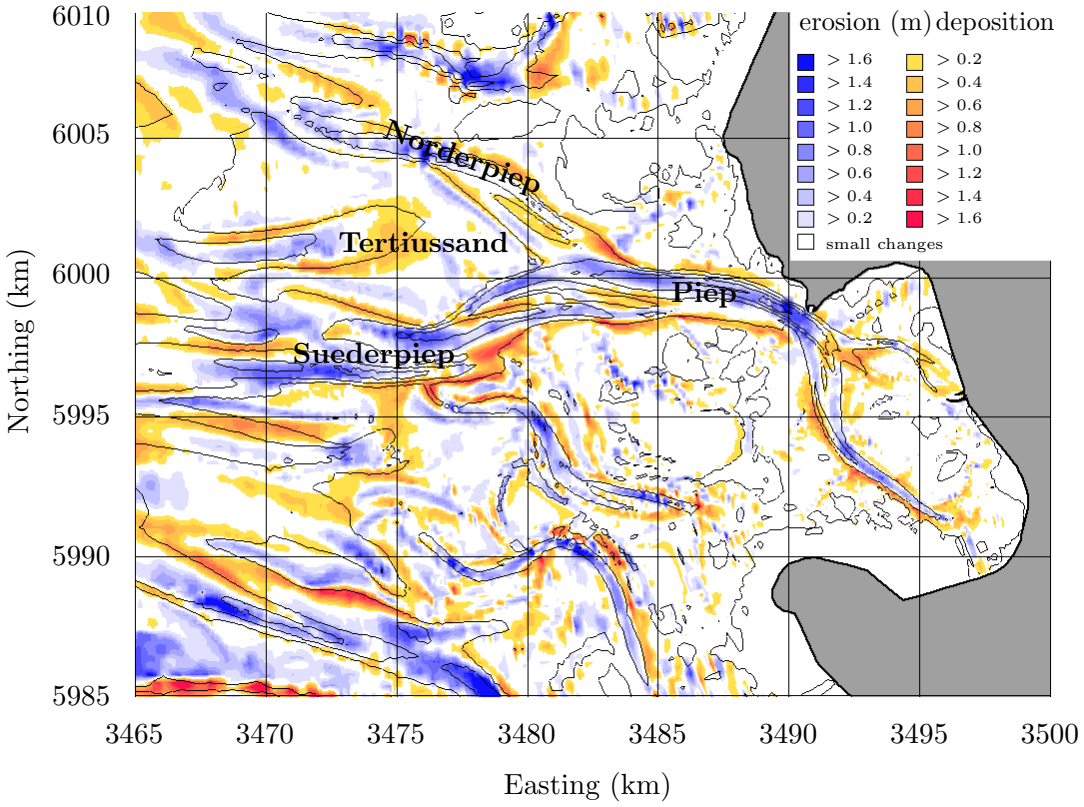

(b) Adapted model set-up and spring-neap cycle.

Figure 4.24: Computed sedimentation and erosion over a period of one year, with representative wind and waves climates.

Chapter 5

Calibration and validation of the medium scale morphodynamic model

5.1 Introduction

On the basis of set-up of the morphodynamic model and its boundary conditions together with the defined representative conditions in terms of tides, swell and wind (Chapter 4), the model calibration and validation have been carried out following the MTM-approach. The calibration of the model is based on the comparison of the computed morphological changes with the observed changes over a 10-year period, from 1977 to 1987. The considered strategy in the calibration is the topic of Section 5.2. The adjustment of the representative open boundary conditions for the medium scale morphological evolution and the calibration of model parameters are discussed in Section 5.3. In the validation the calibrated model has been applied for computation of the morphological changes over the period from 1990 to 1999. This is presented in Section 5.4. The results obtained are discussed in Section 5.5.

5.2 Strategy for the model calibration

To calibrate the medium scale morphodynamic model, a strategy has been defined that consists of two phases. The first – *external* – phase concerns the optimisation of the defined representative conditions for tide, waves and wind. In the second – *internal* – phase the model settings are adjusted to further improve the model results.

Phase 1: Optimisation of the representative conditions

The defined strategy starts of with an evaluation of the model results from a simulation over ten years in which the representative conditions, defined on the basis of

input filtering techniques, were imposed. The correctness of these conditions has been determined, considering the main trends in the morphological changes. The imposed conditions consist of the representative tidal cycle, swell climate and wind climate, as defined in the previous Chapter on the basis of input filtering approaches. As shown in Appendix 4.B, the application of the defined representative tidal cycle yields highly similar results as the imposition of a full spring-neap tidal cycle. Hence, the representative tide has been applied in the calibration without further changes. The model study concerning storm conditions (Appendix 4.A) showed that storms do not have a significant influence on the morphodynamics in the applied model. Therefore it is concluded that storm conditions are sufficiently covered by the representative swell and wind climates (see also Paragraph 4.4.7). The effects of the representative swell and wind climates on the medium scale morphodynamics have not yet been evaluated and have therefore been considered as variables in this initial step of the calibration. The model results have been checked on the basis of the morphological changes of the exposed tidal flats to evaluate the imposed swell and wind conditions, with a focus on the flat Tertiussand in the western part of the study area. The changes in location of the iso-depth contours and the patterns of sedimentation and erosion were considered in the optimisation of the imposed swell and wind conditions. On the basis of these adapted conditions the model results could be improved and the main trends were predicted reasonably well.

Phase 2: Optimisation of the model settings

After phase 1 has been carried out, the morphodynamic model was able to hindcast the main morphological changes correctly, on the basis of the optimised conditions for tide, swell and wind. This formed the basis for further improvements of the model. Again the model results have been evaluated on the basis of changes in location of the iso-depth contours and the sedimentation and erosion patterns. Where in the first phase the focus has been on the exposed, western part of the study area, in the second phase the inner part has been considered. The evaluation was extended with the comparison of the volumetric changes of several sub-domains. This approach led to a calibrated model that is able to reproduce the medium scale morphodynamics of the study area generally correctly.

5.3 Calibration

In the calibration the 10-year period from 1977 to 1987 has been considered. The interpolated bathymetric measurements from 1977 and 1987 are shown in Figure 5.1(a) and (b), followed by the morphological changes in Figure 5.2. The bathymetry from 1977 served as initial bathymetry for the model simulations.

In the first phase of the calibration the model results have been improved through

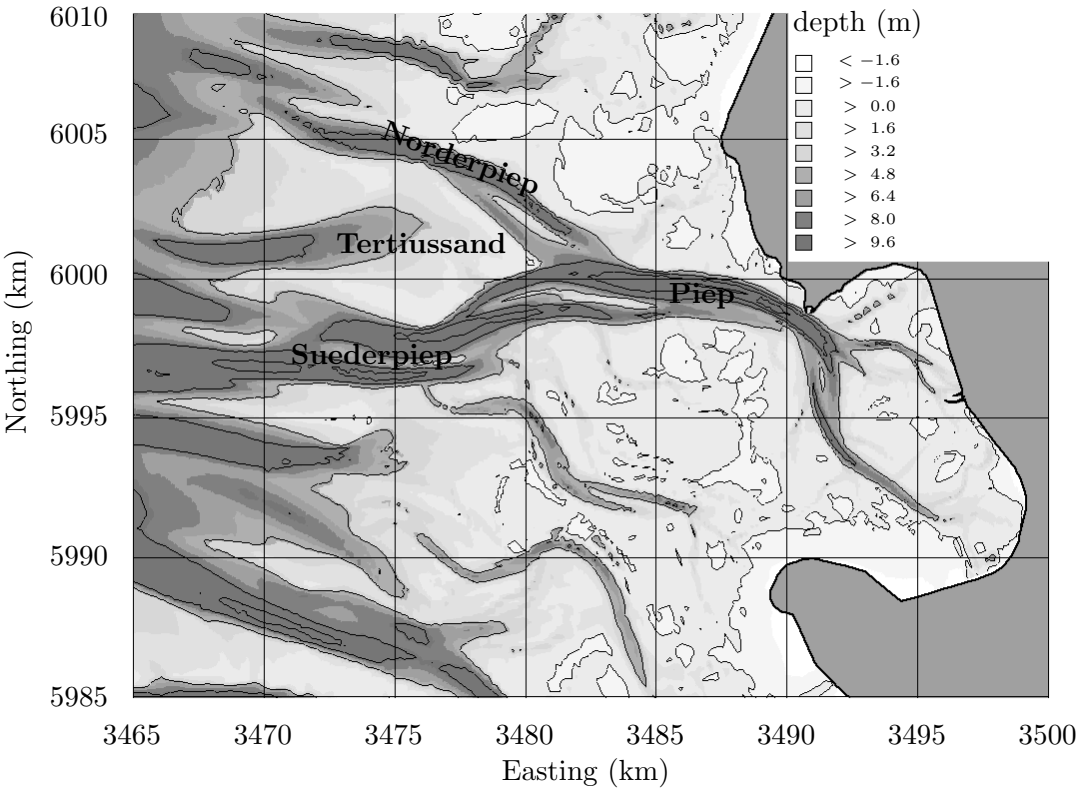

(a) 1977

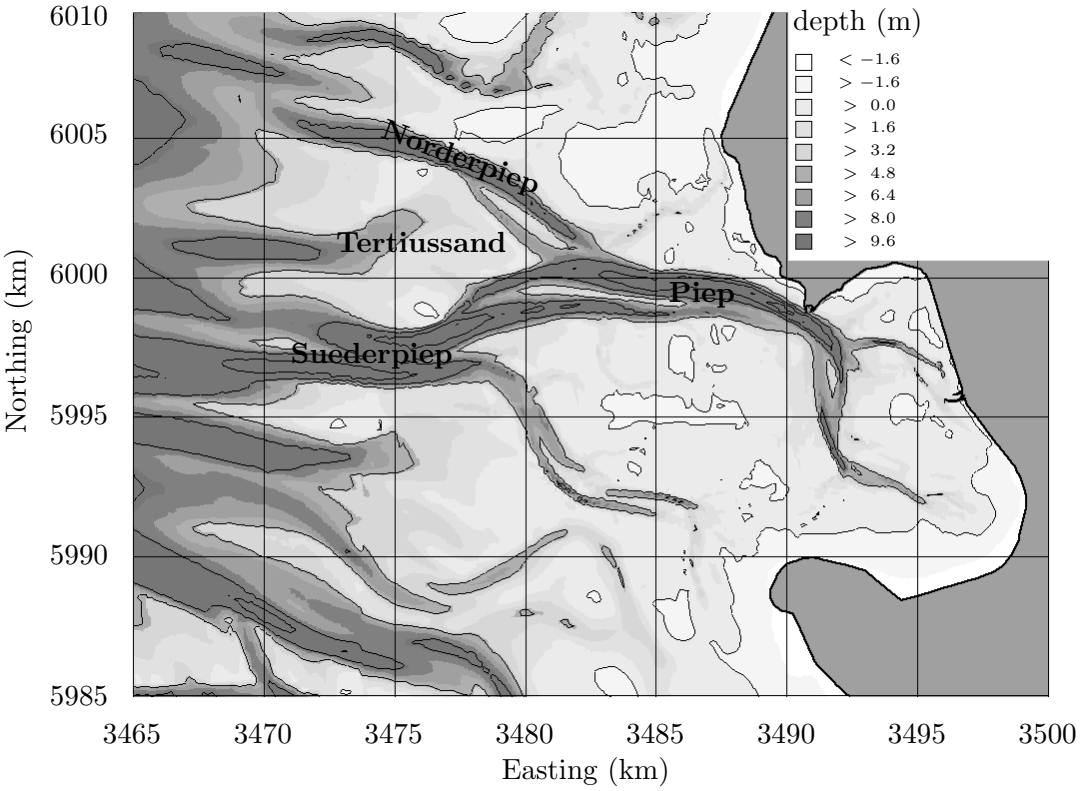

(b) 1987

Figure 5.1: Interpolated bathymetric measurements in the central Dithmarschen Bight for the years (a) 1977 and (b) 1987.

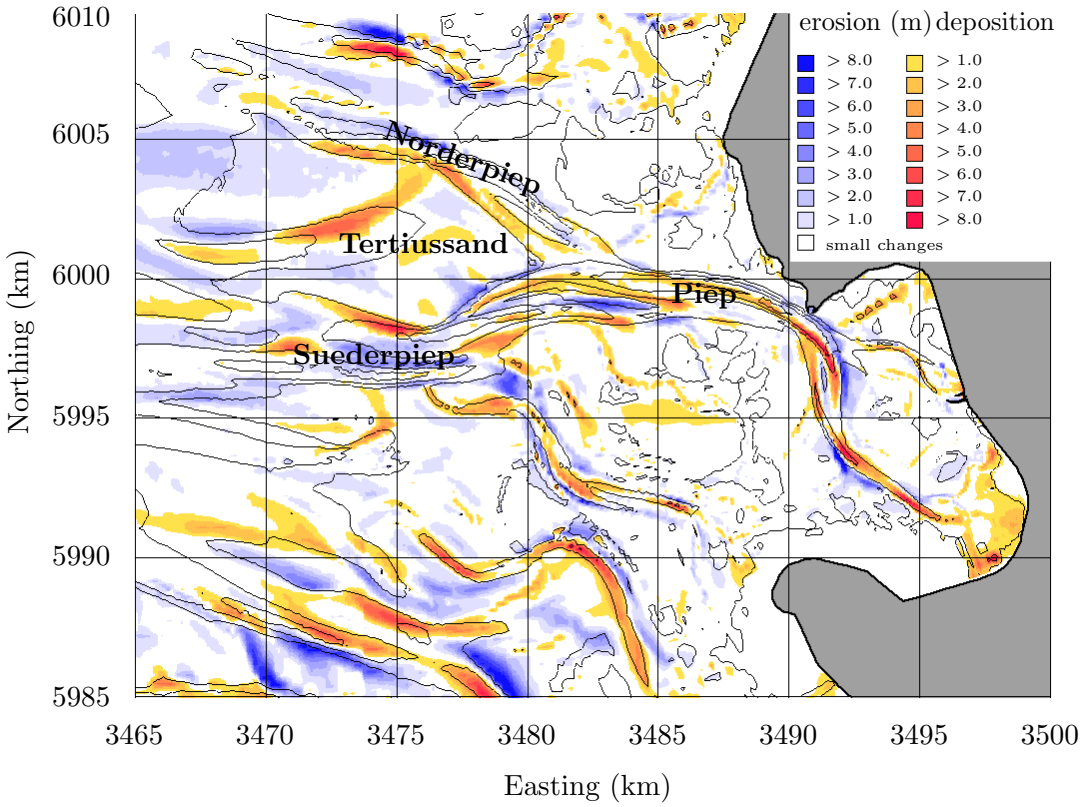

Figure 5.2: Observed sedimentation and erosion patterns between 1977 and 1987 (isolines from 1977).

variation of the imposed swell and wind conditions. Since the representative swell climate has been based on the statistical reduction of the observations from a somewhat distant location into a limited number of conditions, this formed the first topic in the calibration. It has been followed by the calibration on the basis of the defined representative wind conditions. The comparisons between the model results and the observations have been made on the basis of the change in location of the depth contours and patterns of sedimentation and erosion. This is described in Paragraph 5.3.1.

In the second phase further model improvements have been made by adapting several parameters in the sediment transport computation, such as the Bijker constant in the applied sediment transport formula, proposed by Bijker [1971]. The calibration for this variable is discussed exemplarily in Paragraph 5.3.2, as it brought significant improvements. Other settings that were considered in the calibration are for example the slope-induced sediment transport and the definition of the wave boundary layer.

The depth contours and sedimentation and erosion patterns have been considered in this phase, together with a volumetric analysis of several sub-domains. In the analysis the changes of the relative wet volume below MSL are considered. The sub-domains consist of the tidal flat Tertiussand and the main channels of the study area, as shown in Figure 5.3. The volume changes have been indexed to the volumes of the starting

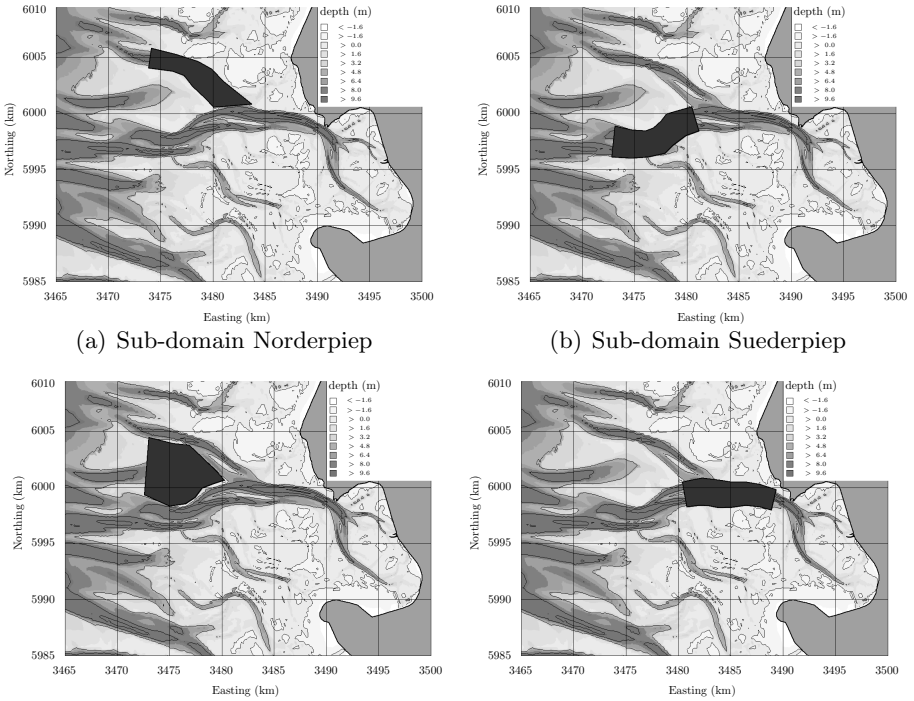

(a) Sub-domain Norderpiep (b) Sub-domain Suederpiep

(c) Sub-domain Tertiussand (d) Sub-domain Piep

Figure 5.3: Location of the considered sub-domains in the volume analysis.

bathymetry for 1977 as follows:

$$V_{rel,i} = \frac{V_i}{V_{1977}} * 100\ \% \tag{5.1}$$

with:

$V_{rel,i}$	relative wet volume below MSL of a sub-domain in year i
V_{1977}	wet volume below MSL of a sub-domain in 1977
V_i	wet volume below MSL of a sub-domain in year i

The bathymetric data for the inner tidal flats do not have a good coverage. The scarce data has to be interpolated onto the model grid to generate a complete, but probably inaccurate, coverage of the tidal flats. Small differences in depth may result in large changes of volume due to the large areas of the tidal flats. Thus, these areas have been omitted in the volume analysis. From the volumetric analysis, conclusions can be drawn about the models ability to predict the correct order of sediment that is imported or exported from a sub-domain, being essential for a good simulation of the medium scale morphodynamics.

5.3.1 Calibration for the wind and swell climate

In the western part of the domain the swell waves generally break on the margins of the tidal flats. Therefore, the waves in the sheltered regions of the study area are mainly locally generated waves. During high tide, the fetch over the tidal flats can

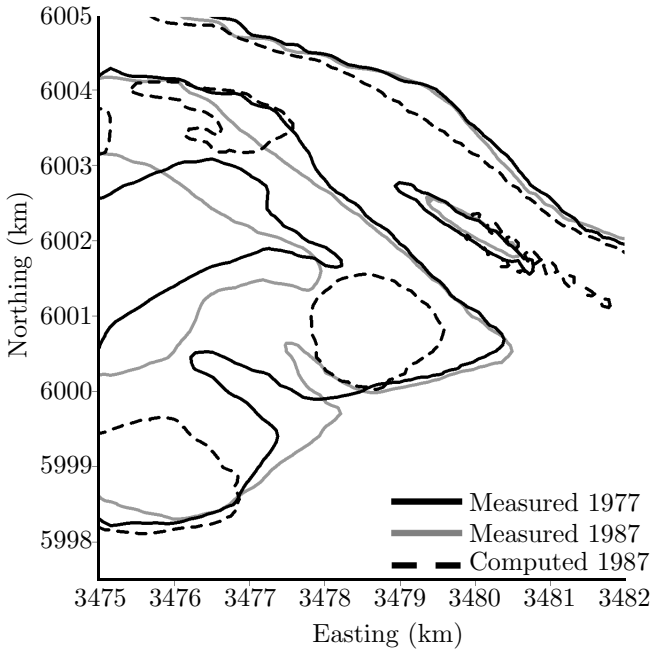

Figure 5.4: Changes of the 3 m depth contours of sub-domain Tertiussand. The model results are based on the originally defined representative swell and wind climates.

get large enough to generate significant wave action. Combined with the limited depth these waves can have a clear influence on the morphodynamics. The correctness of the imposed climate of swell and wind conditions is thus very important.

As a first estimate, the representative swell and wind climates (Paragraph 4.4.6) have been imposed. In Figure 5.4 the change in position of the 3 m depth contours near Tertiussand is shown. It shows the strong reduction of the areas with depths less than 3 m. Only small shallower stretches can be found near its northern, eastern and southern edges. The measurements show that the tidal flat changes its shape at 3 m depth, but does not significantly reduce in area. The computed sedimentation and erosion are shown in Figure 5.5. Compared to the observed changes (see Figure 5.2) the model results show a much too strong erosion of the outer tidal flats, indicating that the imposed conditions were too severe.

Thus an optimisation of the imposed climate has been carried out by defining versions with reduced wave heights and/or wind speeds. In this process, the directions in the wind and swell climates have been kept identical to their original values, to assure that the dominating swell and wind directions in the area are properly represented. Furthermore, the probability of occurrence for each condition has been retained to limit the number of variables.

In the evaluation of the model results, the focus has been mainly on the location and development of the western tidal flats, with an emphasis on Tertiussand. It could be concluded that a reduction of 50 % of the swell wave heights yielded much improved results. Further improvements could be made by lowering the wind speeds with a

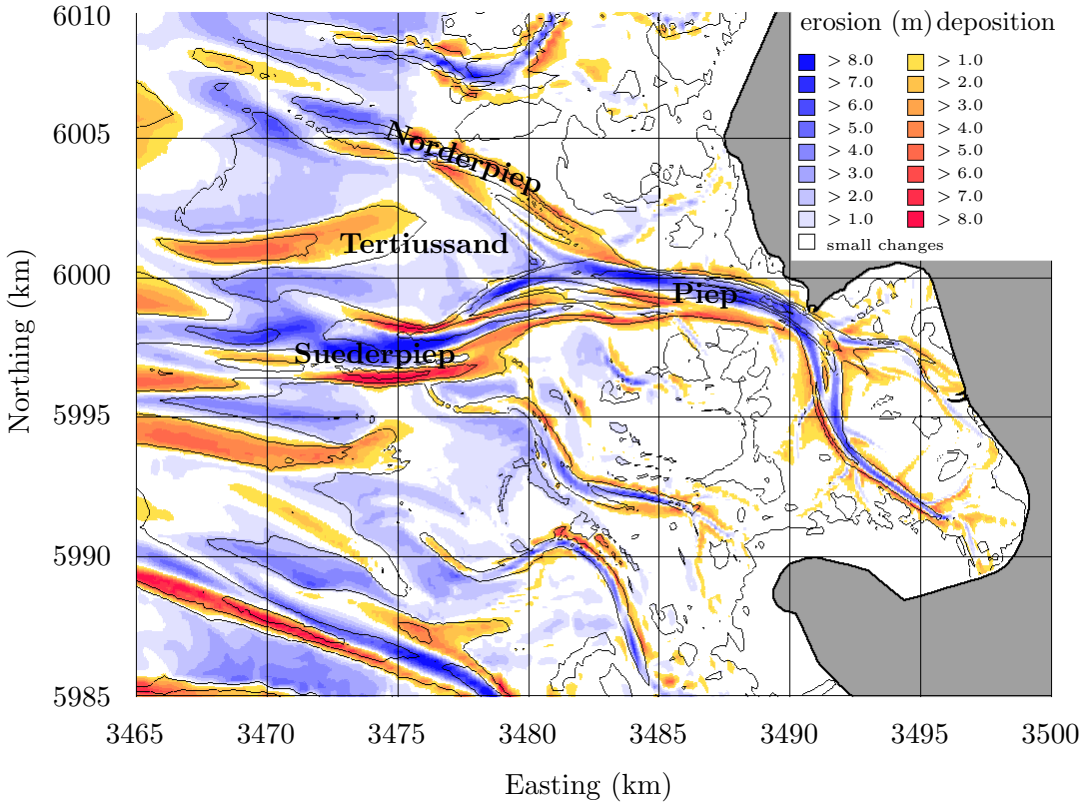

Figure 5.5: Computed sedimentation and erosion patterns between 1977 and 1987 (isolines from 1977). The computation is based on the originally defined representative swell and wind climates.

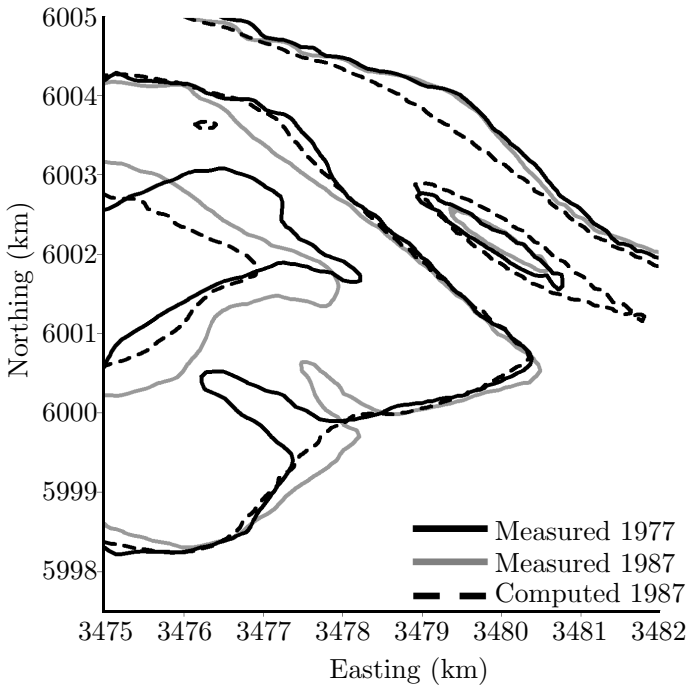

Figure 5.6: Changes of the 3 m depth contours of sub-domain Tertiussand. The model results are based on the optimised swell and wind climates.

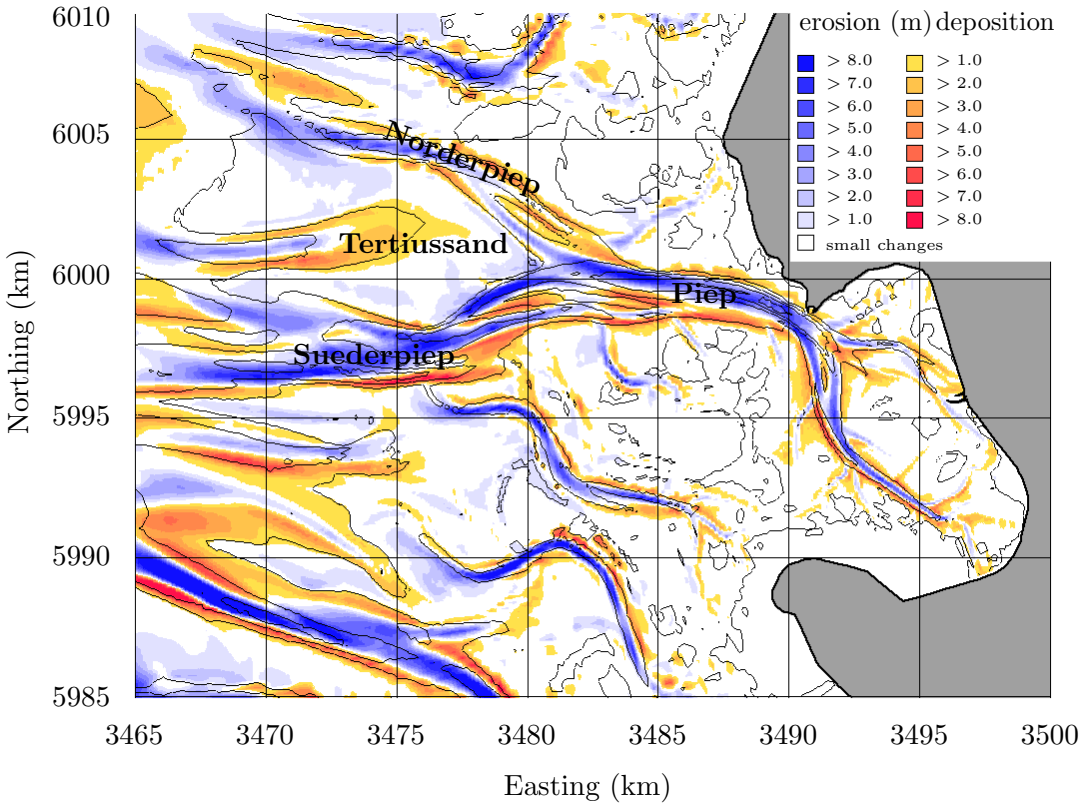

Figure 5.7: Computed sedimentation and erosion patterns between 1977 and 1987 on the basis of the optimised swell and wind climates (isolines from 1977).

factor of two. On the basis of these adaptations, the 3 m depth contours for 1987 are computed as shown in Figure 5.6. It shows a significant improvement of the model results in comparison to the results of the simulation on the basis of the originally defined representative conditions. The sedimentation and erosion patterns resulting from the 10-year simulation with the optimised swell and wind conditions are shown in Figure 5.7.

The changes of the relative wet volume below mean sea level of the sub-domain Tertiussand are shown in Figure 5.8 for both simulations. It shows that the trends in the volume changes are reproduced much better by the simulation with the optimised swell and wind climates. The small decrease of wet volume is computed correctly by the model with the adapted conditions. In the model results for the original swell and wind climates, the wet volume significantly increases, indicating large erosion of Tertiussand. The tidal flat also contains areas above MSL. However, the sediment volume above MSL has not been considered since the interpolated bathymetric measurements showed too much fluctuation over the examined period to make a proper comparison.

5.3.2 Calibration for the Bijker constant

With the optimised swell and wind climates the calibration on the basis of Bijker's constant has taken place. The calibration of the sediment transport model (Section 3.5) has

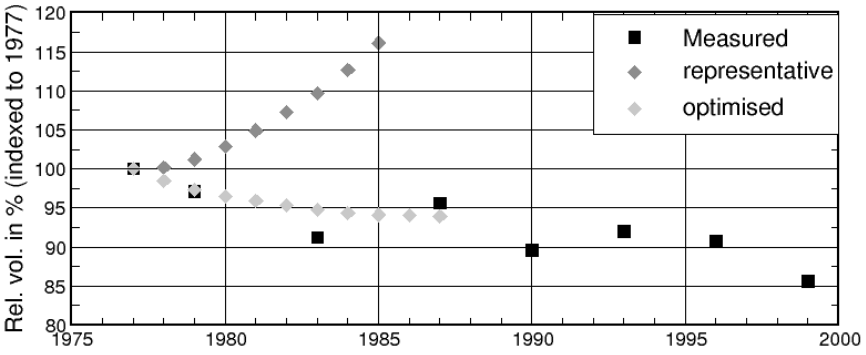

Figure 5.8: Observed and computed changes in the relative wet volume below mean sea level of sub-domain Tertiussand. Comparison of the model results on the basis of the originally defined representative swell and wind climates to those on the basis of the optimised swell and wind climates.

been carried out for relatively calm conditions only. This was limited by the availability of the measurement data of suspended sediment concentrations and flow velocities. These vessel-based measurements could only be carried out during conditions with limited wave heights (see Paragraph 3.5.2). Therefore, the constant in the applied sediment transport formula (Bijker [1971]) has been calibrated for these conditions only. The value of this parameter in the Bijker transport formula (see Paragraph 3.A.4) should generally range between 1 and 5 [WL | Delft Hydraulics, 2003c]. In the validation of the sediment transport model (Paragraph 3.5.2) a constant value of 3 was found to give the best results.

In Delft3D-MOR Bijker's constant can be defined as a constant value or as a value varying with the wave conditions. In the latter case, the value has to be specified for deep water waves and for shallow water waves. For intermediate conditions an interpolation between these values takes place. Thus, the ratio between the significance of the waves and the currents on the sediment transport, as well as its magnitude, can be influenced by variation of the deep water and shallow water values.

This calibration led to the conclusion that the model results could be improved when setting the deep water value to 1 and the shallow water value to 5, effectively enhancing the sediment transport for shallow water conditions with waves and reducing it for situations with deep water waves and without waves.

The changes of the depth contours of Tertiussand and neighbouring channels are shown in Figure 5.9. It shows that the model correctly predicts the slightly eastward extension of the flat in the Northeast and Southeast. The deeper area on Tertiussand is also reduced in size, although the shape does not exactly follow the observed changes. The observed deepening of the minor channel on the Southeast, branching of from the Suederpiep cannot be seen from the computed changes. In the Norderpiep the increase

in area of the submerged bar is reproduced rather well by the model. From the comparison of Figures 5.6 and 5.9 can be seen that, for example for the northeastward expansion of Tertiussand, the simulation with a varying Bijker's constant yielded better results. Furthermore, when considering the computed morphological changes on the basis of these settings in Figure 5.10, the variable definition of the Bijker's constant gives better overall results. It can be seen that the model predictions have improved significantly for the study area.

The strong erosion in the channels has been reduced to values within the range of the observations. Also, the sedimentation in the southeastern part of the Norderpiep (indicated by **A**) is limited to the channel banks, which is in agreement with the measurements. The migration of the flat Tertiussand towards the Northeast (location **B**), depicted by the sedimentation along the middle section of the Norderpiep is predicted correctly as well, although the magnitude is somewhat underestimated. At location **C**, the southward extension of Tertiussand is computed correctly. The magnitude of the sedimentation is slightly less than observed. On the western part of Tertiussand the model does not predict the observed behaviour of the small channel. In the Piep the submerged bar shows deposition together with erosion in the bordering sub-channels. The measured erosion of the southeastern part of Tertiussand can be seen as well.

A comparison between the computed volumetric changes of the simulations with a constant value of 3, respectively with a varying value between 1 and 5, is shown in Figure 5.11 together with the observed changes. For sub-domain Tertiussand the wet volume reduced somewhat less, but is clearly within the range of the measured volumes. A significant improvement was achieved in the Suederpiep, with a much smaller increase in wet volume as in the case with the constant value for Bijker's constant. The changes in the sub-domain Norderpiep have been reduced and follow the observed behaviour better. In the central sub-domain of the channel Piep the increase in volume has been reduced, however the decreasing tendency in the measurements is not reproduced.

Summary

In general can be said that with the calibrated model it was possible to reproduce the medium scale observed changes in the main channels and on Tertiussand. The eastward migration and southward extension of Tertiussand could be reproduced, as well as deepening of the main channels. Also, the accretion on the submerged bar in the Piep can be seen in the model results. The volumetric changes of the examined sub-domains follow the observations, except for the Piep. The smaller scale changes on the flat Tertiussand could not be hindcasted accurately, although some of the computed trends were similar to the observations.

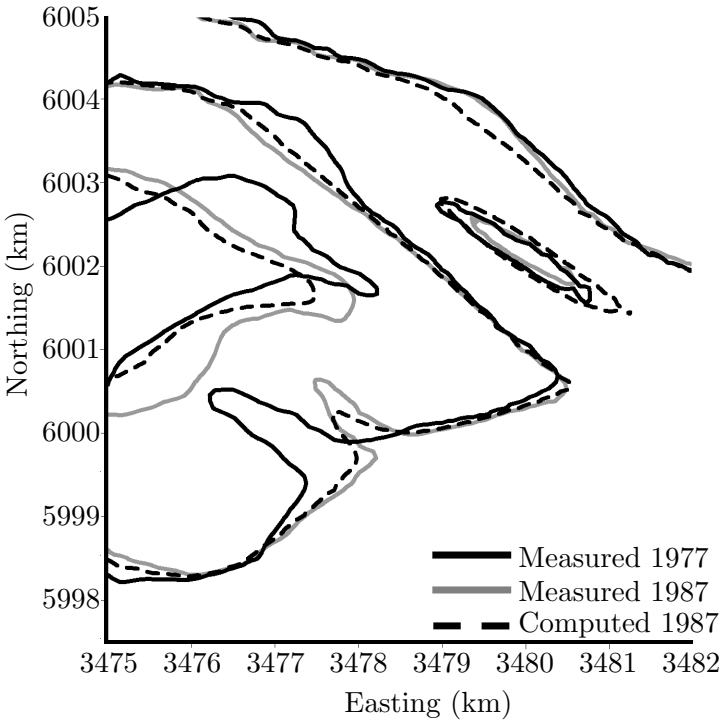

Figure 5.9: Changes of the 3 m depth contours of sub-domain Tertiussand. Model results with the Bijker's constant ranging from 1 for deep water waves to 5 for shallow water waves.

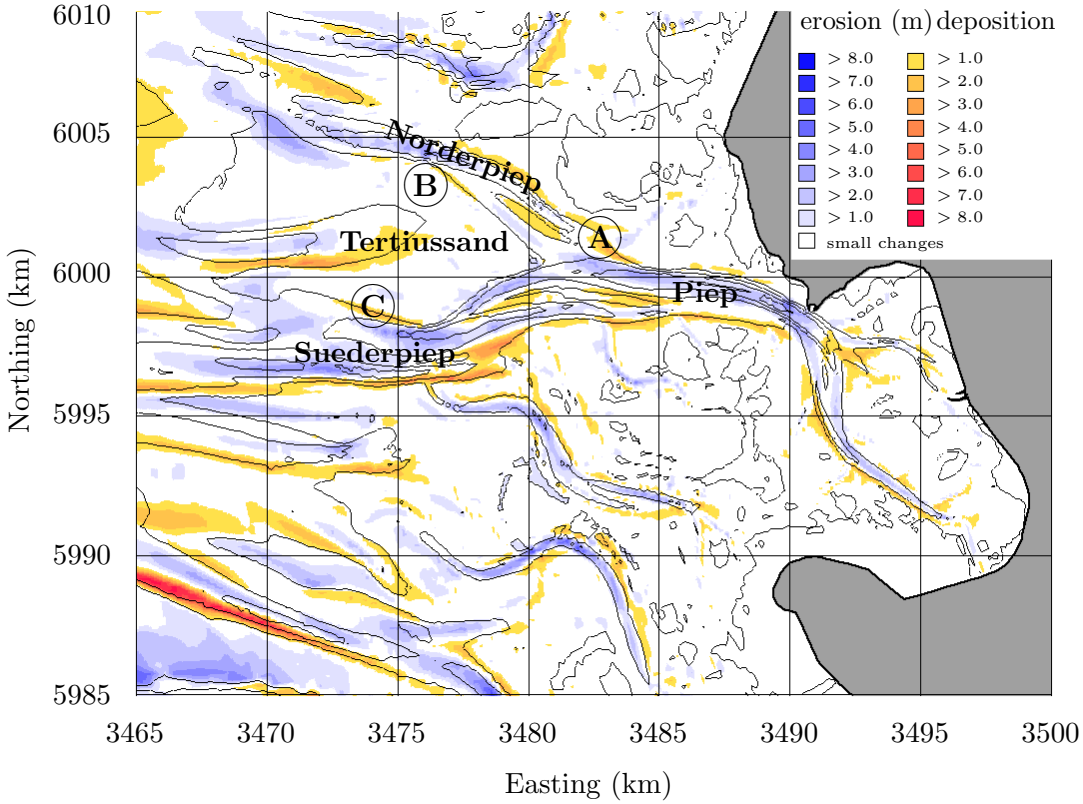

Figure 5.10: Computed sedimentation and erosion patterns between 1977 and 1987. Model results with the Bijker's constant ranging from 1 for deep water waves to 5 for shallow water waves (isolines from 1977).

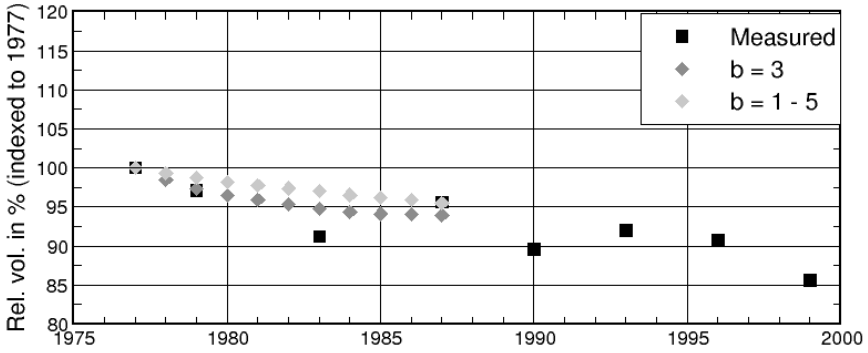

(a) Tertiussand

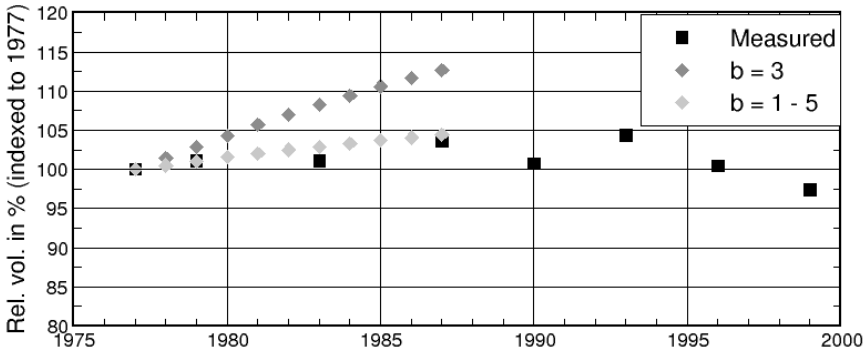

(b) Suederpiep

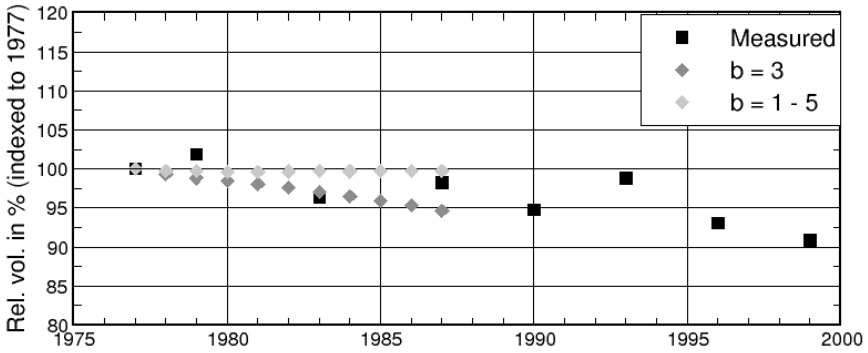

(c) Norderpiep

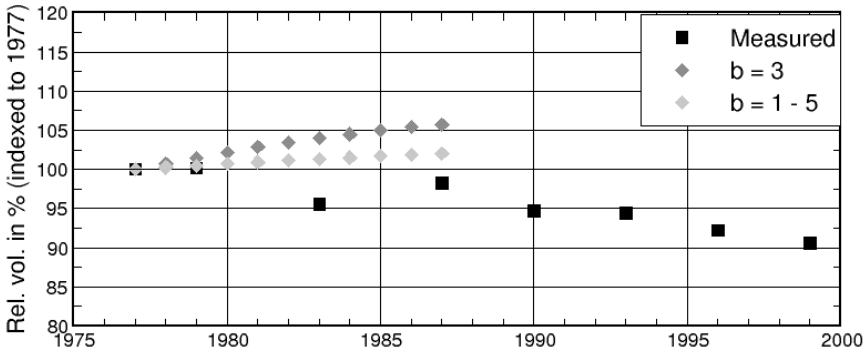

(d) Piep

Figure 5.11: Changes of the relative wet volume below MSL. Model results with the Bijker's constant ranging from 1 for deep water waves to 5 for shallow water waves.

5.4 Validation

In the validation, the adjusted representative boundary conditions and the calibrated model settings have been applied without further changes to evaluate the performance of the morphodynamic model for a different period. The optimal settings and defined swell and wind conditions were considered to model the morphological evolution of the period from 1990 to 1999.

The iso-lines at a depth of 3 m are shown in Figure 5.12 for the validation period. The extension of Tertiussand towards the Northeast is reproduced quite well by the model. At the eastern tip the model results show a retreat of the tidal flat, which cannot be seen in the observations. On the southern side, the minor channel that branches from the Suederpiep onto Tertiussand has significantly increased in length. Here the model predicts a much wider area below 3 m depth. In the Southwest, the southward expansion of Tertiussand is reproduced very well.

The interpolated bathymetric measurements of 1990 and 1999 are shown in Figures 5.13(a) and (b). Based on these interpolated data the observed morphological changes during this period have been computed. These are shown in Figure 5.14. Due to the limited coverage of the shallow areas only the results for the tidal channels and the flat Tertiussand are reliable.

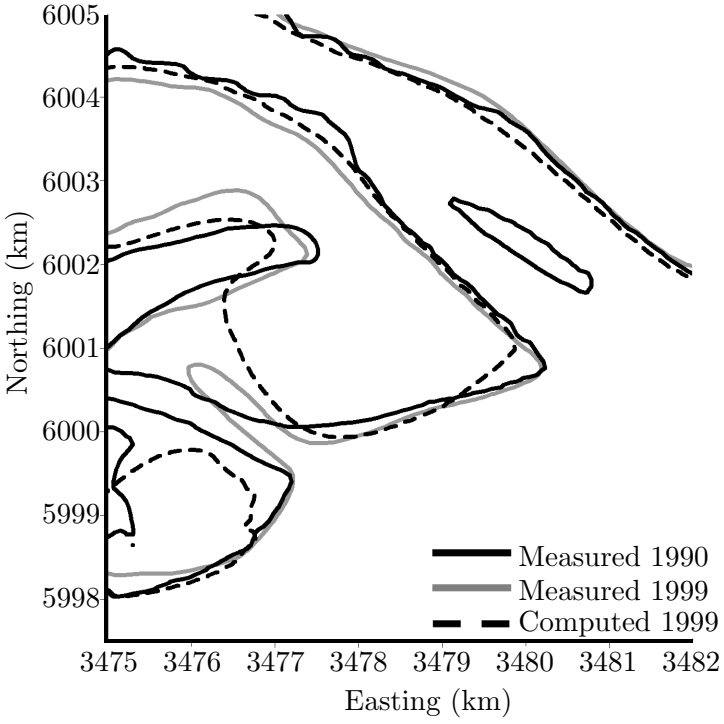

Figure 5.12: Changes of the 3 m depth contours of sub-domain Tertiussand. Model results based on the calibrated morphodynamic model settings and conditions.

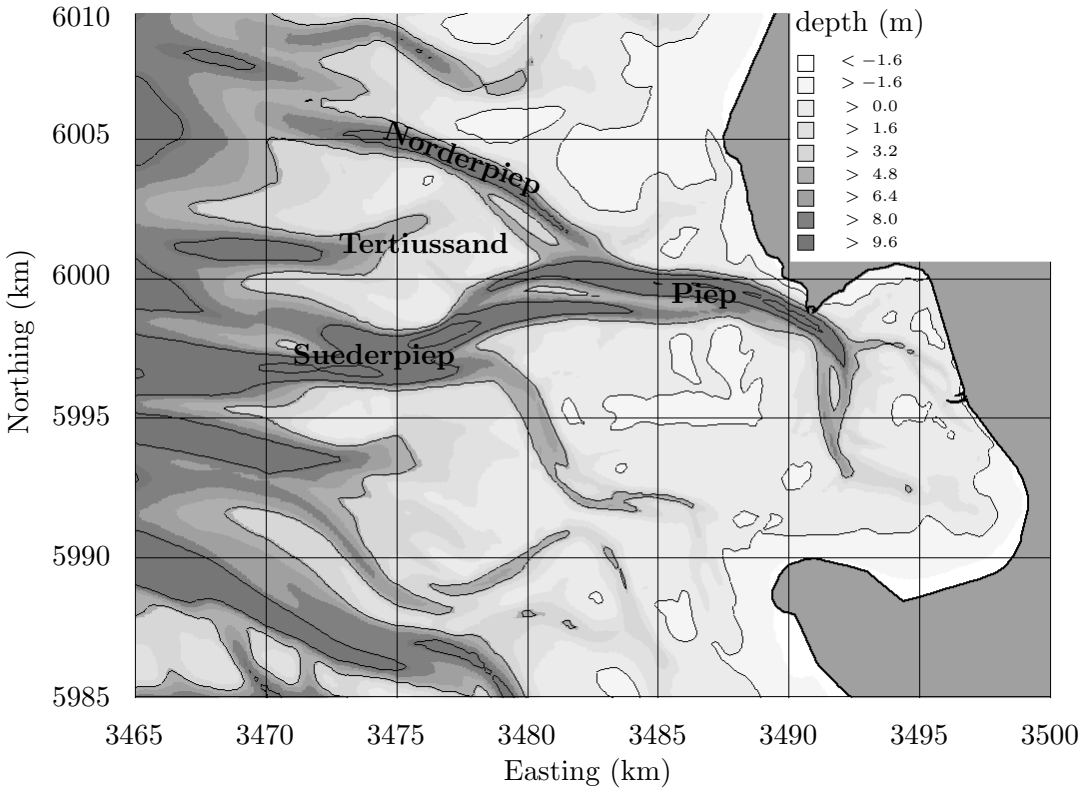

(a) 1990

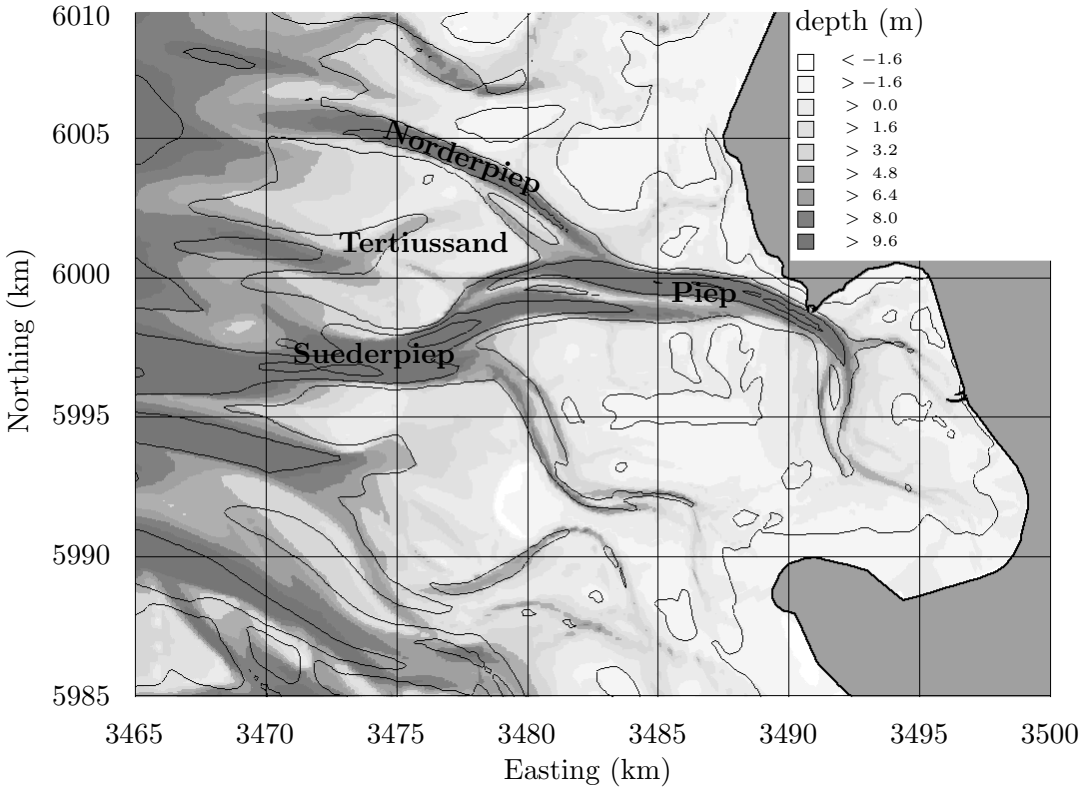

(b) 1999

Figure 5.13: Interpolated bathymetric measurements in the central Dithmarschen Bight for the years (a) 1990 and (b) 1999.

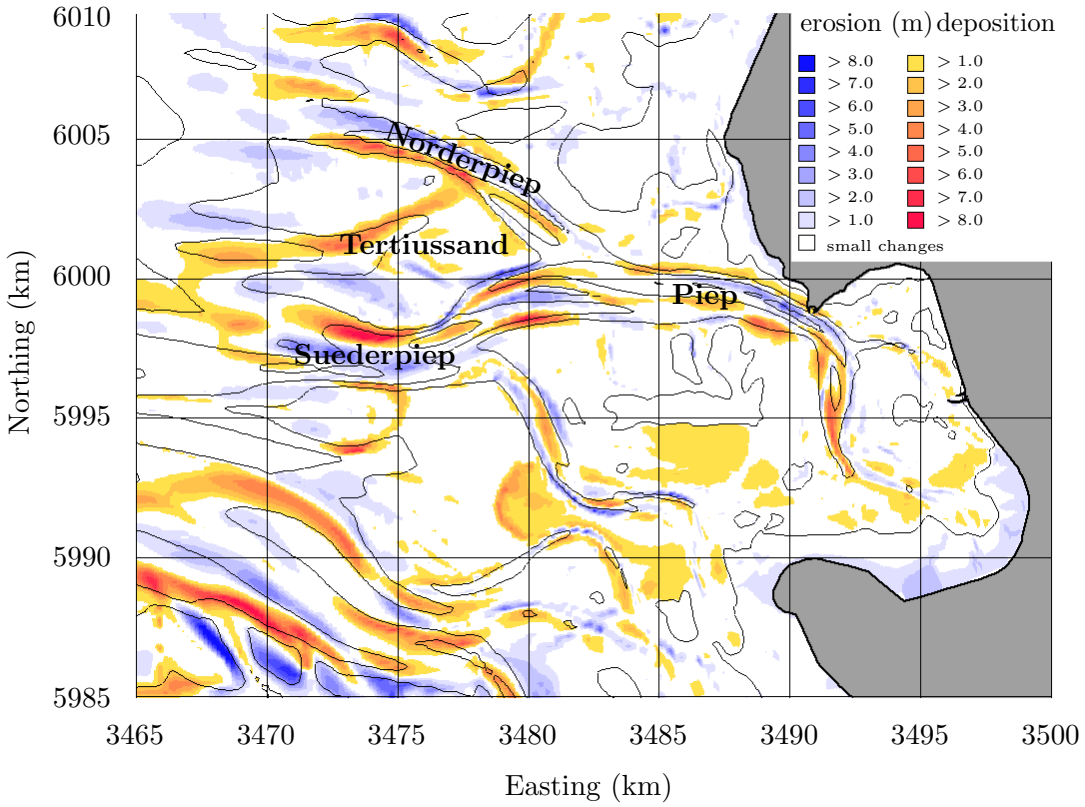

Figure 5.14: Observed sedimentation and erosion between 1990 and 1999 (isolines from 1990).

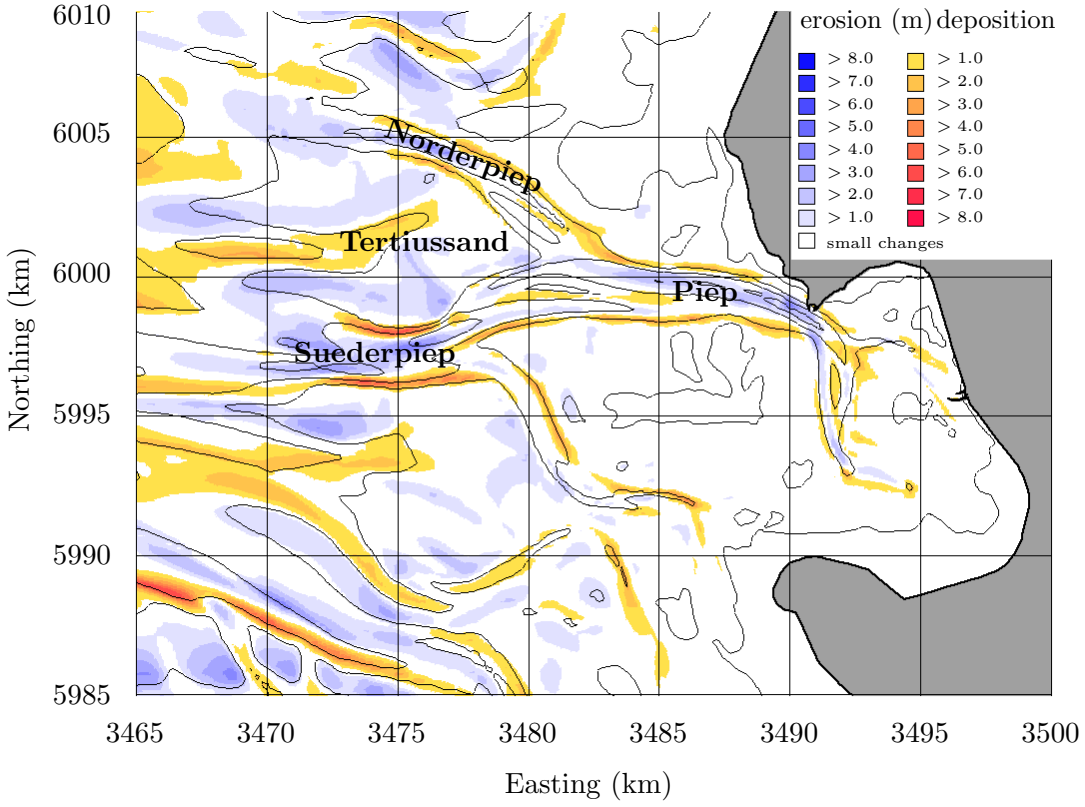

Figure 5.15: Computed sedimentation and erosion between 1990 and 1999 (isolines from 1990). The computation is based on the calibrated morphodynamic model settings and conditions.

The computed morphological changes over this period are shown in Figure 5.15. The model results show a good similarity with the observations. On the flat Tertiussand, the erosion of the higher northwestern and southwestern parts is computed in the correct order of magnitude. The stretch of sedimentation from West to East in the sub-channel in the middle of Tertiussand also matches quite well. Nevertheless, some small scale differences can be found. At its northern and southern edges, bordering the Norderpiep, respectively the Suederpiep, the extension of the tidal flat can be seen in the model results, although the magnitude of the sedimentation near the channel banks is somewhat less.

In the Norderpiep the erosion of the main channel is reproduced, with approximately the same amounts in the northwestern section. In the southeastern section the model predictions sedimentation, where slight erosion has been observed. Here, the accretion of the submerged bar is visible but under-predicted in the model results.

The observed deepening in the western part of the Suederpiep can also be found in the model results, as well as the sedimentation at its southern boundary. In the middle of the channel the model predicts erosion, although sedimentation has been observed. Close to the channel junction, the measured erosion at its northern bank, bordering Tertiussand, can be seen from the model results. However, the amount of erosion is underestimated.

The erosion of the channel Piep is computed rather well, as well as the deposition on the southwestern channel bank. The accretion of the submerged bar is visible in the model results, although it is shifted somewhat southward.

The results of the volume analysis for the four sub-domains (Figure 5.3) are shown in Figure 5.16. For consistency with the volume analysis of the calibration, the volumes have again been indexed to the volumes of 1977. It shows that the computed trends of the relative volume changes are in agreement with the observed trends.

Summary

Although local changes are not always predicted correctly by the model for the considered period of ten years, the overall medium scale behaviour of the main morphological features is reproduced rather well. The computed trends in the volume changes follow those observed for all four considered sub-domains. In the comparison of the sedimentation and erosion patterns good similarity was found as well. The changes in location of the iso-depth lines around Tertiussand are generally in agreement with the observed changes, with some smaller scale exceptions.

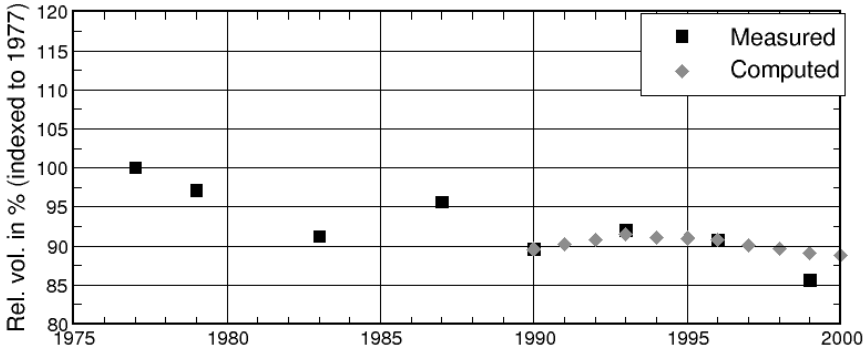

(a) Tertiussand

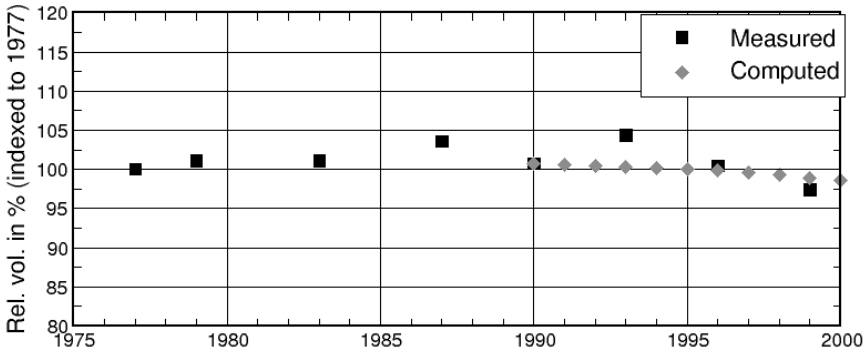

(b) Suederpiep

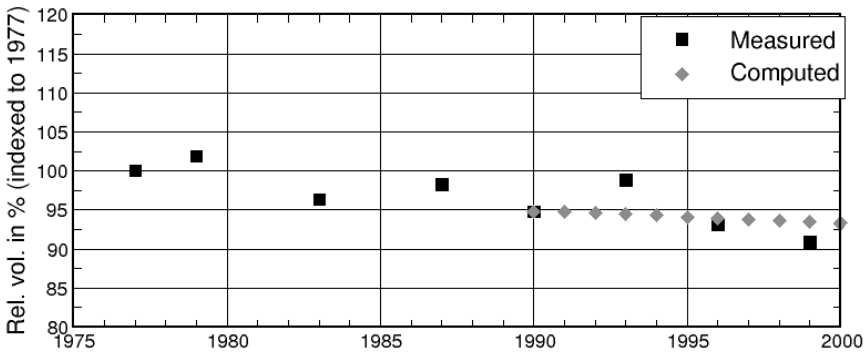

(c) Norderpiep

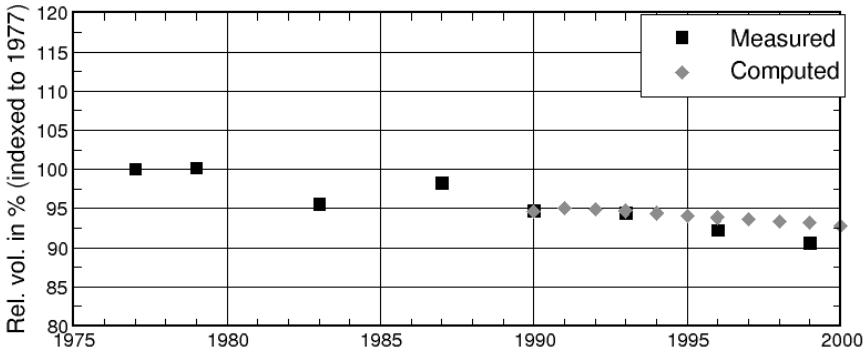

(d) Piep

Figure 5.16: Changes in the relative wet volume below MSL. The computation is based on the calibrated morphodynamic model settings and conditions.

5.5 Discussion

Based on 20 years of bathymetric measurements the morphodynamic model has been evaluated. The first 10 years, from 1977 to 1987 have been used for the calibration of the model. The validation was carried out considering the period from 1990 to 1999. The evaluation has taken place on the basis of volumetric analyses, comparison of sedimentation and erosion patterns and the migration of iso-depth lines.

In the calibration, the model results could be improved significantly by adapting the initially applied representative climates for wind and swell. It was concluded that the effects of the initial wind and swell climates were too strong in the model results. Therefore, the climates have been reduced gradually until the optimal response of the computed morphodynamics was found. It was concluded that with a reduction of the swell climate with 50 % and lowering the wind speeds also by 50 % the computed morphological changes could be brought within the range of the observed changes. Further improvement of the morphodynamic model could be made by adjusting the value of the Bijker's constant. It resulted in a value varying between 1 for locations with deep water wave conditions and 5 for areas with strong wave action. In the intermediate areas Bijker's constant varies between 1 and 5. With these values, a much better agreement with the observations was achieved. Locally, the model could not predict the correct behaviour but on the medium scale the morphological trends of the area of interest were mainly reproduced correctly.

In the validation the calibrated model was applied to hindcast the morphodynamics between 1990 and 1999. Similar to the results of the calibration, the trends in the morphological evolution were reproduced rather well, with the exception of several changes on a smaller scale.

Chapter 6

Medium scale morphodynamic processes and prediction

6.1 Introduction

In the validation of the morphodynamic model it was shown that the model gives a good representation of the medium scale morphodynamics in the considered tidal channels and bordering tidal flats in the Dithmarschen Bight. Hence, the model can be applied for realistic modelling of the medium scale morphological evolution of this area. Two applications considering the medium scale morphodynamics (in MTM-mode) are described in this Chapter.

The first application of the model concerns the analysis of the significance of the driving forces for the morphological evolution of the considered area. The two-year period from 1977 to 1979 was considered, in which the settings of the validated model were used. Several morphodynamic simulations have been made with varying imposed conditions. The descriptions of the intercomparison of the model results and the deduction of relationships between the conditions and occurring morphological changes are given in Section 6.2.

Secondly, the morphodynamic model has been applied to forecast the morphological changes over a period of ten years, starting from the bathymetry of 1999. The results of this prediction are discussed in Section 6.3.

6.2 Significance of the driving forces for the medium scale morphodynamics

Through comparison of the model results of several morphodynamic simulations over a period of two years, the significance of the main driving forces behind the morphological evolution of the study area has been evaluated. The interpolated bathymetric measure-

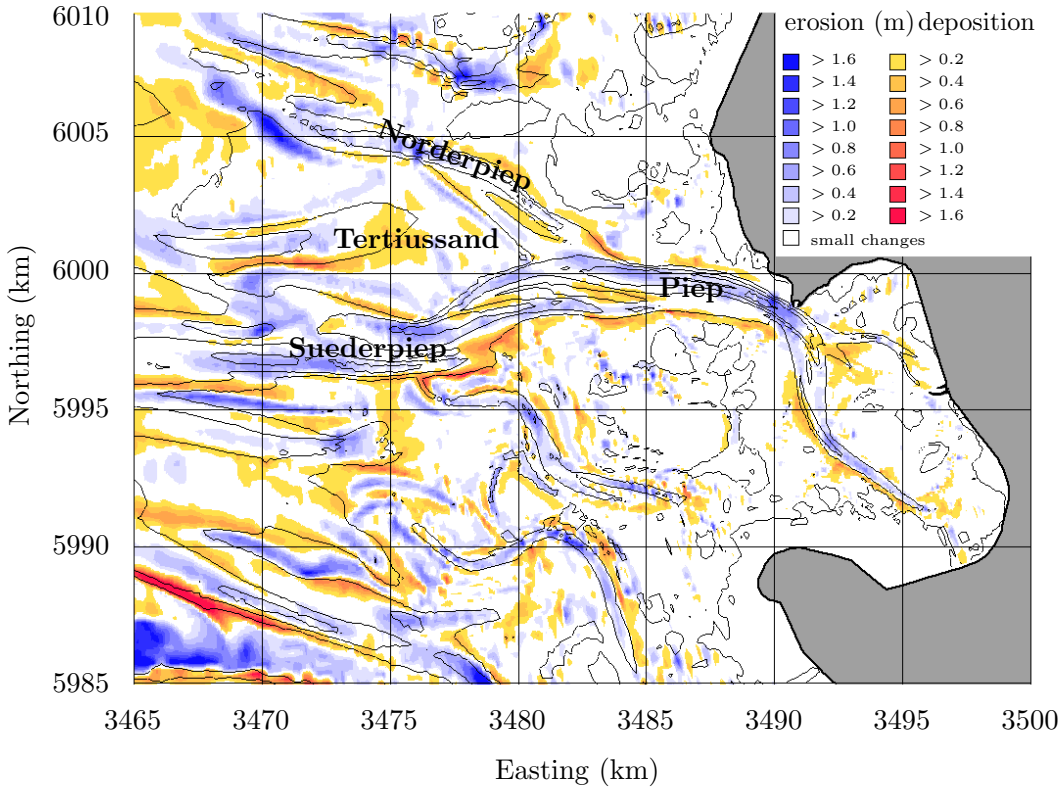

Figure 6.1: Computed morphological changes from 1977 to 1979, based on the optimised swell and wind climates (iso-lines from 1977).

ments from 1977 served as the initial model bathymetry. As described in the previous Chapter, the main driving forces are the tide, the swell and locally generated waves and the local wind. The local wind conditions generate changes in the tidal currents and water levels, and in the locally generated wave conditions. They have therefore been considered indirectly, since eolian effects are not considered in this study.

The evaluation of the significance of each of these forces on the morphodynamics has been based on the analysis of the sedimentation and erosion patterns. Comparisons have been made to the model results of the simulation with the optimised swell and wind conditions of the validated model over the same two-year period. The computed sedimentation and erosion of this simulation, from hereon referred to as the reference simulation, are shown in Figure 6.1.

In Paragraph 6.2.1 the influence of the tidal conditions on the morphological evolution is discussed. This is followed by the description of the effects of the swell in Paragraph 6.2.2. The influence of local wind and wind generated waves are the topic of Paragraph 6.2.3. Since the significance of storm conditions has been described in Appendix 4.A, these conditions have been not been considered here. A synthesis of the results is given in Paragraph 6.2.4.

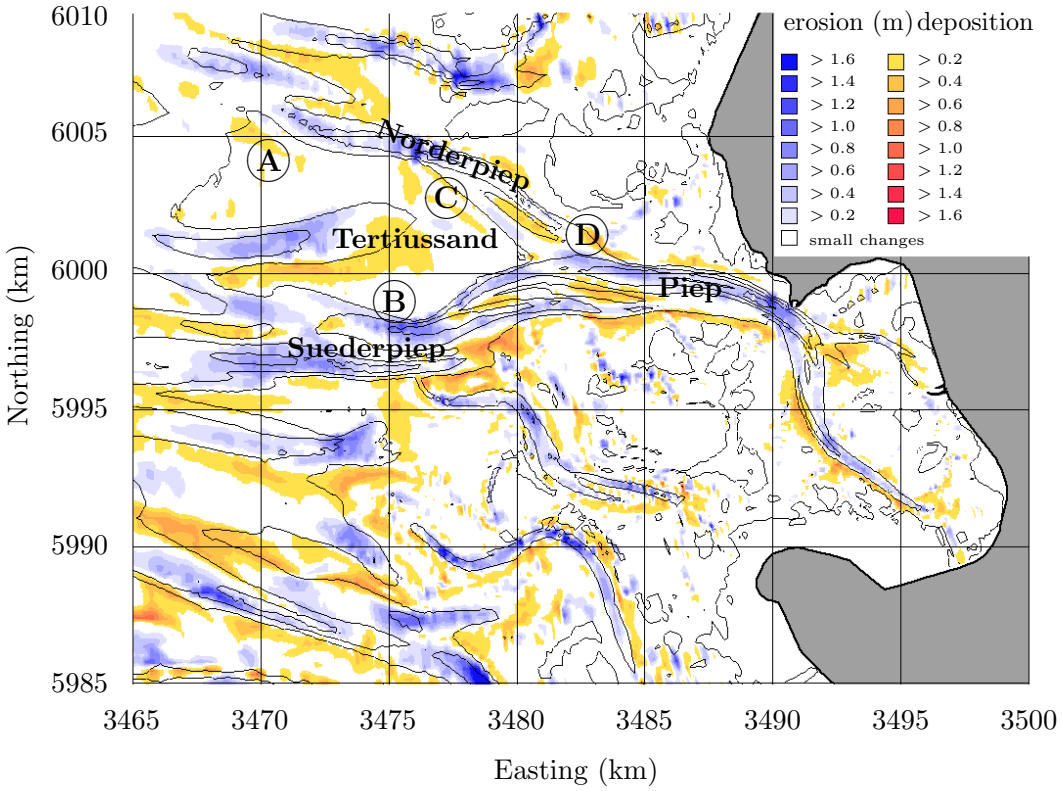

Figure 6.2: Computed morphological changes from 1977 to 1979 without swell and wind (isolines from 1977).

6.2.1 The role of the tide on the morphodynamics

The morphological evolution based on the tide alone is characterised by strong erosion in the channels and sedimentation on the tidal flats. Due to the relatively low current velocities in shallow areas and the absence of waves, sediment is easily deposited here. The absence of the stirring effect of the waves causes that, once deposited, the sediment will not be easily eroded in the shallow areas and fed back to the deeper channels. Thus, less sediment is supplied to the channels and therefore these are deepening.

The computed sedimentation and erosion patterns for the simulation with tide alone are shown in Figure 6.2. Through comparison with the results of the reference simulation (Figure 6.1), it can be seen that in the northwestern part (location **A**) the stretch of strong erosion is replaced by an area of accretion. The middle channel is showing more erosion than in the reference simulation. Southward of this channel up to location **B** the tidal flat shows overall accretion, whereas in the results of the reference simulation a stretch of erosion can be seen. At location **B** the southward expansion of Tertiussand is no longer visible. Near the eastern edge of the flat, at location **C**, the progression towards the Northeast can not be seen in the case without swell and wind. The stretch of erosion from the reference simulation results is replaced by sedimentation. On the basis of the stronger deposition the tidal flat is extending in westward direction.

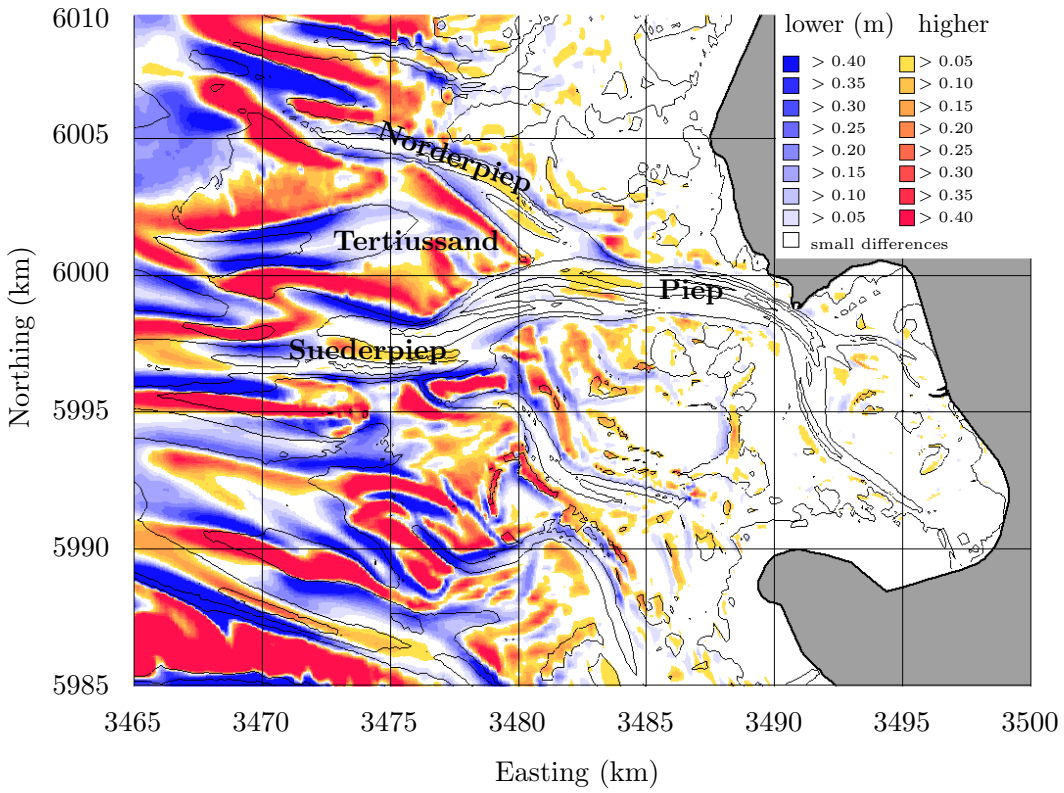

Figure 6.3: Differences in the final bathymetries of the reference simulation and of the simulation without swell and wind, for 1977 to 1979. Blue areas indicate that the bathymetry of the latter simulation is lower; red that it is higher.

The adjacent channels Norderpiep and Suederpiep show a slight increase in erosion. At location **D**, a decrease in sedimentation can be seen. Both effects indicate that when no swell nor wind are imposed the channels are larger than in the reference case where they are considered.

To illustrate the differences between the model results of the simulation without swell and wind and those of the reference simulation, the differences between the resulting bathymetries are shown in Figure 6.3. It shows that differences in the model results are mainly found in the western part of the domain. This area is mostly affected by the waves. In the eastern part of the domain, the differences are very limited. Deepening of the channels is seen throughout the channel system, whereas the submerged bars show accretion. Secondary channels are developing or increasing in size at various locations on the surrounding tidal flats.

Summary

It is concluded that the morphology adapts to purely tidal conditions through a relative increase in wet volume of the main channels. Between these channels the tidal flats and shoals are increasing in sediment volume, where their shape is bound by the location of the adjacent channels. Furthermore, the absence of waves enable the western tidal flats to extend in seaward direction.

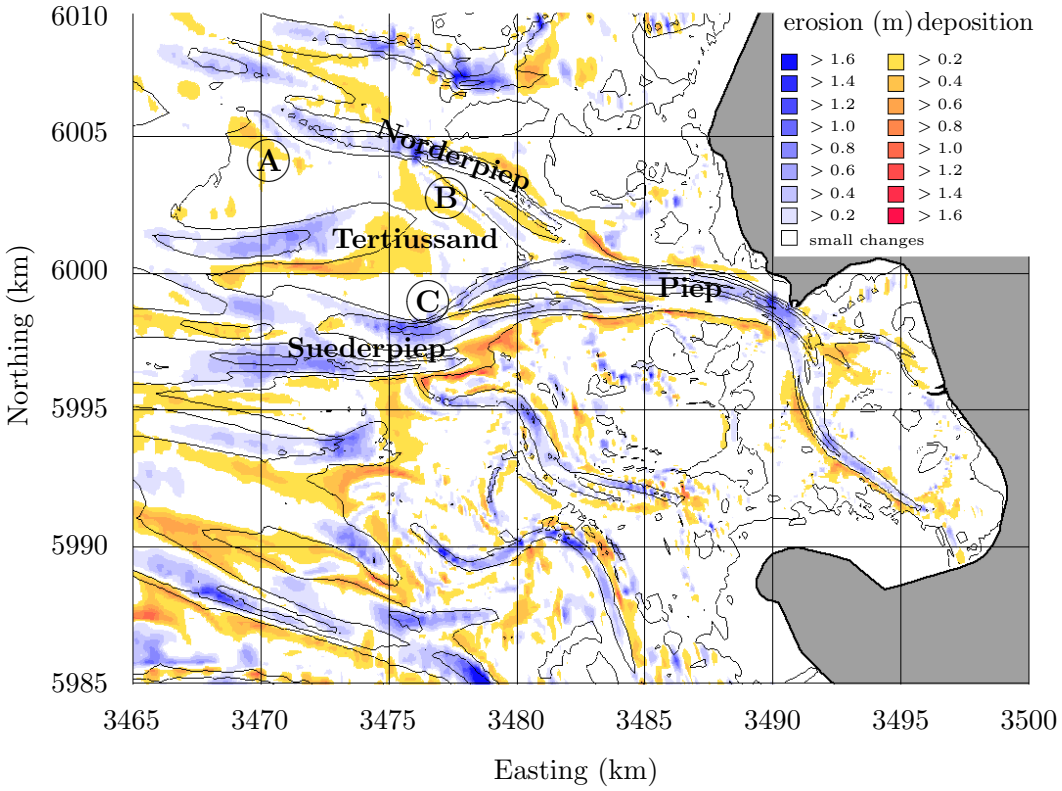

Figure 6.4: Computed morphological changes from 1977 to 1979, including the optimised wind climate without swell (iso-lines from 1977).

6.2.2 The role of swell waves on the morphodynamics

To evaluate the role of swell on the morphodynamics a simulation has been carried out in which no swell conditions have been imposed. Hence, the results of this simulation (Figure 6.4) have been obtained for tide and wind effects only. The local wind climate has been kept identical to the climate imposed in the reference simulation. Thus the differences in the computed bathymetries of this simulation and those of the reference simulation illustrate the effects of the swell waves.

The sedimentation and erosion patterns, from the simulation with tidal and wind conditions and without swell, are shown in Figure 6.4. Near location **A** accretion has replaced the erosion that is seen in the model results of the reference simulation. At location **B**, on the northwestern part of Tertiussand the same can be seen. The narrow stretch of erosion along the Norderpiep, seen from the reference simulation results, has reduced. Much more erosion can be seen in the Norderpiep itself. The expansion of the tidal flat in northeastern direction, as seen in the results of the reference simulation, is not visible here. On the southeastern side of the tidal flat (to the right of location **C**) less erosion is seen. West of location **C**, the erosion that could be seen from the reference simulation results has disappeared. At the southern edge of Tertiussand erosion is seen where in the reference simulation a southward migration was computed.

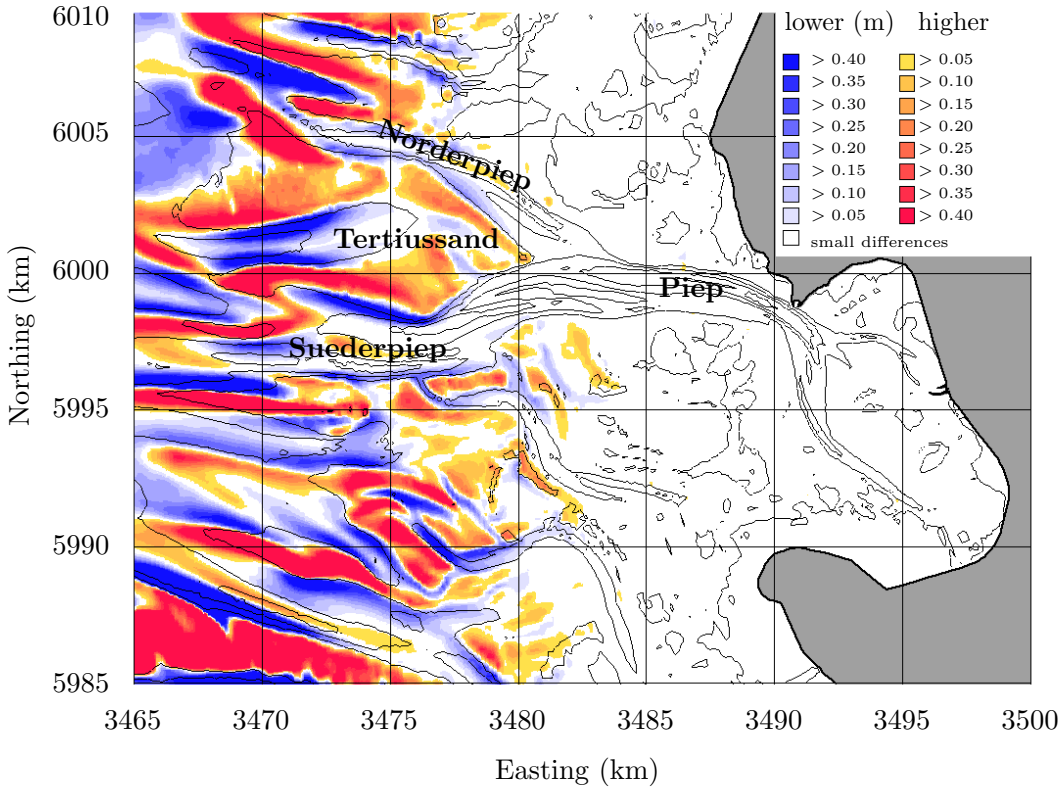

Figure 6.5: Differences in the final bathymetries of the reference simulation and of the simulation without swell, for 1977 to 1979. Blue areas indicate that the bathymetry of the latter simulation is lower; red that it is higher.

The differences in the resulting bathymetries of the reference simulation and the simulation without swell are shown in Figure 6.5. It shows that differences can only be found in the western part of the domain, which is exposed to incoming waves.

To give an indication of the distribution of the wave action over the area, the computed significant wave heights during low and high tide are shown in Figure 6.6.

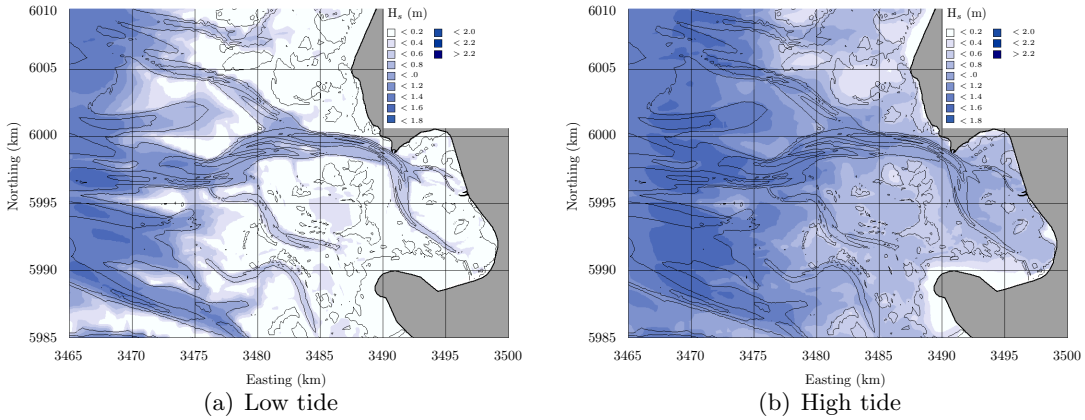

(a) Low tide (b) High tide

Figure 6.6: Computed significant wave heights during (a) low tide and (b) high tide. The results stem from a simulation where swell of 1 m height and 17.5 m/s wind speed were imposed (both from the West).

The results are based on a simulation with a swell of 1 m height and 17.5 m/s wind imposed (both from the West). During low tide the wave energy is mainly dissipated on the western margin of the tidal flats although some waves penetrate into the channels. The high wind speed only has a minor effect in these channels, since the tidal flats are dry. During high tide more wave action can be seen over the area. It can still be noted that the wave heights reduce at the western tidal flat margin, where depth-induced wave breaking takes place. Due the higher water level, some of the energy can penetrate further into the area. Combined with the larger fetch over the now flooded tidal flats this leads to wave action in the entire area.

Summary

The comparison of the model results of the discussed simulations showed that the swell mainly has an influence on the western part of the domain, concentrated on Tertiussand and the adjacent channels. On the basis of the shown computed wave height distributions, this could be expected. However, the extent to which the swell has an effect on the morphodynamics could not be deducted from these wave height distributions. Based on Figure 6.5 and the intercomparison of the sedimentation and erosion patterns of the considered simulations an estimate has been made. It is concluded that swell only has an effect on the area west of approximately 3480 km Easting. The effects are mainly visible as a reduction in height of the shallower areas as well as a reduction of the depth in the neighbouring deeper areas. In other words, due to the swell waves, sediment is stirred up and transported to deeper areas.

6.2.3 The role of wind and locally generated waves

The significance of the wind and locally generated waves has been investigated by comparing the results of a simulation with only the representative tidal conditions and the optimised swell climate imposed to those of the reference simulation. The differences between the model results are thus related to the wind and locally generated waves, which are strongly reduced in the first simulation. It should be noted that a very mild wind climate with wind speeds of 2.5 m/s had to be imposed to ensure stability of the wave model. This concerns swell wakes behind shoals or tidal flats where otherwise infinitesimal wave parameters destabilise the wave computation.

In Figure 6.7 the computed morphological changes from the simulation without wind and locally generated waves are shown. On the flat Tertiussand the main differences in comparison to the model results of the reference simulation are the slightly weaker deposition near locations **A** and **B** and the reduced erosion along its northwestern and southeastern edges. Smaller scale effects are seen along the main channels. The northeastern bank of the Norderpiep is showing less sedimentation than in the reference simulation results. The same can be seen at the southern bank of the Suederpiep.

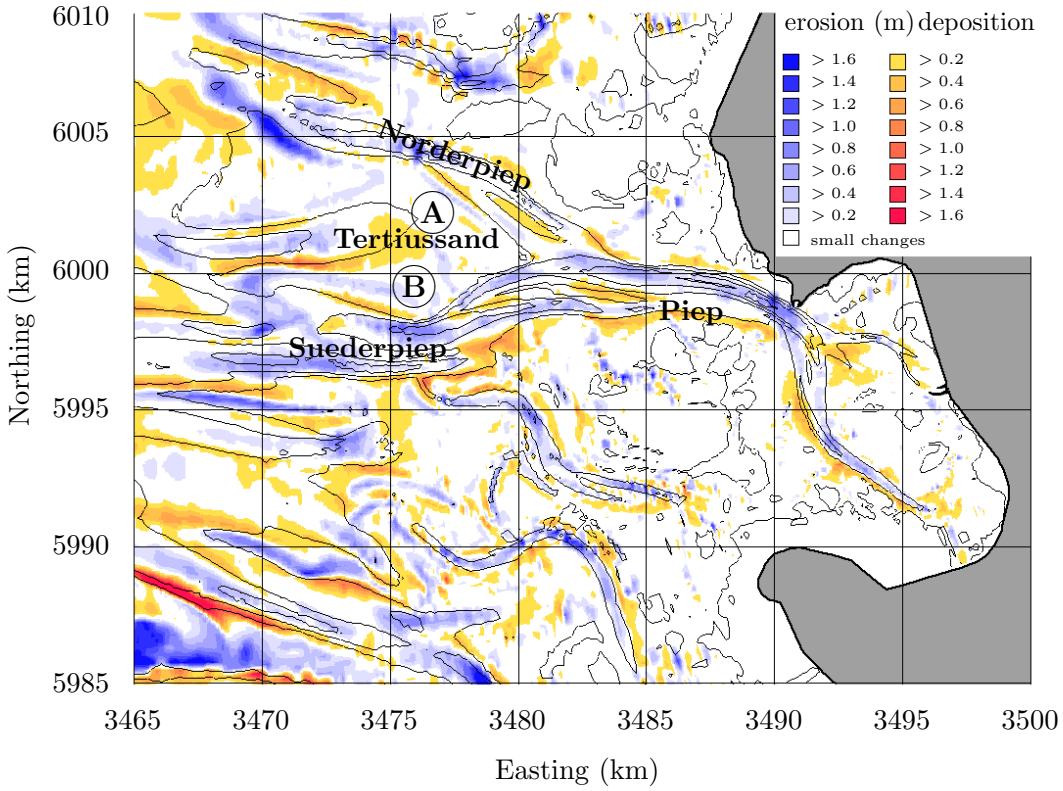

Figure 6.7: Computed morphological changes from 1977 to 1979, including the optimised swell climate and very mild wind conditions (iso-lines from 1977).

The differences between the resulting bathymetries of the reference simulation and the simulation with strongly reduced wind speeds are shown in Figure 6.8. It shows that the differences are mainly in the middle of the domain and not as large as in the difference plots of the previous two Paragraphs.

Summary

From the comparison of the model results can be concluded that the wind and wind generated waves show their main influence in the middle of the domain. However, these effects are limited in comparison to those of the tide and swell. The reason for the more eastward location of the affected area than in the case of the swell can be explained in two ways. Firstly, the locally generated waves are generally smaller and can therefore penetrate further into shallow areas than the higher swell waves. Secondly, the imposed wind also influences the swell waves, which can increase the amount of dissipated energy that in its turn induces stronger currents onto the tidal flats. This may be the case in the reference simulation where both wind and swell were imposed.

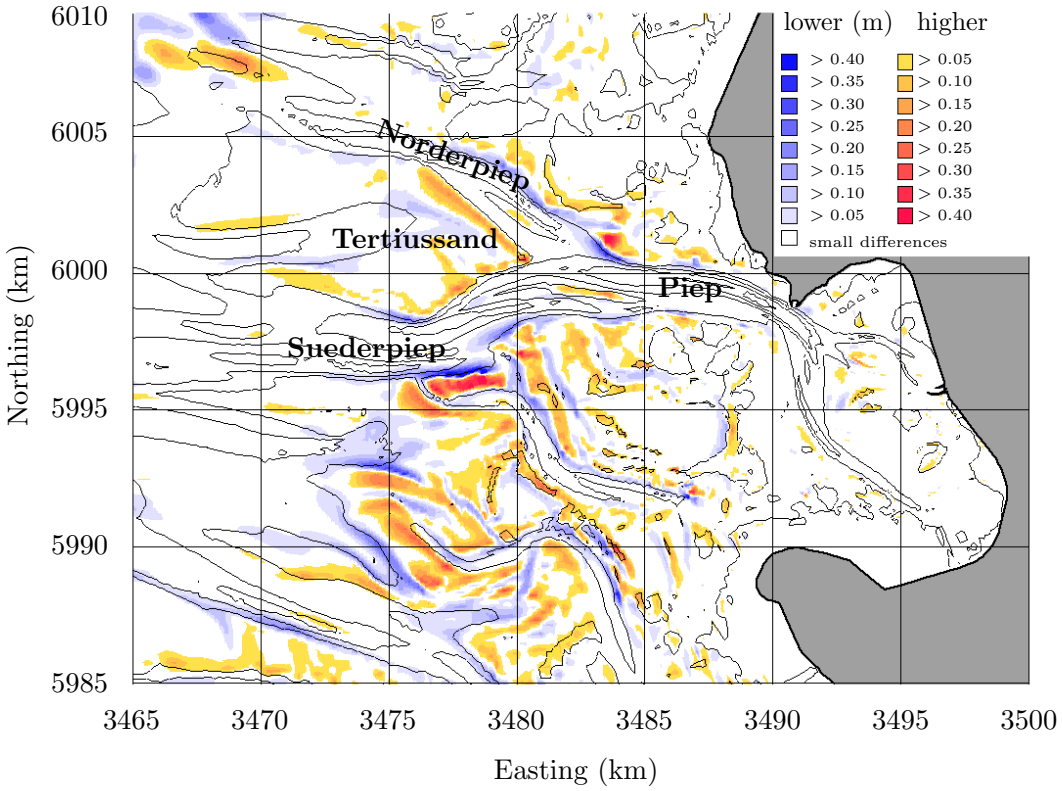

Figure 6.8: Differences in the final bathymetries of the reference simulation and of the simulation without wind and wind generated waves, for 1977 to 1979. Blue areas indicate that the bathymetry of the latter simulation is lower; red that it is higher.

6.2.4 Synthesis of the results

Combining the results of the previous Paragraphs leads to the conclusion that both tide and swell have the larger influence on the medium scale morphodynamics. In Chapter 2 the western area has been classified as lowly tide-dominated and the eastern part as highly tide-dominated, on the basis of the classification by Hayes [1979]. For the eastern part of the domain this fits very well, as no significant differences were seen in the model results of the simulations with and without waves imposed (Figure 6.3). The western part is clearly influenced by the swell and the middle also by the locally generated waves. The western part could thus better be classified as mixed energy instead of lowly tide-dominated.

The evaluation of the model results and their intercomparison showed that the tide is mainly responsible for initiating and maintaining the channels. Without waves it allows the gradual build-up of the tidal flats and shoals, limited by the presence of the channels. The swell causes an equalising of the tidal flats and channels, through erosion of the exposed tidal flats and filling of the channels. Furthermore the swell is the main force behind the expansion of the flat Tertiussand towards the Northeast and South, as well as the erosion of its western part. Wind and locally generated waves have a less distinctive influence on the medium scale morphological evolution, although they

do cause morphological changes in the middle of the domain. If these effects are based on the wind and locally generated waves alone or due to an interaction with the tidal and swell conditions could not be determined from the described simulations. As this influence is relatively small this has not been further investigated.

6.3 Prediction of the medium scale morphodynamics over ten years

The validated morphodynamic model has been applied to predict the morphological evolution of the area over a period of ten years, from 1999 to 2009. Based on the optimised swell and wind climates the model could reproduce the medium scale morphodynamics in the area in a good manner. Thus the same climates have been imposed in the simulation for the prediction, assuming that no significant changes occur in the general characteristics of these conditions. Possible changes, e.g. a considerable increase in the number of storms or a sea level rise are thus not considered here.

The initial bathymetry for 1999 and the resulting bathymetry for this simulation are shown in Figure 6.9. Figure 6.10 shows the computed morphological changes over the considered ten years. As can be seen, some significant changes are predicted by the model, mainly around Tertiussand. The small channel, branching of from the Suederpiep is gradually breaking through the tidal flat and connecting the open sea. The cut-off part of Tertiussand on the south is migrating further southward towards the Suederpiep. This migration causes a narrowing of the Suederpiep as the southern channel bank is maintained by the presence of the shoal D-Steert.

On the northeastern side of Tertiussand the observed progress towards the Northeast is continued. The southwestern sub-channel of the Norderpiep is gradually filled, creating a connection between the tidal flat and the submerged bar in this channel. At the southeastern side the channel Suederpiep is further eroding the edge of Tertiussand, a process that is now enhanced by the presence of the newly created channel over the tidal flat. More eastward deepening of the Piep is predicted. The submerged bar shows erosion, where it showed deposition in the computations and observations for the periods between 1977 and 1999. This change may also be related to the initiation of the channel over Tertiussand.

The relative volume changes are shown in Figure 6.11. Like before, the volumes have been indexed to the volumes of 1977 for consistency. The results of the calibration and validation have been added as well to give an overview. In contrast to the calibration and validation period, Tertiussand is showing a significant increase in wet volume for the period considered in the prediction. This increase is related to the breakthrough of the tidal channel over the tidal flat. This phenomenon was not seen in the periods for calibration and validation. The fact that the model predicts this breakthrough for the prediction period (1999 – 2009) and does not show this in the last years of the validation period (1990 – 1999) is related to the initial bathymetry of the prediction simulation. The initial bathymetry of the prediction simulation for 1999 already shows a tendency towards the breakthrough. This tendency is not so distinctly present in the computed bathymetry for 1999, resulting from the validation simulation.

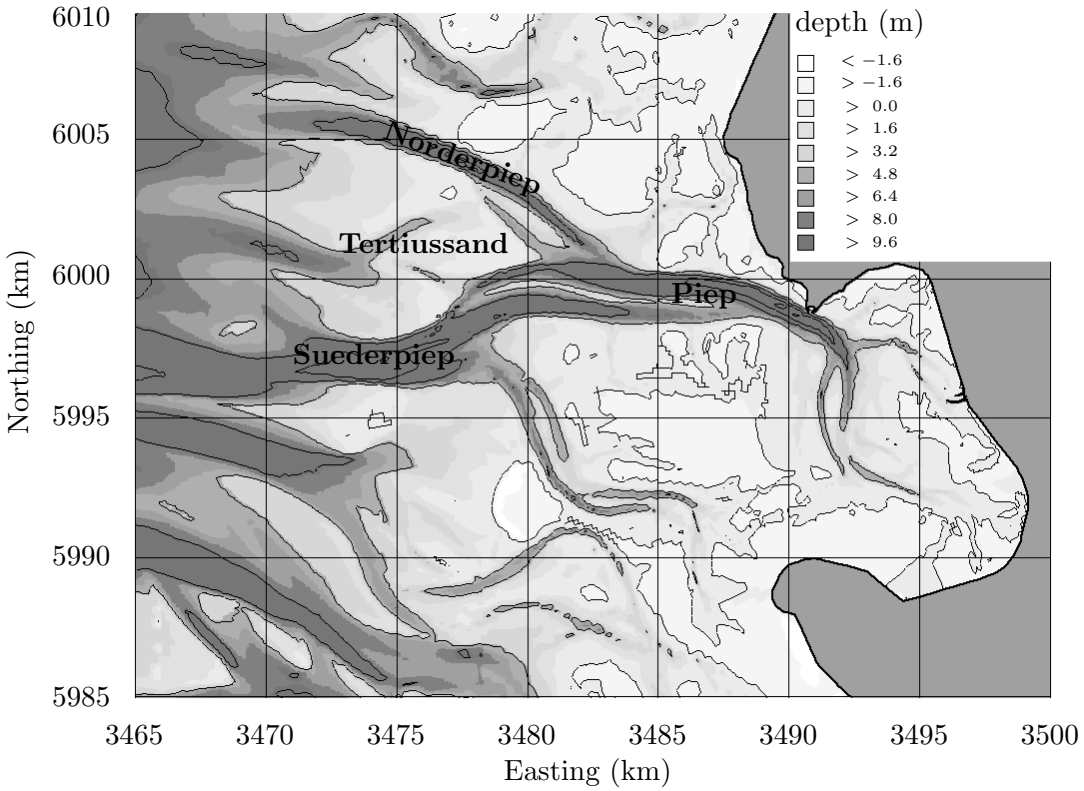

(a) Initial bathymetry for 1999

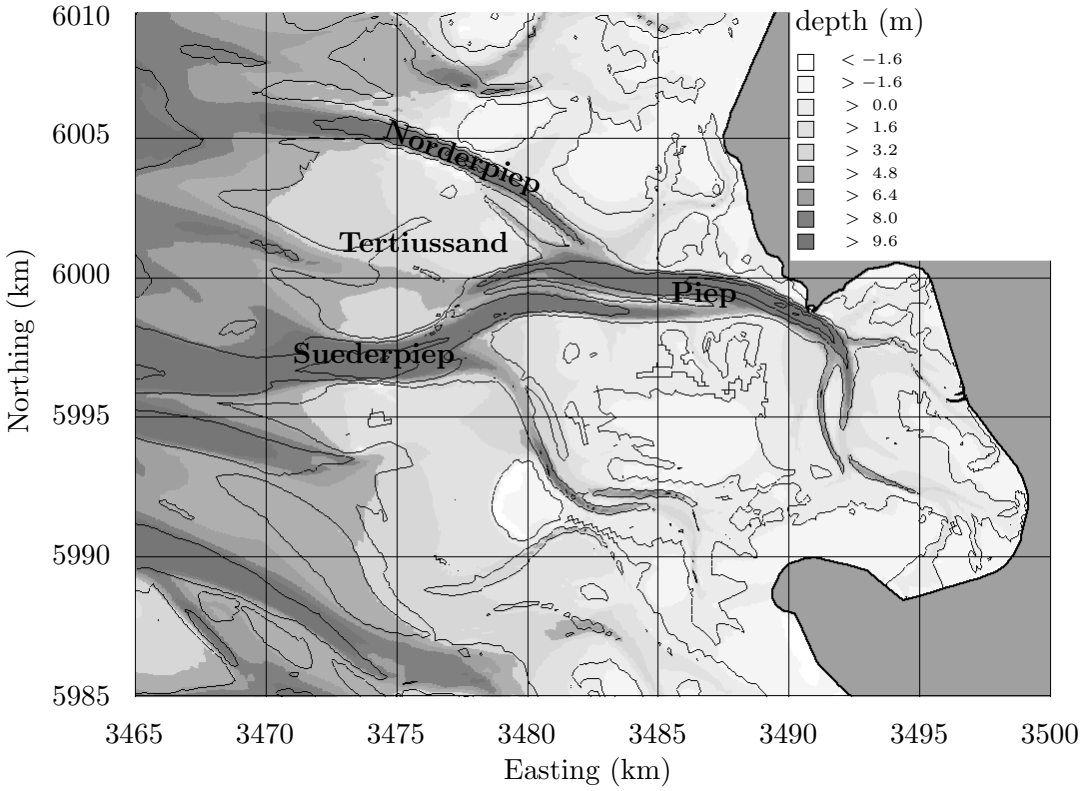

(b) Prediction for 2009

Figure 6.9: (a) Initial model bathymetry for 1999 and (b) predicted bathymetry for 2009 (isolines from 1999). Computation on the basis of the validated model settings and optimised swell and wind climates.

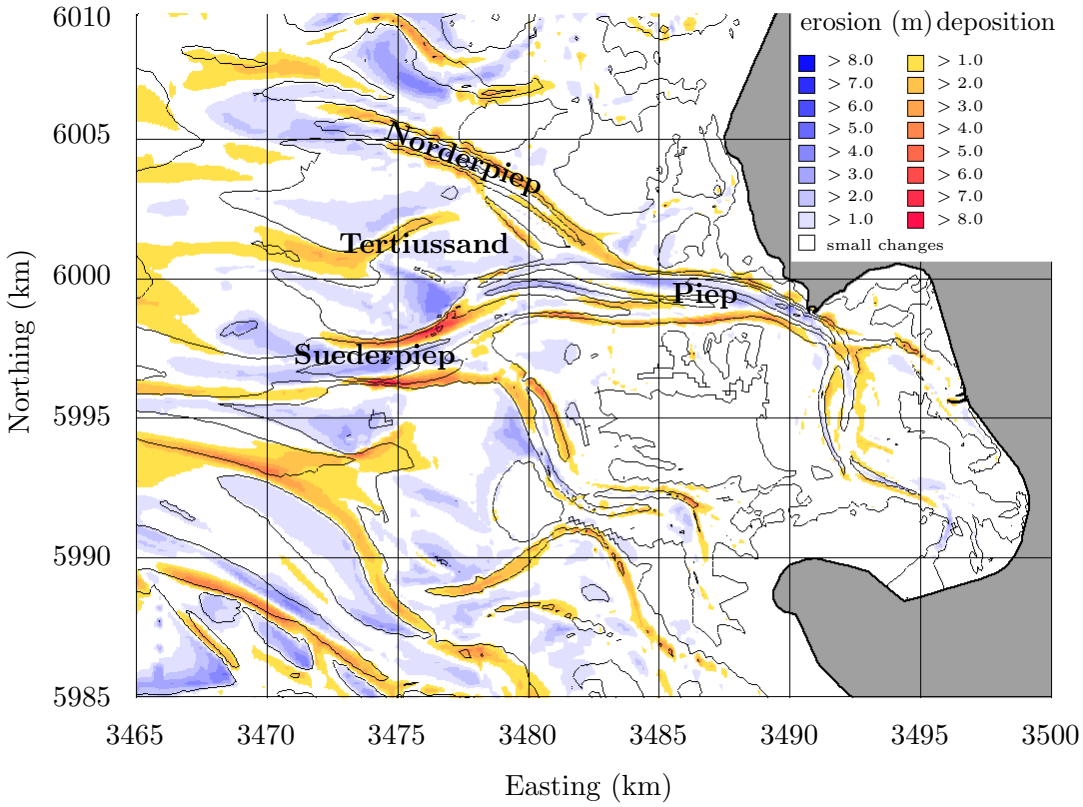

Figure 6.10: Predicted morphological changes from 1999 to 2009 (isolines from 1999). Computation on the basis of the validated model settings and optimised swell and wind climates.

These bathymetric differences lead to a different behaviour of the modelled morphodynamics, as can be seen from the different trends in the volumetric changes of both simulations, especially for the sub-domain Tertiussand. The sub-domains Suederpiep and Piep show trends similar to those found from the calibration and validation results. These trends also follow the general trend of the measurements. The deepening of the Suederpiep (see Figure 6.10) partly compensates the narrowing due to the southward migration of Tertiussand. Therefore the reduction of the wet volume of the sub-domain Suederpiep is more moderate. The sub-domain Norderpiep shows a stronger reduction of the volume, which is related to the predicted deposition in its southwestern sub-channel.

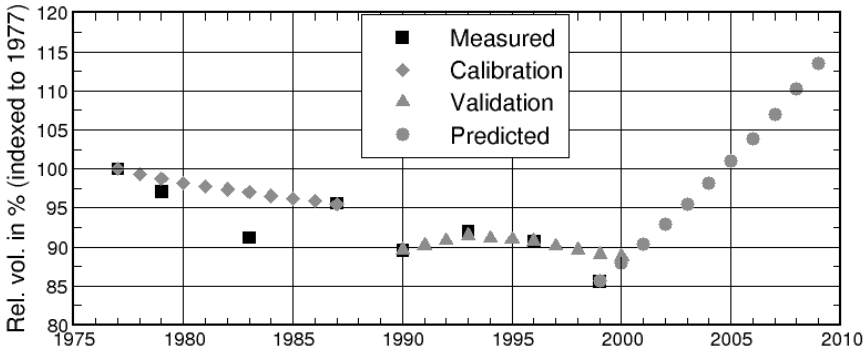

(a) Tertiussand

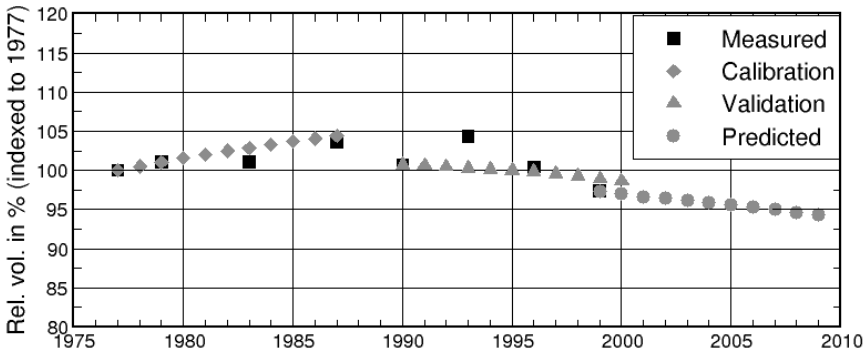

(b) Suederpiep

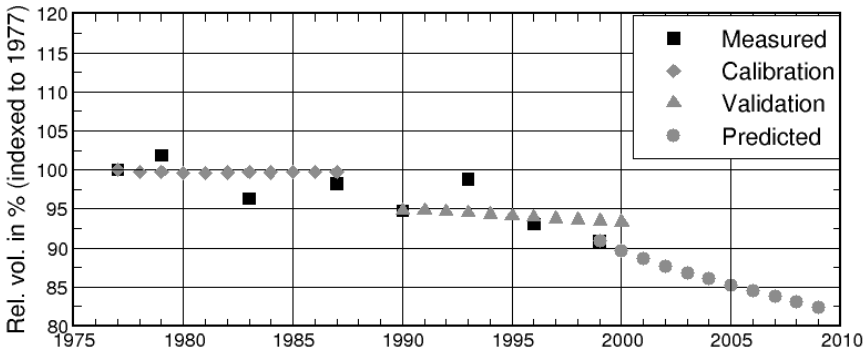

(c) Norderpiep

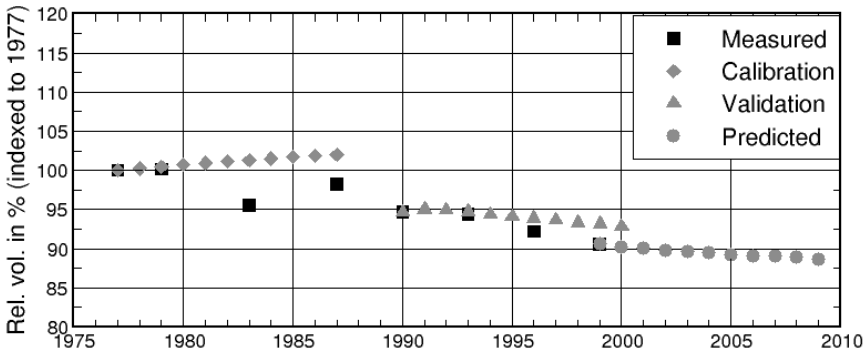

(d) Piep

Figure 6.11: Relative changes in the wet volume below sea level. Model results of the prediction simulation based on the optimised swell and wind climates. The results of the model calibration and validation have been added.

6.3.1 Summary

The results of the model prediction of the medium scale morphodynamics in the study area showed some significant changes. Enhanced by the breakthrough of the channel over the tidal flat Tertiussand, the adjacent tidal channels Norderpiep and Suederpiep showed a narrowing and deepening. The predicted new channel is located at the western end of the northern sub-channel of the Piep and thus forms an extension of this sub-channel. Therefore the morphodynamics of the Piep are subject to changes as well. The northern channel seems to change its orientation to create a smoother connection, resulting in erosion of the submerged bar in the Piep.

Although the model predicts some rather extensive changes in the morphology of the area, they do not seem to be unrealistic. Considering that the model showed rather good results on the medium scale in the calibration and validation, together with the fact that the underlying individual process models were also subjected to extensive calibration and validation studies, the model results appear to be reliable. The prediction has been based on the optimised representative conditions for tides, swell and wind. It is thus based on the assumption that these imposed conditions are also valid for the considered period from 1999 to 2009. Around the year 2009 it will be interesting to evaluate the occurred morphological changes to evaluate the quality of the above presented prediction.

Chapter 7

Conclusions and recommendations

7.1 Conclusions

Analysis of the measurements

The medium scale morphological evolution over the last twenty years of the tidal channel system in the central Dithmarschen Bight has been analysed on the basis of the available bathymetric measurements. The combination of previous investigations and the extensive measurement data provided a solid basis for the characterisation of the hydrodynamics, sediment dynamics and geomorphological background of the study area. This led to a comprehensive understanding of the dominant processes for the morphodynamics, which served as a basis for the set-up, evaluation and application of the medium scale morphodynamic model.

Set-up of the medium scale morphodynamic model

Based on validated individual process models for simulating flow, waves and sediment transport, the morphodynamic model was set-up. The validations of the individual models showed that each of them was able to reproduce the complex behaviour of the hydrodynamics and sediment dynamics of the investigated area very well. The coupling of these models was defined in such a way, that the mutual interactions between the processes are properly represented in the resulting morphodynamic model.

Medium scale modelling approach and representative boundary conditions

For the morphodynamic modelling on a medium scale, an approach has been defined in which a limited number of representative conditions in terms of tides, swell, wind and storm conditions has been defined. The definition of these conditions has been based on widely accepted input filtering techniques.

It is concluded that a tidal cycle with a tidal range close to the mean tidal range in the area yielded optimal results, whereas slightly higher ranges (between 7 and 20 % higher) are proposed in the literature. It was shown that the application of the representative tide and the application of a full spring-neap tidal cycle yielded highly similar morphodynamic model results.

Representative swell and wind climates were defined on the basis of long-term data sets of wave and wind characteristics. These climates formed first estimates and have been adjusted in the calibration.

Furthermore, it is be concluded that the influence of storm conditions on the medium scale morphodynamic model results was very limited in comparison to the changes induced by representative conditions. Therefore, storm conditions have been considered as part of the representative swell and wind climates.

Calibration and validation of the medium scale morphodynamic model

In the calibration and validation of the medium scale morphodynamic model evaluation periods of approximately ten years have been considered. The model results have been evaluated on the basis of changes in the location of depth contours, volumetric analysis of several sub-domains and comparison of the medium scale sedimentation and erosion patterns.

In the calibration the most significant improvements were achieved by adjusting the first estimates of the representative swell and wind climates and through the application of a variable definition of the Bijker's constant in the applied sediment transport formula. It is be concluded that the reduction of the representative swell and wave climates by 50 % in terms of the significant wave heights and the wind speeds led to significant improvements. Through a spatial and temporal variation of the Bijker's constant on the basis of the wave conditions the model results could be further improved. The calibration led to a model that could reproduce the majority of the observed medium scale morphodynamics during the considered period from 1977 to 1987 rather well.

In the validation, the results of the calibrated morphodynamic model were evaluated for the period from 1990 to 1999. The medium scale behaviour of the investigated tidal area was reproduced in a good manner by the model.

Thus it is concluded that the morphodynamic model gives a good representation of the medium scale morphodynamics of the investigation area and that the model can be applied for realistic modelling of the medium scale morphological evolution.

Analysis of the morphodynamic processes

The validated morphodynamic model has been applied to analyse the significance of the main driving forces, i.e. the tide, the swell, locally generated waves and wind, on the medium scale morphodynamics.

It is concluded that the tidal and swell conditions have the most significant influence

on the medium scale morphodynamics of the western part of the investigated area. In the centre of the domain the locally generated waves form an additional force in the medium scale morphodynamics, although the significance is less pronounced than the significance of the tidal and swell conditions. Hence, western and middle parts of the area can better be classified as mixed energy than as lowly tide-dominated, as it followed from the classification by Hayes [1979] on the basis of the mean tidal range and the mean wave height. In the East of the investigation area the medium scale morphodynamics were concluded to be highly tide-dominated, in agreement with Hayes' classification.

The swell has been identified as the main force behind the observed expansion of the central tidal flat Tertiussand to the Northeast and South, as well as the erosion on its western part. In general, the morphological evolution mainly depends on the balance of the tide, responsible for initiating and maintaining the channels, and the swell, causing an equalising of the tidal flats and channels.

Prediction of ten years of morphological evolution

The results of the prediction of the medium scale morphodynamics showed some significant morphological changes, mainly induced by a breakthrough of the central tidal flat. The prediction does not seem unrealistic, however, in the light of the observed morphodynamics over the last twenty years. The fact that the underlying individual process models as well as the medium scale morphodynamic model have been subjected to extensive calibration and validation studies increases the confidence in the prediction.

7.2 Recommendations for future research

Sediment grain size

In the described morphodynamic model a uniform distribution of the sediment grain size has been imposed, based on the results of the validation of the sediment transport model. Although good results were achieved, both in the sediment transport modelling and in the medium scale morphodynamic modelling, and the fact that the sieve curves showed quite uniform grain sizes, improvements may be made when considering a varying distribution. Furthermore, only the median grain size d_{50} and 90th percentile grain size d_{90} are considered in the computation of the sediment transport. On the basis of an area-wide data set of sediment sieve curves, multiple grain sizes could be defined to give a better representation.

Small scale morphodynamics

It was shown that the morphodynamic model represents the medium scale morphodynamics in a good manner. It would be interesting to examine the quality of the model

with respect to smaller scale morphodynamics. To this purpose the spatial resolution should be increased at the cost of the computational efforts.

Three-dimensional modelling

In this study a two-dimensional depth-averaged approach has been applied for the morphodynamic modelling. It was shown that this is suitable for the representation of the medium scale morphological evolution. When considering smaller scale hydrodynamic and morphodynamic processes it may be required to consider the three-dimensional approach in the individual process models. It could give more accurate results for the behaviour of smaller scale features, e.g. submerged bars or the meandering effect of curved channels due to spiral flow.

References

Asp, N.E., 2003, Long to short-term morphodynamics of the tidal flats in the Dithmarschen Bight, German North Sea, Ph.D. thesis, University of Kiel, Germany.

Asp, N.E., Wilkens, J., Ricklefs, K., and Mayerle, R., 2001, Geology and morphodynamics of a tidal flat area of the German North Sea coast: A comparison of field measurements and medium-scale morphodynamic modelling results, Proceedings of the 8th ABEQUA Congress.

Behre, K.E., 1994, Die deutsche Nordseeküste, In: Liedtke, H. and J. Marcinek, Physische Geographie Deutschlands, Gotha, In German.

Bijker, E.W., 1971, Longshore transport computations, Journal of the waterways, harbors and coastal engineering division, WW4:687–701.

BMFT, 1994, Optimierung des Küstenschutzes auf Sylt - Phase II, Bundesministerium für Forschung und Technologie, Amt für Ländliche Räume, Husum, In German.

Booij, N., Ris, R.C., and Holthuijsen, L.H., 1999, A third-generation wave model for coastal regions, Part I, Model description and validation, Journal of Geophysical Research, 104(C4):7649–7666.

Brown, J., Colling, A., Park, D., Phillips, J., Rothery, D., and Wright, J., 1989, Waves, tides and shallow-water processes, Open University course team, Open University, Walton Hall, Milton Keynes, England, Butterworth-Heinemann, Oxford.

Davies, J.L., 1964, A morphogenetic approach to world shorelines, Zeitschrift für Geomorphologie, Sonderheft zum 70. Geburtstag Prof. H. Mortensen, pages 127–142.

De Vriend, H.J., 1997, Prediction of aggregated-scale coastal evolution (PACE), In: Thornton, M.B., and Huntley, D.A. (eds.), Coastal Dynamics '97.

De Vriend, H.J., Capobianco, M., Chesher, T., De Swart, H.E., Latteux, B., and Stive, M.J.F., 1993a, Approaches to long-term modelling of coastal morphology: a review, Coastal Engineering, 21:225–269.

De Vriend, H.J., Zyserman, J., Nicholson, J., Roelvink, J.A., and Southgate, H.N., 1993b, Medium-term 2DH coastal area modelling, Coastal Engineering, 21:193–224.

Dingemans, M.W., Radder, A.C., and De Vriend, H.J., 1987, Computation of the driving forces of wave-induced currents, Coastal Engineering, 11:539–563.

Dittmer, E., 1938, Schichtenaufbau und Entwicklungsgeschichte des dithmarscher Alluviums, Westküste, No. 1 (2): pp. 105-150, In German.

Dittmer, E., 1960, Neue Beobachtungen und kritische Bemerkungen zur Frage der Küstensenkung, Die Küste, H. 8, In German.

Dronkers, J., 1986, Tidal assymetry and estuarine morphology, Netherlands Journal of Sea Research, 20(2/3):117–131.

DWD, 2000, Orkantief Anatol vom 3./4. Dezember 1999, Homepage of the German Meteorological Service (Deutsche Wetter Dienst), In German.

Ehlers, J., 1988, The morphodynamics of the Wadden Sea, A.A. Balkema, Rotterdam.

Figge, K., 1981, Begleitheft zur Karte der Sedimentverteilung in der Deutschen Bucht 1:250000 (Nr. 2900), Bericht des Deutsches Hydrographisches Instituts, In German.

Froehle, P. and Kohlhase, S., 1995, Long-term statistical evaluation of sea state in storm surges, Proceedings of the 1995 International Conference on Coastal and Port Engineering in Developing Countries.

Galappatti, R., 1983, A depth integrated model for suspended transport, Communications of Hydraulics.

Gast, R., 1980, Die Sedimente der Meldorfer Bucht (Deutsche Bucht): Ihre Sedimentpetrographie und Besiedlung, Typisierung und Schwermetallgehalte, Ph.D thesis, University of Kiel, Germany, In German.

Gast, R., Köster, R., and Runte, K.H., 1984, Die Wattsedimente in der nördlichen und mittleren Meldorfer Bucht, Die Küste, H. 40, In German.

Hanson, H., Aarninkhof, S., Capobianco, M., Jimenez, J.A., Larson, M., Nicholls, R.J., Plant, N.G., Southgate, H.N., Steetzel, H.J., Stive, M.J.F., and De Vriend, H.J., 2003, Modelling of coastal evolution on yearly to decadal time scales, Journal of Coastal Research, 19(4):790–811.

Hartsuiker, G., 1997, Deutsche Bucht and Dithmarschen Bucht, Set-up and calibration of tidal flow models, Delft Hydraulics, report no. H1821.

Hayes, M.O., 1975, Morphology of sand accumulations in estuaries, In Cronin, L.E. (ed.), Estuarine Research, 2:3–22.

Hayes, M.O., 1979, Barrier island morphology as a function of tidal and wave regime, In: Leatherman, S.P. (eds.) Barrier Islands from the Gulf of St. Lawrence to the Gulf of Mexico.

Hirschhäuser, T. and Zanke, U.C.E., 2002, Morphologische Langfristprognose für das System Tidebecken-Aussensände am Beispiel Sylts und der Dithmarscher Bucht, Die Küste, H. 64, In German.

Holthuijsen, L.H., Booij, N., and Herbers, T.H.C., 1989, A prediction model for stationary, short-crested waves in shallow water with ambient currents, Coastal Engineering, 13:23–54.

Hoyme, H., 2002, Mesoskalige morphodynamische Modellierungen am Beispiel der Meldorfer Bucht, Ph.D. dissertation, Fachbereich Bauingenieur- und Vermessungswesen, University of Hanover, In German.

Kesper, J., 1992, Sedimentdynamik ausgewählter Außensände vor der schleswig-holsteinische Westküste, Ph.D. thesis, University of Kiel, Germany, In German.

Latteux, B., 1995, Techniques for long-term morphological simulation under tidal action, Marine Geology, 126:129–141.

Luthardt, H., 1987, Analyse der wassernahen Druck- und Windfelder über der Nordsee aus Routinebeobachtungen, Hamburger Geophysikalische Einzelschriften, Reihe A 83, In German.

Mayerle, R. and Palacio, C., 2002, Open boundary condition approaches for near coastal area models, Proceedings of the 13th congress of the Asia and Pacific division of IAHR.

Niemeyer, H.D., Goldenbogen, R., Schroeder, E., and Kunz, H., 1995, Untersuchungen zur Morphodynamik des Wattenmeeres im Forschungsvorhaben WADE, Die Küste, H. 57, In German.

Palacio, C., 2002, Metodología para la validación de modelos hidrodinámicos utilizando amplia información de campo: aplicación a la Bahía Meldorf en la costa del Mar del Norte Alemán, Ph.D. thesis, National University of Colombia, Medellin, In Spanish.

Palacio, C., Winter, C., and Mayerle, R., 2001, Set-up of a hydrodynamic model for the Meldorf Bight, Proceedings of the World Water and Environmental Resources Congress.

Poerbandono, 2003, Measurement and Modelling of Sediment Transport in the Meldorf Bight Tidal Channels, German North Sea Coast, Ph.D. thesis, University of Kiel, Germany.

Poerbandono and Mayerle, R., 2003, Modelling of suspended sediment concentration dynamics. Case study: Meldorf Bight tidal channels, German North Sea coast, Proceedings of the International Conference on Coastal Engineering (ICCE), Lisbon, 2004.

Reimers, H.C., 1999, Wirkungsweise von Buschlahnungen auf den Sedimenthaushalt von aufwachsenden Deichvorländern, Research and Technology Centre Westcoast, University of Kiel, Büsum, Germany, Report no. 17, In German.

Reimers, H.C., 2003, Sedimentverteilung und Benthosverbreitung in den Watten der Dithmarscher Bucht als Indikator für morphodynamische Veränderungen, Abschlußbericht zum Forschungsvorhaben SEDIMORV im GKSS-Hochschulprogramm, GKSS Research Centre Geesthacht, Germany, Report no. GKSS 2003/18, In German.

Reineck, H.E., 1978, Das Watt, Ablagerungs- und Lebensraum, Kramer, Frankfurt, second edition, In German.

Ris, R.C., Booij, N., and Holthuijsen, L.H., 1999, A third generation wave model for coastal regions, Part II, Verification, Journal of Geophysical Research, 104(C4): 7667–7682.

Rizzo, R., 2003, Open boundary conditions for sediment transport in near coastal area models, M.Sc. thesis, Coastal Geosciences and Engineering, University of Kiel, Germany.

Roelvink, J.A. and Van Banning, G.K.F.M., 1994, Design and development of DELFT3D and application to coastal morphodynamics, Hydroinformatics 1994, Verwey, Minns, Babovic and Maksimovic (eds), Balkema, Rotterdam.

Roelvink, J.A., Walstra, D.J.R., and Chen, Z., 1994, Morphological modelling of Keta Lagoon case, Proceedings of the 24th international conference on coastal engineering.

Rohde, H., 1977, Sturmfluthöhen und saekularer Wasserstandsanstieg an der deutschen Nordseeküste, Die Küste, H. 30, In German.

Runte, K.H., 1994, Sedimenttransport unter Sturmflutbedinungen in einem Wattrückensystem des Blauortsandes, Meyniana, No. 46, pp. 107 - 125, In German.

Steijn, R.C., 1992, Input filtering techniques for complex morphological models, Delft Hydraulics Report, H 824.53.

Stelling, G., 1984, On the construction of computational methods for shallow water flow problems, Rijkswaterstaat communications, No. 35.

Van Rijn, L.C., 1984, Sediment transport: Part I: Bed load transport; Part II: Suspended load transport, Journal of Hydraulic Engineering, 110.

Van Rijn, L.C., Grasmeijer, B.T., and Ruessink, B.G., 2002a, Accuracy of measurement instruments, In: Van Rijn, L.C., Ruessink, B.G. and Mulder, J.P.M. (Editors), The Behaviour of a Straigh Sandy Coast on the Time Scale of Storms and Seasons: Process Knowledge and Guidelines for Coastal Management, EC MAST Project, MAS3-CT97-0086 COAST3D-EGMOND, Aqua Publications, Amsterdam, The Netherlands, pages E1–E21.

Van Rijn, L.C., Walstra, D.J.R., Grasmeijer, B., Sutherland, J., Pan, S., and Sierra, J.P., 2002b, Simulation of nearshore hydrodynamics and morphodynamics on the time scale of storms and seasons using process-based profile models, COAST3D-Egmond End Document.

Vela Diez, S., 2001, Sediment mapping of the tidal flat channels off Büsum, M.Sc. thesis, Coastal Geosciences and Engineering, University of Kiel, Germany.

Verboom, G.K., De Ronde, J.G., and Van Dijk, R.P., 1992, A fine grid tidal flow and storm surge model of the North Sea, Continental Shelf Research, 12(2/3):213–233.

Westlake, S.J. ET AL., 1996, Accuracy of NOURTEC bathymetric surveys, Report NOURTEC project, RIKZ, Rijkswaterstaat, The Netherlands.

Wieland, P., 1984, Untersuchung über geomorphologische Veränderungen in der Dithmarscher Bucht, Die Küste, H. 40, In German.

Wieland, P., Fladung, B., and Bergheim, V., 1984, Tidedynamische und meteorologische Randbedingungen im Bereich des Schlick-Testfeldes Dithmarscher Bucht, Die Küste, H. 40, In German.

Wilkens, J., Asp, N.E., Ricklefs, K., and Mayerle, R., 2001, Medium-scale morphodynamic modelling in the Meldorf Bight, Proceedings of the EWRI/ASCE world water and environmental resources congress.

Wilkens, J. and Mayerle, R., 2002, Calibration of coupled flow-wave models and generation of boundary conditions for the central Dithmarschen Bight, Germany, Proceedings of the Conference on physics in estuaries and coastal seas (PECS), Hamburg, 2002.

Winter, C., 2003, Validation of the CSM-GBM Nesting, Determination of open sea boundary conditions for small scale coastal models, Coastal Research Laboratory, University of Kiel, Germany, Report no. 04-03.

Winter, C. and Mayerle, R., 2003, Calibration and validation of a sediment transport model with extensive data-sets for a tidal channel system in the German Wadden Sea, Proceedings of Coastal Sediments, Clearwater Beach, 2003.

WL | Delft Hydraulics, 2003a, Delft3D-FLOW, Simulation of multi-dimensional hydrodynamic flows and transport phenomena, including sediments, User Manual, WL | Delft Hydraulics, the Netherlands.

WL | Delft Hydraulics, 2003b, Delft3D-WAVE, Simulation of short-crested waves with HISWA or SWAN, User Manual, WL | Delft Hydraulics, the Netherlands.

WL | Delft Hydraulics, 2003c, Delft3D-MOR, Simulation of the long-term interaction of waves, currents, sediment transport and morphological development, User Manual, WL | Delft Hydraulics, the Netherlands.

Zeiler, M., Schulz-Ohlberg, J., and Figge, K., 2000, Mobile sand deposits and shoreface dynamics in the inner German Bight (North Sea), Marine Geology, 170:363–380.

Zielke, W., Gross, G., Hoyme, H., Mayerle, R., Ricklefs, K., Winter, C., Eppel, D.P., and Witter, G., 2000, Predictions of medium-scale morphodynamics - PROMORPH, Proceedings of the 27th International Conference on Coastal Engineering.

Nomenclature

Symbol	Description	Unit
Δs	Local grid cell size in the sediment transport direction	$[m]$
Δt	Time step	$[s]$
$\Delta t_{bed,max}$	Maximal time step for bed evolution calculation	$[s]$
Δt_{bed}	Time step for bed evolution calculation	$[s]$
Δx	Grid cell size in x-direction	$[m]$
Δy	Grid cell size in y-direction	$[m]$
Δ	Relative density $(\rho_s - \rho_w)/\rho_w$	$[-]$
η	Horizontal co-ordinate along the Delft3D grid	$[m]$
λ_x	Sediment transport representativity factor in x-direction	$[-]$
λ_y	Sediment transport representativity factor in y-direction	$[-]$
μ	Ripple factor	$[-]$
ν_{2Dh}	Horizontal viscosity coefficient	$[m^2/s]$
ρ_s	Density of the sediment	$[kg/m^3]$
ρ_w	Density of the water	$[kg/m^3]$
σ	Relative wave frequency	$[s^{-1}]$
τ_{cw}	Combined current- and wave-induced bed shear stress	$[N/m^2]$
$\tau_{w,rel}$	Relative contribution to the total stirring effect	$[-]$
$\tau_{w,tot}$	Total stirring effect, summed over all wave heights and directions	$[kg/ms^2]$
$\tau_w(H,\theta)$	Stirring effect contribution for wave height H and direction θ	$[kg/ms^2]$
θ	Wave direction	[°N]
θ_w	Wind direction	[°N]
ξ	Horizontal co-ordinate along the Delft3D grid	$[m]$
ζ	Water level with respect to MSL (pos. upward	$[m]$
b	Bijker calibration constant	$[-]$
C	Chézy bottom roughness coefficient	$[m^{1/2}/s]$
c_σ	Propagation velocity in σ-space	$[m/s]$
c_θ	Propagation velocity in θ-space	$[m/s]$
c_x	Propagation velocity in x-direction	$[m/s]$
c_y	Propagation velocity in x-direction	$[m/s]$
c_{bed}	Bed celerity	$[m/s]$
Cr	Courant-Friedrich-Levy number	$[-]$

Cr_{bed}	Courant number for the bed	$[-]$
d	Bottom level with respect to MSL (pos. downward)	$[m]$
D_h	Horizontal eddy diffusivity coefficient	$[m^2/s]$
d_{50}	Median sediment grain size	$[\mu\text{m}]$
d_{90}	90^{th} Percentile of the sediment grain size distribution	$[\mu\text{m}]$
$E(\sigma, \theta)$	Spectral wave energy density	$[J/m^2]$
g	Gravitational acceleration	$[m/s^2]$
h	Water depth	$[m]$
H_s	Significant wave height	$[m]$
I_1, I_2	Einstein integrals, functions of the relative bottom roughness	$[-]$
k_s	Bed roughness	$[m]$
MSL	Mean Sea Level	
$N(\sigma, \theta)$	Spectral wave action density	$[Js/m^2]$
NN	Normal Null, German notation for the mean sea level	
$P(H, \theta)$	Energy flux contribution for wave height H and direction θ	$[N/m]$
$p(H, \theta)$	Probability of occurrence for wave height H and direction θ	$[-]$
P_{rel}	Relative contribution to the total energy flux	$[-]$
P_{tot}	Total energy flux, summed over all wave heights and directions	$[N/m]$
q_η	Discharge in η-direction per unit of width	$[m^2/s]$
q_ξ	Discharge in ξ-direction per unit of width	$[m^2/s]$
r_c	Bed roughness height for currents	$[m]$
S	Wave energy source term	$[J/m^2]$
S_b	Bed load sediment transport	$[kg/m^2s^2]$
S_s	Suspended load sediment transport	$[kg/m^2s^2]$
S_x	Total sediment transport in x-direction per unit width	$[m^2/s]$
S_y	Total sediment transport in y-direction per unit width	$[m^2/s]$
$S_{ds,br}(\sigma, \theta)$	Source term for dissipation through wave breaking	$[J/m^2]$
$S_{ds,b}(\sigma, \theta)$	Source term for dissipation through bottom friction	$[J/m^2]$
$S_{ds,w}(\sigma, \theta)$	Source term for dissipation through white-capping	$[J/m^2]$
$S_{in}(\sigma, \theta)$	Source term for wind generation	$[J/m^2]$
T_p	Peak period of a wave spectrum	$[s]$
t_i	Time i in a simulation	$[s]$
T_m	Morphological time scale	$[s]$
U	Horizontal flow velocity magnitude	$[m/s]$
U_w	Wind speed	$[m/s]$
V_{1977}	Wet volume below MSL of a sub-domain in 1977	$[m^3]$
V_i	Wet volume below MSL of a sub-domain in year i	$[m^3]$
$V_{rel,i}$	Relative wet volume below MSL of a sub-domain in year i	$[-]$

About the author

Jort Wilkens was born in Blokzijl, the Netherlands, on March 24^{th}, 1974, and has the Dutch nationality. From 1986 he attended the Zuyderzee College in Emmeloord and graduated in 1992 to receive his V.W.O. diploma. Subsequently, he moved to Allendale, Michigan, to attend the senior year at the Allendale High School, from which he received the diploma in 1993.

Back in the Netherlands, in the same year, the author started his academic study in Civil Engineering and Management at the University of Twente in Enschede. During a three-month traineeship in 1997 at Alkyon Hydraulic Consultancy & Research, Emmeloord, he studied the distribution and characteristics of sand waves in the southern North Sea. He completed his study with a masters project at WL | Delft Hydraulics, carried out for the Rijksinstituut voor Kust en Zee (RIKZ, National Institute for Coastal and Marine Management). In this model study the morphological development of the spit Bornrif at the head of the Wadden Sea island of Ameland was investigated. The author received his M.Sc. degree in 1999.

From the middle of 1999 to 2004 he conducted his doctorate study at the Coastal Research Laboratory of the Research and Technology Centre Westcoast, University of Kiel, Germany. His research on the morphodynamics of the central Dithmarschen Bight was funded by the Bundesministerium für Bildung und Forschung (BMBF, Federal Ministry of Education and Research) as part of the research project PROMORPH.

Currently, the author is working as a postdoc at the Coastal Research Laboratory in Kiel.